UiT
THE ARCTIC
UNIVERSITY
OF NORWAY

Faculty of Science, Department of Geology

Post-Caledonian brittle faults along the SW Barents Sea Margin

Onshore-offshore margin architecture and fault rock-forming conditions

—

Kjetil Indrevær

A dissertation for the degree of Philosophiae Doctor – August 2014

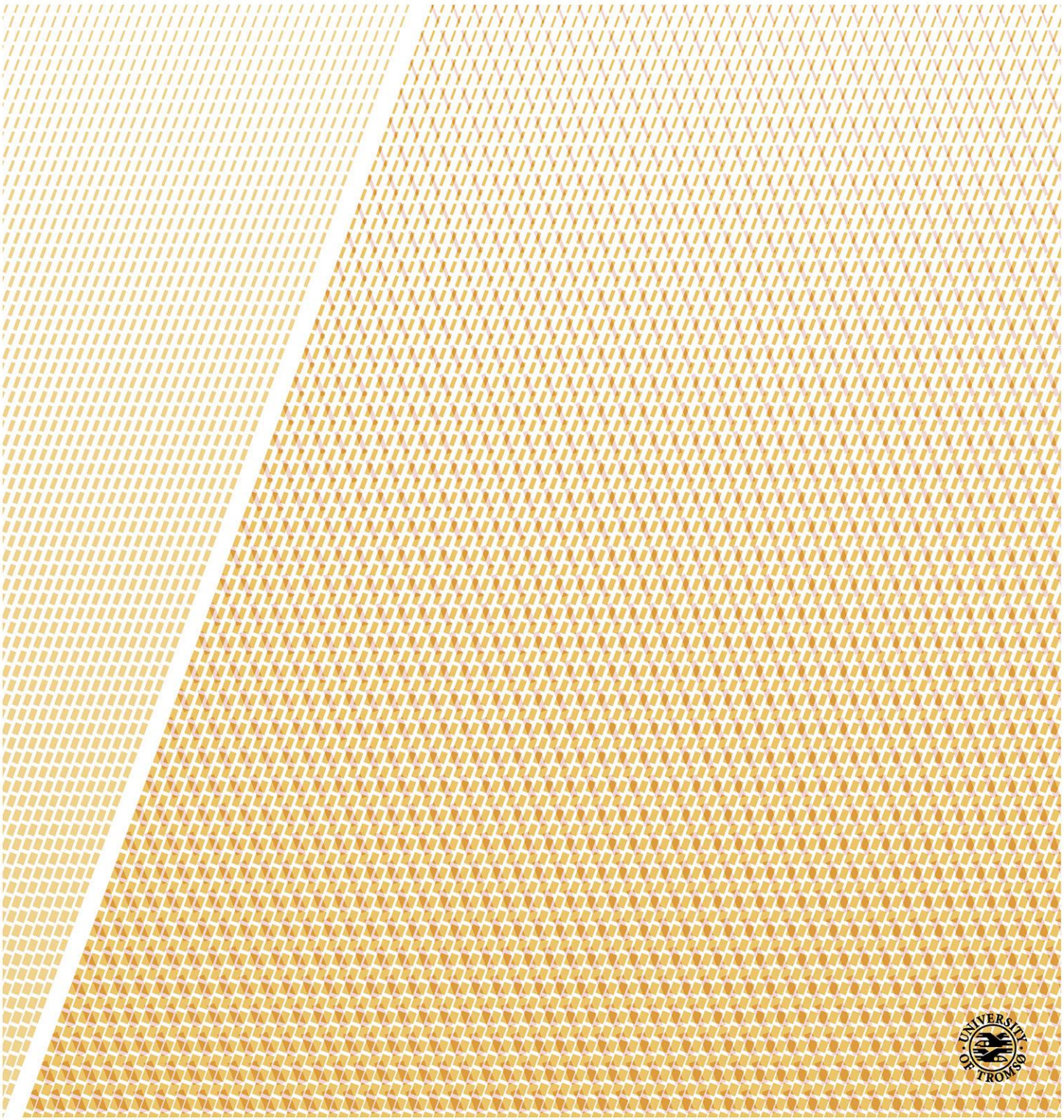

Table of content

Preface

This thesis is a result of a PhD-project that was carried out in accordance with the Industrial PhD-scheme as organized by the Norwegian Research Council. The project has been funded by the council and DONG E&P Norge. The University of Tromsø is the degree-awarding institution. Supervisors have been Professor Steffen G. Bergh (main) and Professor Holger Stunitz from the University of Tromsø and Arild Ingebrigtsen from DONG E&P Norge.

The thesis presented herein aims to unravel the evolution and finite stage architecture of the SW Barents Sea Margin, which formed as a part of the rifting of present day Greenland and Scandinavia and the opening of the North Atlantic Ocean (cf. Faleide et al., 2008). The SW Barents Sea Margin studied in this thesis starts just north of the Lofoten-Vesterålen archipelago, continues northward outboard northern Troms and into western Finnmark. This thesis focus on (i) *if* and *how* onshore Post-Caledonian brittle faults correlate with major offshore, basin-bounding fault complexes and (ii) under which conditions onshore faulting occurred.

As a part of the PhD, I have been employed at Front Exploration (August 2011-June 2012) and DONG E&P Norge (July 2012-present). The Industrial PhD-scheme has allowed me to move freely between offices at DONG E&P and the University of Tromsø as a fully integrated member of both institutions. As a part of my PhD, I have had a stay at NGU, Trondheim, a 6-weeks field course in the Mojave Desert, California, followed by 2 weeks of structural fieldwork in a similar tectonic setting as the western Barents Sea, mapping the San Andreas Fault and associated structures (These data are published elsewhere). The stays has given me a broadened view on the world's geology, expanded my contact network and led me into new, ongoing projects as co-author on related topics to those presented as part of my PhD (Bergh et al. 2014, unpublished; Schermer et al., unpublished). Further, I have attended several scientific cruises with the research vessel FF Helmer Hanssen in the Barents Sea and Greenland Sea and attended several scientific conferences presenting results from the PhD-project, including the "Onshore-Offshore relationships on the North-Atlantic margin" (Trondheim, Oct. 2012) and the EGU General Assembly 2014 in Vienna. Although I have not been obliged to do duty work, I have had the pleasure of teaching undergraduate students during exercises and excursions in structural geology at the University of Tromsø.

The PhD-project has resulted in three papers, which includes the tasks of (i) mapping basement structures and brittle fault zones onshore, on the shallow shelf and on the deep shelf using different techniques and (ii) unravelling details on the conditions under which these fault zones formed. The papers presented herein are:

Paper 1: Indrevær, K., Bergh, S.G., Koehl, J.-B., Hansen, J.-A., Schermer, E.R. & Ingebrigtsen, A., 2013: Post-Caledonian brittle fault zones on the hyperextended SW Barents Sea margin: New insights into onshore and offshore margin architecture. *Norwegian Journal of Geology, Vol 93 (3-4)*, pp. 167–188.

Paper 2: Indrevær, K., Stunitz, H., & Bergh, S. G., in press: On Palaeozoic-Mesozoic brittle normal faults along the SW Barents Sea margin: fault processes and implications for basement permeability and margin evolution. *Journal of the Geological Society, London*.

Paper 3: Indrevær, K. & Bergh, S. G., in press: Linking onshore-offshore basement rock architecture and brittle faults on the submerged strandflat along the SW Barents Sea Margin using high-resolution (5x5m) bathymetry data. *Norwegian Journal of Geology*.

Acknowledgements

I would like to express my utmost gratitude to my main supervisor Professor Steffen G. Bergh for taking me under his wings and introducing me to his exiting research. His skills within- and enthusiasm for geology has been very inspiring to me.

I would also like to thank my co-supervisors Professor Holger Stunitz (UiT) and Arild Ingebrigtsen (DONG E&P Norway). Holger Stunitz's support and good advice has led to exciting discoveries on fault-rock forming processes during this project. I thank Arild Ingebrigtsen for guidance related to seismic data, for making sure that all administrative issues were sorted out and for being very supportive in every way during these three years.

I send my gratitude to Professor Elizabeth R. Schermer for enriching my PhD-experience by introducing me to the amazing geology of the US and for constructive collaboration, feedback and reviews during this project. I thank John-Are Hansen for help, especially within the start-up of the project and I thank Jean-Baptiste Koehl for exciting fieldwork.

I sincerely thank DONG E&P Norge (and Front Exploration) for taking on this project. I would like to thank all of my colleagues in DONG, especially Tom Arne Rydningen, Rikke Bruhn and Tanni Juul Abramovitz for project-related discussions and feedback.

This work has been a part of the Industrial PhD-scheme organized by the Norwegian Research Council. I would like to express my gratitude to all persons involved from this institution. I would also like to thank Odleiv Olesen and Laurent Gernigon at NGU for letting me visit and see the benefits of working with gravimetric and magnetic anomaly data.

I thank all of my colleagues at the Department of Geology, UiT. Especially Trine, Edel and others at the laboratory and Jan P. Holm for his help on finding long lost figures. Finally, I thank all of my fellow PhD-students at UiT for fun times during these three years.

Introduction

Background and scope of thesis

This work was initiated as a cooperation between Front Exploration (and later DONG E&P Norge) and the University of Tromsø as a part of the Industrial PhD-scheme organized by the Norwegian Research Council.

The work is the continuation of the project "Tectonic development of faults on the Lofoten-Vesterålen continental margin; comparisons with land" that was initiated in 2002 by Professor Steffen G. Bergh, as a collaboration between the University of Tromsø, the Geological Survey of Norway and the industry. This project led to an increase in the understanding of the Lofoten-Vesterålen margin and is summarized in the papers Bergh et al. (2007, 2008) and the PhD-theses of Karsten Eig and John-Are Hansen (Eig, 2008; Hansen, 2009).

The project presented herein has aimed to study the SW Barents Sea margin situated just north of Lofoten and Vesterålen (Figs. 1 & 2) in order to obtain knowledge on onshore-offshore structural relationships off northern Troms and western Finnmark. The work has included:

(1) Onshore fieldwork focussing on brittle fault structures, their kinematics and their relations to pre-existing basement structures on the outer islands of Troms, including Senja, Kvaløya, Ringvassøya and Vanna (Fig. 2).
(2) Detailed microstructural study of fault rocks with emphasis on fault-rock forming conditions, revealing details about P-T conditions, fluid flow characteristics and fault rock healing processes during and after faulting.
(3) Mapping of fault zones and fault complexes on the deep shelf based on the interpretation of seismic data, focusing on the Troms-Finnmark, Ringvassøy-Loppa, Nysleppen and Måsøy fault complexes, their associated basins (Harstad-, Tromsø- and Hammerfest basins) and the Finnmark Platform (Fig. 1).
(4) Using magnetic anomaly data and high-resolution bathymetry data from the shallow shelf (strandflat) along the margin in an effort to map ductile basement fabrics and link brittle fault complexes mapped onshore with fault complexes mapped offshore.

Geological setting

As a part of the breakup of the North Atlantic Ocean, the continental margin off mid-Norway (Fig. 1) was subjected to multiple rift events in the Palaeozoic through Early Cenozoic times (e.g. Doré 1991; Faleide et al. 1993; Blystad et al. 1995; Doré & Lundin 1996; Brekke et al. 2001; Osmundsen et al. 2002; Eig 2008; Faleide et al. 2008). The fault timing and evolution of different rift events are well constrained by seismic and potential field data offshore mid-Norway, but less constrained from the SW Barents Sea margin (e.g. Gudlaugsson et al. 1998; Dore et al. 1999; Brekke 2000; Faleide et al. 2008; Redfield & Osmundsen, 2013). On the mid- and north-Norwegian margin, the earliest events occurred in the mid-Carboniferous, Carboniferous-Permian and Permian-Early Triassic times (Doré 1991). On the Lofoten-Vesterålen margin (Fig. 1), rifting occurred during multiple tectonic events in the Permian-Early Triassic, Mid/Late Jurassic-Early Cretaceous and latest Cretaceous-Paleogene (Brekke 2000; Osmundsen et al. 2002; Bergh et al., 2007; Eig, 2008; Hansen et al., 2012). The Vestfjorden and northern Træna basins show large-scale fault activity in the Permian to Early Triassic (Brekke 2000; Osmundsen et al. 2002; Hansen et al. 2012), followed by Late Triassic regional subsidence (Faleide et al. 2008). The main fault array on the Lofoten-Vesterålen margin likely developed during the syn-rift, Late Jurassic and Early Cretaceous phase (Hansen et al. 2012) as the Atlantic rifting propagated northwards.

In the SW Barents Sea, north of Lofoten (Fig. 1), Carboniferous rift structures are widespread (Gudlaugsson et al. 1998) and led to the formation of early rift basins such as the Nordkapp and Tromsø basins (Faleide et al., 2008). The most prominent offshore fault complex in the region, the Troms-Finnmark Fault Complex, experienced long-term activity from the Carboniferous through the Eocene, with a main fault-related subsidence in Late Jurassic to Early Cretaceous times (Gabrielsen et al., 1990; Faleide et al., 2008) leading to the formation of the Harstad and Hammerfest basins and further deepening of the Tromsø Basin (Fig. 1). A Late Cretaceous to Paleocene rifting event was accomplished by dextral transform movement along the mega-shear system defined by the Senja Shear Zone (Fig. 1), which may be traced northwards from Senja to west of Spitsbergen, where it is known as the Hornsund-De Geer Fault Zone (Fig. 1; Gabrielsen et al., 1991; Faleide et al., 1993, 2008). The transform movement led to the formation of the Bjørnøya and Sørvestnaget basins and the further development of the Tromsø and Harstad basins as combined extensional and pull-apart basins (Gabrielsen et al. 1997; Knutsen & Larsen 1997; Faleide et al. 2008). Final lithospheric

break-up along the margin occurred at c. 55-54Ma, leaving the SW Barents Sea as a passive continental margin since Oligocene time (Faleide et al. 2008).

Onshore Troms (Fig. 2), dating of fault rocks using 40Ar/39Ar and apatite fission track methods indicates that faulting in western Troms largely occurred during the Permian to Early Triassic rifting phase, thus corresponding with the initial large-scale fault activity on the Lofoten-Vesterålen margin, including the Vestfjorden and Træna basins, but with no major fault activity during the Mesozoic and Cenozoic (Hendriks et al. 2010; Davids et al., 2013). However, Mesozoic fault activity is suggested to have taken place onshore further north, in Finnmark (Roberts & Lippard 2005; Torgersen et al., 2013), and to the south in Lofoten-Vesterålen and Andøya (Dalland, 1981; Fursich & Thomsen, 2005; Hansen, 2009; Hendriks et al., 2010; Osmundsen et al., 2010; Davids et al., 2013). Paleomagnetic evidence for Permian as well as Cenozoic to recent phases of faulting and cataclasis has been obtained for the Kvaløysletta-Straumsbukta fault zone, which is a part of the Vestfjorden-Vanna Fault Complex (Olesen et al., 1997).

The margin off northern Troms and western Finnmark marks the transition between the spreading, normal passive margin off Lofoten-Vesterålen and the Barents Sea transform margin off the WTBC, marked by the Senja Shear Zone (Figs. 1 & 2), and is thus very important when discussing the evolution of the North-Norwegian margin as a whole. However, only a few onshore-offshore structural studies have previously been undertaken north of Lofoten, of which are mainly in northern Finnmark (Roberts & Lippard, 2005; Roberts et al., 2011).

The present thesis aims to fill this gap and focuses on the network of Palaeozoic-Mesozoic faults along the coast of Troms, and their genetic relationship with major structural elements in the deeper portions of the SW Barents Sea, such as the Troms-Finnmark Fault Complex (TFFC), the Ringvassøy-Loppa Fault Complex (RLFC) and the Måsøy and Nysleppen fault complexes, in addition to their relation with the Senja Shear Zone and the transition to a transform margin (Figs. 1 & 2; Ramberg et al. 2008; Smelror et al. 2009). Onshore western Troms, these brittle faults are manifested mainly as NNE-SSW and ENE-WSW trending normal faults (Fig. 2). They are constrained to the West Troms Basement Complex (WTBC, Zwaan, 1995), a major basement horst that extends from Lofoten in the south to island of Vanna in the north and comprises the islands of Senja, Kvaløya, Ringvassøy and Vanna, as

well as several other smaller islands (Figs. 1 & 2; Olesen et al., 1997; Bergh et al., 2010). The WTBC horst can be traced southwestward to link up with the Lofoten Ridge, which is flanked by major normal faults (Blystad et al., 1995; Bergh et al., 2007; Hansen et al., 2012) that border the offshore Ribban and Vestfjorden basins. In Troms, corresponding fault zones can be divided into the Vestfjorden-Vanna Fault Complex (VVFC), which marks the southeastern boundary of the WTBC, down-dropping Caledonian nappes to the east in the order of 1-3 km (Forslund, 1988; Opheim & Andresen, 1989; Olesen et al., 1997) and a system of less prevalent, SE-dipping, faults situated along the outer rim of the islands of the WTBC (Fig. 2; Antonsdottir 2006; Thorstensen 2011).

Summary of papers

Paper 1: Indrevær, K., Bergh, S.G., Koehl, J.-B., Hansen, J.-A., Schermer, E.R. & Ingebrigtsen, A., 2014: Post-Caledonian brittle fault zones on the hyperextended SW Barents Sea margin: New insights into onshore and offshore margin architecture. *Norwegian Journal of Geology, Vol 93 (3-4)*, pp. 167–188.

The aim of this paper is to investigate the regional fault pattern and discuss how these faults are genetically linked across the SW Barents Sea Margin. It focus on the geometry and kinematics of selected previously described and undescribed fault zones onshore Troms, in an effort to elaborate all onshore fault data into a common frame of reference. Onshore brittle faults have been studied and compared with offshore fault complexes interpreted from seismic data, and correlated with offshore fault complexes by the use of bathymetry data and magnetic anomaly data. This is done in order to get a regional control on the behaviour of brittle structures and thus margin architecture.

The main conclusions of the paper are that the Palaeozoic-Mesozoic rift-related activity on the west Troms margin (Fig. 1 & 3) resulted in widespread NNE-SSW and ENE-WSW trending brittle normal faults that constitutes at least two major fault complexes, the Vestfjorden-Vanna and the Troms-Finnmark Fault Complexes and two subsidiary NW-SE trending transfer fracture systems, one present northwest of Senja and another near the island of Nord-Fugløya (Fig. 3). The onshore fault zones can be separated into (1) the major Vestfjorden-Vanna Fault Complex, which marks the southeastern boundary of the WTBC (Opheim & Andresen, 1989; Olesen et al. 1997) and continues offshore north of Vanna to link up with the offshore Måsøy and Nysleppen fault complexes, and (2) a less prevalent system

of right-stepping fault segments that run along the outer rim of the islands of the WTBC, best exposed at Rekvika. This fault system is mainly SE-dipping with displacement in the order of 100's of meters or less (Fig. 2). Offshore, the Troms-Finnmark Fault Complex is the dominant basin-bounding fault complex and defines the northwestern boundary of the WTBC, that down-drops basement rocks from 4-5km depth on the Finnmark Platform to more than ~10km depth in the Harstad Basin (Fig. 1). The Troms-Finnmark Fault Complex can be traced from the Lofoten Ridge in the south to link up with the Ringvassøy-Loppa Fault Complex in the north. Thus, both the Troms-Finnmark and Vestfjorden-Vanna Fault Complexes can be traced for 100's of kilometers along strike along the North-Norwegian margin (Fig. 1; Olesen et al., 1997; Dore et al., 1997; 1999). The margin is segmented along strike by at least two major transfer zones, the Senja Shear Zone (e.g. Olesen et al., 1997) and the Fugløya transfer zone, the latter named after the nearby island of Nord-Fugløya. These two transfer zones mark a pronounced switch in fault polarity and/or amount of displacement of the Vestfjord-Vanna and the Troms-Finnmark Fault Complexes and spatially overlap with the ~NW trending, Proterozoic-Palaeozoic basement-seated Bothnian-Senja Fault Complex (and Senja Shear Belt) and the Bothnian-Kvænangen Fault Complex, respectively. The Bothnian-Kvænangen Fault Complex is suggested to be the controlling element for the location of the Fugløya transfer zone, the Ringvassøya-Loppa Fault Complex, and potentially also the transform Hornsund-De Geer Fault Zone that lie along strike of the Fugløya transfer zone farther north along the Barents Sea margin.

In the context of rifting along the SW Barents Sea margin, our results suggest a widespread initial distributed rifting event in the Carboniferous and Late Permian/Early Triassic along the NE-SW striking VVFC and TFFC. This early event was followed by a main, Late Jurassic/Early Cretaceous syn-rift extension in the Hammerfest Basin and a corresponding switch in localization of fault movements to the Troms-Finnmark and Ringvassøy-Loppa fault complexes. These major offshore, basin-bounding faults are characterized by a listric geometry and large-magnitude displacement, whereas a planar geometry is inferred for the onshore Vestfjorden-Vanna Fault Complex and related horst-internal faults. The contrast in fault geometry, where the dominant movement was localized to the Troms-Finnmark Fault Complex by Late Jurassic/Early Cretaceous, resulted in the formation of a short tapered, hyper-extended margin after final break-up in the Paleocene/Eocene (c. 55Ma). Later on, the West Troms Basement Complex was uplifted and exhumed as a short-tapered margin due to unloading and crustal flexure with continued uplift and erosion to the present stage level.

Paper 2: Indrevær, K., Stunitz, H., & Bergh, S. G., in press: On Palaeozoic-Mesozoic brittle normal faults along the SW Barents Sea margin: fault processes and implications for basement permeability and margin evolution. *Journal of the Geological Society*.

This paper focuses on the microstructural characteristics of onshore brittle fault rocks within the West Troms Basement Complex. It aims to estimate temperature and depth of faulting and to increase our understanding of processes that may have controlled margin-parallel faulting during the onshore Late Permian/Early Triassic rifting phase. The main conclusions from the study are that the minimum P-T conditions during early stages of brittle faulting is estimated to ~300°C and ~240MPa (~10km depth) based on the presence of greenschist facies mineral assemblages in the cataclasites. Later fault movement introduced pumpellyite, yielding minimum P-T condition of ~275°C and ~220MPa (~8.5km depth). Quartz-rich ultracataclasites occur within granitoid fault rocks and are interpreted as preserved fault rocks from early (deep) stages of faulting that formed due to the chemical breakdown of feldspar to epidote and chlorite with the release of quartz. Due to the lack of any subsequent formation of phyllosilicates within the process fault zone, which is common for cataclasis of granitoid rocks at shallower crustal levels (Wintsch et al., 1995; Janecke & Evans, 1998; Wibberley, 1999; Rutter et al., 2001; Holdsworth, 2004; Jefferies et al., 2006), the main fault activity is interpreted to have ceased during early stages of rifting.

Microstructural observations of the brittle fault rocks indicate that pore pressures locally reached lithostatic levels (240MPa) during faulting. Thus, the studied faults within the basement rocks acted as fluid conduits during rifting in the Late Permian/Early Triassic. Based on the presence of injected cataclasites, a minimum co-seismic fluid velocity is calculated to have been on the order of 10^{-1} m/s. However, evidence for grain growth and mineral precipitation suggest that the fault zones sealed of rapidely after faulting, thereby evolving from a fluid conduit to a fluid barrier through a fault cycle.

The occurrence of pumpellyite allowed for the estimation of a maximum geothermal gradient during faulting in the Late Permian/Early Triassic, which is calculated to ~30°C/km. This un-elevated geothermal gradient suggests either that faulting occurred during early stages of continental rifting or that the studied fault zones were located along the rift flanks where little or no subsidence took place. A minimum average exhumation rate of ~40m/Ma is estimated

for the outer islands of the West Troms Basement Complex since Late Permian times. When considering normal erosion rates, the proposed late Cenozoic uplift, which has been discussed widely in the literature (c.f. Doré et al., 2002), may be explained by erosion alone, possibly as an effect of climate deterioration after the formation of the North-Atlantic Ocean, causing a faster rate of erosion along the margin, which led to a subsequent isostatic crustal re-calibration and greater isostatic uplift of the marginal crust, compared to inland.

Finally, a model is proposed, showing how fluid flow within a fault zone may be controlled by processes such as grain growth, mineral precipitation and hydrothermal alteration, which may alter fluid flow characteristics within a fault zone through a fault cycle. As the studied fault zones are the onshore portions of large fault complexes that continue offshore (Indrevær et al., paper 1), it is likely that the studied fault zones are analogue to basement-seated faults offshore. This implies that the conditions and nature of faulting observed onshore may be valid for offshore faults and that, at present, basement-seated fault zones offshore (e.g. on the Finnmark Platform and Loppa High) acted as fluid barriers and thus, have the potential to control hydrocarbon flow.

Paper 3: Indrevær, K. & Bergh, S. G., in press: Linking onshore-offshore basement rock architecture and brittle faults on the submerged strandflat using high-resolution (5x5m) bathymetry data in Troms, Northern Norway. *Norwegian Journal of Geology*.

Traditionally, the Norwegian Army has, within 12 nautical miles of the coast, considered a resolution finer than 50x50m of the MAREANO data as classified information, although it is collected with a resolution down to as much as 1x1m (depending on depth). An effort to get access to higher resolution MAREANO data for the correlation work in paper 1 was undertaken, but initially not successful. We were, however, later given access and permission to publish illustrations of high-resolution (5x5m) data. This has allowed us to identify and study astonishingly detailed morphological features visible on the strandflat outboard Troms, which shed light on the shallow shelf distribution of basement rocks, Caledonian thrust nappes and Post-Caledonian brittle faults. To our knowledge, high-resolution bathymetry data has never been used to this extent for the purpose of mapping offshore ductile and brittle fabrics visible on the seafloor.

The main results of the paper are that morphological features observed on the high-resolution bathymetry data in great detail mimic basement structures commonly observed onshore western Troms, i.e. Archaean-Palaeoproterozoic ductile fabrics (steep foliation, macrofolds, shear zones), gently dipping Caledonian nappe structures and post-Caledonian brittle faults. Our interpretations suggest firstly, that the basement lithologies of the WTBC continue onto the strandflat, secondly, that the contact between the WTBC units and the Caledonian thrust nappes crops out in the sound southwest of Nord-Fugløya, and thirdly, that post-Caledonian, rift-related and horst-bounding brittle normal faults are widespread on the shallow shelf. Importantly, the Caledonian nappe boundary correspond with the same strait that marks the location of the Mesozoic Fugløya transfer zone, the possible continuation of the Proterozoic-Palaeozoic Bothnian-Kvænangen Fault Complex (Indrevær et al., paper 1). The spatial overlap of these features suggests that the Precambrian and Caledonian structures both exerted an important role in controlling the rifting and passive margin deformation through the late Paleozoic, Mesozoic and Cenozoic time span.

The basement fabrics visible on the strandflat are transected by numerous NNE-SSW to ENE-WSW trending, mostly linear trenches that are interpreted as rift-related brittle normal faults, based on similar orientation with onshore and offshore faults and fault segments mapped on the continental shelf from seismic data (see paper 1). These faults overlap with scarps bounding asymmetric landscapes or rotated fault blocks (Osmundsen et al., 2009, 2010) that offset bedrock lithologies and structures across the trenches with estimated displacement in the order of kilometers. The structural relationship between strandflat escarpments and faults of different orientation suggests that the fault zones, independent of their orientations, formed during the same period. Our detailed investigation of the strandflat bathymetry and various strandflat aspects demonstrates a strong correlation with basement structures and brittle faults onshore and thus would support a strong tectonic influence on the present day coastal landscape and the SW Barents Sea margin architecture.

Synthesis

Onshore-offshore correlation studies on the Lofoten-Vesterålen margin have in the recent years significantly increased our understanding of the fault architectures and evolution of the North-Atlantic passive margin (e.g. Bergh et al., 2007, 2008; Eig, 2008; Faleide et al., 2008; Hansen, 2009; Hendriks et al., 2010; Osmundsen et al., 2010; Hansen et al., 2012). North of Lofoten, however, very few comparable margin studies have been undertaken. Roberts and

Lippard (2005) and Roberts et al. (2011) correlated onshore fault zones in Finnmark with offshore fault zones mapped from seismic data and bathymetry data. Previous work in western Troms, however, is mostly limited to the study of individual fault zones onshore (Andresen & Forslund 1987; Forslund 1988; Opheim & Andresen 1989; Gagama, 2005; Antonsdottir, 2006; Thorstensen, 2011) and large scale, basin-bounding fault complexes offshore (Gabrielsen 1984; Sund et al., 1986; Gabrielsen et al., 1990; Faleide et al., 1993; Waqas, 2012). Whilst the Vestfjorden-Vanna Fault Complex was previously identified and discussed in a regional context (Opheim & Andresen, 1989; Olesen et al., 1997), the continuation of this fault complex to north of Vanna, has not yet been considered in detail. Due to a vast amount of available seismic data from the offshore regions, the distribution and tectonic evolution of basin-bounding faults are relatively well known (cf. Gabrielsen et al., 1990; Smelror et al., 2001). However, an effort to correlate fault complexes onshore with those from offshore basins has not previously been done.

The present work is a first attempt to fully correlate major offshore and onshore brittle zones that bound the WTBC horst (Fig. 2). The present work also adresses other important unresolved issues concerning P-T conditions of margin faulting, timing of rifting events, extent of faulting, fault rock-forming processes, fluid flow, pore pressure and permeability.

Recent dating of brittle fault rocks in western Troms (Davids et al. 2013), supported by paleomagnetic dating of fault gouge from the VVFC (Olesen et al., 1997), has enabled us to infer onshore fault activities to a specific rifting event. Most important, the obtained ages suggest that only one phase of rifting (Late Permian/Early Triassic) is preserved onshore. By contrast, along other portions of the margin farther south and north, this early rifting phase was strongly overprinted by later Late Jurassic/Early Cretaceous and Late Cretaceous-Palaeocene fault activity. As a consequence, the study of brittle fault zones in western Troms gives a unique opportunity to obtain detailed information on the nature and significance of the earliest phases of the North-Atlantic rifting events.

Margin architecture

Our synthesis show that post-Caledonian brittle faults in western Troms on average display NNE-SSW and ENE-WSW trends and constitute two major NE-SW trending fault complexes, the TTFC and the VVFC, that bound the WTBC horst (Fig. 2 & 3). These boundary fault zones run partly onshore and offshore along the studied portion of the margin, linking up with the onshore Lofoten and offshore Nordland Ridges to the south, and with the

Ringvassøy-Loppa, Nysleppen and Måsøy fault complexes in the north (Indrevær et al. paper 1). The southeastern boundary of the WTBC horst is marked by the VVFC, which down-drops Caledonian thrust nappes to the east. Westward, the study of detailed bathymetry data reveal that the strandflat outboard the islands of Senja, Kvaløya and Ringvassøy and west of Vanna are made up of the same basement lithologies and structural fabrics (Fig. 2). This demonstrates that the WTBC horst extends offshore, at least to the western edge of the strandflat (Indrevær & Bergh, paper 3). Seismic sections that cover parts of the Finnmark Platform and the Harstad Basin are interpreted to suggest that the WTBC units are to a lesser extent down-faulted on the Finnmark Platform and that the TFFC defines the northwestern boundary of the WTBC horst down-dropping basement rocks more than 5 km into the Harstad Basin (Indrevær et al., paper 1). Remnants of Caledonian nappes on down-faulted basement units are thought to be present within large regions of the SW Barents Sea (Gernigon & Brönner, 2012) and may also be present on the Finnmark Platform offshore the WTBC. The planar geometry obtained for the VVFC (with displacement in the order of 1-3km) and the listric geometry of the TFFC (with estimated displacement of >5km) resulted in an overall asymmetric WTBC horst geometry (Indrevær et al., paper 1).

At least two transfer zones, the Senja Shear Zone and the Fugløya transfer zone seem to have segmented the margin along strike, allowing fault segments to step and change fault polarity across the transfer zones (Fig. 3) (Indrevær et al., paper 1), similar to the Lofoten Ridge (Tsikalas et al., 2005; Bergh et al., 2007). The dextral Senja Shear Zone is believed to mark the position of the initial, SW Barents Sea transform continent-continent boundary, which evolved to a continent-ocean transform boundary in the Eocene (Olesen et al., 1997; Faleide et al., 2008). The Fugløya transfer zone is considered by us to be genetically linked to the Senja Shear Zone and apparently displacing sinistrally both Mesozoic brittle normal faults (Indrevær et al. paper 1) and the contact between basement rocks and the Caledonian thrust nappes (Indrevær & Bergh, paper 3). The Fugløya transfer zone is suggested to be related to the Senja Shear Zone by accommodating for lateral differences in strain along the margin, due to the transition from a normal rift setting to a transform rift setting in Troms.

Fault timing

The derived ages of brittle fault-associated rocks onshore (Davids et al. 2013) are essential for the interpretation and implications of our results and conclusions. The obtained ages indicate that faulting onshore Troms occurred during Late Permian/Early Triassic, with few or no later

significant fault movement. The only exception is a Late Cenozoic reactivation inferred from paleomagnetic dating of fault gouge from the VVFC (Olesen et al. 1997).

The present work contributes in a number of ways on the timing of faulting and possible later reactivation of faults both onshore as well as on the shallow shelf:

First, the presence of a widespread healed silica-rich cataclasite in the Rekvika fault zone suggests that faulting as observed onshore Troms, occurred in the deeper parts of the brittle deforming crust, with no later reactivation. This is supported by the estimates of P-T conditions during faulting, which indicate that faulting occurred at 8.5-10km depth. This implies that onshore fault activity came to a stop during *early and deep stages* of the continental rifting (Indrevær et al. paper 2). Thus, both the observed silica-rich cataclasite and the P-T conditions are consistent Late Permian/Early Triassic ages obtained for fault activity onshore Troms, with the general lack of evidence for any post-Triassic reactivation (Davids et al., 2013; Olesen et al., 1997).

Second, curved relationships of NNE-SSW and ENE-WSW trending faults and fractures are common in western Troms, suggesting that the two populations of faults formed contemporaneously (Indrevær & Bergh, paper 3). This is in contrast with the Lofoten-Vesterålen margin faults, where the NNE-SSW trending fault segments formed first due to WNW-ESE directed extension, and where later on replaced by ENE-WSW trending faults due to a switch to NNW-SSE directed extension (Bergh et al. 2007). Our work largely supports Hansen (2009) who suggested that the NNE-SSW striking fault segments in Lofoten formed as *en echelon*, right-stepping faults that were linked by NE-SW to E-W trending fault segments acting as transfer faults. In western Troms, our kinematic analysis of onshore fault zones has not enabled to solve the timing relationships between the two fault sets. Slickensided fault surfaces from the studied fault zones onshore as well indicate both normal dip-slip and oblique- normal senses of shear, independent of the fault trends.

Thirdly, the nature of displacement of fault zones and offset of the basement-Caledonian thrust nappe boundary across the Fugløya transfer zone indicate that this transfer zone was active during post Caledonian times (Indrevær & Bergh, paper 3). As this transfer zone displaces and/or accommodates a major shift in fault polarity across the zone for fault segments belonging to the Late Permian/Early Triassic Vestfjorden-Vanna Fault Complex

(Davids et al., 2013; Indrevær et al. paper 1), the activity may likely be tied to both the Late Permian/Early Triassic and the Late Jurassic/Early Cretaceous rifting phases.

Fourthly, the regionally sub-planar, Quaternary strandflat outboard of western Troms, is in several locations observed to be down-dropped by possible brittle normal faults (Indrevær & Bergh, paper 3). This observation suggests that certain post-Caledonian faults have modified the strandflat and thus been active during the Quaternary.

Basement control

Several indicators for basement control on post-Caledonian brittle structures have been observed through the present work. First, the studied onshore brittle fault zones, at least on a local scale, commonly formed close to, or along favourably oriented Precambrian or Caledonian structural trends such as lithological boundaries, foliation surfaces and/or ductile shear zones (Indrevær et al. paper 1). This suggests that brittle faulting utilized pre-existing zones of weakness in the basement to achieve brittle reactivation.

Second, on a larger scale, steep basement-seated Precambrian ductile shear zones, e.g. the NW-SE trending Bothnian-Senja Fault Complex (and Senja Shear Belt) and the Bothnian-Kvænangen Fault Complex, seem to have affected the NE-SW trending brittle fault complexes by allowing portions of these pre-existing structures to be reactivated as the Senja Shear Zone and the Fugløya transfer zone, respectively, which accommodated shifts in polarity and/or the stepping of fault segments to a new position along strike (Indrevær et al. paper 1; Indrevær & Bergh, paper 3). The conspicuous overlap of (i) the Fugløya transfer zone, (ii) the contact between the WTBC and Caledonian thrust nappes, (iii) a possible Svecofennian high-strain zone and (iv) the Proterozoic-Palaeozoic Bothnian Kvænangen Fault Complex (Indrevær & Bergh, paper 3) suggests that this zone has played a major role in accommodating margin-oblique crustal deformation through time. This zone may initially have formed as a ductile shear zone (or terrain boundary) in the Archean-Palaeoproterozic, possibly the Svecofennian, and later been covered by thrust nappes during the Caledonian orogeny. Post-Caledonian crustal rifting, which led to the opening of the North-Atlantic Ocean, have potentially reactivated this zone as a transfer zone, allowing Palaeozoic-Mesozoic brittle faults to step and change fault polarity across the transfer zone (Indrevær et al. paper 1), displacing the Caledonian thrust nappes sinistrally (Indrevær & Bergh, paper 3). It is suggested that the ~NW-trending Bothnian-Kvænangen Fault Complex also may be the controlling element for the Ringvassøya-Loppa Fault Complex and potentially also the

transform Hornsund-De Geer Fault Zone further north on the Barents Sea margin, as they are located along strike of the Fugløya transfer zone (Indrevær et al. paper 1).

Thirdly, aspect analysis of the topography and bathymetry within the study area suggest that the coastal landscape and the strandflat are tectonically influenced (Indrevær & Bergh, paper 3). The analysis reveals that surface slopes and escarpments trending NNE-SSW and ENE-WSW, and subsidiary NW-SE trend, dominate the landscape and strandflat topography, thus reflecting the two populations of post-Caledonian brittle faults commonly observed in western Troms and the in general NW-SE trending ductile basement fabric, respectively.

Margin evolution

Based on the results and synthesis of the three papers, we propose a model for the evolution of the SW Barents Sea margin (Fig. 4). Initial NW-SE oriented extension occurred in the Carboniferous and Late Permian/Early Triassic along a distributed network of NE-SW trending, NW and SE dipping normal fault complexes (Fig. 4a). The onshore studies of fault rocks linked to the Late Permian/Early Triassic rift activity show that the present day surface was located in the deeper parts of the seismogenic zone (~8.5-10km depth) (Indrevær et al. paper 2). This is supported by the observation of preserved deep-forming silica-rich ultracastaclasites from granitoid fault rocks, and the lack of any subsequent formation of phyllosilicates within the core zones (Indrevær et al. paper 2). Faulting was characterized by high-pressure fluid infiltration of a mafic composition and processes such as mineral precipitation and grain growth influenced fault permeability through time (Indrevær et al. paper 2).

The termination of onshore fault activity after Early Triassic and the exhumation and preservation of the fault zones is believed to be due to a westward migration of fault activity to the offshore TFFC by the onset of the Late Jurassic/Early Cretaceous rifting phase. The reason(s) for such a westward migration of faulting to the TFFC is not known, but a reasonable explanation may be that the onset of the transform/strike-slip movement along the Senja Shear Zone and Fugløya transfer zone was involved. The hard-linkage of the Senja Shear Zone and the TFFC may have been the reason for the shutdown of faulting onshore in western Troms. If so, the effect of this onset came into place prior to the Late Jurassic/Early Cretaceous, in order to completely abandon the onshore fault zones by this time (Fig. 4b). It is therefore likely that the Senja Shear Zone and the Fugløya transfer zone initially only modestly influenced the nature and stepping of brittle normal faulting along the margin

(during Late Permian/Early Triassic) and that any significant strike-slip motion along the transfer zones occurred later, during the Late Jurassic/Early Cretaceous rifting event.

The Late Jurassic/Early Cretaceous rifting event was accompanied by extension in the Hammerfest Basin and the activation of the adjoining Ringvassøy-Loppa and Troms-Finnmark fault complexes (Fig. 4b). The listric geometry and large amount of displacement along these few, along-strike basin-boundary faults offshore compared to the planar geometry and less amounts of displacement along the onshore VVFC, resulted in the formation of a short tapered, hyper-extended margin after final break-up in the Paleocene/Eocene (Fig. 4c). Offshore, further reactivation, listric faulting and sediment deposition in the offshore basins (e.g. Harstad and Tromsø Basins) continued in the Cenozoic, due to transform plate motion along the Senja Shear Zone. In onshore areas, the WTBC was uplifted and exhumed in the Early Cenozoic as a short-tapered margin due to unloading and crustal flexure of the crust (Indrevær et al. paper 1). Continued uplift, reactivation of faults and erosion followed in the Late Cenozoic due to climate deterioration linked to the formation of the North-Atlantic Ocean, which caused subsequent flexure and greater uplift of the marginal crust due to a faster rate of erosion along the margin than inland (Fig. 4d).

Implications for hydrocarbon exploration in basement rocks

The results from Indrevær et al. (paper 2) shows that the onshore Late Permian/Early Triassic fault zones likely became completely sealed shortly after faulting by the processes of mineral precipitation and grain growth. As the studied fault zones are shown to correlate with offshore basin-bounding faults and faults on the Finnmark Platform and possibly also the Loppa High (Indrevær et al., paper 1), the same processes may have been valid for offshore basement-involved fault zones as well. This implies that these faults at present will act as fluid barriers. As is evident from the evidence for fluid flow from the study, a reactivation of a fault zone after any potential entrapment of hydrocarbons, will temporary increase fault permeability significantly and allow for along- and across-fault migration of hydrocarbons.

Further, Olesen et al. (2013) discuss the presence of saprolites in northern Norway, in context with Triassic to Jurassic deep weathering of basement rocks. The saprolites commonly occur as chemically weathered, highly permeable grus deposits. It implies that within basement highs such as the Finnmark Platform and the Loppa High, highly permable weathered grus may be juxtaposed with impermeable Palaeozoic-Mesozoic fault zones due to normal

faulting. Alternatively, highly fractured basement rocks may act as a reservoir. Important factors for the formation of hydrocarbon reservoirs may thus be present on basement highs in the Barents Sea.

Future research

The following suggestions on future research are given to further verify and/or evolve the results and models presented herein:

- The considerable gap between onshore fault outcrops and offshore seismic data has to some extent been made clearer by the study of high-resolution bathymetry and magnetic anomaly data. Still, large portions of the Finnmark Platform have a poor coverage of seismic data and are covered with glacigenic sediments, leaving the bathymetry data useless in these areas. Access to the new generation of magnetic anomaly data (BASAR, NGU) may increase the accuracy of fault correlation across the Finnmark Platform.
- Grav-mag modelling within the study area would further increase our understanding of the SW Barents Sea Margin, especially in relation to the structure of the deeper crust, including the depth to MOHO and the location of the taper break.
- The identification and existence of the Fugløya transfer zone may be verified by geological fieldwork on the islands of Nord-Fugløya and Spenna. These islands are difficult to access and have not been possible to visit as a part of this PhD.
- An XRF-analysis and pseudosection study of the metabasites used for determination of P-T conditions during faulting could further restrain the pressure and temperature stability fields for different stages of faulting during the Late Permian/Early Triassic rifting phase.
- The differences in derived ages on fault activity in Lofoten-Vesterålen, Troms and Finnmark needs further attention. The shut-off of onshore faulting in Troms has been tentatively explained by the hard-linkage of the Troms-Finnmark Fault Complex and the Senja Shear Zone prior to the Late Jurassic/Early Cretaceous rifting phase (this thesis) and would explain why rifting continued in the Lofoten Vesterålen, but not Troms. However, one would expect that such a hard-link would prevent Mesozoic fault activity in Finnmark as well, but evidence suggest otherwise (Roberts & Lippard, 2005; Torgersen et al., 2013).
- The genetic relationship between ductile shear zones, brittle-ductile shear zones and brittle faults within the West Troms Basement Complex is still uncertain. It is

important to settle if they represent distinct tectonic events, a progressive evolution by exhumation of the margin, or alternatively, both, with a progressive re-use of pre-existing structures from earlier events and the formation of new structures with the onset of a new tectonic event.

References

Andresen, A. & Forslund, T. 1987: Post-Caledonian brittle faults in Troms: geometry, age and tectonic significance. The Caledonian and Related Geology of Scandinavia. Cardiff, 22-23 Sept., 1989 (Conf. Abstract).

Antonsdòttir, V. 2006: *Structural and kinematic analysis of the post-Caledonian Rekvika Fault Zone, Kvaløya, Troms*. Unpublished Master thesis, University of Tromsø, 84 pp.

Bergh, S. G., Eig, K, Kløvjan, O. S., Henningsen, T., Olesen, O. & Hansen, J-A. 2007: The Lofoten-Vesteralen continental margin: a multiphase Mesozoic-Palaeogene rifted shelf as shown by offshore-onshore brittle fault-fracture analysis. *Norwegian Journal of Geology*, v. 87, 29 - 58.

Bergh, S. G., Corfu, F. & Corner, G. D. 2008: Proterozoic igneous and metamorphic rocks: a template for Mesozoic-Cenozoic brittle faulting and tectonic inherited landscapes in Lofoten-Vesterålen, North Norway. *33 IGC Excursion Guidebook No 38*, IGC The Nordic Countries, 71 pp.

Bergh, S. G., Kullerud, K., Armitage, P. E. B., Zwaan, K. B., Corfu, F., Ravna, E. J. K. & Myhre, P. I. 2010: Neoarchaean through Svecofennian tectono-magmatic evolution of the West Troms Basement Complex, North Norway. *Norwegian Journal of Geology*, v. 90, 21-48.

Bergh, S. G., Sylvester, A.G, Damte, A. & Indrevær, K. 2014: Evolving transpressional strain fields along the San Andreas fault in southern California: implications for fault branching, fault dip segmentation and strain partitioning. Abstract, EGU General Assembly 2014.

Blystad, P., Brekke, H., Færseth, R. B., Larsen, B. T., Skogseid, J. & Tørudbakken, B. 1995: Structural elements of the Norwegian continental shelf, Part II. *The Norwegian Sea Region*. *Norwegian Petroleum Directorate Bulletin*, v. 8. 45pp.

Brekke, H. 2000: The tectonic evolution of the Norwegian Sea continental margin with emphasis on the Vøring and Møre basins: *Special Publications - Geological Society of London*, v. 136, 327-378.

Brekke, H., Sjulstad, H. I., Magnus, C. & Williams, R. W. 2001: Sedimentary environments offshore Norway - an overview. *Norwegian Petroleum Society*, *Special Publication 10,* 7-37.

Dalland, A. 1981: Mesozoic sedimentary succession at Andøya, Northern Norway, and relation to structural development of the North Atlantic area. In: Kerr, J. W. & Fergusson, A. J. (eds.) Geology of the North Atlantic borderlands. *Canadian Society of Petroleum Geologists, Memoir 7*, 563-584.

Davids, C., Wemmer, K., Zwingmann, H., Kohlmann, F., Jacobs, J. & Bergh, S.G. 2013: K–Ar illite and apatite fission track constraints on brittle faulting and the evolution of the northern Norwegian passive margin. *Tectonophysics 608*, 196–211.

Doré, A. G. 1991: The structural foundation and evolution of Mesozoic seaways between Europe and the Arctic. *Palaeogeograhy, Palaeoclimatology, Palaeoecology*, v. 87, 441-492.

Doré, A. G. & Lundin, E. R. 1996: Cenozoic compressional structures on the NE Atlantic margin: nature, origin and potential significance for hydrocarbon exploration: *Petroleum Geoscience*, v. 2, 299-311.

Doré, A. G., Lundin, E. R., Jensen, L. N., Birkeland, Ø., Eliassen, P. E. & Fichler, C. 1999: Principal tectonic events in the evolution of the northwest European Atlantic margins. In: Fleet, A. J. & Boldy, S. A. R. (eds.), Petroleum Geology of Northwest Europe*: Proceedings of the 5th Conference*. *Geological Society of London*, 41-61.

Doré, A. G., Lundin, E. R., Fichler, C. & Olesen, O. 1997: Patterns of basement structure and reactivation along the NE Atlantic margin. *Journal of the Geological Society of London 154*, 85-92

Doré, A. G., Lundin, E. R., Jensen, L. N., Birkeland, Ø., Eliassen, P. E. & Fichler, C. 1999: Principal tectonic events in the evolution of the northwest European Atlantic margins. In: Fleet, A. J. & Boldy, S. A. R. (eds.), Petroleum Geology of Northwest Europe*: Proceedings of the 5th Conference*. *Geological Society of London*, 41-61.

Doré, A. G., Cartwright, J. A., Stoker, M. S., Turner, J. P. & White, N. (eds.) 2002. Exhumation of the North Atlantic Margin: Timing, Mechanisms and Implications for Petroleum Exploration, *Special Publications - Geological Society of London*, v. **196**, 45-65.

Eig, K. 2008: *Onshore and offshore tectonic evolution of the Lofoten passive margin, North Norway*. Unpublished PhD thesis, University of Tromsø, 256 pp.

Faleide, J. I., Vågnes, E., & Gudlaugsson, S. T. 1993: Late Mesozoic-Cenozoic evolution of the south-western Barents Sea in a regional rift-shear tectonic setting. *Marine and Petroleum Geology*, *10*(3), 186-214.

Faleide, J. I., Tsikalas, F., Breivik, A. J., Mjelde, R., Ritzmann, O., Engen, O., Wilson, J. & Eldholm, O. 2008: Structure and evolution of the continental margin off Norway and Barents Sea. *Episodes 31(1),* 82-91.

Forslund, T. 1988: *Post-Kaledonske forkastninger i Vest-Troms, med vekt på Kvaløyslettaforkastningen, Kvaløya*. Unpublished Cand. Scient. thesis, University of Tromsø. 173 pp.

Fürsich, F. & Thompsen, E. 2005: Jurassic biota and biofacies in erratics from the Sortland area, Vesterålen, northern Norway. *Geological Society of Norway, Bulletin 443*, 37-53.

Gabrielsen, R. H. 1984: Long-lived fault zones and their influence on the tectonic development of the southwestern Barents Sea. *Journal of the Geological Society*, *141*(4), 651-662.

Gabrielsen, R.H., Færseth, R.B., Jensen, L.N., Kalheim, J.E. & Riis, F. 1990: Structural elements of the Norwegian continental shelf — Part I: the Barents Sea Region. *Norwegian Petroleum Directorate Bulletin 6*, 33 pp.

Gabrielsen, R. H., Grunnaleite, I. & Rasmussen, E. 1997: Cretaceous and Tertiary inversion in the Bjørnøyrenna Fault Complex, south-western Barents Sea. *Marine and Petroleum Geology 14(2),* 165-178.

Gagama, M. F. V. 2005: *Strukturell analyse av post-kaledonske lineamenter ved Sifjorden, Vest-Senja, Troms*. Unpublished Master thesis, University of Tromsø, 85 pp.

Gernigon, L. & Brönner, M. 2012. Late Palaeozoic architecture and evolution of the southwestern Barents Sea: insights from a new generation of aeromagnetic data. *Journal of the Geological Society*, **169**(4), 449-459.

Gudlaugsson, S. T., Faleide, J. I., Johansen, S. E. & Breivik, A. J. 1998: Late Paleozoic structural development of the south-western Barents Sea: *Marine and Petroleum Geology*, v. 15, 73-102.

Hansen, J.-A. 2009: *Onshore-offshore tectonic relations on the Lofoten and Vesterålen Margin - Mesozoic to early Cenozoic structural evolution and morpological implications*. PhD thesis, University of Tromsø, 229 pp.

Hansen, J-A, Bergh, S. G. & Henningsen, T. 2012: Mesozoic rifting and basin evolution on the Lofoten and Vesterålen Margin, North-Norway; time constraints and regional implications. *Norwegian Journal of Geology*, v. 91 (1-2), 203 - 228.

Hendriks, B. W. H., Osmundsen, P. T. & Redfield, T. F. 2010: Normal faulting and block tilting in Lofoten and Vesterålen constrained by apatite fission track data. *Tectonophysics 485*, 154-163.

Knutsen, S. M. & Larsen, K. I. 1997: The late Mesozoic and Cenozoic evolution of the Sørvestsnaget Basin: A tectonostratigraphic mirror for regional events along the Southwestern Barents Sea margin? *Marine and petroleum geology 14(1),* 27-54.

Olesen, O., Torsvik, T. H., Tveten, E., Zwaan, K. B., Løseth, H. & Henningsen, T. 1997: Basement structure of the continental margin in the Lofoten-Lopphavet area, northern Norway: constraints from potential field data, on-land structural mapping and palaeomagnetic data, *Norwegian Journal of Geology*, v. 77, 15-30.

Opheim, J.A. and Andresen, A. 1989: Basement-cover relationships on northern Vanna, Troms, Norway. *Norwegian Journal of Geology*, v. 69(2), 67-81.

Osmundsen, P.T., Sommaruga, A., Skilbrei, J.R. & Olesen, O. 2002: Deep structure of the Mid Norway rifted margin. *Norwegian Journal of Geology*, v. 82, 205-224.

Osmundsen, P. T., Henderson, I., Lauknes, T. R., Larsen, Y., Redfield, T. F., & Dehls, J. 2009: Active normal fault control on landscape and rock-slope failure in northern Norway. *Geology*, *37*(2), 135-138.

Osmundsen, P. T., Redfield, T. F., Hendriks, B. H. W., Bergh, S., Hansen, J. A., Henderson, I. H. C., Dehls, J., Lauknes, T.R., Larsen, Y., Anda, E. & Davidsen, B. 2010: Fault-controlled alpine topography in Norway. *Journal of the Geological Society*, *167*(1), 83-98.

Ramberg, I. B., Bryhni, I., Nøttvedt, A. & Rangnes, K. 2008. *The making of a land*. *Geology of Norway*. The Norwegian Geological Association, Oslo.

Redfield, T. F. & Osmundsen, P. T. 2013: The long-term topographic response of a continent adjacent to a hyperextended margin: A case study from Scandinavia. *Geological Society of America Bulletin 125(1-2),* 184-200.

Roberts, D. & Lippard, S.J. 2005: Inferred Mesozoic faulting in Finnmark: current status and offshore links. *Geological Survey of Norway Bulletin 443*, 55-60.

Smelror, M., Mørk, A., Mørk, M. B. E., Weiss, H. M. & Løseth, H. 2001: Middle Jurassic-Lower Cretaceous transgressive-regressive sequences and facies distribution off northern Nordland and Troms, Norway. *Norwegian Petroleum Society Special Publications*, v. 10, 211-232.

Smelror, M., Petrov, O.V., Larssen, G.B. & Werner, S.C. (eds.) + 16 co-authors 2009: Geological history of the Barents Sea. *Geological Survey of Norway*, Trondheim, 135 pp.

Sund, T., Skarpnes, O., Jensen, L. N., & Larsen, R. M. 1986: Tectonic development and hydrocarbon potential offshore Troms, northern Norway.

Thorstensen, L. 2011*: Land-sokkel korrelasjon av tektoniske elementer i ytre del av Senja og Kvaløya i Troms*. Unpublished Master thesis, University of Tromsø, 107 pp.

Torgersen, E, Viola, G & Zwingmann, H., 2013: How can K-Ar geochronology of clay-size mica/illite help constrain reactivation histories of brittle faults? An example from a Paleozoic thrust fault in Northern Norway. EGU General Assembly Conference Abstracts 15, 2986.

Tsikalas, F., Eldholm, O., & Faleide, J. I. 2005: Crustal structure of the Lofoten–Vesterålen continental margin, off Norway. *Tectonophysics*, *404*(3), 151-174.

Waqas, A. 2012: *Structural Analysis of the Troms--Finnmark Fault Complex, SW Barents Sea*. Master thesis, University of Oslo.

Zwaan, K. B. 1995: Geology of the West Troms Basement Complex, northern Norway, with emphasis on the Senja Shear Belt: a preliminary account. *Geological Survey of Norway, Bulletin 427*, 33-36.

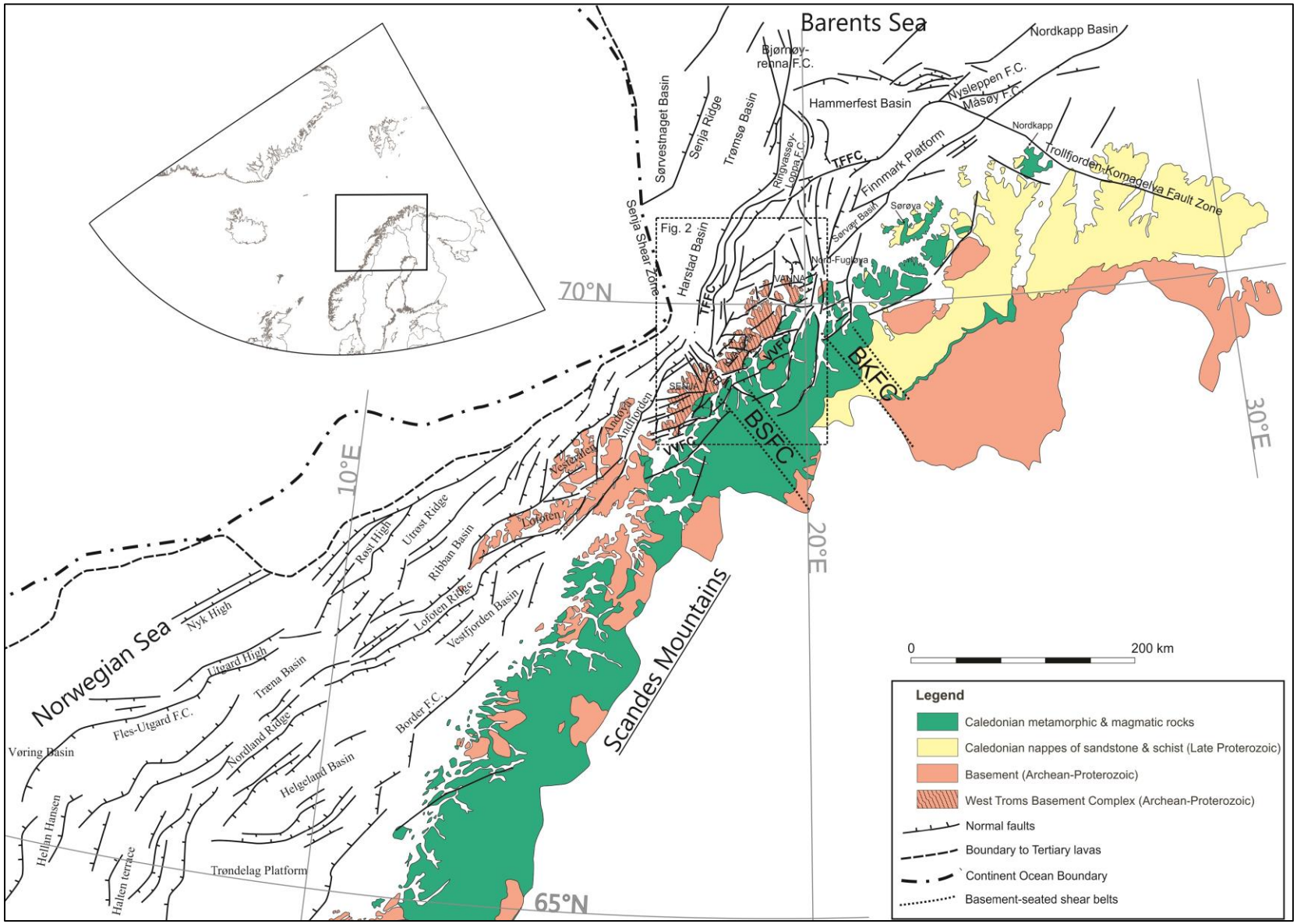

Figure 1: Regional onshore-offshore tectonic map and setting of the mid-Norwegian shelf, the West Troms Basement Complex and the SW Barents Sea margin (after Blystad et al., 1995; Mosar et al., 2002; Bergh et al., 2007; Faleide et al., 2008; Hansen et al., 2012; Indrevær et al., 2014). Onshore geology is from the Geological Survey of Norway. The yellow box outlines Fig. 2. Abbreviations: TFFC=Troms-Finnmark Fault Complex, VVFC=Vestfjorden-Vanna Fault Comple

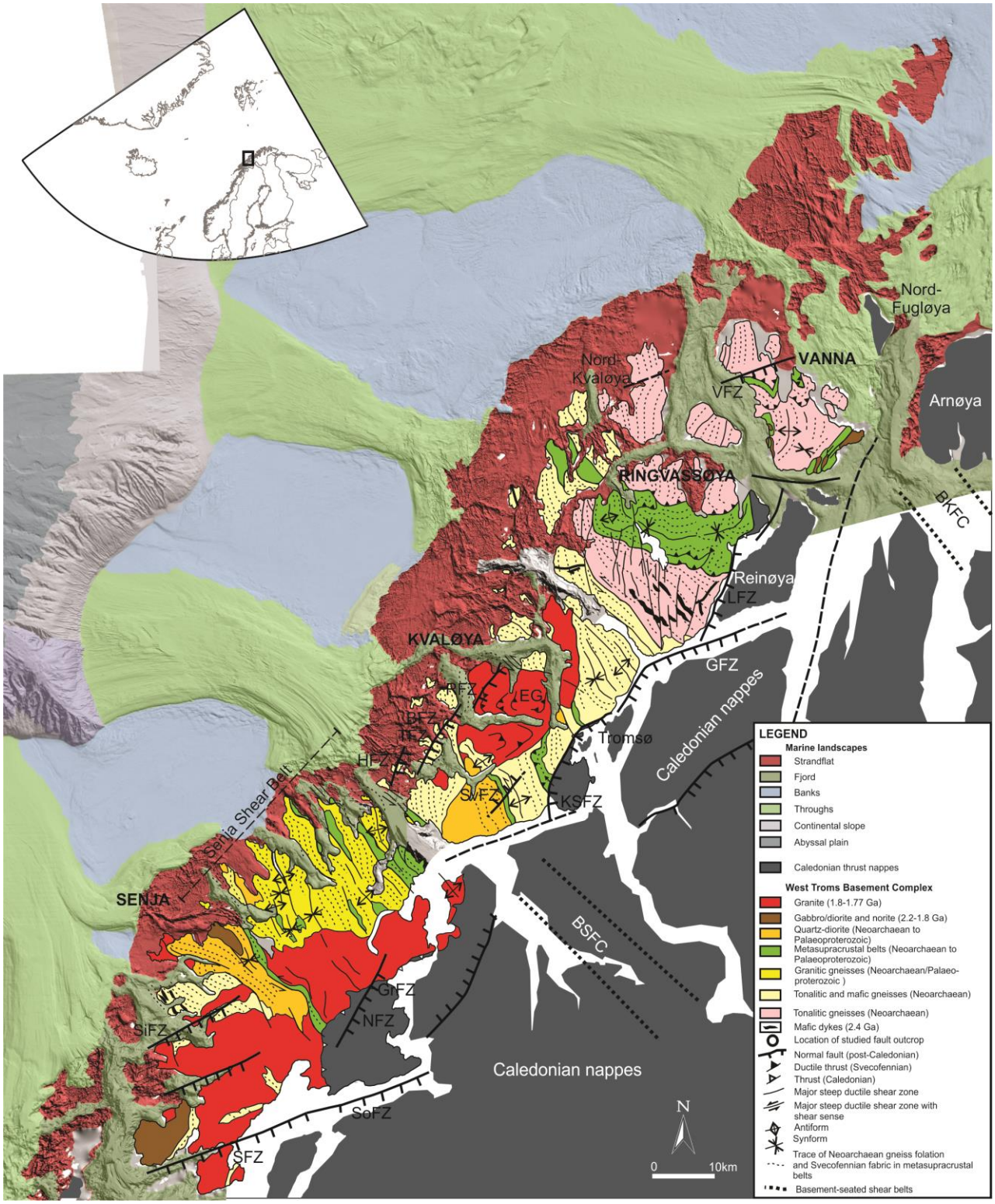

Figure 2: Detailed geological map of the West Troms Basement Complex showing main Archaean-Palaeoproterozoic fabrics and post-Caledonian brittle normal faults that separate the basement horst from down-dropped Caledonian nappes to the east (after Bergh et al., 2010). Offshore, marine landscape types are given, including the lateral distribution of the strandflat (mareano.no). Abbreviations: BFZ = Bremneset fault zone, BKFC=Bothnian-Kvænangen Fault Complex, BSFC=Bothnian-Senja Fault Complex, EG=Ersfjord Granite, GFZ=Grøtsundet fault zone, GrFZ=Grasmyrskogen fault zone, HFZ = Hillesøy fault zone, KSFC=Kvaløysletta-Straumsbukta fault zone, LFZ=Langsundet fault zone, NFZ=Nybygda fault zone, RFZ=Rekvika fault zone, SFZ=Stonglandseidet fault zone, SiFZ=Sifjorden fault zone, SoFZ=Solbergfjorden fault zone, SvFZ=Skorelvvatn fault zone, TFZ=Tussøya fault zone, VFZ=Vannareid-Brurøysund fault zone, VVFC=Vestfjorden-Vanna Fault Complex.

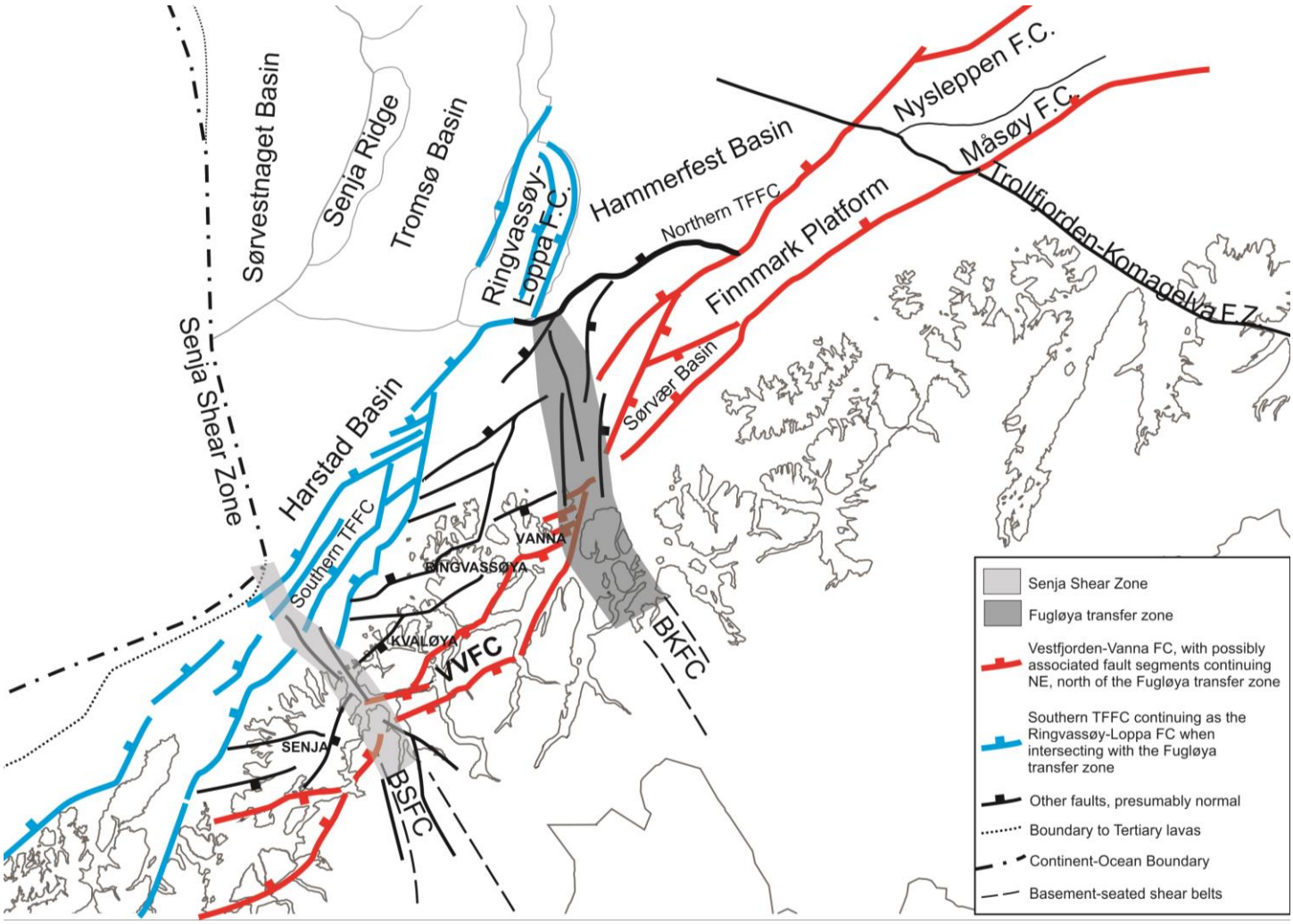

Figure 3: Simplified tectonic map of the SW Barents Sea region linking major NNE-SSW and ENE-WSW trending fault complexes onshore and offshore. At least two transfer zones, one located along the Precambrian Senja Shear Belt (BSFC = Bothnian-Senja Fault Complex) and the second, the Fugløya transfer zone, the continuation of the Bothnian-Kvænangen Fault Complex (BKFC), accommodate change in polarity and stepping of fault zones along the margin.

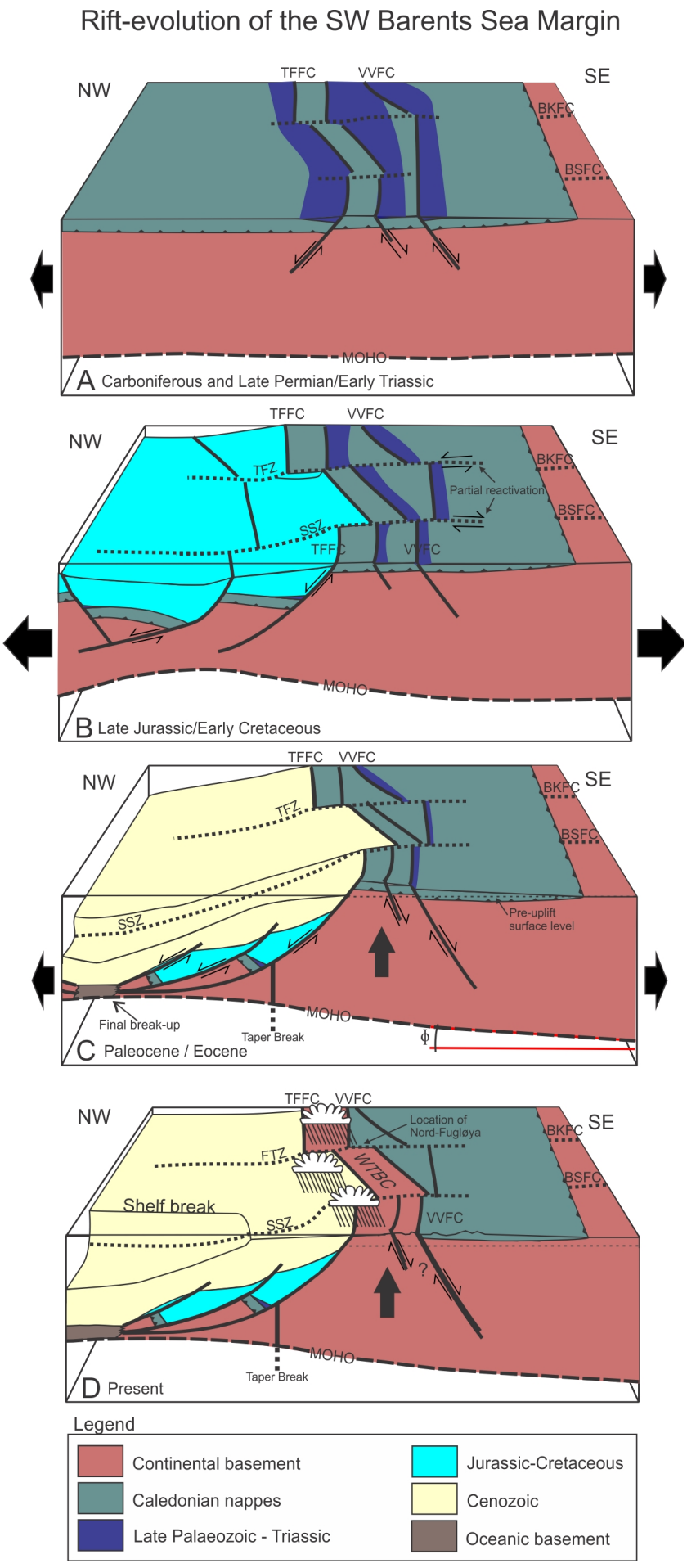

Figure 4: Schematic proposed tectonic evolution of the SW Barents Sea margin and the exhumation of the West Troms Basement Complex (WTBC). (a) Intial shallow and distributed NE-SW faulting in the Carboniferous and Late Permian/Early Triassic along the Troms-Finnmark and the Vestfjorden-Vanna fault complexes. Partial reactivation of the Bothnian-Kvænangen and Bothnian-Senja fault complexes as transfer zones allowed for changes in fault polarity along the margin. (b) Continued rifting in the Late Jurassic/Early Cretaceous was accompanied by the hard link of the Senja Shear Zone (SSZ) and the Troms-Finnmark FC and dextral and sinistral displacement along the SSZ and the Fugløya transfer zone, respectively (c) Paleocene/Eocene extension and transform movement along the SSZ caused final break-up, further listric faulting offshore and uplift of the short-tapered margin due to unloading and crustal flexure. (d) Continued uplift and exhumation of the WTBC due to climate detoriation and associated increase in coastal erosion rates. BKFC=Bothnian-Kvænangen Fault Complex, BSFC=Bothnian-Senja Fault Complex, TFFC=Troms-Finnmark Fault Complex, SSZ=Senja Shear Zone, FTZ=Fugløya transfer zone, VVFC= Vestfjorden-Vanna Fault Complex.

Paper 1

Post-Caledonian brittle fault zones on the hyperextended SW Barents Sea margin: New insights into onshore and offshore margin architecture

Kjetil Indrevær, Steffen G. Bergh, Jean-Baptiste Koehl, John-Are Hansen, Elizabeth R. Schermer & Arild Ingebrigtsen

Indrevær, K., Bergh, S.G., Koehl, J.-B., Hansen, J.-A., Schermer, E.R. & Ingebrigtsen, A.: Post-Caledonian brittle fault zones on the hyperextended SW Barents Sea margin: New insights into onshore and offshore margin architecture. *Norwegian Journal of Geology,* Vol 93, pp. 167–188. Trondheim 2013, ISSN 029-196X.

Onshore-offshore correlation of brittle faults and tectonic lineaments has been undertaken along the SW Barents Sea margin off northern Norway. The study has focused on onshore mapping of fault zones, the mapping of offshore fault complexes and associated basins from seismic interpretation, and the linkage of fault complexes onshore and offshore by integrating a high-resolution DEM, covering both onshore and offshore portions of the study area, and processed magnetic anomaly data. This study shows that both onshore and offshore brittle faults manifest themselves mainly as alternating NNE–SSW- and ENE–WSW-trending, steeply to moderately dipping, normal fault zones constituting at least two major NE-SW-trending fault complexes, the Troms-Finnmark and Vestfjorden-Vanna fault complexes. These fault complexes in western Troms bound a major basement horst (the West Troms Basement Complex), run partly onshore and offshore and link up with the offshore Nysleppen and Måsøy fault complexes. Pre-existing structures in the basement, such as foliation, lithological boundaries and ductile shear zones are shown, at least on a local scale, to have exerted a controlling effect on faulting. On a larger scale, at least two major transfer fault zone systems, one along the reactivated Precambrian Senja Shear Belt and the other, the Fugløya transfer zone, accommodate changes in brittle fault polarity along the margin. Our results suggest that distributed rifting during Carboniferous and Late Permian/Early Triassic time was followed by a northwestward localisation of displacement to the Troms–Finnmark and Ringvassøy–Loppa fault complexes during the Late Jurassic/Early Cretaceous, resulting in the formation of a short-tapered, hyperextended margin with final break-up at ~55 Ma. An uplift of the margin and preservation of the West Troms Basement Complex as a basement outlier is suggested to be due to unloading and crustal flexure of the short-tapered margin in the region.

Indrevær, Kjetil, Department of Geology, University of Tromsø, 9037 Tromsø, Norway. DONG E&P Norge AS, Roald Amundsens Plass 1, 9257 Tromsø, Norway. Bergh, Steffen G., Department of Geology, University of Tromsø, 9037 Tromsø, Norway. Koehl, Jean-Baptiste, Department of Geology, University of Tromsø, 9037 Tromsø, Norway. Hansen, John-Are, Department of Geology, University of Tromsø, 9037 Tromsø, Norway. Schermer, Elizabeth R., Department of Geology, Western Washington University, Bellingham, WA 98225, United States. Ingebrigtsen, Arild, DONG E&P Norge AS, Roald Amundsens Plass 1, 9257 Tromsø, Norway.

E-mail corresponding author (Kjetil Indrevær): kjetil.indrevar@uit.no

Introduction

The continental margin off Central/Mid Norway was subjected to multiple rift events in the Palaeozoic through to Early Cenozoic times as a part of the break-up of the North Atlantic Ocean (e.g., Doré, 1991; Faleide et al., 1993; Blystad et al., 1995; Doré & Lundin, 1996; Brekke et al., 2001; Osmundsen et al., 2002; Eig, 2008; Faleide et al., 2008). The fault timing and evolution of these rifting events and the resulting margin architecture are well constrained by seismic and potential field data offshore Mid Norway (e.g., Dore et al., 1999; Brekke, 2000; Redfield & Osmundsen, 2013). On the Lofoten–Vesterålen margin (Fig. 1), recent work on the linking of onshore and offshore fault systems and morphotectonic elements has established a very complex rift evolution (Olesen et al., 1997, 2007; Tsikalas et al., 2001, 2005, 2008; Wilson et al., 2006; Bergh et al., 2007; Eig, 2008; Hansen, 2009; Hansen et al., 2012). However, north of Lofoten, on the West Troms margin, few onshore-offshore structural studies have been undertaken (Gabrielsen et al., 1990; Roberts & Lippard, 2005). This region marks the transition between the spreading, normal passive margin and the Barents Sea transform margin (Fig. 1). Along the West Troms margin, onshore brittle faults manifest themselves mainly as NNE–SSW- and ENE–WSW-trending normal faults, as in the Lofoten–Vesterålen archipelago. They are constrained to a major basement horst that extends from Lofoten in the south to Vanna in the north (Fig. 1) and comprises the islands of Senja, Kvaløya, Ringvassøy and Vanna, as well as several other smaller islands (Figs. 1, 2; Olesen et al., 1997; Bergh et al., 2010). The basement horst is named the West Troms Basement Complex (WTBC) (Zwaan, 1995) and is flanked in the south by major normal faults (Blystad et al., 1995; Bergh et al., 2007; Hansen et al., 2012) that border the offshore Ribban and Vestfjorden basins. Northwards it is bound to the east by

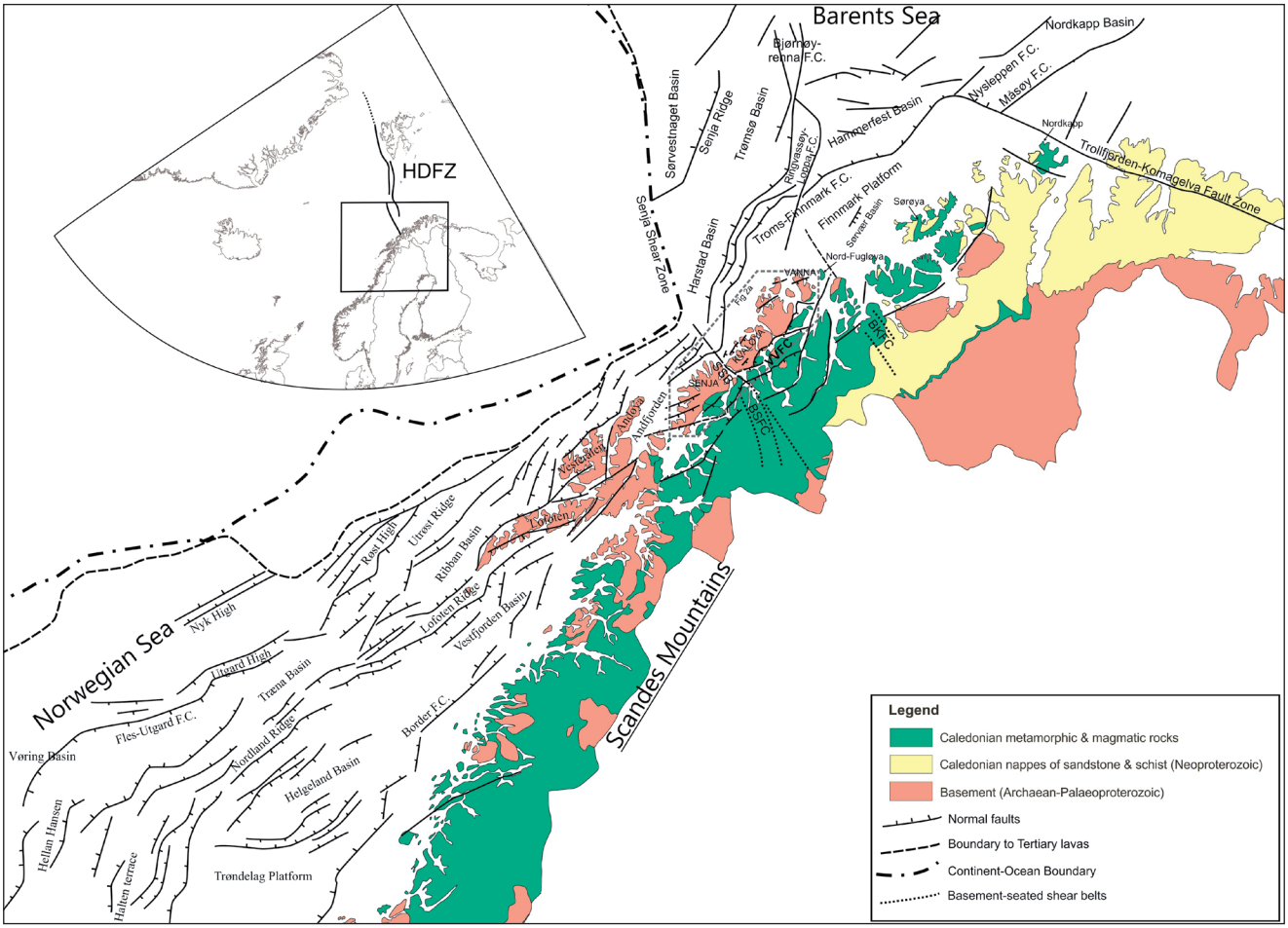

Figure 1. *Regional onshore-offshore tectonic map and setting of the Mid-Norwegian shelf, the Lofoten–Vesterålen archipelago and the SW Barents Sea margin (after Blystad et al., 1995; Mosar et al., 2002; Bergh et al., 2007; Faleide et al., 2008; Hansen et al., 2012). Onshore geology is from the Geological Survey of Norway. The boxed area in the inset map outlines Fig. 2A. Abbreviations: BKFC – Bothnian–Kvænangen Fault Complex, BSFC – Bothnian–Senja Fault Complex, HDFZ – Hornsund–De Geer Fault Zone, SSB – Senja Shear Belt, VVFC – Vestfjorden–Vanna Fault Complex.*

the SE-dipping Vestfjorden–Vanna Fault Complex that down-drops Caledonian nappes (Andresen & Forslund, 1987; Forslund, 1988; Opheim & Andresen, 1989; Olesen et al., 1997; Roberts & Lippard, 2005).To the west of the WTBC, no specific major faults or fault zones have yet been observed that may correspond to horst-bounding faults offshore.

The present work focuses on the network of Palaeozoic–Mesozoic faults in the West Troms Basement Complex and their relationship to major structural elements in the SW Barents Sea, such as the Troms–Finnmark Fault Complex (TFFC), the Ringvassøy–Loppa Fault Complex (RLFC) and the Måsøy and Nysleppen fault complexes (Figs. 1, 2; Ramberg et al., 2008; Smelror et al., 2009). We aim to identify and characterise rift-related fault zones exposed onshore, and to discuss the possible controls of inherited basement fabrics as a framework for regional correlation. Particular emphasis will be given to proposed boundary faults of the onshore basement horst, e.g., the Rekvika fault zone in the west, suggested to be a possible onshore portion of the Troms–Finnmark Fault Complex (Antonsdottir, 2006; Thorstensen, 2011; Hansen et al., 2012), and the Kvaløysletta–Straumsbukta fault zone (and others) on the landward side of the WTBC (Andresen & Forslund, 1987; Forslund, 1988; Olesen et al., 1997). Comparisons with offshore fault zones will be made based on seismic data. We have performed detailed mapping in regions where major structural elements converge, diverge or change orientation, in order to understand their origin and relationships. We have used a digital elevation model (DEM) and magnetic anomaly data to link up and/or extend fault traces between and beyond exposures of onshore faults and to map tectonic lineaments in offshore regions where seismic data coverage is insufficient. The compiled data on fault behaviour in the region will be evaluated in the context of a hyperextended Norwegian margin, as proposed by Redfield & Osmundsen (2013).

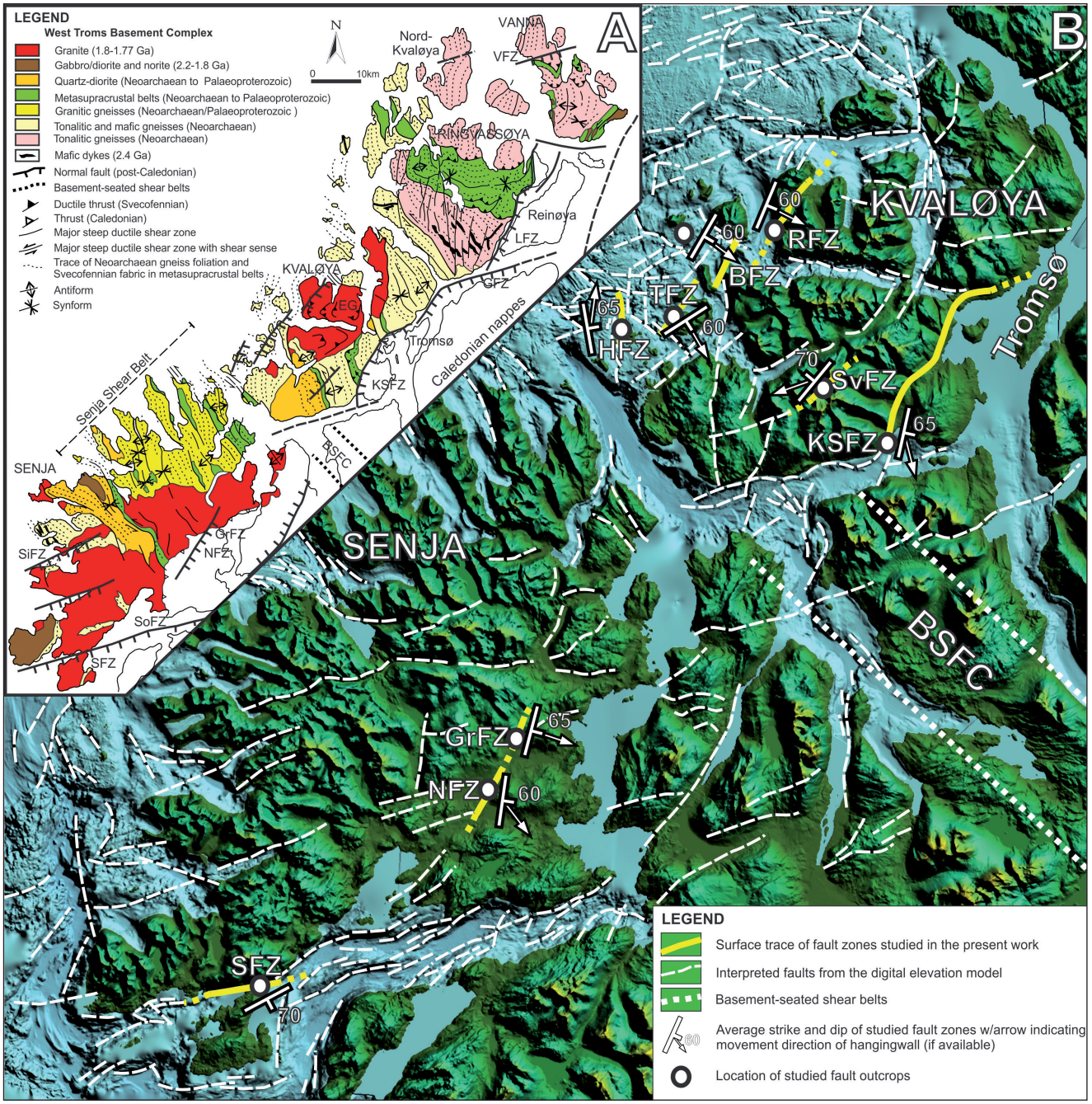

Figure 2. *(A) Detailed geological map of the West Troms Basement Complex showing the main Archaean–Palaeoproterozoic foliations and post-Caledonian brittle normal faults that separate the basement horst from down-dropped Caledonian nappes to the east and Late Palaeozoic–Mesozoic basins to the west (after Olesen et al., 1997; Bergh et al., 2010). Note the step-wise pattern of normal faults that correspond with the general orientation of fjords and sounds and offshore fault-bounding basins. (B) Digital elevation model (DEM) showing the location of studied fault outcrops from Fig. 4, with interpreted lineaments and synthesised fault data. Note that most lineaments trend NNE–SSW and ENE–WSW, with a subsidiary set trending ~NW–SE, both onshore and on the shallow shelf. Abbreviations: BFZ – Bremneset fault zone, BSFC – Bothnian–Senja Fault Complex, EG – Ersfjord Granite, GFZ – Grøtsundet fault zone, GrFZ – Grasmyrskogen fault zone, HFZ – Hillesøy fault zone, KSFC – Kvaløysletta–Straumsbukta fault zone, LFZ – Langsundet fault zone, NFZ – Nybygda fault zone, RFZ – Rekvika fault zone, SFZ – Stonglandseidet fault zone, SiFZ – Sifjorden fault zone, SoFZ – Solbergfjorden fault zone, SvFZ – Skorelvvatn fault zone, TFZ – Tussøya fault zone, VFZ – Vannareid–Brurøysund fault zone.*

Geological setting and margin evolution

Precambrian structures of the West Troms Basement Complex

The West Troms Basement Complex horst (Fig. 2) is made up of various Meso- and Neoarchaean (2.9–2.6 Ga) tonalitic, trondhjemitic and granitic TTG-gneisses, metasupracrustal rocks/greenstone belts (2.85–1.9 Ga), and felsic and mafic igneous rocks (1.8–1.75 Ga) (Corfu et al., 2003; Bergh et al., 2010). The ductile deformation within the WTBC is mostly of Svecofennian age (1.8–1.7 Ga) and includes macro-scale upright and vertical folds linked to NW–SE-trending, steep deformation zones or terrane boundaries (Fig. 2A). These structural trends are

largely parallel with the Archaean and Palaeoproterozoic orogenic belts of the Fennoscandian Shield that stretch from Kola Peninsula in Russia through Finland and Sweden into the Bothnian Basin of central Scandinavia (Gaal & Gorbatschev, 1987; Hölttä et al., 2008; Lahtinen et al., 2008). The younger Caledonian overprint is generally weak (Corfu et al., 2003; Bergh et al., 2010).

Post-Caledonian structures

The Palaeozoic–Mesozoic rift-related activity on the West Troms margin is manifested within the horst by widespread, NNE–SSW- and ENE–WSW-trending, brittle normal faults and fractures arranged in a zigzag pattern along its southeastern and northwestern limits (cf., Hansen et al., 2012) and a subsidiary NW–SE-trending fracture system that is best developed in Lofoten (Fig. 1; Eig & Bergh, 2011; Hansen & Bergh, 2012). The Vestfjorden–Vanna Fault Complex (VVFC, Figs. 1, 2A; Olesen et al., 1997) can be traced for hundreds of kilometres southwestwards along the North Norwegian margin, as it links up and continues along the Lofoten and Nordland ridges, as well as along the Halten terrace farther south (Dore et al., 1997, 1999). The zigzag-shaped map pattern of the VVFC in western Troms can be traced northwards to Vanna, outlined by several smaller-scale fault segments (Fig. 2; Andresen & Forslund, 1987; Forslund, 1988; Opheim & Andresen, 1989; Olesen et al., 1997), where it continues offshore as a part of the boundary fault system of the Sørvær Basin (Fig. 1; Olesen et al., 1997). From this point it has not been mapped farther northwards. The fault zones within the VVFC in general show down-to-southeast normal displacement on the order of 1–3 km based on the offset of Caledonian nappes with known thickness (Forslund, 1988; Opheim & Andresen, 1989; Olesen et al., 1997).

On the seaward side of the West Troms Basement Complex horst, no major, hard-linked boundary-fault complex similar to the VVFC on the landward side has yet been identified. Instead, less prevalent fault zones exist (Fig. 2; Olesen et al., 1997; Antonsdottir, 2006; Thorstensen, 2011) that run along the outer islands of the horst. In addition, a few fault zones within the central parts of the WTBC have been identified (Fig. 2; Opheim & Andresen, 1989; Armitage & Bergh, 2005; Gagama, 2005). The western zone of faults is not well known from previous studies. The kinematics, timing and evolution of these faults, as well as possible controlling effects on basement structures for the location of Palaeozoic–Mesozoic brittle fault reactivation, will be discussed in the present paper.

Margin evolution and fault timing

The Mid-Norwegian and SW Barents Sea continental margin experienced multiple periods of rifting during the Palaeozoic and Mesozoic that were linked to the break-up of Pangea, and the final stages of opening of the North Atlantic Ocean in the Cenozoic (cf., Gabrielsen et al., 1990; Faleide et al., 2008; Smelror et al., 2009). The earliest events occurred in Mid Carboniferous, Carboniferous–Permian and Permian–Early Triassic times (Doré, 1991). In the western Barents Sea, Carboniferous rift structures are widespread (Gudlaugsson et al., 1998) and led to the formation of early rift basins such as the Nordkapp and Tromsø basins (Faleide et al., 2008). On the Lofoten–Vesterålen margin, rifting is thought to have occurred during multiple tectonic events in the Permian–Early Triassic, Mid/Late Jurassic–Early Cretaceous and latest Cretaceous–Palaeogene (Brekke, 2000; Osmundsen et al., 2002; Bergh et al., 2007; Eig, 2008; Hansen et al., 2012). The Vestfjorden and northern Træna basins show large-scale fault activity in the Permian to Early Triassic (Brekke, 2000; Osmundsen et al., 2002; Hansen et al., 2012), followed by Late Triassic regional subsidence (Faleide et al., 2008). The main fault array on the Lofoten–Vesterålen margin likely developed during the syn-rift, Late Jurassic and Early Cretaceous phase (Hansen et al., 2012), as the Atlantic rifting propagated northwards leading to the formation of the Harstad, Tromsø, Bjørnøya and Sørvestnaget basins in the SW Barents Sea (Gabrielsen et al., 1997; Knutsen & Larsen, 1997; Faleide et al., 2008). Similarily, the Troms–Finnmark Fault Complex experienced a long-term activity from the Carboniferous through to the Eocene, with the main fault-related subsidence in Late Jurassic to Early Cretaceous times (Gabrielsen et al., 1990; Faleide et al., 2008).

A Late Cretaceous to Palaeocene rifting event preceded the final lithospheric break-up at *c.* 55–54 Ma. This rifting event was accomplished by transform movement along the Senja Shear Zone and the Hornsund-De Geer Fault Zone west of Svalbard (Gabrielsen et al., 1990; Faleide et al., 1993, 2008), leading to the further development of the Tromsø and Harstad basins as pull-apart basins. Simultaneously, inversion occurred in the Bjørnøyrenna and Ringvassøy–Loppa fault complexes (Gabrielsen et al., 1997). Since Oligocene time, the SW Barents Sea has been a passive continental margin (Faleide et al., 2008).

Onshore, recent datings using $^{40}Ar/^{39}Ar$ and apatite fission-track dating methods have been interpreted to indicate that faulting in western Troms largely occurred during the Permian to Early Triassic rifting phase, corresponding with the large-scale fault activity identified in the Vestfjorden and Træna basins, with no major fault displacement during the Mesozoic and Cenozoic (Hendriks et al., 2010; Davids et al., 2013). However, Mesozoic fault activity is suggested to have taken place onshore both farther north in Finnmark (Roberts & Lippard, 2005), and to the south in Lofoten–Vesterålen and Andøya (Dalland 1981; Fürsich & Thomsen, 2005; Hansen, 2009; Hendriks et al., 2010; Osmundsen et al., 2010; Davids et al., 2013). Palaeomagnetic evidence for Permian as well as Cenozoic to recent phases of faulting and cataclasis has been obtained for the Kvaløysletta–Straumsbukta fault zone which is a part of the Vestfjorden–Vanna Fault Complex (Forslund, 1988; Olesen et al., 1997).

Methods and databases

The present work is centred on understanding the distribution, geometry and kinematic behaviour of faults in the study area using: (1) descriptions of onshore fault characteristics, (2) the distribution of major offshore fault complexes and associated structures from interpretation of seismic data and (3) correlation and linkage of fault complexes onshore and offshore by integrating a high-resolution DEM and processed magnetic anomaly data. The data allows for a high-confidence interpretation of faults and tectonic lineaments on the shallow shelf where the coverage of seismic data is insufficient for fault interpretation.

Fieldwork

Fault zone outcrops were mapped with emphasis on gathering data on fault/fracture patterns, fault rock types, mineral precipitation on fault/fracture planes and orientation of pre-existing structures such as foliation and lithological boundaries in the host rock. Slickensided fault surfaces were used to determine slip sense. Fault orientation data are plotted as great circles and poles to planes with directions of slip-linears for the hanging wall in lower-hemisphere equal-area stereonets.

Seismic database and wells

The seismic data used in the present work include all available public 2D and 3D seismic data in the region (Fig. 3; pdp.diskos.com). Variable ages and quality of the seismic data may have influenced the fault interpretation and correlation in some areas. Horizons were picked using available public well data (Fig. 3; see later offshore section for more details). Depth conversion of seismic sections was done using the commercial *Aker hiQbe* velocity model (http://www.akersolutions.com) covering the SW Barents Sea.

Magnetic anomaly data

Magnetic anomaly data from the Geological Survey of Norway have been used to map faults and tectonic lineaments in the WTBC and adjacent coastal areas (Henkel, 1991; Olesen et al., 1997), using a similar method as for the Lofoten–Vesterålen margin (cf., Tsikalas et al., 2005; Eig, 2008; Hansen et al., 2012; Hansen & Bergh, 2012). The surveys used in this study are the tilt derivative of the HRAMS–98 and NGU69/70.

The tilt derivative (Miller & Singh, 1994) is chosen for

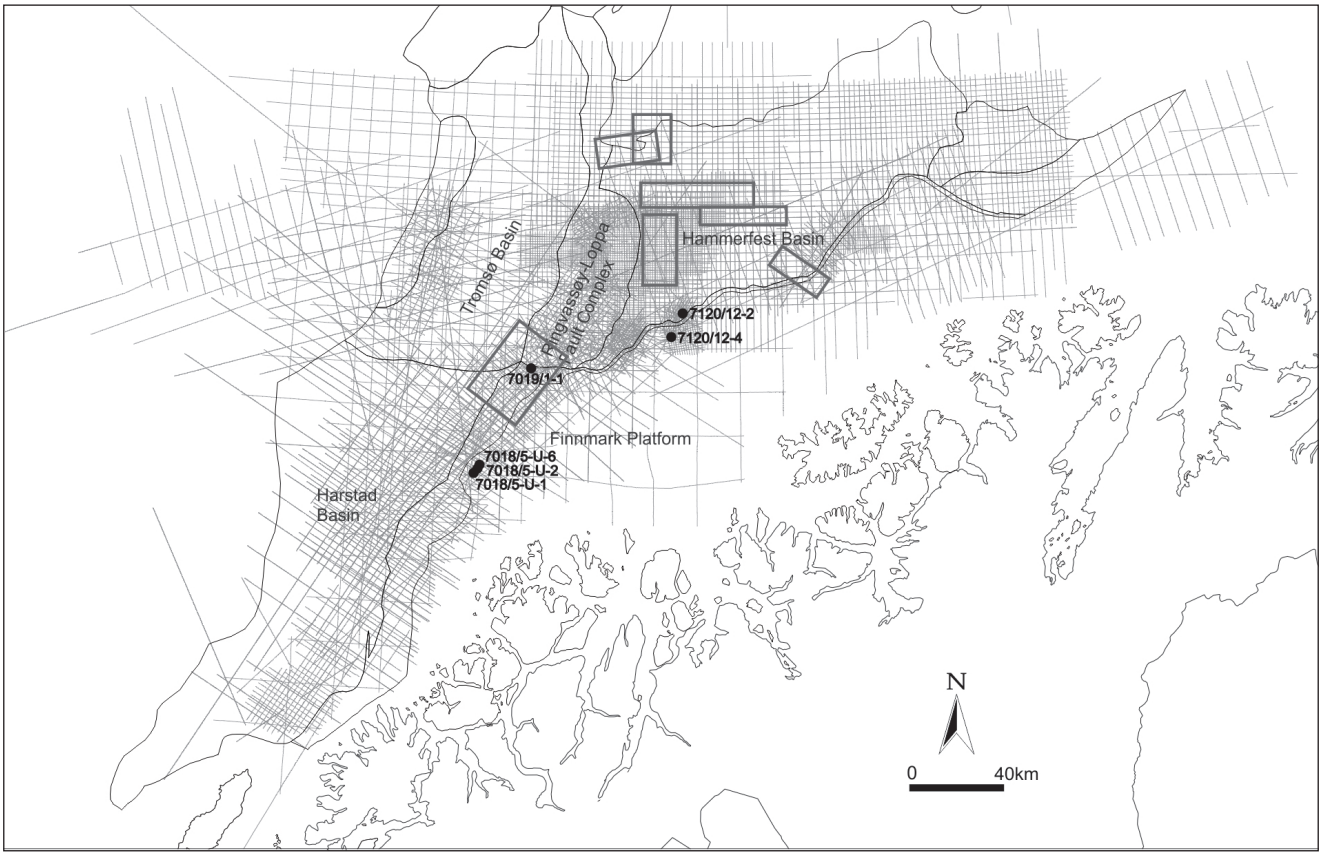

Figure 3. *Overview of the available 2D and 3D seismic data used in the study with the location of wells (numbered) used for seismic correlation (pdp.diskos.com).*

mapping because it enhances subtle magnetic anomalies in the subsurface such as those produced by faults. This is due to the nature of the arctan trigonometric function used in the calculation of the tilt derivative, restricting all values to ±90° regardless of the amplitude of the vertical or the absolute value of the total horizontal gradient (Verduzco et al., 2004).

Digital Elevation Model (DEM) data

The use of high-resolution bathymetric and topographic data for fault trace mapping is a method that has recently been adopted in the region (e.g., Roberts et al., 2011), made possible due to the availability of high-resolution bathymetry data and digital terrain models. A continuous 50 x 50 m digital elevation model (DEM) covering both onshore and offshore areas has been constructed for the area of study, based on the MAREANO (mareano.no), IBCAO (Jacobsson et al., 2012) and Norway Digital (norgedigitalt.no) databases.

The interpretation of DEM data builds on the assumption that the alpine topography is, in part, tectonically controlled and hence allows us to map tectonic lineaments from either aerial photography or terrain models (Gabrielsen et al., 2002; Gagama, 2005; Wilson et al., 2006; Bergh et al., 2008; Osmundsen et al., 2010). To assure an adequate quality of the interpretations, the method should only be used in combination with a good, field-based geological understanding of the study area. Offshore, many of the same assumptions are valid for bathymetry data. It is imperative to be able to clearly differentiate between glacial and tectonic lineaments, and bathymetric data should only be used cautiously and in combination with seismic data in order to identify true tectonic lineaments.

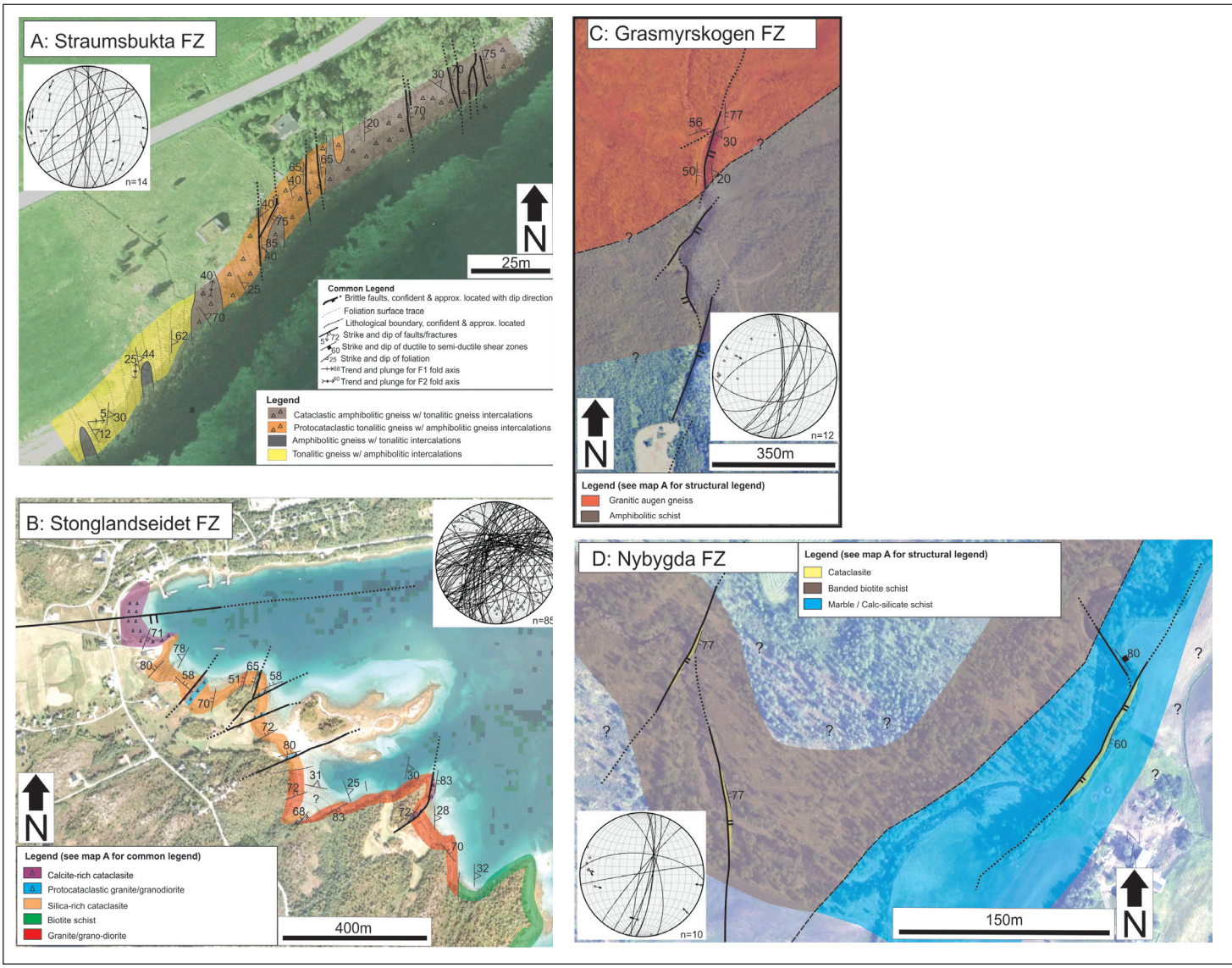

Results

Onshore fault zones

Several outcropping fault zones in and adjacent to the WTBC horst have been investigated (Figs. 2, 4). Many of the fault zones have been described in varying detail by other authors, but all of the mentioned fault-zone outcrops have been revisited and mapped for this work. This common platform of reference ensures a proper characterisation and comparison of fault geometries and kinematics for the different fault zones. The results presented here are therefore from this work unless stated otherwise.

The studied fault zones are located on (i) the eastern, or landward rim of the WTBC, (ii) the onshore western, seaward side, and (iii) inside the horst itself (Figs. 2, 4). In general, the fault zones delimit two major trends, NNE–SSW and ENE–WSW with variable dips to the SE and NW, and one minor structural trend striking NW–SE. The NNE–SSW- and the ENE–WSW-trending faults dominate the regional map pattern and alternate along strike, generating a zigzag pattern and enclosing fault-block domains.

Landward fault zones

The eastern horst-bounding networks of faults (i.e., the VVFC) include the NNE–SSW- to ENE–WSW-trending and ESE- and SSE-dipping Kvaløysletta–Straumsbukta, Stonglandseidet, Grasmyrskogen and Nybygda fault zones (Figs. 2, 4A–D). The SE-dipping Kvaløysletta–Straumsbukta fault zone (first described by Forslund, 1988) runs along the eastern shore of Kvaløya, juxtaposing Precambrian gneisses in the footwall with Caledonian nappes in the hanging wall. Near Straumsbukta, the damage zone of the footwall crops out within foliated tonalitic and amphibolitic gneisses (Fig. 4A). Fault surfaces

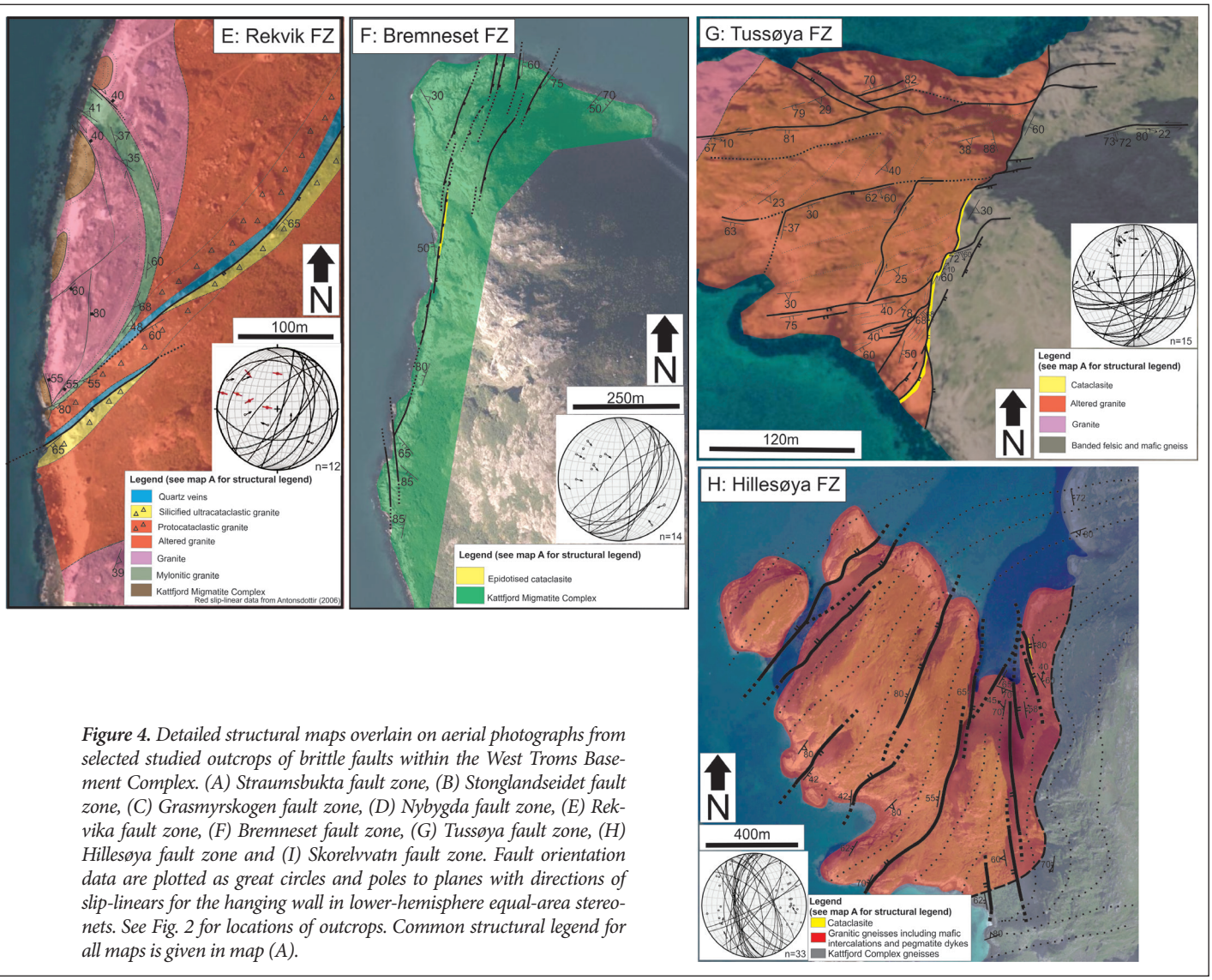

Figure 4. *Detailed structural maps overlain on aerial photographs from selected studied outcrops of brittle faults within the West Troms Basement Complex. (A) Straumsbukta fault zone, (B) Stonglandseidet fault zone, (C) Grasmyrskogen fault zone, (D) Nybygda fault zone, (E) Rekvika fault zone, (F) Bremneset fault zone, (G) Tussøya fault zone, (H) Hillesøya fault zone and (I) Skorelvvatn fault zone. Fault orientation data are plotted as great circles and poles to planes with directions of slip-linears for the hanging wall in lower-hemisphere equal-area stereonets. See Fig. 2 for locations of outcrops. Common structural legend for all maps is given in map (A).*

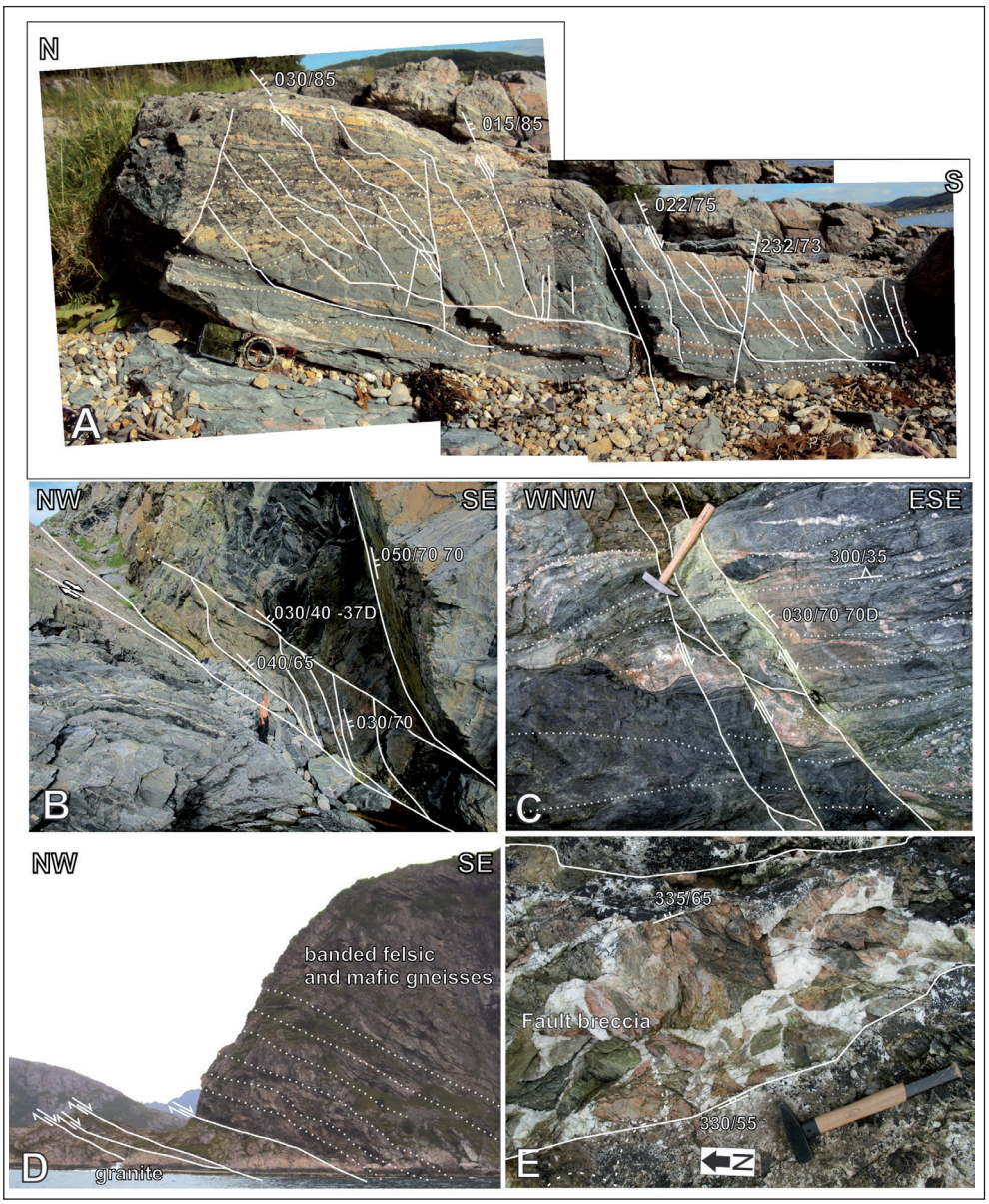

Figure 5. Selected field photos of brittle faults studied within the WTBC. (A) Mesoscale brittle faults in outcrop from the footwall of the Kvaløysletta–Straumsbukta fault zone at Straumsbukta. Note the red-stained colour of the tonalitic gneiss bands due to hydrothermal alteration. (B) Outcrop of the Bremneset fault zone at Bremneset, showing a 2 m-wide, epidote-rich cataclastic zone that cuts the foliation of mafic gneisses at a high angle. Note splaying and deflection of fractures within the cataclastic core zone towards its boundaries, supporting a dextral component of displacement. (C) Small-scale brittle normal faults that offset foliated amphibolite gneisses within the Bremneset fault zone. The offsets indicate down-to-the-ESE fault motion. (D) Overview of the Tussøya fault zone localised at the lithological boundary between banded felsic and mafic gneisses and foliation-parallel granite. The height of the cliff is c. 300 m. (E) Calcite-rich breccia from the Hillesøya fault cropping out in a ~1.5 m-thick zone.

commonly trend N–S, locally also NE–SW, and are parallel to a moderately E-dipping foliation in the gneisses. The footwall outcrop is increasingly deformed towards the east, with the occurrence of cataclastic rocks within the amphibolitic gneiss. The tonalitic gneisses are commonly red-stained from hydrothermal alteration (Fig. 5A) and fracture surfaces coated with chlorite are cut by fractures coated by quartz, which, in turn, are cut by fractures coated with hematite. The slip-linear fault data (Fig. 4A) indicate an oblique-dextral normal movement with down-to-the-SE displacement of the hanging wall.

The Stonglandseidet and Sifjorden fault zones on Senja occur largely within massive to weakly foliated granite (Fig. 2). The Stonglandseidet fault zone strikes *c.* ENE–WSW (Fig. 4B) and its fault core zone is *c.* 100 m wide and associated with carbonate-rich, cataclastic fault rocks. Faults trend mainly ENE–WSW with variable dips to the SE and NW, in addition to a subordinate set of faults trending NNE–SSW, also dipping both SE and NW. The damage zone on the southern, hanging-wall side extends for *c.* 400 m and comprises granitic and silica-rich fault zones. A presumed Caledonian foliation in the granites on the southern side dips gently to the southeast when approaching the biotite schist in the southernmost portion of the mapped area (Fig. 4B). The Stonglandseidet fault zone has a presumed down-to-the-SSE sense of shear (Forslund, 1988), based on an apparent down-drop of a Caledonian thrust that encircles the Stonglandeidet peninsula. The Sifjord fault zone (Fig. 2A) has not been studied in association with the present work, but defines a system of alternating NW- and SE-dipping, conjugate, normal fault zones with numerous epidote- and chlorite-rich fracture sets and slickensides indicating oblique-normal fault movement, down-to-the-SE (Gagama, 2005).

Other minor fault zones on Senja include the Grasmyrskogen and Nybygda faults (Fig. 2B), located within Caledonian rocks of the Upper Allochthon Lyngsfjellet Nappe Complex (Zwaan et al., 1998) or close to the thrust contact between the Lyngsfjellet Nappe Complex and the basement rocks in the southeastern part of Senja. The Grasmyrskogen fault (Fig. 4C) strikes NNE–SSW, dips to the E, and makes up a left-stepping, partly linked system of fault traces, partly excavated by a river that cuts through granitic augen gneiss in the outcrop's northern parts and amphibolitic schist in the southern part. The slickensided surfaces indicate a normal, dip-slip, down-to-the-ESE fault movement.

The Grasmyrskogen fault is connected to the NNE–SSW-striking and E-dipping Nybygda fault (Fig. 4D) farther south, which is located within banded biotite schist in the northwestern part of the locality and marbles and calc-silicate rocks in the southeastern part. Foliation dips gently NE. Minor faults predominantly dip steeply to ESE. A normal, down-to-the-ESE sense of movement is interpreted from slickensided surfaces (Fig. 4D).

The landward fault zones are generally poorly exposed, but they are interpreted to have had a considerable impact on the younger valley, fjord and sound topography. The fault cores and damage zones most likely caused the faults to act as preferred zones of ice-sheet drainage during the last glacial periods.

Seaward fault zones

The most important fault zones exposed on the western side of the WTBC include the NNE–SSW- to NE–SW-striking, east-dipping Rekvika, Bremneset, Tussøya and Hillesøya fault zones (Figs. 2, 4E–H). These faults do not display the same significant influence on the topography as the landward fault zones, but locally coincide with fault escarpments along strike. These western fault zones are located within variably foliated tonalitic and quartz-dioritic gneisses of the Kattfjord Complex (Zwaan et al., 1998; Bergh et al., 2010), and the enclosed Ersfjord granite, a massive to well foliated granitic intrusion (Andresen, 1980).

The Rekvika fault zone (first described by Antonsdottir, 2006) strikes NE–SW, dips SE (Fig. 4E) and cuts through the contact between weakly foliated Ersfjord granite and the Kattfjord Complex, which runs partly onshore and partly offshore along the coastline. The fault is characterised by a ~200–300 m-wide zone of hydrothermally altered red granite and minor cataclastic fault rocks that can be traced for *c.* 300 m along strike. The contact between the Ersfjord granite and the Kattfjord Complex is characterised by a boundary-parallel foliation within the granite, and with NE–SW- and NNW–SSE-striking, ductile shear zones splaying out from the contact. One large, curvilinear shear zone striking NNW–SSE bends into parallelism with the Rekvika fault zone. The latter consists mainly of protocataclastic and altered granite in the footwall, increasingly cut by quartz veins when approaching the core zone. The core zone is 2–3 m thick and consists of completely silicified ultracataclastic fault rocks with minor hematite. The damage zone in the footwall is typically 30–50 m wide, while the hanging wall shows little or no damage. The granite surrounding the Rekvika fault zone shows conspicuous hydrothermal alteration (red-coloured, iron-oxide staining in granite). Slickensided surfaces indicate oblique, normal, down-to-the-SE movement (Fig. 4E; Antonsdottir, 2006).

Farther south, at Bremneset and Tussøya (Fig. 4F, G), similar fault zones crop out (Fig. 2). They contain prominent cataclastic fault rocks and a hydrothermal alteration similar to that observed in Rekvika. The faults dip *c.* 60° southeast, largely parallel to the foliation of the host rock gneisses. At Bremneset, the fault zone occurs as a 0–3 m-thick, NNE–SSW-striking, E-dipping, cataclastic zone, *c.* 200 m long in the Kattfjord Complex (Fig. 5B). Fracture/fault surfaces commonly carry an epidote precipitate, and they are locally cut by younger faults/fractures with hematite staining. The gneiss foliation is locally at a moderate angle to the fault zone (Fig. 4F). Slickensided surfaces and minor fault offsets (Figs. 4F, 5C) suggest normal, down-to-the-ESE fault movement.

The Tussøya fault zone (Fig. 4G) strikes NNE–SSW, dips moderately southeast and juxtaposes granite in the footwall against banded gneisses in the hanging wall (Fig. 5D). Foliation in the gneisses is gently folded, but generally subparallel to the fault zone. The fault crops out as a 1–3 m-thick, proto- to ultracataclastic zone, characterised by altered granite in the host rock cut by dark bands of ultracataclasite. The granite in the footwall is red–stained through hydrothermal alteration, as observed at Rekvika, with the alteration occurring within a 200 m-thick zone approaching the fault. The footwall is more deformed than the hanging wall, although altered granite also occurs in the hanging wall. Subsidiary, ENE–WSW-trending, dextral normal faults interact with the overall main NNE–SSW fault trend and are displaced by the main fault (Fig. 4G). Slickensided surfaces suggest oblique-sinistral, normal, down-to-the-SE movement along the main fault trace (Fig. 4G).

The Hillesøya fault zone (Fig. 4H) in southwestern Kvaløya is defined by segments of parallel faults trending NNE–SSW, dipping to the east, and commonly merging with subsidiary NNW–SSE faults. It is located on the steep northwestern limb of a macro-scale subvertical fold that may have controlled its location (Thorstensen, 2011). The fault zone is parallel to the foliation in amphibolitic gneisses and confined to granitic pegmatite sheets within the gneisses. Zones of breccia, 1.5–2 m wide with angular clasts of red pegmatite granite and amphibolite embedded in a matrix of calcite, are common (Fig. 5E). Clasts are cross-cut by epidotised veins, which, in turn, are cut by calcite-bearing veins. Other, less prevalent

faults with slickensides are common, revealing oblique-sinistral normal movement, down-to-the-ENE (Fig. 4H).

The subsidiary NNW–SSE-striking, ENE-dipping faults on Hillesøya are atypical compared with most other brittle fault zones in the WTBC, and are subparallel to the Svecofennian, NNW–SSE-trending Senja Shear Belt (Zwaan, 1995).

Central fault zones

Two major fault zones located in the interior parts of the WTBC horst have been studied and are further described here. These include the Vannareid–Burøysund fault zone on Vanna (first described by Opheim & Andresen, 1989) and a brittle fault zone that truncates the Mjelde–Skorelvvatn belt (Armitage, 1999; Armitage & Bergh, 2005) (Figs. 2, 4I). The ENE–WSW-trending and *c.* 60° southward-dipping Vannareid–Burøysund fault zone is developed in Neoarchaean tonalitic and quartz-dioritic gneisses and downdrops the presumed Palaeoproterozoic Skipsfjord Nappe by at least 3 km (Opheim & Andresen, 1989). The fault zone is marked in the topography by an ENE-WSW-trending valley in the northern parts of Vanna, showing an at least 20 m-wide cataclastic zone composed of proto- to ultracataclasites. Slickensided surfaces indicate a pure dip-slip, down-to-the-SSE displacement along the fault.

The Skorelvvatn fault zone (Fig. 4I) strikes ENE–WSW, dips steeply NNW and offsets distinctive metavolcanic rocks of the Palaeoproterozoic Skorelvvatn Formation (Armitage, 1999) as well as adjacent host-rock migmatites and diorites of the Neoarchaean gneisses. Cataclasites, 0.5–5 m thick, occur along the escarpment, and individual fault surfaces show great variation in geometry, with interacting ENE–WSW and NE–SW fault segments constituting the main fault zone. The main fault zone displays oblique-sinistral, normal fault movement (Fig. 4I). The fault is at a high angle to foliation and fault surfaces are in general epidotised with minor faulting increasing in frequency from <100 m when approaching the core zone. Slickensides on the main fault surfaces indicate an oblique-sinistral, normal sense of shear (Fig. 4I). A minimum of 250 m down-to-the-SSE displacement is calculated for the fault zone, by assuming *c.* 100 m apparent dextral, horizontal displacement of the Bakkejord diorite and perpendicular surface traces of the fault relative to the host-rock foliation.

Offshore fault complexes and associated basins

The relationship between onshore fault complexes and faults on the Finnmark Platform, and how they correlate, both spatially and temporally with basin-bounding faults in the SW Barents Sea, is not well understood. The present work is focused on linking major faults associated with the Tromsø, Hammerfest and Harstad basins, including the Troms–Finnmark, Ringvassøy–Loppa, Måsøy and Nysleppen fault complexes (Fig. 1), with faults on the Finnmark Platform and onshore fault complexes (Fig. 6).

Seismic stratigraphy

The seismic stratigraphy within different offshore basins and platforms was determined based on correlation with available well data (Fig. 3). Horizons in the Hammerfest Basin were tied to the well 7120/12–2 which penetrates most of the Palaeozoic and Mesozoic succession and terminates in crystalline basement composed of biotite augen gneisses. In the Harstad Basin, well 7019/1–1 and IKU's shallow stratigraphic cores (Fig. 3; wells 7018/5 –1, –2 & –6, cf., Smelror et al., 2001) have been used to tentatively identify top Cretaceous and top Jurassic seismic reflection events (Fig. 7A, B). Since none of these wells penetrate deeper than Mid Jurassic, top crystalline basement in the Harstad Basin has been picked on a deep, gently dipping, seismic reflection into which the interpreted faults deflect and merge (Fig. 7A, B). This seismic reflection is interpreted to represent a low–angle detachment zone forming the continuation of the listric TFFC in depth. Due to the extreme extension and rotation of basement fault blocks along the TFFC in this region, the detachment is interpreted to represent the boundary between Palaeozoic–Mesozoic sedimentary strata and basement. On the Finnmark Platform, the top of the crystalline basement may be traced as a seismic unconformity, dipping gently seawards towards the Harstad and Hammerfest basins from the WTBC and terminating against the TFFC (Fig. 7A–D). The unconformity clearly divides younger strata from the acoustically chaotic to transparent reflection pattern interpreted to represent basement rocks. The depth of the unconformity is verified by well 7120/12–4 on the Finnmark Platform that terminates in the Late Carboniferous Ugle Formation. In the adjacent well 7120/12–2, located ~10 km north of 7120/12–4 in the Hammerfest Basin, the Ugle Formation is ~100 m thick, overlying basement.

Description of offshore structures

The Troms–Finnmark Fault Complex (TFFC) is one of the most distinct fault complexes offshore and is composed of alternating NNE–SSW and ENE–WSW- to E–W-striking fault segments linked together in a zigzag pattern similar to that seen onshore (Fig. 6). The fault complex can be traced from Andfjorden in the south, as a northward continuation of the fault systems of the Lofoten Ridge, running outboard and parallel to the West Troms Basement Complex (Fig. 1). In this region, the TFFC is composed of a set of parallel, NW-dipping, listric faults with a large amount of displacement, down-faulting the basement from about 4 s twt, or ~4–5 km depth on the Finnmark Platform, to possibly more than ~7 s twt, corresponding to ~10 km depth in the Harstad Basin (Fig. 7A, B). The Finnmark Platform in this region is characterised by Late Palaeozoic to Early Mesozoic sedimentary strata overlying presumed crystalline basement (Smelror et al., 2001). The presence of a thick

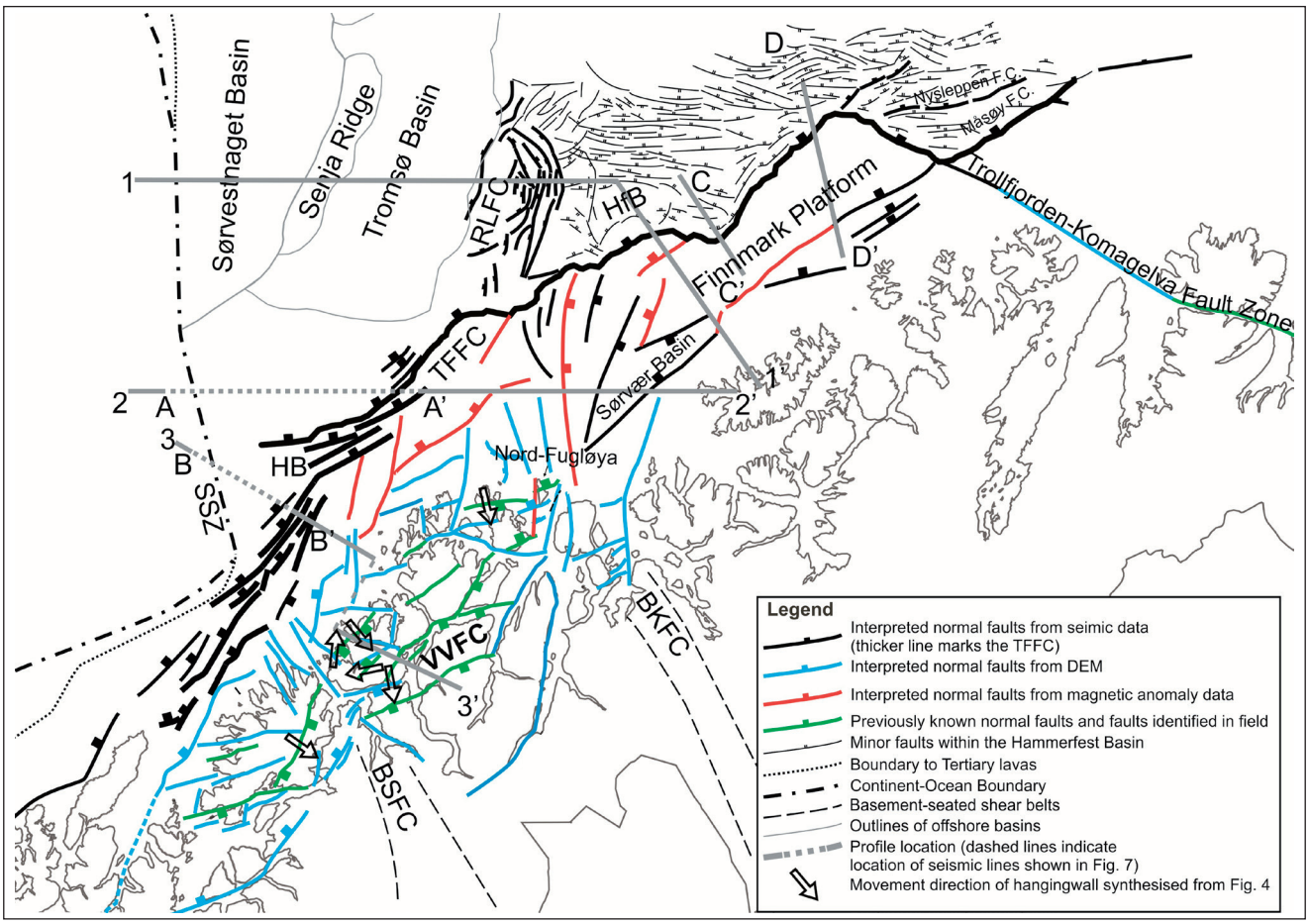

Figure 6. Regional map summarising the architecture of the SW Barents Sea margin based on interpreted lineaments from onshore fieldwork (green lines), DEM (blue lines), magnetic anomaly data (red lines) and seismic interpretation (black lines). Arrows indicate synthesised hanging-wall movement direction from the different fault zones given in Fig. 4. Profiles 1–1', 2–2' and 3–3' are shown in Fig. 10. The dashed parts of the profile lines indicate location of seismic sections A–A' to D–D' given in Fig. 7. Abbreviations: BKFC – Bothnian–Kvænangen Fault Complex, BSFC – Bothnian–Senja Fault Complex, RLFC – Ringvassøy–Loppa Fault Complex, SSZ – Senja Shear Zone, TFFC – Troms–Finnmark Fault Complex, VVFC – Vestfjorden–Vanna Fault Complex.

Cretaceous sedimentary succession in the Harstad Basin indicates that the southern portion of the TFFC had its most important phase of activity in the Cretaceous (cf., Gabrielsen et al., 1990). Close to the intersection between the TFFC and the Ringvassøy–Loppa Fault Complex, the TFFC changes its orientation to an ENE–WSW strike, and becomes a complex, anastomosing series of left-stepping fault segments (Fig. 6). East of the intersection between the Troms–Finnmark and Ringvassøy–Loppa fault complexes, the amount of displacement along the TFFC decreases to less than 3 km of down-to-the-NW movement in the Hammerfest Basin (Fig. 7C, D; cf., well 7120/12–2 and 7120/12–4, npd.no). Seismic interpretation reveals that N–S-striking steep faults dominate on the Finnmark Platform side of the TFFC in the area of shift, and that this may be linked to a change in TFFC characteristics (Fig. 6). The TFFC is therefore divided into a northern and a southern segment in the description herein, based on structural style and orientation, with the divide marked by the intersection with the Ringvassøy–Loppa Fault Complex (Fig. 8).

The Ringvassøy–Loppa Fault Complex (Fig. 6) divides the relatively shallow Hammerfest Basin in the east from the deep Tromsø Basin in the west, down-faulting base Cretaceous from less than 2 s twt in the Hammerfest Basin to more than 7 s twt in the Tromsø Basin within a distance of 30 km (Brekke et al., 1992). The fault complex is made up of a series of west-dipping curvilinear faults, and a very thick sequence of Cretaceous strata reveals that the main subsidence of the Tromsø Basin occurred during the Cretaceous. Even so, early phases of subsidence during the Carboniferous may have allowed for the deposition of evaporites within the Tromsø Basin, visible today by the occurrence of salt diapirs within younger strata in the basin (e.g., Brekke et al., 1992).

The northern segment of the TFFC separates the Finnmark Platform on the landward side from the Hammerfest Basin in the north (Fig. 6). This segment of the TFFC is characterised by faulting localised on one major fault, not several, at least as observed within the given seismic resolution. On the Finnmark Platform, top basement dips gently northwards and can be traced

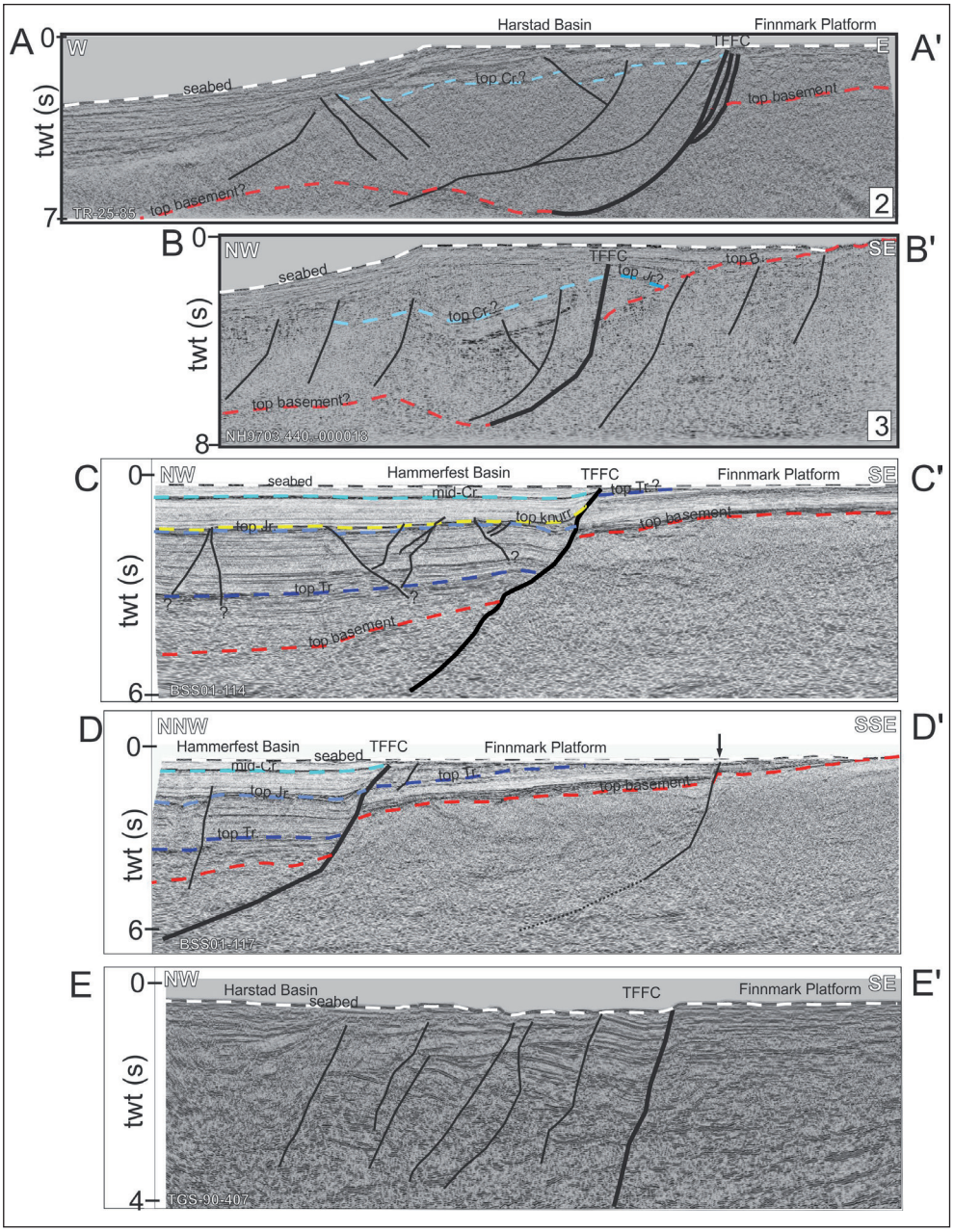

Figure 7. *Examples of interpreted seismic sections from the SW Barents Sea margin. (A) Interpreted seismic section showing faults and important horizons along profile B (Fig. 6) from the Finnmark Platform into the Harstad Basin. This section is part of onshore-offshore profile 2 in Fig. 10. (B) Interpreted section along profile C (Fig. 6). Note how basement is down-faulted along the listric Troms–Finnmark Fault Complex in the Harstad Basin. This section is part of onshore-offshore profile 3 in Fig. 10. (C) Interpreted seismic section C–C' (Fig. 6) showing faults and important horizons traced from the Finnmark Platform into the Hammerfest Basin. Note that the basement is much less down-faulted than in the Harstad Basin and is overlain by Late Palaeozoic and Early Mesozoic sedimentary strata on the Finnmark Platform. (D) Interpreted seismic section D–D' (Figs. 6, 9B) showing that the magnetic anomaly lineament identified in Fig. 9B is a listric normal fault, dipping towards the NW (black arrow). (E) Interpreted seismic section E–E' (Figs. 6, 9A) showing how the Troms–Finnmark Fault Complex reaches the seabed and influences seabed morphology in the Håkjerringdjupet.*

from the coast, where it crops out at the seabed, towards the TFFC where it lies at ~2.5 km depth (Larssen et al., 2002; cf., 7120/12–4, npd.no). Basement is overlain by a wedge-shaped prism of Carboniferous to Early Triassic sediments that onlap crystalline basement southward towards the Norwegian mainland (Fig. 7C). Internally, the Hammerfest Basin shows distributed Late Jurassic/Early Cretaceous faults that control the distribution of the Ryazanian–Hauterivian Knurr Formation which thickens toward the TFFC, indicating that the main subsidence started in the Late Jurassic, with displacement localising to the TFFC during the Early Cretaceous (Fig. 7C).

Farther east-northeast, along the northern segment of the TFFC, the Måsøy and Nysleppen fault complexes are situated where the seaward extension of the Trollfjorden–Komagelva Fault Zone truncates the TFFC, northwest of Nordkapp (Fig. 6). Notably, the northeastern portion of the TFFC and the Måsøy Fault Complex are composed of a series of linked fault segments that trend NE–SW and E–W to NW–SE. NE–SW-striking fault segments commonly splay out from the main TFFC trace where fault segments of different orientations meet, continuing onto the Finnmark Platform (Fig. 6).

Onshore-offshore relationships using DEM and magnetic anomaly data

It is challenging to link the offshore parts of the fault complexes to the onshore parts on account of the physical separation of the datasets and the differences in their spatial resolution. However, a link may be provided from

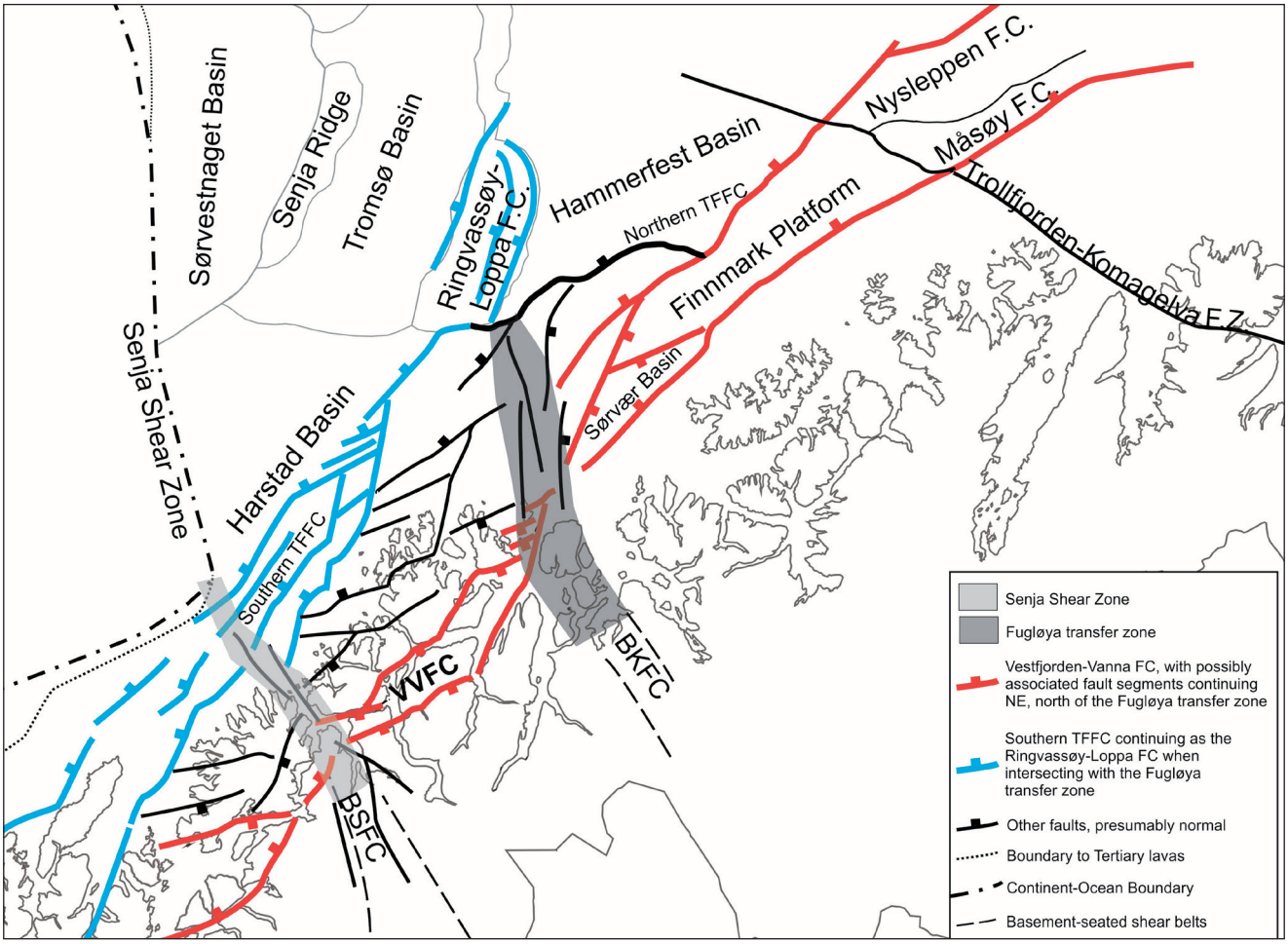

Figure 8. *Simplified tectonic map of the SW Barents Sea region linking major NNE–SSW- and ENE–WSW-trending fault complexes onshore and offshore. At least two major transfer zones accomodate change in polarity and stepping of fault zones along the margin: (i) The Senja Shear Zone, located along the reactivated Precambrian Senja Shear Belt and Bothnian-Senja Fault Complex (BSFC) and (ii) the Fugløya transfer zone, a possible continuation and reactivated section of the Bothnian Kvænangen Fault Complex (BSFC).*

bathymetry (DEM) and magnetic anomaly data from the shallow shelf portion of the margin, and consequently a valid fault correlation may thus be possible. In order to correlate and/or extend offshore and onshore fault traces, we mapped tectonic lineaments onshore and on the shallow and deep shelf areas, where seismic data coverage is insufficient, using DEM and magnetic data (Figs. 2B, 9).

Onshore DEM data show that relatively high mountain peaks and deep fjords, typical for glaciated margins, characterise the coastal region of western Troms and Finnmark. The fjords, sounds and large valleys are commonly oriented NNE–SSW and ENE–WSW, possibly reflecting the network of brittle faults in the region and resulting in a zigzag pattern of the fjords and sounds (Fig. 2). Where fault zones splay out and converge again, e.g., near the islands of Tromsø and Reinøya, they leave behind rhombohedra-shaped islands (Fig. 2A).

The shallow shelf is characterised by a gentle relief surface at 0–100 m below sea level with many shallow, semi-linear, elongated depressions up to tens of kilometres long (Figs. 2B, 9A). Locally, these features can be traced onshore as continuous lineaments (Fig. 2B). The shallow shelf appears as a 5–15 km-wide zone between the islands and the deep shelf, and is identified as a strandflat (Fig. 9A; Thorsnes et al., 2009), i.e., flat coastal regions eroded into crystalline basement rocks. Any minor relief produced by brittle palaeo-faults and/or fractures such as narrow scarps, ridges and/or depressions would therefore be easy to identify. The same is apparent for Precambrian (ductile) elements such as folds, foliations and ductile shear zones (cf., Thorstensen, 2011) that may have controlled the location of brittle faulting. Interpretation of lineaments on the strandflat is therefore a very useful tool in mapping orientations of faults and fractures close to shore.

A key observation in verifying bathymetry (DEM) as a valid correlation tool on the shallow shelf is where bathymetric lineaments can be traced onshore where they coincide with known onshore fault outcrops, for instance at the Stonglandseidet and Kvaløysletta–Straumsbukta fault zones (Fig. 2B). Another key observation is when

the transition from strandflat to glacial deposits is linear and sharp. In such cases, if these sharp transitions define the same geometric (map) patterns and orientations as the observed (onshore-offshore) faults, the transition is then interpreted to mark the surface trace of a fault. Our interpretation reveals that NNE–SSW- and ENE–WSW-trending faults/fractures caused by down-faulting of the crystalline basement, allowing it to be covered by glacigenic sedimentary strata, are common on the strandflat (Fig. 9A). Furthermore, interpreted faults/fractures on the internal portions of the strandflat generally show the same orientations as onshore faults (Figs. 2B, 9A).

NW–SE-trending lineaments locally dominate the seabed relief, such as between Senja and Kvaløya near the location of the Svecofennian Senja Shear Belt. A similar area, dominated by NW–SE- to N–S-trending lineaments in the crystalline bedrock, occurs around Nord-Fugløya (Fig. 9A). The lineaments there continue N to NW off Nord-Fugløya and presumably extend all the way to the TFFC, although the northern part is covered by glacigenic sediments on Nordvestbanken (Fig. 9A).

The deep portion of the shelf in the region has, in general, a glacially controlled morphology with troughs, banks and other glacial features (cf., Rydningen et al., 2013),

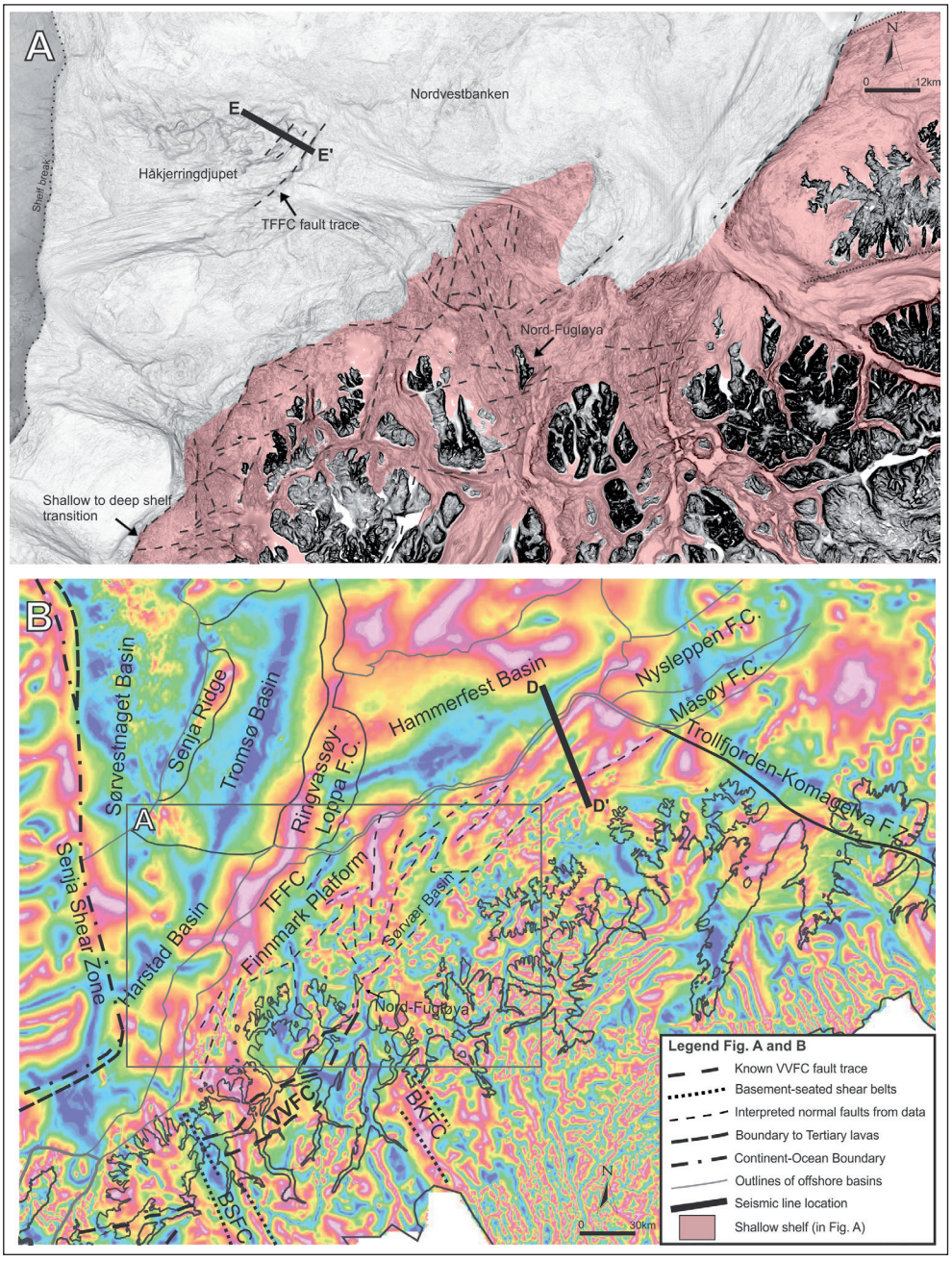

Figure 9. Examples of interpreted DEM and magnetic data from the SW Barents Sea margin. (A) Enlargement of the DEM showing the strandflat (light pink) and interpretations of lineaments within the onshore- and strandflat portion of the margin (see Fig. 9B for location). Note the shallow to deep shelf transition traceable as interchanging NNE–SSW- and ENE–WSW-trending lineaments, interpreted as normal faults, and the NW–SE-trending lineaments around Nord-Fugløya, proposed to be the surface traces of a transfer fault zone. The Håkjerringdjupet area is the only part of the deep shelf where bathymetry lineaments have positively been identified as tectonic, in this case the surface trace of the TFFC. Seismic line E–E' is shown in Fig. 7. (B) The tilt-derivative of the HRAM–98 and NGU69/70 provided by the Geological Survey of Norway. Major structures are shown offshore. Thin lines show lineaments which are interpreted to be normal faults. Profile D–D' is shown in Fig. 7 and confirms that the lineament shown is a normal fault dipping NW. Boxed area shows location of Fig. 9A.

and lineaments on the deep shelf are largely a product of glacial erosion and deposition rather than tectonically generated lineaments. Even the prominent structural elements such as the TFFC and the Ringvassøy–Loppa Fault Complex do not influence the seafloor morphology in any clear way, except at one locality in the Håkjerringdjupet where likely glacial erosion has exposed the TFFC escarpment by plucking blocks of sediment that detached along the fault plane (Figs. 7E, 9A).

The magnetic anomaly data (Fig. 9B) show many distinct lineaments traceable over tens of kilometres, defined by either continuous high or low values or as changes in the appearance of anomalies across a lineament, such as wavelength (Fig. 9B). From seismic interpretation the mapped TFFC locally coincides well with a high-value, subcontinuous, anomaly lineament traceable along the coast and thereby supports the notion that some visible magnetic lineaments may be the product of faults (Fig. 9B). Even so, the known boundary faults of the West Troms Basement Complex, i.e., the Vestfjord–Vanna Fault Complex, only partly produce a linear anomaly pattern, expressed at its clearest along its northern portion, southwest of Nord-Fugløya (Fig. 9B). Anomalies produced by the VVFC are thus interpreted to be locally too weak in comparison with other magnetic sources (e.g., the Ersfjord granitic intrusion) and cannot, at least onshore, be mapped with sufficient confidence, as other sources, such as spatial variations in crust lithology (e.g., magmatic intrusions, shear zones, mafic and felsic rocks, etc.), may also influence the signal.

However, the magnetic data may be used to support the interpretation of the DEM and seismic data, to provide an additional basis for correlation of faults, and to strengthen interpretations in areas on the shelf where the crystalline basement is covered by glacigenic sediments and therefore not visible on the DEM. For instance, in the area around and north of Nord-Fugløya (Fig. 9A), bathymetric lineaments strike NW–SE and N–S and presumably continue across the sediment-covered Nordvestbanken. The magnetic anomaly data show a distinct high-value anomaly, trending ~N–S and continuing all the way to the TFFC (Fig. 9B), suggesting that the bathymetric lineaments identified in the vicinity of Nord-Fugløya on the DEM are part of a feature that may link with the TFFC. Other magnetic lineaments also coincide with the transition between the strandflat and the deeper shelf outboard of western Troms and on the Finnmark Platform, thereby supporting the interpretation that these transitions represent faults where the basement has been down-faulted adequately to produce a notable change in magnetic anomaly pattern, thus indicating that this transition is tectonically controlled. Another example is in regions where the TFFC changes strike from NE–SW to E–W or ESE–WNW along the southern border of the Hammerfest Basin (Fig. 9B). Magnetic lineaments suggest that fault segments splay out from the TFFC, southwest onto the Finnmark Platform (Fig. 9B). These faults, which can partly be confirmed by seismic data (Fig. 7D), may be traced for tens of kilometres onto the Finnmark Platform, running parallel to the coast. In fact, the easternmost of these lineaments can be traced southwestwards from the Måsøy Fault Complex, parallel to the coast, continuing along the southeastern boundary fault of the Sørvær Basin and all the way to the island of Nord-Fugløya, where it meets up with the Vestfjorden–Vanna Fault Complex (Fig. 9B). Seismic data from this area show that this lineament is a likely listric normal fault zone dipping towards the NW with *c.* 500 m of displacement (Figs. 7D, 9B). Similarly, a magnetic anomaly lineament can be traced southwestwards from the intersection between the TFFC and the Nysleppen Fault Complex, trending parallel to the TFFC and onto the Finnmark Platform, and continuing SW to the above-described, ~N–S-trending anomaly close to Nord-Fugløya (Fig. 9B).

All the above-mentioned lineaments visible on the available magnetic anomaly data are expressed more clearly in newer data, published by Gernigon & Brönner (2012, their Fig. 3). Their data show that the NW–SE- to N–S-trending lineaments in the vicinity of Nord-Fugløya can be traced outboard to the TFFC (Fig. 9B), and that the lineament produced by the NE–SW-trending, NW-dipping listric fault as identified in Figs. 7D & 9B defines the southeastern boundary fault of the Sørvær Basin and merges with the southeastern boundary fault of the Nordkapp Basin in the northeast.

Discussion

In this section we argue for a correlation of onshore and offshore major fault zones based on the field mapping and interpretation of seismic, DEM and magnetic anomaly data. We use the structural relationships as a basis for discussing structural architecture, fault timing, basement control and evolution of the SW Barents Sea margin. We focus the discussion on faults linked to the WTBC and surrounding coastal areas of western Troms (Figs. 1, 2).

Correlation and margin architecture

The West Troms Basement Complex horst is bounded to the southeast by the SE-dipping VVFC (Figs. 6, 8), which displays 1–3 km of down-to-the-SE normal movement (Andresen & Forslund, 1987; Forslund, 1988; Opheim & Andresen, 1989; Olesen et al., 1997). Interpreted magnetic anomaly and seismic data (Figs. 6, 9B) show that the onshore VVFC largely mimics the zigzag geometry of the offshore TFFC. Offshore, just east of the island of Vanna, the VVFC is replaced by a set of NW-dipping fault segments that is interpreted to link up with the Måsøy Fault Complex and continue farther NE into the Nordkapp Basin (Smelror et al., 2009).

The westernmost mapped fault zones of the WTBC include the Rekvika, Bremneset, Tussøya and Hillesøy fault zones (Fig. 8). These individual fault zones show similarities in geometry, fault rocks and movement character (Figs. 2, 4E–H), indicating that they are associated with each other and constitute fault segments within a common fault system running along the outer rim of the islands of the WTBC. These western fault zones of the WTBC are characterised by NE–SW- to N–S-trending fault segments that commonly show red staining of host-rock granites, and comprise cataclastic fault rocks and hydrothermal alteration zones with precipitates of epidote, chlorite, quartz, calcite and/or hematite on fault/fracture surfaces. Kinematic data mostly reveal normal to oblique-normal, down-to-the–SE fault movement. From these similarities, we suggest that the fault zones may link up as en échelon, right-stepping, fault segments that run parallel to the VVFC. On the other hand, these fault zones clearly do not define the northwestern limit of the WTBC horst, since: (i) the kinematic data yield down-to-the-SE displacement, opposite of what would be expected for the bounding fault complex, (ii) the observed data do not match the VVFC in the form of amount of displacement, damage-zone width or impact on topography, and (iii) they do not juxtapose WTBC rocks with other (e.g., Caledonian) rocks. It is suggested that these fault zones only accommodated horst-internal displacement in the order of hundreds of metres or less, based on similarity with the Skorelvvatn fault zone, where the minimum displacement was estimated to 250 m. Instead, the actual west-bounding limit or boundary fault(s) of the WTBC horst is located farther northwest, at the southern segment of the TFFC (Figs. 6, 8). Seismic interpretation (Fig. 7A, B) suggests that the WTBC horst stretches all the way to the TFFC with only minor, horst-internal, down-faulting of basement occurring on the Finnmark Platform.

The northern segment of the TFFC (northeastwards from the intersection with the Ringvassøy–Loppa Fault Complex) is clearly different from the southern segment, displaying considerably less displacement and, locally, a WNW–ESE trend (Figs. 7C, 8). The Ringvassøy–Loppa Fault Complex, however, based on similarities in fault segment orientations and amount of displacement, is suggested to be the natural continuation of the southern segment of the TFFC (Figs. 6, 8).

The above-mentioned changes in the characteristics of the TFFC where it intersects with the Ringvassøy–Loppa Fault Complex are suggested to be due to the interaction with an inferred NW–SE- to N–S-trending zone that continues onto the Finnmark Platform with a comparable trend to that of the Trollfjorden–Komagelva Fault Zone and the Senja Shear Zone (Figs. 1, 8). This NW–SE-trending zone is confirmed by studies of shallow shelf bathymetry, onshore DEM data and magnetic anomaly data, showing a complex pattern of interacting lineaments trending NW–SE to N–S (Figs. 6, 9) across the Finnmark Platform close to Nord-Fugløya. Moreover, the NE–SW-trending fault segments traceable across the Finnmark Platform from the Troms–Finnmark, Nysleppen and Måsøy fault complexes, meet up and terminate against this same zone (Figs. 6, 8). From the south, the VVFC and the horst-internal fault zones, such as the Vannareid–Brurøysund fault zone, also terminate against the same NW–SE-trending zone. Thus, we suggest the presence of a previously not described transfer zone that runs NW–SE from the mainland near Nord-Fugløya, as a continuation of the Bothnian–Kvænangen Fault Complex, to link up with the TFFC. This transfer zone is termed the Fugløya transfer zone (Fig. 8). The fault segments bounding the Sørvær Basin and continuing northeastward may, tentatively, all be associated with the VVFC. This interpretation is supported by the similarities in fault trends and amount of displacement. If so, the fault segments change polarity and are apparently offset sinistrally across the Fugløya transfer zone. Comparable domains or segments where the fault zones define a shift in polarity and/or step to a new position along strike can be observed farther south, where the VVFC intersects with the Senja Shear Zone, a possible continuation of the reactivated Precambrian Senja Shear Belt and Bothnian–Senja Fault Complex (Figs. 2, 8; Henkel, 1991; Olesen et al., 1997).

In summary, the architecture of the SW Barents Sea margin is controlled by at least two major fault complexes, the VVFC and the TFFC, which define the southeastern and northwestern boundary faults of the WTBC horst, respectively. The WTBC horst and potentially also other segments along strike of the horst are cut by widespread, internally distributed, fault zones with only modest displacements, as illustrated by the seaward fault zones of the WTBC (Figs. 2, 6). Faulting is clearly controlled by, and possibly offset across, the Senja Shear Zone and the Fugløya transfer zone, causing fault stepping and polarity change across the transfer zones. The Fugløya transfer zone also marks a change in characteristics of the TFFC, both in the amount of displacement and in geometry.

Basement control

The network of brittle faults that frame the SW Barents Sea margin (Figs. 6, 8) may, to some extent, have been controlled by ductile basement fabrics, such as the Svecofennian and/or Caledonian foliations and ductile shear zones, and possible later reactivation of these pre-existing structures. The Svecofennian fabrics are largely steeply inclined, NW–SE-trending, gneissic foliations and ductile shear zones (Bergh et al., 2010), whereas the Caledonian fabrics are gently NW- and SE-dipping (NE–SW-trending) thrusts and intra-nappe foliations (e.g., Roberts et al., 2007). Although it is not an easy task to document inheritance from older structures, some obvious controls may be inferred, at least on a local scale, from the onshore fault data:

Firstly, the Kvaløysletta–Straumsbukta and Rekvika fault zones are oriented parallel to Svecofennian foliations and/or ductile shear zones (Fig. 4A, E), and the Hillesøya fault zone (Fig. 4H), notably, is situated on the steep western limb of a Svecofennian macro-fold (Thorstensen, 2011). Furthermore, the core of the Tussøya fault zone (Fig. 4G) is located along a SE-dipping boundary between granite and foliated amphibolite gneisses, thus demonstrating that lithological boundaries, at least on a local scale, controlled localisation of brittle faulting.

Secondly, basement-seated, NW–SE-trending, Svecofennian ductile shear zones seem to have exerted a controlling effect on, e.g., the right-stepping, zigzag nature of Palaeozoic–Mesozoic brittle faults on the SE boundary of the WTBC. Similarly to the possible controlling element of the Precambrian Bothnian-Senja Fault Complex and Senja Shear Belt on the Senja Shear Zone, the NW–SE-trending, Bothnian–Kvænangen Fault Complex (Doré et al., 1997; Olesen et al., 1997) (Figs. 1, 2) may extend offshore as a controlling element for the Fugløya transfer zone (Fig. 8), the Ringvassøya–Loppa and Bjørnøyrenna fault complexes (Gabrielsen et al., 1997) and potentially also for the transform Hornsund–De Geer Fault Zone (Faleide et al., 1993) farther north (Fig. 1, inset map).

Implications for timing of margin evolution and exhumation

The finite stage architecture of the SW Barents Sea margin in western Troms is a complex network of Late Palaeozoic–Mesozoic, rift-related, brittle fault zones bounding onshore basement horsts and adjacent offshore basins (Fig. 6). It is apparent from the proposed correlation of margin fault systems (Fig. 8) that not only were the offshore Barents Sea basins affected by Late Palaeozoic–Mesozoic rift tectonics, but also a large portion of its surrounding onshore continental margin, including the Finnmark Platform, the WTBC and even areas east of the VVFC. The timing of faulting onshore in relation to offshore faulting, however, is still a matter of uncertainty and debate (Gabrielsen et al., 1990; Faleide et al., 2008; Davids et al., 2013).

The timing of initial (pre-) and syn-rift tectonic activity on the SW Barents Sea margin that led to the formation and evolution of the Harstad, Tromsø and Sørvestnaget basins and adjoining ridges, is constrained to the Carboniferous–Early Triassic from seismic data (Faleide et al., 2008), whereas onshore faults have recently been radiometrically dated to show Permian/Early Triassic movement (Davids et al., 2013). From the correlation of margin-bounding fault complexes in western Troms and Finnmark, one may infer that, as the precursor rift basins to the opening of the North Atlantic continued from south to north along the Norwegian margin, distributed Carboniferous–Early Triassic rifting propagated northward into the SW Barents Sea. The rifting occurred along at least two major, NE–SW-trending fault complexes, the southern segment of the TFFC and the VVFC, including fault segments continuing northeastwards north of the Fugløya transfer zone (Fig. 8). These faults then became the precursor boundary faults of, e.g., the Nordkapp and Hammerfest Basins, which further evolved in the Late Jurassic to Early Cretaceous (Gabrielsen et al., 1990; Faleide et al., 2008). In the Early Cretaceous, in association with the formation of the Hammerfest Basin, these early faults were linked by E–W- to ESE–WNW-trending faults to form the northern segment of the TFFC. In the same period, transform plate movements initiated along the Hornsund–De Geer Fault Zone (Faleide et al., 1993) causing a switch in strain, with localisation of displacement along the southern TFFC and the Ringvassøy–Loppa Fault Complex. This switch led to the deepening of the Harstad, Tromsø and Sørvestnaget basins and their further evolution as pull-apart basins throughout Cretaceous times (Faleide et al., 2008).

In the Late Cenozoic, the coastal part of the SW Barents Sea margin was uplifted as part of the Scandes mountains (Corner, 2005). The timing and nature of such uplift(s), including exhumation of basement ridges like the Lofoten Ridge and the West Troms Basement Complex and the corresponding rejuvenation of the margin, are still much debated (cf., Olesen et al., 1997; Mosar et al., 2002; Eig, 2008; Osmundsen & Ebbing, 2008; Steltenpohl et al., 2009; Hendriks et al., 2010; Redfield & Osmundsen, 2013). Various causes of uplift have been proposed, e.g., rapid switches in the regional strain and stress fields (Bergh et al., 2007; Eig, 2008), stress perturbations within transfer zones (Eig & Bergh, 2011), passive margin exhumation due to NW–SE–aligned ridge-push forces (cf., Grønlie et al., 1991; Gabrielsen et al., 2002; Mosar et al., 2002) and asthenospheric diapiric rise due to emplacement of the Iceland Plume and later climate deterioration with increased erosion (e.g., Rohrman & van der Beek, 1996; Nielsen et al., 2002; Pascal & Olesen, 2009). Recent work by Osmundsen & Redfield (2011) and Redfield & Osmundsen (2013) has proposed yet another driving force, suggesting that the uplift has been controlled by the hyperextended character of the Norwegian passive margin (e.g., Lundin & Doré, 2011). Even though the character of the hyperextended margin when crossing the Senja Shear Zone has not yet been discussed in the literature, the margin along the southern portion of the WTBC horst is characterised by a relatively short taper length (Redfield & Osmundsen, 2013). Due to the large amount of down-faulting of the basement along the southern segment of the TFFC, identified from interpreted seismic sections (Fig. 7A, B), the taper break is identified to run just west of, and parallel to the TFFC northwards in the Harstad Basin and into the Tromsø Basin, using depth-to-MOHO estimates from Faleide et al. (2008) and top-basement estimates from this study (Fig. 10). A short taper length is thought to give increased uplift due to unloading and flexure of the crust, resulting

in a higher topography in the hinterland and proximal margin (onshore regions) compared to portions of the margin with longer taper lengths (Osmundsen & Redfield, 2011). Our interpreted cross-sections of the West Troms margin (Fig. 10) illustrate how the different fault zones identified on land and offshore may have interacted to produce an overall narrow taper margin, thus providing a frame for discussing taper-controlled uplift and exhumation.

Onshore in the study area, faulting is characterised by presumably planar fault zones with modest displacements (hundreds of metres) within the WTBC horst, and steep, most likely deep-seated, horst-bounding major faults (VVFC) with 1–3 km displacement. These landward faults are presumed to be planar as no roll-over of foliation is observed when approaching the fault zones, as would be expected if the faults were listric. On the other hand, the corresponding northwestern limit of the WTBC horst is identified as the major listric, deep-seated, southern segment of the TFFC, which down-drops basement more than 5 km in the Harstad Basin (Fig. 10). Thus, the WTBC horst is clearly not a symmetric basement horst as seen, e.g., in the Lofoten or Senja ridges (Figs. 1, 10), where both sides of the horst are marked by major listric, deep-seated normal faults, but rather an asymmetric horst where most of the displacement was localised along the listric TFFC and the Ringvassøy–Loppa Fault Complex during the main phases of continental rifting. This geometry of the WTBC horst leads to a narrow taper length with a relatively high topography in the hinterland compared to areas of longer taper length, e.g., as in Mid Norway (see sections in Faleide et al., 2008; Osmundsen & Redfield, 2011; Redfield & Osmundsen, 2013). This relationship is inferred for the Troms region, as illustrated by the high peaks of the WTBC and the Lyngen Alps to the east of the WTBC. As final break-up occurred along this portion of the margin, the short tapered margin acted as a stiff body of crust rebounding due to unloading and ridge-push forces along the break-up axis. These forces may have been the controlling factors in the uplift of the WTBC, reactivating fault complexes such as the VVFC. A reactivation of brittle faults has been recorded in Mid Norway, constrained to have taken place after 100 Ma, suggesting displacements during reactivation of up to 2–3 km (Redfield et al., 2005). Similar reactivation may have occurred in western Troms as indicated by the presence of Cenozoic to recent fault gouge along some of the major fault zones (Olesen et al., 1997). Recent radiometric dating, however, suggests that any recent reactivation must have been only moderate in the Troms region in order to prevent a reset of the recorded Late Permian/Early Triassic, K–Ar and Ar–Ar ratios and fission-track ages within the fault rocks (Davids et al., 2013).

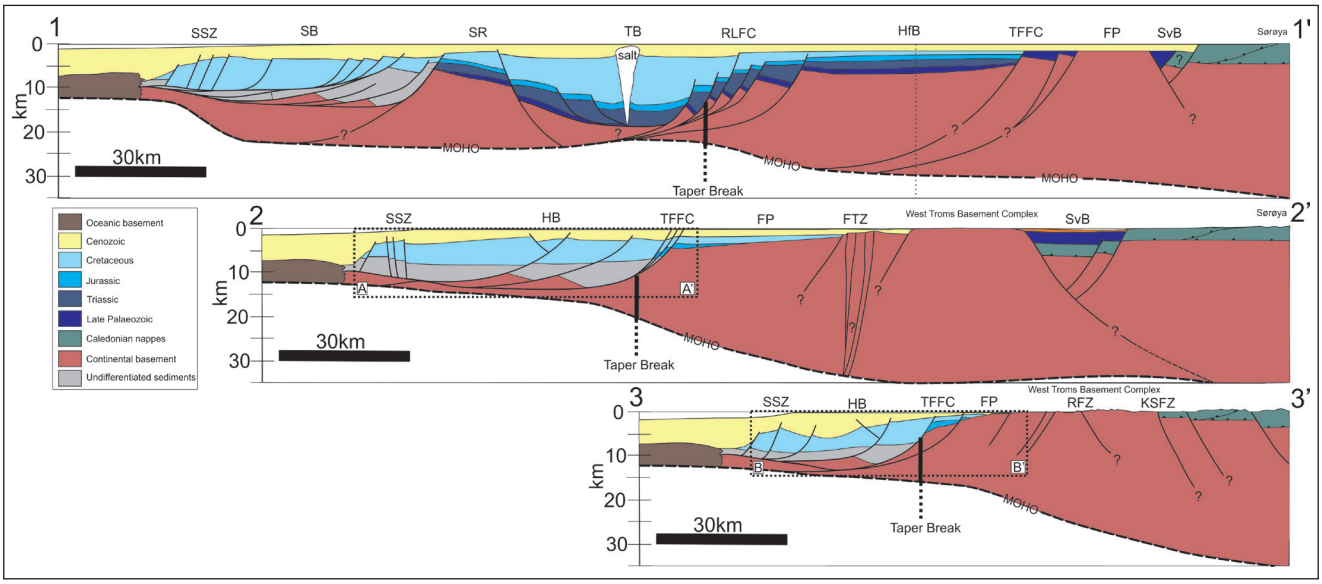

Figure 10. *Tentative crustal-scale, onshore-offshore sections across the SW Barent Sea margin based on interpreted seismic profiles and onshore fault data. Locations of the profiles are shown in Fig. 6. Location of the taper break is inferred from the seismic sections B–B' and C–C'. Moho depth is from Faleide et al. (2008). Dashed boxes in profiles B and C show the locations of seismic sections in Fig. 7. 1–1': Interpreted section extending from Sørøya westward to the continent-ocean transition. Note the moderate down-faulting of basement in the Hammerfest Basin compared to the significant down-faulting within the Tromsø Basin. From the RLFC westward, the section is based on Faleide et al. (2008). 2–2': Section running from Sørøya and into the Harstad Basin. Note that the basement is down-dropped considerably in the Harstad Basin. 3–3': Section extending from the mainland east of Tromsø and into the Harstad Basin. Note the asymmetric shape of the West Troms Basement Complex horst. Abbreviations: FP – Finnmark Platform; HB – Harstad Basin, HfB – Hammerfest Basin, FTZ – Fugløya transfer zone, RFZ – Rekvika fault zone, RLFC – Ringvassøy–Loppa Fault Complex, KSFZ – Kvaløysletta–Straumsbukta fault zone, SB – Sørvestnaget Basin, SSZ – Senja Shear Zone, SvB – Sørvær Basin, SR – Senja Ridge, TB – Tromsø Basin, TFFC – Troms–Finnmark Fault Complex.*

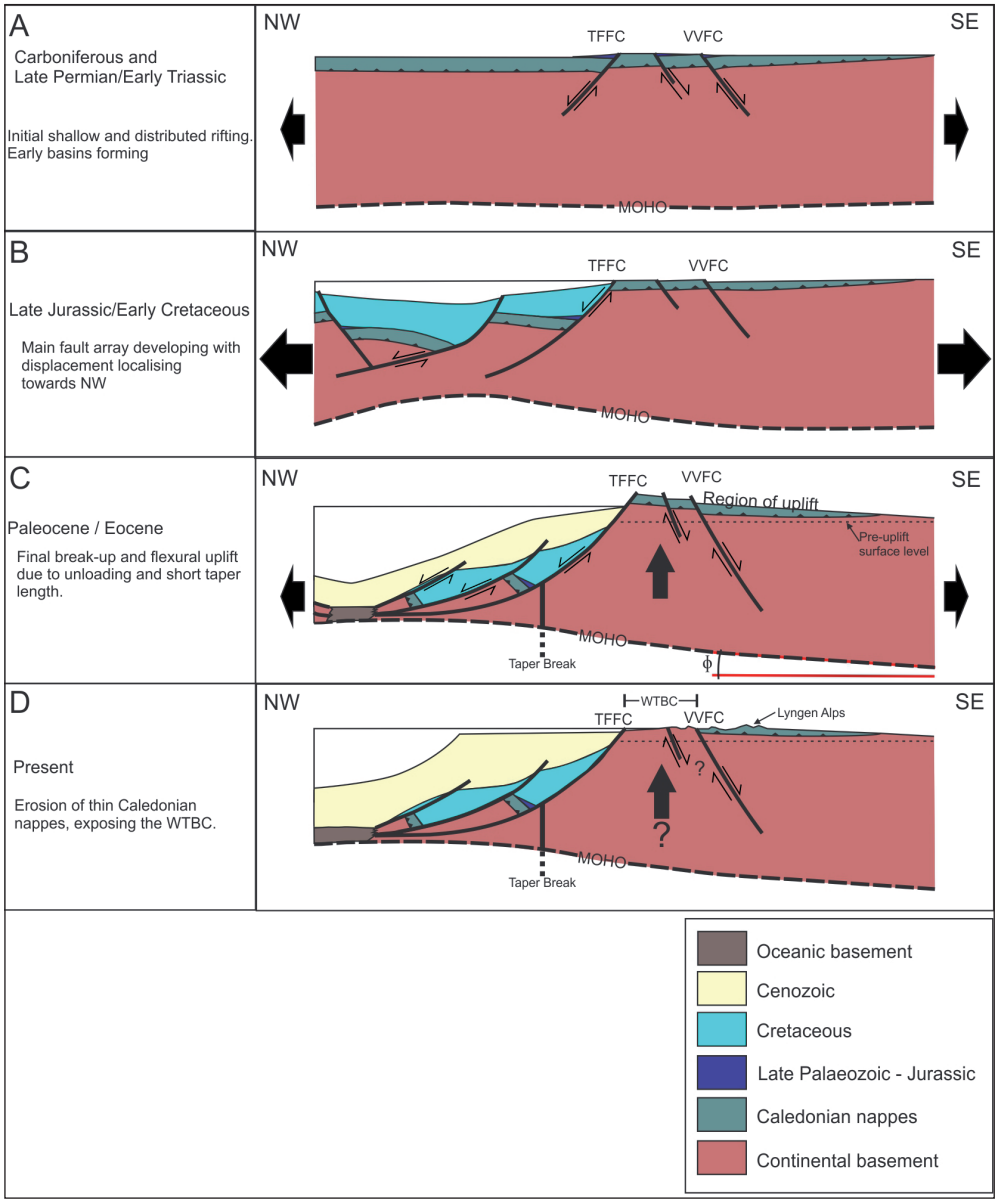

Figure 11. Schematic proposed tectonic evolution of the SW Barents Sea margin and the exhumation of the West Troms Basement Complex. (A) Initial shallow and distributed NE–SW faulting in the Carboniferous and Late Permian/Early Triassic along major fault complexes, the Troms–Finnmark Fault Complex, Ringvassøy–Loppa Fault Complex and the Vestfjorden–Vanna Fault Complex. (B) Late Jurassic/Early Cretaceous syn-rift extension in the Hammerfest Basin and adjoining Ringvassøy–Loppa Fault Complex and Troms–Finnmark Fault Complex. Note the listric geometry and large amount of displacement of the basin-boundary faults offshore, and the planar geometry of the onshore Vestfjorden–Vanna Fault Complex, resulting in the formation of a short-tapered, hyperextended margin after final break-up in the Palaeocene/Eocene. (C) Palaeocene/Eocene extension and further listric faulting and deposition of Cenozoic units in the offshore Harstad, Tromsø and Sørvestnaget basins and reactivation of the basins by transform motion. In onshore areas, the WTBC was uplifted and exhumed as a short-tapered margin due to unloading and crustal flexure. (D) Continued uplift and erosion to the present-day level, resulting in the development of high topographic relief, as illustrated by e.g., the Lyngen Alps, east of the Vestfjorden–Vanna Fault Complex.

We propose an evolutionary model of brittle faulting in the western Troms part of the SW Barents Sea margin as outlined in Fig. 11, based on the above data and discussion. Initial NW–SE-oriented extension occurred in the Carboniferous and Late Permian/Early Triassic along a distributed network of NE–SW-trending, NW- and SE-dipping normal faults (Fig. 11A). This event was followed by a Late Jurassic/Early Cretaceous extension in the Hammerfest Basin, activating the adjoining Ringvassøy–Loppa and Troms–Finnmark fault complexes (Fig. 11B). The listric geometry and large amount of displacement along these basin-boundary faults offshore, and the planar geometry of the onshore VVFC, resulted in the formation of a short-tapered, hyperextended margin after final break-up in the Palaeocene/Eocene (Fig. 11C). Offshore, further reactivation, listric faulting and sediment deposition in the offshore basins (e.g., Harstad and Tromsø Basins) followed in the Cenozoic, due to transform plate motion in the North Atlantic. In onshore areas, the WTBC was uplifted and exhumed as a short-tapered margin due to unloading and crustal flexure with continued uplift, reactivation of faults and erosion to the present stage level, forming high mountains in, for instance, the Lyngen area, east of the VVFC (Fig. 11D).

Conclusions

- The SW Barents Sea margin in western Troms is characterised by a network of onshore and offshore, steeply to moderately dipping, brittle normal faults, trending NNE–SSW and ENE–WSW, bounding major horsts (onshore) and basins (offshore). This fault pattern is also present on the Finnmark Platform farther north, where it connects with segments of the

major, offshore, basin-bounding Troms–Finnmark Fault Complex.

- Two major fault complexes, the Vestfjorden–Vanna and the Troms–Finnmark fault complexes, are localised partly onshore and partly offshore, and bound a major horst, the West Troms Basement Complex. The southern portion of the Troms–Finnmark Fault Complex, which defines the northwestern boundary of this horst, changes character northeastwards as it merges into the N–S–trending Ringvassøy–Loppa Fault Complex. The Ringvassøy–Loppa Fault Complex is interpreted as the northward continuation of the southern segment of the Troms–Finnmark Fault Complex, based on similarities in geometry, kinematics and amount of displacement. The northern segment of the Troms–Finnmark Fault Complex shows less displacement and is suggested to be younger than the southern segment of the Troms–Finnmark Fault Complex and formed in association with the formation of the Hammerfest Basin.
- The horst-bounding faults, including the Vestfjorden–Vanna Fault Complex, change character along strike northwards near the island of Nord-Fugløya, where they terminate and/or are offset sinistrally against a probable major, margin-wide transfer zone, the Fugløya transfer zone. This transfer zone marks a pronounced switch in the fault polarity and/or amount of displacement of the Vestfjord–Vanna and the Troms–Finnmark fault complexes. North of the Fugløya transfer zone, major NW-dipping fault segments occur on the Finnmark Platform, possibly representing a continuation of the Vestfjorden–Vanna Fault Complex, and inferred to link up with the Nysleppen and Måsøy fault complexes.
- The studied onshore brittle fault zones, at least on a local scale, formed close to, or along favourably oriented Precambrian or Caledonian structures such as lithological boundaries, foliations and/or ductile shear zones, suggesting a reactivation of these pre-existing structures. On a larger scale, steep, basement-seated, Precambrian ductile shear zones, e.g., the NW-SE-trending Botnian-Senja Fault Complex and the Senja Shear Belt and the Bothnian–Kvænangen Fault Complex, seem to have affected the NE–SW-trending brittle fault complexes by accommodating shifts in polarity and/or the stepping of fault segments to a new position along strike. The ~NW-SE-trending Bothnian-Kvænangen Fault Complex may thus be the controlling element for the Fugløya transfer zone, the Ringvassøya–Loppa Fault Complex, and potentially also the transform Hornsund–De Geer Fault Zone farther north on the Barents Sea margin.
- In the context of rifting along the SW Barents Sea margin, our data suggest initial distributed rifting in the Carboniferous and Late Permian/Early Triassic along at least two NE–SW-striking fault complexes. This early event was followed by a main, Late Jurassic/Early Cretaceous, syn-rift extension in the Hammerfest Basin, and a corresponding northwestward localisation of displacement along the Troms–Finnmark and Ringvassøy–Loppa fault complexes offshore. These offshore, basin-bounding faults are characterised by a listric geometry and large-magnitude displacement/extension, whereas a planar geometry is inferred for the onshore Vestfjorden–Vanna Fault Complex and related horst-internal faults. This contrast in fault geometry, with displacement largely localising to the Troms–Finnmark Fault Complex, may have resulted in the formation of a short-tapered, hyperextended margin after final break-up in the Palaeocene/Eocene (at *c.* 55 Ma). The West Troms Basement Complex was finally uplifted and exhumed in the Late Cenozoic as a short-tapered margin due to unloading and crustal flexure with continued uplift and erosion to its present-day level.

Acknowledgements. This work was part of the Industrial Ph.D. scheme organised by the Norwegian Research Council. The project is a collaboration between DONG Energy and the University of Tromsø, financed by DONG Energy and the Norwegian Research Council. We would like to show our gratitude to all persons involved from these institutions. We would also like to acknowledge NGU for sharing and allowing us to publish the magnetic anomaly surveys NGU69/70 and HRAM–98. Lastly, we would like to thank Rikke Bruhn and the referees Per Terje Osmundsen and Roy H. Gabrielsen for constructive feedback during the review process.

References

Andresen, A. 1980: The age of the Precambrian basement in western Troms, Norway. *Geologiska Föreningen i Stockholm Förhandlingar 101*, 291–298.

Andresen, A. & Forslund, T. 1987: Post-Caledonian brittle faults in Troms: geometry, age and tectonic significance. *The Caledonian and Related Geology of Scandinavia, Cardiff, 22–23 Sept., 1989 (Conf. Abstract)*.

Antonsdòttir, V. 2006: *Structural and kinematic analysis of the post-Caledonian Rekvika Fault Zone, Kvaløya, Troms*. MSc thesis, University of Tromsø, 84 pp.

Armitage, P.E.B. 1999: *Kinematic analysis of a Precambrian metasupracrustal deformation zone between Mjelde and Skorelvvatn, Kvaløya, Troms.* Cand. scient. thesis, University of Tromsø, 173 pp.

Armitage, P.E.B. & Bergh, S.G. 2005: Structural development of the Mjelde–Skorelvvatn Zone on Kvaløya, Troms: a metasupracrustal Shear Belt in the Precambrian West Troms Basement Complex, North Norway. *Norwegian Journal of Geology 85*, 117–132.

Bergh, S.G., Eig, K, Kløvjan, O.S., Henningsen, T., Olesen, O. & Hansen, J.-A. 2007: The Lofoten–Vesteralen continental margin: a multiphase Mesozoic–Palaeogene rifted shelf as shown by offshore-onshore brittle fault-fracture analysis. *Norwegian Journal of Geology 87*, 29–58.

Bergh, S.G., Corfu, F. & Corner, G.D. 2008: Proterozoic igneous and metamorphic rocks: a template for Mesozoic–Cenozoic brittle faulting and tectonic inherited landscapes in Lofoten–Vesterålen, North Norway. *33 IGC Excursion Guidebook No 38, IGC The Nordic Countries*, 71 pp.

Bergh, S.G., Kullerud, K., Armitage, P.E.B., Zwaan, K.B., Corfu, F., Ravna, E.J.K. & Myhre, P.I. 2010: Neoarchaean through Svecofennian tectono-magmatic evolution of the West Troms Basement Complex, North Norway. *Norwegian Journal of Geology 90*, 21–48.

Blystad, P., Brekke, H., Færseth, R.B., Larsen, B.T., Skogseid, J. & Tørudbakken, B. 1995: Structural elements of the Norwegian continental shelf, Part II. The Norwegian Sea Region. *Norwegian Petroleum Directorate Bulletin 8*, 45 pp.

Brekke, H. 2000: The tectonic evolution of the Norwegian Sea continental margin with emphasis on the Vøring and Møre basins. *Geological Society of London Special Publication 136*, 327–378.

Brekke, H., Kalheim, J.E., Riis, F., Egeland, B., Blystad, P., Johnson, S. & Ragnhildstveit, J. 1992: Two-way time map of the unconformity at the base of Upper Jurassic (north of 69°N) and the unconformity at the base of the Cretaceous (south of 69°N), offshore Norway, including the main geological trends onshore, scale 1:2 million. *NPD Continental Shelf Map No. 1, The Norwegian Petroleum Directorate / The Geological Survey of Norway.*

Brekke, H., Sjulstad, H.I., Magnus, C. & Williams, R.W. 2001: Sedimentary environments offshore Norway – an overview. *Norwegian Petroleum Society Special Publication 10*, 7–37.

Corfu, F., Armitage, P.E.B., Kullerud, K. & Bergh, S.G. 2003: Preliminary U–Pb geochronology in the West Troms Basement Complex North Norway: Archaean and Palaeoproterozoic events and younger overprints. *Geological Survey of Norway Bulletin 441*, 61–72.

Corner, G.D. 2005: Atlantic coast and fjords. *In* Seppälä, M. (ed.): *The physical Geography of Fennoscandia*, Oxford Regional Environments Series, Oxford University Press, pp. 203–228.

Dalland, A. 1981: Mesozoic sedimentary succession at Andøya, Northern Norway, and relation to structural development of the North Atlantic area. *In* Kerr, J.W. & Fergusson, A.J. (eds.): *Geology of the North Atlantic borderlands*. Canadian Society of Petroleum Geologists, Memoir 7, pp. 563–584.

Davids, C., Wemmer, K., Zwingmann, H., Kohlmann, F., Jacobs, J. & Bergh, S.G. 2013: K–Ar illite and apatite fission track constraints on brittle faulting and the evolution of the northern Norwegian passive margin. *Tectonophysics 608*, 196–211.

Doré, A.G. 1991: The structural foundation and evolution of Mesozoic seaways between Europe and the Arctic. *Palaeogeograhy, Palaeoclimatology, Palaeoecology 87*, 441–492.

Doré, A.G. & Lundin, E.R. 1996: Cenozoic compressional structures on the NE Atlantic margin: nature, origin and potential significance for hydrocarbon exploration. *Petroleum Geoscience 2*, 299–311.

Doré, A.G., Lundin, E.R., Fichler, C. & Olesen, O. 1997: Patterns of basement structure and reactivation along the NE Atlantic margin. *Journal of the Geological Society of London 154*, 85–92.

Doré, A.G., Lundin, E.R., Jensen, L.N., Birkeland, Ø., Eliassen, P.E. & Fichler, C. 1999: Principal tectonic events in the evolution of the northwest European Atlantic margins. *In* Fleet, A.J. & Boldy, S.A.R. (eds.): *Petroleum Geology of Northwest Europe: Proceedings of the 5th Conference*. Geological Society of London, pp. 41–61.

Eig, K. 2008: *Onshore and offshore tectonic evolution of the Lofoten passive margin, North Norway*. PhD thesis, University of Tromsø, 256 pp.

Eig, K. & Bergh, S.G. 2011: Late Cretaceous–Cenozoic fracturing in Lofoten, North Norway: Tectonic significance, fracture mechanisms and controlling factors. *Tectonophysics 499*, 190–205.

Faleide, J.I., Vågnes, E. & Gudlaugsson, S.T. 1993: Late Mesozoic–Cenozoic evolution of the southwestern Barents Sea in a regional rift-shear tectonic setting. *Marine and Petroleum Geology 10*, 186–214.

Faleide, J.I., Tsikalas, F., Breivik, A.J., Mjelde, R., Ritzmann, O., Engen, O., Wilson, J. & Eldholm, O. 2008: Structure and evolution of the continental margin off Norway and Barents Sea. *Episodes 31*, 82–91.

Forslund, T. 1988: *Post-Kaledonske forkastninger i Vest-Troms, med vekt på Kvaløyslettaforkastningen, Kvaløya*. Cand. Scient. thesis, University of Tromsø. 173 pp.

Fürsich, F. & Thompsen, E. 2005: Jurassic biota and biofacies in erratics from the Sortland area, Vesterålen, northern Norway. *Geological Society of Norway Bulletin 443*, 37–53.

Gaal, G. & Gorbatschev, R. 1987:An outline of the Precambrian evolution of the Baltic Shield. *Precambrian Research 35*, 15–52.

Gabrielsen, R.H., Færseth, R.B., Jensen, L.N., Kalheim, J.E. & Riis, F. 1990: Structural elements of the Norwegian continental shelf — Part I: the Barents Sea Region. *Norwegian Petroleum Directorate Bulletin 6*, 33 pp.

Gabrielsen, R.H., Grunnaleite, I. & Rasmussen, E. 1997: Cretaceous and Tertiary inversion in the Bjørnøyrenna Fault Complex, south-western Barents Sea. *Marine and Petroleum Geology 14*, 165–178.

Gabrielsen, R.H., Braathen, A., Dehls, J. & Roberts, D. 2002: Tectonic lineaments of Norway. *Norwegian Journal of Geology 82*, 153–174.

Gagama, M.F.V. 2005: *Strukturell analyse av post-kaledonske lineamenter ved Sifjorden, Vest-Senja, Troms*. Master thesis, University of Tromsø, 85 pp.

Gernigon, L. & Brönner, M. 2012: Late Palaeozoic architecture and evolution of the southwestern Barents Sea: insights from a new generation of aeromagnetic data. *Journal of the Geological Society of London 169*, 449–459.

Grønlie, A., Nilsen, B. & Roberts, D. 1991: Brittle deformation history of fault rocks on the Fosen Peninsula, Trøndelag, Central Norway. *Geological Survey of Norway Bulletin 421*, 39–57.

Gudlaugsson, S.T., Faleide, J.I., Johansen, S.E. & Breivik, A.J. 1998: Late Paleozoic structural development of the south-western Barents Sea: *Marine and Petroleum Geology 15*, 73–102.

Hansen, J.-A. 2009: *Onshore-offshore tectonic relations on the Lofoten and Vesterålen Margin – Mesozoic to early Cenozoic structural evolution and morpological implications*. PhD thesis, University of Tromsø, 229 pp.

Hansen, J.-A & Bergh, S.G. 2012: Origin and reactivation of fracture systems adjacent to the Mid-Norwegian continental margin on Hamarøya, North Norway: use of digital geological mapping and morphotectonic lineament analysis. *Norwegian Journal of Geology 92*, 391–403.

Hansen, J.-A., Bergh, S. G. & Henningsen, T. 2012: Mesozoic rifting and basin evolution on the Lofoten and Vesterålen Margin, North-Norway; time constraints and regional implications. *Norwegian Journal of Geology 91*, 203–228.

Hendriks, B.W.H., Osmundsen, P.T. & Redfield, T.F. 2010: Normal faulting and block tilting in Lofoten and Vesterålen constrained by apatite fission track data. *Tectonophysics 485*, 154–163.

Henkel, H. 1991: Magnetic crustal structures in Northern Fennoscandia. *Tectonophysics 192*, 57–79.

Hölttä, P., Balagansky, V., Garde, A.A., Mertanen, S., Peltonen, P., Slabunov, A., Sorjonen-Ward, P. & Whitehouse, M. 2008: Archean of Greenland and Fennoscandia. *Episodes 31*, 13–19.

Jakobsson, M., Mayer, L., Coakley, B., Dowdeswell, J. A., Forbes, S., Fridman, B., Hodnesdal, H., Noormets, R., Pedersen, R., Rebesco, M., Schenke, H.W., Zarayskaya, Y., Accettella, D., Armstrong, A., Anderson, R.M., Bienhoff, P., Camerlenghi, A., Church, I., Edwards, M., Gardner, J.V., Hall, J.K., Hell, B., Hestvik, O., Kristoffersen, Y., Marcussen, C., Mohammad, R., Mosher, D., Nghiem, S.V., Pedrosa, M.T., Travaglini, P.G. & Weatherall, P. 2012: The international bathymetric chart of the Arctic Ocean (IBCAO) version 3.0. *Geophysical Research Letters 39*, doi:10.1029/2012GL052219.

Knutsen, S.M. & Larsen, K.I. 1997: The late Mesozoic and Cenozoic evolution of the Sørvestsnaget Basin: A tectonostratigraphic mirror for regional events along the Southwestern Barents Sea margin? *Marine and petroleum geology 14*, 27–54.

Lahtinen, R., Garde, A.A. & Melezhik, V.A. 2008: Paleoproterozoic evolution of Fennoscandia and Greenland. *Episodes 31*, 20–28.

Larssen, G.B., Elvebakk, G., Henriksen, L.B., Kristensen, S.E., Nilsson, I., Samuelsberg, T. J., Svånå, T.A., Stemmerik, L. & Worsley, D. 2002: Upper Palaeozoic lithostratigraphy of the Southern Norwegian Barents Sea. *Norwegian Petroleum Directorate Bulletin 9*, 76 pp.

Lundin, E.R. & Doré, A.G. 2011: Hyperextension, serpentinization, and weakening: A new paradigm for rifted margin compressional deformation. *Geology 39*, 347–350.

Miller, H.G. & Singh, V. 1994: Potential-field tilt—a new concept for location of potential-field sources. *Journal of Applied Geophysics 32*, 213–217.

Mosar, J., Torsvik, T.H. & the BAT team 2002: Opening the Norwegian and Greenland Seas: Plate tectonics in Mid Norway since the Late Permian. *In* Eide, E.A. (coord.): *BATLAS – Mid Norway plate reconstruction atlas with global Atlantic perspectives*, pp. 48–59.

Nielsen, S.B., Paulsen, G.E., Hansen, D.L., Gemmer, L., Clausen, O.R., Jacobsen, B.H., Balling, N., Huuse, M. & Gallagher, K. 2002: Paleocene initiation of Cenozoic uplift in Norway. *In* Doré, A.G., Cartwright, J.A., Stoker, M.S., Turner, J.P. & White, N. (eds.): *Exhumation of the North Atlantic Margin: Timing, Mechanisms and Implications for Petroleum Exploration*, Geological Society of London Special Publication 196, pp. 45–65.

Olesen, O., Torsvik, T.H., Tveten, E., Zwaan, K.B., Løseth, H. & Henningsen, T. 1997: Basement structure of the continental margin in the Lofoten–Lopphavet area, northern Norway: constraints from potential field data, on-land structural mapping and palaeomagnetic data. *Norwegian Journal of Geology 77*, 15–30.

Olesen, O., Ebbing, J., Lundin, E., Mauring, E., Skilbrei, J.R., Torsvik, T.H., Hansen, E.K., Henningsen, T., Midbøe, P. & Sand, M. 2007: An improved tectonic model for the Eocene opening of the Norwegian–Greenland Sea: Use of modern magnetic data. *Marine and Petroleum Geology 24*, 53–66.

Opheim, J.A. and Andresen, A. 1989: Basement-cover relationships on northern Vanna, Troms, Norway. *Norwegian Journal of Geology 69*, 67–81.

Osmundsen, P.T. & Ebbing, J. 2008: Styles of extension offshore mid Norway and implications for mechanisms of crustal thinning at passive margins. *Tectonics 27*, DOI:10.1029/2007TC002242.

Osmundsen, P.T. & Redfield, T.F. 2011: Crustal taper and topography at passive continental margins. *Terra Nova 23*, 349–361.

Osmundsen, P.T., Sommaruga, A., Skilbrei, J.R. & Olesen, O. 2002: Deep structure of the Mid Norway rifted margin. *Norwegian Journal of Geology 82*, 205–224.

Osmundsen, P.T., Redfield, T.F., Hendriks, B., Bergh, S.G., Hansen, J.-A., Henderson, I., Dehls, J., Lauknes, T.R., Larsen, Y., Anda, E., Fredin, O. & Davidsen, B. 2010: Fault-controlled alpine topography in Norway. *Journal of the Geological Society of London 167*, 83–98.

Pascal, C. & Olesen, O. 2009: Are the Norwegian mountains compensated by a mantle thermal anomaly at depth? *Tectonophysics 475*, 160–168.

Ramberg, I.B., Bryhni, I., Nøttvedt, A. & Rangnes, K. 2008. *The making of a land. Geology of Norway.* The Norwegian Geological Association, Oslo.

Redfield, T.F., Osmundsen, P.T. & Hendriks, B.W.H. 2005: The role of fault reactivation and growth in the uplift of western Fennoscandia. *Journal of the Geological Society of London 162*, 1013–1030.

Redfield, T.F. & Osmundsen, P.T. 2013: The long-term topographic response of a continent adjacent to a hyperextended margin: A case study from Scandinavia. *Geological Society of America Bulletin 125*, 184–200.

Roberts, D. & Lippard, S.J. 2005: Inferred Mesozoic faulting in Finnmark: current status and offshore links. *Geological Survey of Norway Bulletin 443*, 55–60.

Roberts, D., Nordgulen, Ø. & Melezhik, V. 2007: The Uppermost Allochthon in the Scandinavian Caledonides: From a Laurentian ancestry through Taconian orogeny to Scandian crustal growth on Baltica. *In* Hatcher Jr., R.D., Carlson, M.P., McBribde, J.H. & Martínez Catalán, J.R. (eds.): *4-D Framework of Continental Crust*, Geological Society of America Memoir 200, pp. 357–377.

Roberts, D., Chand, S. & Rise, L. 2011: A half-graben of inferred Late Palaeozoic age in outer Varangerfjorden, Finnmark: evidence from seismic-reflection profiles and multibeam bathymetry. *Norwegian Journal of Geology 91*, 191–200.

Rohrman, M. & van der Beek, P. 1996: Cenozoic postrift domal uplift of North Atlantic margins: an asthenospheric diapirism model. *Geology 24*, 901–904.

Rydningen, T.A., Vorren T.O., Laberg, J.S. & Kolstad, V. 2013: The marine-based NW Fennoscandian ice sheet: glacial and deglacial dynamics as reconstructed from submarine landforms. *Quaternary Science Reviews 68*, 126–141.

Smelror, M., Mørk, A., Mørk, M.B.E., Weiss, H.M. & Løseth, H. 2001: Middle Jurassic–Lower Cretaceous transgressive-regressive sequences and facies distribution off northern Nordland and Troms, Norway. *Norwegian Petroleum Society Special Publications 10*, 211–232.

Smelror, M., Petrov, O.V., Larssen, G.B. & Werner, S.C. (eds.) 2009: *Geological history of the Barents Sea*. Geological Survey of Norway, Trondheim, 135 pp.

Steltenpohl, M.G., Carter, B.T., Andresen, A. & Zeltner, D.L. 2009: $^{40}Ar/^{39}Ar$ thermochronology of late- and postorogenic extension in the Caledonides of north–central Norway. *The Journal of Geology 117*, 399–414.

Thorsnes, T, Erikstad, L., Dolan, M.F.J. & Bellec, V.K. 2009: Submarine landscapes along the Lofoten–Vesterålen–Senja margin, northern Norway. *Norwegian Journal of Geology 89*, 5–16.

Thorstensen, L. 2011: *Land-sokkel korrelasjon av tektoniske elementer i ytre del av Senja og Kvaløya i Troms*. MSc thesis, University of Tromsø, 107 pp.

Tsikalas, F., Faleide, J.I. & Eldholm, O. 2001: Lateral variations in tectono-magmatic style along the Lofoten–Vesterålen volcanic margin off Norway. *Marine and Petroleum Geology 18*, 807–832.

Tsikalas, F., Eldholm, O. & Faleide, J.I. 2005: Crustal structure of the Lofoten–Vesterålen continental margin, off Norway. *Tectonophysics 404*, 151–174.

Tsikalas, F., Faleide, J. I. & Kusznir, N. J. 2008: Along-strike variations in rifted margin crustal architecture and lithosphere thinning between northern Vøring and Lofoten margin segments off mid-Norway. *Tectonophysics 458*, 68–81.

Verduzco, B., Fairhead, J.D., Green, C.M. & MacKenzie, C. 2004: New insights into magnetic derivatives for structural mapping. *The Leading Edge 23*, 116–119.

Wilson, R.W., McCaffrey, K.J.W., Holdsworth, R.E., Imber, J., Jones, R., Welbon, A. & Roberts D.J. 2006: Complex fault pattern, transtension and structural segmentation of the Lofoten Ridge, Norwegian Margin: Using digital mapping to link onshore and offshore geology. *Tectonics 25*, doi:10.1029/2005TC001895.

Zwaan, K.B. 1995: Geology of the West Troms Basement Complex, northern Norway, with emphasis on the Senja Shear Belt: a preliminary account. *Geological Survey of Norway, Bulletin 427*, 33–36.

Zwaan, K.B., Fareth, E. & Grogan, P.W. 1998: Tromsø, bedrock geology map, scale 1:250,000, *Geological Survey of Norway*.

Paper 2

On Palaeozoic-Mesozoic brittle normal faults along the SW Barents Sea margin: fault processes and implications for basement permeability and margin evolution

Kjetil Indrevær[1,2,*], Holger Stunitz[1] & Steffen G. Bergh[1]

1) Department of Geology, University of Tromsø, N-9037 Tromsø, Norway
2) DONG E&P Norge AS, Roald Amundsens Plass 1, N-9257 Tromsø, Norway

* Corresponding author (e-mail: kjetil@indrevar.no)

Abstract: Palaeozoic–Mesozoic brittle normal faults onshore along the SW Barents Sea passive margin off northern Norway give valuable insight into fault and fluid flow processes from the lower brittle crust. Microstructural evidence suggests that Late Permian–Early Triassic faulting took place during multiple phases, with initial fault movement at minimum *P–T* conditions of *c*. 300 °C and *c*. 240 MPa (*c*. 10 km depth), followed by later fault movement at minimum *P–T* conditions of *c*. 275 °C and *c*. 220 MPa (*c*. 8.5 km depth). The study shows that pore pressures locally reached lithostatic levels (240 MPa) during faulting and that faulting came to a halt during early (deep) stages of rifting along the margin. Fault permeability has been controlled by healing and precipitation processes through time, which have sealed off the core zone and eventually the damage zones after faulting. A minimum average exhumation rate of *c*. 40 m Ma^{-1} since the Late Permian is estimated. It implies that the debated Late Cenozoic uplift of the margin may be explained by increased erosion rates in the coastal regions owing to climate detoriation, which caused subsequent isostatic recalibration and uplift of the marginal crust. The studied faults may be used as analogues of basement-involved fault complexes offshore, revealing details about the offshore nature of faulting, including past and present basement and fault zone permeability.

Introduction

It is well known that the strength of the crust depends not only on the frictional strength of dry rocks, but also on pore pressure at depth (e.g. Hubbert & Rubey 1959). The consequence is that the brittle strength of the crust can be of the order of several hundred MPa under hydrostatic pore pressure conditions (depending on depth) or negligible as pore pressures approach lithostatic values (Sibson 1973; Byerlee 1978; Brace & Kohlstedt 1980; Jaeger *et al*. 2009). The importance of this effect on crustal strength was first fully appreciated when attempts to model earthquakes had to involve fluids to replicate the strength of the brittle crust (e.g. Sibson *et al*. 1975; Sibson 1977, 1989; Byerlee 1990, 1993; Zoback 1991; Rice 1992; Blanpied *et al*. 1992; Bruhn *et al*. 1994). These models implied that pore pressures within fault zones were commonly elevated, also at deeper levels of the seismogenic zone.

Several studies have since discovered that faults act as important pathways for fluids in the upper crust as they represent high-permeability zones owing to fracturing and cataclasis (e.g.

Sibson 1973, 1977; Hickman *et al*. 1995; Seront *et al*. 1998; Gudmundsson *et al*. 2001; Zoback & Townend 2001; Crampin *et al*. 2002; Ganerød *et al*. 2008). Experimental data have shown that fluid-involved processes, which control fault strength and permeability, include fault healing through pressure solution and hydrothermal precipitation of minerals (Karner *et al*. 1997; Olsen *et al*. 1998; Bos & Spiers 2000; Kanagawa *et al*. 2000; Nakatini & Scholz 2004). However, observations and analysis of fault rock, fluid interactions and fluid behaviour (including fluid pore pressure) from natural examples are relatively scarce in the literature (e.g. Bruhn *et al*. 1994; Eichhubl & Boles 2000; Caine *et al*. 2010; Faulkner *et al*. 2010). In particular, this appears to be the case for preserved examples from the deeper parts of the seismogenic zone (5–12 km), which are crucial to understand fault and fault–fluid behaviour at depth (see Faulkner *et al*. 2010).

In the present study, we present observations from naturally occurring fault rocks, which show evidence for elevated pore pressure and fluid flow during faulting in the deeper parts of the seismogenic zone. The fault zones crop out as a network of Late Permian–Early Triassic brittle normal faults in Troms, northern Norway (Fig. 1; Andresen & Forslund 1987; Forslund 1988; Opheim & Andresen 1989; Olesen *et al*. 1997; Davids *et al*. 2013; Indrevær *et al*. 2013) and constitute major fault complexes that run partly onshore, partly offshore along the SW Barents Sea passive margin (Indrevær *et al*. 2013). The fault zones display mostly Permian–Early Triassic ages of faulting (Davids *et al*. 2013) and varying amounts of displacement (>3 km to <100 m) (Forslund 1988; Opheim & Andresen 1989; Olesen *et al*. 1997; Indrevær *et al*. 2013). We describe and characterize features indicating fault–fluid interactions and high pore pressures in fault rocks from selected onshore fault zone outcrops in the region (Fig. 2), and we aim to estimate *P–T* conditions and fluid pressures during faulting from mineral assemblages and microstructures. This approach may yield insight into important processes operating during faulting in the intermediate to deeper levels of the brittle crust (<15km). The implications of syn- and post-deformation fault rock permeability will be discussed in the context of the potential for hydrocarbon migration and entrapment within basement rocks in the region. Lastly, the results will be set into context with the current understanding of evolution of the SW Barents Sea passive margin (see Gabrielsen *et al*. 1990; Faleide *et al*. 2008; Smelror *et al*. 2009).

Geological Setting

The studied fault rock outcrops are located within the West Troms Basement Complex, a basement horst situated on the SW Barents Sea margin, northern Norway (Fig. 1). The horst is

bounded by the Lofoten igneous and high-grade metamorphic province to the SW (Corfu 2004) and by largely Permian–Early Triassic high-angle normal faults, which down-drop Caledonian nappes, to the east (Andresen & Forslund 1987; Zwaan 1995; Davids *et al*. 2013; Indrevær *et al*. 2013). The West Troms Basement Complex is made up of various Meso- and Neoarchaean tonalitic, trondhjemitic and granitic gneisses and meta-supracrustal belts, intruded by felsic and mafic igneous rocks (Corfu *et al*. 2003; Bergh *et al*. 2010).

The Permian–Early Triassic rift-related activity in the region is manifested within the horst by widespread NNE–SSW- and ENE–WSW-trending brittle normal faults and fractures arranged in a zig-zag pattern along the southeastern and northwestern limits of the West Troms Basement Complex. A subsidiary NW–SE-trending fracture system is also present (Fig. 1; see Indrevær *et al*. 2013). The onshore fault zones can be divided into the Vestfjorden–Vanna Fault Complex, which marks the southeastern boundary of the West Troms Basement Complex, down-dropping Caledonian nappes to the east by some 1–3km (Forslund 1988; Opheim & Andresen 1989; Olesen *et al*. 1997), and a less prevalent, SE-dipping, segmented fault array that runs along the outer rim of the islands of the West Troms Basement Complex (Antonsdóttir 2006; Thorstensen 2011; Indrevær *et al*. 2013) with displacement of the order of hundreds of metres or less (Indrevær *et al*. 2013; Fig. 2).

The northwestern limit of the West Troms Basement Complex is identified as the Troms–Finnmark Fault Complex (Indrevær *et al*. 2013), which runs offshore, parallel to the West Troms Basement Complex, where basement is down-faulted more than 5km in the Harstad Basin, to *c*. 10km depth (Fig. 1; Indrevær *et al*. 2013). Preserved Caledonian nappes thrust on top of Precambrian basement, as observed in the mainland of northern Norway, are indicated to be present within large regions of the SW Barents Sea (Gernigon & Brönner 2012) and may be present offshore from the West Troms Basement Complex, overlying down-faulted Precambrian basement.

The Troms–Finnmark and Vestfjorden–Vanna fault complexes (Figs 1 and 2) can be traced for hundreds of kilometres along strike of the north Norwegian margin, linking up major structural elements in the south, such as the Lofoten and Nordland ridges, with offshore fault complexes in the north, such as the Ringvassøy–Loppa, Nysleppen and Måsøy fault complexes (Doré *et al*. 1997, 1999; Olesen *et al*. 1997; Indrevær *et al*. 2013). Because the Vestfjorden–Vanna Fault Complex, which runs partly onshore, links up with offshore fault complexes, the fault zones in western Troms act as a unique natural laboratory for studying

offshore-correlative basement-seated fault zones and their characteristics.

Timing of faulting

Ages of onshore rocks and fault rocks derived using the $^{40}Ar/^{39}Ar$ and/or apatite fission-track methods are interpreted to indicate that faulting in western Troms largely occurred in the Permian to Early Triassic with insignificant fault displacement or reactivation later in the Mesozoic and Cenozoic (Hendriks *et al*. 2010; Davids *et al*. 2013). Instead, Mesozoic fault activity took place offshore, along the Troms–Finnmark Fault Complex (Gabrielsen *et al*. 1990), further north in Finnmark (Roberts & Lippard 2005; Torgersen *et al.* 2013) and to the south in Vesterålen and Andøya (Dalland 1981; Fürsich & Thomsen 2005; Eig 2008; Hansen 2009; Hendriks *et al*. 2010; Osmundsen *et al*. 2010; Davids *et al*. 2013). The onshore faults in Troms are therefore believed to have been abandoned after the Late Permian–Early Triassic rifting phase and thus reflect conditions of early stages of rifting (Davids *et al*. 2013; Indrevær *et al*. 2013). However, palaeomagnetic evidence for Permian as well as Cenozoic to recent phases of faulting has been obtained for fault segments within the Vestfjorden–Vanna Fault Complex in Troms (Olesen *et al*. 1997), suggesting that the major offshore fault activity triggered minor reactivation on some onshore faults.

Methods

Several fault segments with good outcrops of fault rocks in the West Troms Basement Complex have been investigated through structural mapping, including extensive sampling of rocks from both the core zones and damage zones. Fault rock studies using polarizing light microscopy and SEM analysis, including backscatter detection (BSD) and energy-dispersive spectrometry (EDS), have been conducted to identify mineral assemblages, which have been used in estimation of *P–T* conditions during faulting, and to identify and describe fault rocks to provide insight into fault and fluid flow characteristics.

Results

Described fault segments with distinct fault rocks include the Rekvika, Bremneset, Tussøya and Kvaløysletta–Straumsbukta fault zones (Fig. 2; Forslund 1988; Opheim & Andresen 1989; Olesen *et al*. 1997; Antonsdóttir 2006; Thorstensen 2011; Indrevær *et al*. 2013). These and other fault rocks of the West Troms Basement Complex have been mapped and discussed in a regional context by Indrevær *et al*. (2013). The Rekvika, Bremeset and Tussøya faults have estimated amounts of displacement of the order of hundreds of metres or less (Indrevær

et al. 2013). The Kvaløysletta–Straumsbukta fault zone is a fault segment of the Vestfjorden–Vanna Fault Complex with an estimated amount of displacement of 1–3 km (Forslund 1988). In the following, we aim to describe the meso- and microscopic petrological characteristics of the fault rocks from these fault zones as a basis for discussing *P–T* conditions, fault evolution, fluid flow characteristics, and fluid pressures during faulting.

Rekvika fault zone

Mesoscale observations. The sinistral-normal Rekvika fault zone (Fig. 2, map A; Antonsdóttir 2006; Indrevær *et al*. 2013) dips SE and cuts through parts of a granitic intrusion. The damage zone ranges in width from 30 to 50m into the footwall, consisting mainly of protocataclastic red stained granite. It is abundantly cut by irregular quartz veins and enriched in epidote (Fig. 3a and b). The process zone occurs as a *c*. 2 m wide, light green, ultracataclasite composed of dominantly quartz and minor hematite (Fig. 3c). The ultracataclasite is cut by later irregular quartz veins (Fig. 3c). Both the hanging wall and the footwall are characterized by a >400m wide zone along strike of conspicuous red staining of the granite (Fig. 3d).

Microscale observations. In thin section, at least three generations of cataclasites are observed within the light green core zone (Fig. 3e and f). The first generation cataclasite is preserved as sub-angular 0.2– 1mm clasts of very fine-grained quartz ultracataclasite (internal grain size of 5 μm to <1 μm) containing *c*. 99% quartz and 1% hematite. The first generation cataclastic aggregates are embedded within rounded to sub-rounded clasts of a second generation of quartz ultracataclasite (Fig. 3e and f), which is composed of *c*. 80% quartz and *c*. 20% hematite. The sub-rounded clasts of the second generation are, again, embedded within a third generation, composed of 99% quartz and less than 1% hematite with a grain size in the range from 50 μm to <1 μm. The fine-grained domains show microstructural characteristics of healing and grain growth, evident from the development of cuspate grain boundaries (Fig. 3g), indicating that the initial clast grain size was less than what is observed in thin section.

Later extensional fractures with infill of quartz cut both generations of cataclasites (Fig. 3e and f). These fractures are cut first by fractures containing both hematite and quartz, and subsequently by fractures showing only hematite. A lens of mafic gneiss that shows an amphibolite-facies mineral assemblage away from the fault zone (Fig. 2, map A) is statically retrograded to chlorite (60%), quartz (30%), epidote (5%), albite (5%), and accessory titanite and muscovite within the damage zone of the fault zone (Fig. 3h).

Tussøya fault zone

Mesoscale observations. This sinistral-normal fault zone dips moderately ESE and separates granite in the footwall from banded mafic and felsic gneisses in the hanging wall (Fig. 2, map B and Fig. 4a; Indrevær *et al*. 2013). The fault crops out as a 1–3 m thick proto- to ultracataclastic zone (Fig. 4b). The granite in the footwall is stained red, similar to the Rekvika fault zone, within a 200 m wide zone and is commonly cut by dark bands of ultracataclasite (Fig. 4c). Altered granite also occurs in the hanging wall in the southern parts of the outcrop area. Subsidiary, ENE–WSW-trending, dextral normal faults interact with the overall main NNE–SSW fault trend and are displaced by the main fault. In general, the footwall is more deformed than the hanging wall.

The dark bands of ultracataclasite are injected into fractures in the sidewall of the faults (Fig. 4c and d). These injections show a lack of internal foliation, indicating no significant amount of displacement along the fracture, which would be needed to produce the observed cataclasite *in situ*, and a lack of any significant damage to the side-walls of the fracture. Also, the fractures that are filled with cataclasites are commonly at high angles to the main fault zone. However, the fractures do have some displacement along them, as the side-walls of the fracture do not match up properly (Fig. 4d).

Microscale observations. Within the core zone, at least three generations of cataclasites are observed in thin sections (Fig. 4e and f). The oldest generation consists of angular to sub-rounded clasts, 5 mm to <1 μm in size, made up of quartz (90%) and feldspar (10%) within a matrix composed of quartz (80%), epidote (20%) and accessory hematite (Fig. 4e and f). The second generation is characterized by sub-angular to rounded clasts of quartz (90%) and feldspar (20%) within a matrix of epidote (40%), hematite (30%), quartz (20%) and chlorite (10%) (Fig. 4e and f). The third generation of cataclasite is observed in association with microfaults, which cut the two previous generations (Fig. 4e and f) and consist of quartz (60%), albite (30%), pumpellyite (10%) and hematite (1%).

Microstructural study of the inferred injected ultracataclasites confirms the lack of any high-strain zone within the cataclasite, supporting its injected nature inferred from outcrop observations. The ultracataclasites have formed elsewhere (probably along larger fault segments) and been transported into fractures (Fig. 4g and h), resulting in the dark bands of ultracataclasites observed in outcrops (Fig. 4d).

Within the damage zone, biotite is locally fractured and dilated by the precipitation of quartz

(Fig. 5a). Larger clasts of quartz show undulatory extinction (Fig. 5b) and both quartz and feldspar show healed fractures, with nucleation of new grains along the healed fractures (Fig. 5b and c). Comparing unaltered and altered granite under a polarizing microscope reveals that the red staining is limited to grains of plagioclase (Fig. 5d–g). Micro-grains of iron oxides (<1 μm in size) in larger plagioclase grains produce the red staining (Fig. 5f and g).

Bremneset fault zone

Mesoscale observations. This normal fault (Fig. 2, map C) dips ESE and occurs as a 0–3 m thick cataclastic zone that can be traced along the shore for *c*. 200m, cutting migmatitic, banded gneisses (Fig. 6a and b). The gneiss foliation is in general at a moderate angle to the fault zone. Fault and fracture surfaces commonly show epidote precipitation, and they are locally cut by younger faults or fractures with hematite staining. The core zone is composed of epidote-rich cataclasite with minor quartz and chlorite (Fig. 6b).

Microscale observations. A fractured amphibolite gneiss from the damage zone of the Bremneset fault zone consists of albite (40%), quartz (30%), chlorite (5%), epidote (5%), apatite (1%) and accessory titanite and calcite (Fig. 6c and d). Clasts of fractured epidote (Fig. 6e) show typical grain growth features including the formation of idiomorphic grain boundaries. Later faulting has fractured the annealed epidote grains. EDS analysis shows that pumpellyite occurs along these fractures (Fig. 6f and g). Chlorite grains are observed being fractured and dilated by titanite infill (Fig. 6h).

Plagioclase grains are commonly stained red, but the staining is not present along healed fractures when they cut plagioclase grains (see Fig. 5f and g). Preserved larger quartz and feldspar grains show traces of healed fractures similar to those in the Tussøya fault zone (Fig. 5c and d). The larger quartz grains show undulatory extinction. Late-stage microfaults cut the cataclasite without forming new cataclasite along the faults (Fig. 7a and b). Within healed fractures, fluid inclusions are observed, indicating the presence of fluids during fracturing.

Away from the Bremneset fault zone, viscously deformed amphibolites are preserved outside the fault zones. Foliation-parallel plastically boudinaged quartz veins are commonly found within the gneisses. As they are boudinaged, they clearly predate the brittle deformation (Fig. 7c). Approaching the fault zone, the amphibolite-facies ductile microstructure is progressively retrograded to a greenschist-facies mineral assemblage through static recrystallization, except in zones around the boudinaged quartz veins (Fig. 7d and e). As static retrogression is indicative of the percolation of fluids through the rock, the preserved amphibolite-facies

metamorphic mineral assemblage along the outer rim of the quartz veins indicates that the quartz veins have prevented fluid flow across these zones.

Kvaløysletta–Straumsbukta fault zone

Mesoscale observations. This is an oblique-dextral normal fault zone (Fig. 2, map D; Forslund 1988; Olesen *et al*. 1997; Indrevær *et al*. 2013), which dips SE and runs along the eastern rim of Kvaløya, juxtaposing Precambrian gneisses in the footwall and Caledonian nappes in the hanging wall. Near Straumsbukta, parts of the footwall damage zone crop out within foliated tonalitic and amphibolitic gneisses (Fig. 8a and b). Fault surfaces commonly trend north–south and locally NE–SW, and are parallel to a moderately east-dipping foliation in the gneisses. The footwall outcrop is increasingly deformed towards the east. The tonalitic gneisses are commonly stained red, as observed along the other studied fault zones. In outcrops, related fault and fracture surfaces are coated with chlorite and quartz, and systematically are cut by fractures coated with hematite.

Microscale observations. At least two generations of cataclasites are observed in mafic rocks of the damage zone in Straumsbukta. The first generation consists of very fine-grained (<1 μm) epidote (40%), chlorite (40%) and quartz (20%) aggregates, which appear as clasts within a second generation of cataclasite composed of quartz (50%), chlorite (30%) and epidote (20%) in the matrix (Fig. 8c and d). Chlorite within the second generation of cataclasite commonly shows radial growth (Fig. 8e and f). Both generations of the fault rocks are cut by quartz and chlorite veins, in successive order.

Plagioclase grains from the tonalitic gneisses of the damage zone are commonly stained red, similar to the other studied fault zones. Notably, the plagioclase within the amphibolite gneisses is retrograded to sericitic albite with overgrowth of white mica and epidote, which is also present within amphibolitic gneisses from Bremneset (Fig. 7d).

In summary, a common feature to all of the studied fault zones and related fractures is the red staining of plagioclase within the fault damage zone and hydrothermal precipitation of epidote, quartz, chlorite, calcite and/or hematite along fracture surfaces and in the matrix of cataclasites. Cross-cutting relationships demonstrate that epidote, quartz and chlorite veins formed first and were later cut by veins composed dominantly of hematite. At least two generations of cataclasites were formed during faulting, accompanied by mineral recrystallization and/or growth. Both the cataclasites and the statically recrystallized mafic gneisses show the mineral assemblage epidote + quartz + chlorite + albite + titanite ± apatite

± calcite ± muscovite. Subsequent fracturing and cataclasis introduced pumpellyite to the mineral assemblage.

Discussion

P–T conditions during faulting

The mineral assemblage epidote + quartz + chlorite + albite + titanite ± apatite ± calcite ± muscovite is identified in the first generations of cataclasites in mafic gneisses of the Bremneset and Tussøya fault zones. This mineral assemblage indicates that greenschist-facies metamorphic conditions were present during faulting. The same mineral assemblage is observed in statically recrystallized mafic gneisses from the damage zones of the Rekvik and Bremneset fault zones. The formation of pumpellyite in later-stage fractures in cataclastic mafic gneisses at Bremneset and in granitoid fault rocks at Tussøya further suggests decreasing *P–T* conditions of faulting through time, as pumpellyite is stable at sub-greenschist-facies conditions.

The presence of greenschist-facies mineral assemblage (epidote + quartz + albite + chlorite ± white mica) is indicative of a minimum temperature during the formation of the early generations of cataclasites at *c*. 300 °C (Fig. 9; Bucher & Grapes 2011). Fractured grains of epidote show grain growth and the development of idiomorphic grain boundaries (Fig. 6e). As grains of epidote are fractured, this implies that epidote and thus, greenschist-facies metamorphic conditions, were reached prior to fracturing. The post-fracturing grain growth and the development of idiomorphic grain boundaries of the fractured epidote indicate that greenschist-facies metamorphic conditions persisted after the early event(s) of brittle faulting. Later fault movement fractured the idiomorphic grains, and fine-grained pumpellyite formed along these fractures. Pumpellyite forms at temperatures ranging from *c*. 250 to 300°C (Fig. 9; Bucher & Grapes 2011). Thus, the presence of pumpellyite suggests that the temperature decreased below *c*. 300 °C during later stages of faulting.

The observed microstructures and greenschist-facies mineral assemblages do not allow for a precise estimate of confining pressure during deformation owing to the relatively wide pressure range of stability for greenschist-facies assemblages. The occurrence of pumpellyite, however, yields a minimum pressure for the later-stage faulting of *c*. 220MPa corresponding to a minimum depth of *c*. 8.5 km, assuming an average meta-MORB (mid-ocean ridge basalt) composition of the amphibolites and an upper lithospheric density of 2600 kg m^{-3} (Fig. 9).

From these estimates, it is possible to infer the highest possible geothermal gradient during the time of faulting as *c*. 30 °C km^{-1}.

A minimum estimate for pressures during the earlier greenschist-facies fault activity may be obtained by extrapolating this geothermal gradient up to *c*. 300°C (the minimum temperature estimate for the greenschist faulting conditions). This yields a minimum pressure of the early stage faulting at *c*. 245MPa, corresponding to *c*. 10 km depth (Fig. 9).

Fault rocks and fluid interactions

The Rekvika and Tussøya fault zones run partly within granitic rocks. Fault zones within feldspar-rich host rocks commonly develop phyllonites within core zones of faults, as a result of the breakdown of feldspars to phyllosilicates (Wintsch *et al*. 1995; Janecke & Evans 1988; Wibberley 1999; Rutter *et al*. 2001; Holdsworth 2004; Jefferies *et al*. 2006). In Rekvika and Tussøya, however, the formation of phyllonites within the core zones is not observed. Rather, within the core zone of the Rekvika fault zone, a *c*. 2 m wide zone of quartzitic ultracataclasite occurs. Wibberley (1999) described preserved clasts of 'cemented quartz–albite-ultracataclasite' within phyllonites and attributed them to early stages of faulting, where the chemical breakdown of orthoclase feldspars to muscovite leads to the release of quartz. The chemical reactions are (Wibberley 1999)

$$3NaAlSi_3O_8 + K^+ + 2H^+ = 4KAl_3Si_3O_{10}(OH)_2 + 6SiO_2 + 3Na^+$$
(albite) (muscovite) (silica)

$$3KAlSi_3O_8 + 2H^+ = KAl_3Si_3O_{10}(OH)_2 + 6SiO_2 + 2K^+$$
(K-feldspar) (muscovite) (silica)

These reactions are favoured in meteoric water-dominated granitic fault systems (Wintsch *et al*. 1995).

The occurrence of the quartzitic ultracataclasite at Rekvika may thus be preserved early stages of faulting, which, in contrast to the Wibberley (1999) study, are preserved where these fault rocks form relict clasts within phyllonites. If so, at least three generations of such cataclasites can be observed in Rekvika and suggest that the fault zone was abandoned after early stages of rifting so that subsequent fault activity and progressive formation of phyllosilicates (inducing fault weakening) did not occur.

Within the Rekvika and Tussøya fault zones, no extensive formation of muscovite is observed, as would be predicted if the abundance of quartz within the core zone of the

Rekvika fault zone were due to the above-described breakdown of feldspars. Instead, the fault rocks are enriched in epidote, chlorite, calcite and hematite (in addition to quartz). Bruhn *et al*. (1994) described common mineral reactions for feldspars under *P–T* conditions of intermediate to deeper levels of normal faulting involving fluids. With a mafic fluid composition involving dissolved Ca^{2+}, Fe^{3+} and Mg^{2+}, important chemical reactions include

(1) $2NaAlSi_3O_8 + 2Ca^{2+} + Fe^{3+} + 3H_2O = Ca_2Al_2FeSi_3O_{12}(OH) + 2Na^+ + 5H^+ + 3SiO_2$
(albite) (epidote) (silica)

(2) $2KAlSi_3O_8 + 2Ca^{2+} + Fe^{3+} + 3H_2O = Ca_2Al_2FeSi_3O_{12}(OH) + 2K^+ + 5H^+ + 3SiO_2$
(K-feldspar) (epidote) (silica)

(3) $2KAlSi_3O_8 + 5Mg^{2+} + 8H_2O = Mg_5Al_2Si_3O_{10}(OH)_8 + 2K^+ + 8H^+ + 3SiO_2$
(K-feldspar) (chlorite) (silica)

(4) $Ca^{2+} + 2Fe^{3+} + CO_2 + 4H_2O = CaCO_3 + Fe_2O_3 + 8H^+$
(calcite) (hematite)

These reactions are more consistent with the observed mineral compositions of the Rekvika and Tussøya fault zones and suggest that the fluid may originate from a mafic source. A potential mafic source of the infiltrating fluids does not preclude a meteoric origin, but may favour a metamorphic origin of the fluids. One way to generate metamorphic fluids is by prograde reactions during down-faulting of a mafic rock to a deeper crustal level (Caine *et al*. 1996).

Mafic rocks are abundantly found close to all of the studied fault zones. Prograde metamorphism, however, is not consistent with the overall retrograding conditions inferred for the studied fault rocks, but may have been the case for rocks situated at deeper levels during faulting.

Red staining

The red staining of feldspars, as observed within the damage zones of the Rekvika, Tussøya and Kvaløysletta–Straumsbukta fault zones (Figs 3d and 5f, g), is yet another indication of fault-related fluid infiltration; the red staining may in general be attributed to subsolvus alteration of feldspar minerals through hydrothermal alteration (Boone 1969; Taylor 1977; Smith & Brown 1988; Nakano *et al*. 2005; Drake *et al*. 2008), where plagioclase interacts with fluids to form pseudomorphs after plagioclase occupied by albite and K-feldspar. The red staining itself has been demonstrated to occur as a result of the precipitation of hematite within feldspar pores (Putnis *et al*. 2007). The iron is suggested to originate from either fluids

(Putnis *et al*. 2007) or iron-rich plagioclase, where albitization of plagioclase leads to exsolution of iron from the plagioclase crystal at lower temperatures, and its reaction and oxidization in contact with fluids to form distributed hematite (Tegner 1997). Our microstructural studies also suggest that some of the iron may originate from biotite, which has retrograded to chlorite.

Healed fractures cutting plagioclase pseudomorphs are observed to have narrow zones without red staining along them. This indicates that, during later stages of fluid flow, fluids permeated through the fractures as they opened and removed hematite along the now healed fractures (Fig. 5f and g). This may explain the enrichment of hematite within some of the cataclasites and the wide occurrence of later stage precipitation of hematite on fault and fracture surfaces. The ubiquitous epidote in addition to the abundant hematite suggests that conditions were oxidizing during faulting.

Pore pressure and stress conditions

Pore pressure is a critical controlling factor of crustal strength. High pore pressure will effectively decrease the confining pressure and, depending on the differential stress, fracturing will occur as pore pressure approaches lithostatic values (e.g. Hubbert & Rubey 1959; Haimson & Fairhurst 1967). In the following, we will discuss observations that are consistent with fluids having dilated or created open space within the fault rocks, which is indicative of lithostatic pore pressures during faulting. For simplicity, we define lithostatic pressure as equal to σ_3.

The microstructural observations include the following.

(1) Mineral precipitation on fault or fracture surfaces. For fluids to hold fractures open (at least by very small amounts) to allow precipitation of minerals in the dilatant sites, the fluid pressure must exceed the normal stress acting on a fracture plane and as a minimum, be equal to σ_3 (Delaney *et al*. 1986).

(2) Fracturing and dilatation. Microstructural evidence for fracturing and dilatation of the fault rocks is observed and interpreted in the form of fractured biotite with injection of fluids and precipitation of quartz (Fig. 5g), and fractured chlorite with injection of fluids and precipitation of titanite (Fig. 6h). For fluid injection and crack dilatation, the pore pressure needs to equal or exceed σ_3.

(3) Radial growth of chlorite within cataclasites. Undeformed (and thus post-faulting) radial aggregates of chlorite are observed in thin section (Fig. 8f). The radial shape suggests that it has grown into an open pore space. For pore space to exist at depth, the porepressure must, as a minimum, have been equal to σ_3.

(4) Injection of ultracataclasite into the host rock. As pore pressures were sufficient for opening veins for cataclasites to be injected during deformation (Figs 4c, d, g and h), the pore pressure must, as a minimum, have reached σ_3.

Owing to the above-mentioned indications for pore pressures reaching σ_3, a minimum estimate of the pore pressure during faulting is thus *c*. 240MPa, corresponding to the pressure of deformation obtained from estimations based on mineral assemblages from earlier sections. It follows that the differential stress must have been relatively low for the fluid pressure to have reached lithostatic values without causing hydraulic fracturing during earlier phases of pore pressure build-up. Assuming a typical Mohr–Coloumb failure criterion (see Goodman 1989), the differential stress needed to fracture a rock that is subjected to lithostatic pore pressure is of the order of tens of MPa at the most (Fig. 10). The inferred lithostatic pore pressure thus implies that the middle crust was relatively weak during faulting.

The high pore pressure within the fault zones may be explained by episodic flow of high-pressure fluids, also known as seismic pumping (e.g. Sibson *et al*. 1975; Byerlee 1993). The cyclic nature of seismic pumping fits with the inference of episodic rupture in the studied fault zones as suggested by the range of mineral precipitates and several generations of cataclasites.

Fluid flow velocity

The presence of injected ultracataclasites into veins of the fault rocks (Fig. 4g and h) provides an opportunity to roughly estimate the co-seismic fluid velocity during faulting and injection. For cataclasites to be injected, they need to be fluidized.

Stokes' Law, describing the settling of a sphere, provides a good approximation to the fluidization velocity of a granular material (Rodrigues *et al*. 2009). Fluidizing occurs as the fluid velocity (*V*) surpasses the settling velocity (*U*) of a granular material. The minimum fluid flow needed to fluidize and inject the observed ultracataclasite is

$$V \geq U = \frac{2(\rho_s - \rho_f)gR^2}{9\mu}$$

where ρ_s and ρ_f are the density of a sphere (clast) and fluid, respectively, g is the gravitational constant, R is the radius of a sphere (clast), here set to 100μm as observed in thin section (Fig. 5g and h), and μ is the dynamic viscosity, set to 10^{-4} kg m^{-1} s^{-1} for water (for simplicity) at 300 °C (Schmidt & Mayinger 1963). We obtain a value on the order of 10^{-1} m s^{-1} using the parameters derived from this study.

Eichhubl & Boles (2000) calculated palaeo-fluid flow rates during co-seismic fluid expulsion events of a minimum of 0.01 m s^{-1}. The value obtained in the present study suggests that co-seismic rates of fluid flow may exceed those estimated by Eichhubl & Boles (2000) by one order of magnitude.

Fault zone permeability

The above discussion supports that the studied fault zones have acted as fluid conduits during faulting. In addition to their conduit properties such as grain growth and mineral precipitation, other microstructural observations have been made, which shed light on pre- and syn-faulting basement rock permeability.

First, the observed static recrystallization of pre-existing, Archaean–Proterozoic amphibolite-facies ductile fabrics, which are retrograded to greenschist-facies minerals, indicates that fluid infiltration has taken place in the adjacent gneisses. Consequently, permeability within the basement rocks must have been sufficiently large to allow for adequate fluid flow through the rock. Furthermore, basement permeability prior to the brittle deformation has been highly anisotropic, as illustrated by the impregnating properties of pre-existing, boudinaged, foliation-parallel quartz veins (Fig. 7c–e), which have protected its immediate surroundings from static retrogradation, hence limiting permeability across the vein. Thus, pre-existing, extensive, foliation-parallel quartz veining will allow for fluid flow parallel to foliation, but impede across-foliation fluid flow.

Second, the large amount of precipitation of hydrothermal minerals on fault and fracture surfaces in the damage and process zones implies that the fault zones have acted as fluid transport paths. The red staining of feldspar-rich host rocks may also influence fault zone permeability. Drake *et al*. (2008) have shown that the red staining process of plagioclase pseudomorphs increases the porosity compared with unaltered samples. This implies that, as

fluid infiltration and red staining occurs in a plagioclase-rich rock, the permeability within these hydrothermally altered zones will increase with time, as more plagioclase grains are pseudomorphed, giving a positive feedback mechanism for the red staining process.

A model is proposed, using the terminology of fluid flow characteristics of Caine *et al*. (1996), describing faults as fluid conduits, fluid barriers, or fluid conduit–barriers (Fig. 11). The model summarizes the observed feedback mechanisms that may influence fault zone permeability by illustrating the dynamic evolution of three end-member fault zones: (1) a fault zone within granitic host rocks (the Rekvika fault zone); (2) a fault zone within foliated gneisses (the Bremneset fault zone); (3) a fault zone separating granitic rocks in the footwall from banded gneisses in the hanging wall (the Tussøya fault zone).

Prior to faulting, the permeability with granites is assumed to be isotropic. Within sub-horizontal banded gneisses, the horizontal permeability is assumed similar to the permeability within granites, whereas the vertical permeability is strongly impeded owing to pre-existing, impermeable foliation-parallel layers, such as quartz veins. The observed microstructures suggest that, as faulting initiates, fracturing and cataclasis in the core zone and immediate damage zone leads to an increase in permeability and hence an increase in vertical fluid flow within the central parts of the fault (Fig. 11a). As silica walls form owing to pressure release, the permeability within the core zone decreases rapidly and this zone probably becomes completely sealed. The trapped fluids are forced into the surrounding damage zone (Fig. 11b). Here, fluid flow is more restricted, but increases through time within feldspar-rich host rocks, as the red staining process increases permeability. Thus, the damage zone will become the preferred fluid pathway for along-fault fluid flow during periods after faulting (Fig. 11b). In the banded gneisses, however, any vertical (along-fault) fluid flow will be restricted by impermeable foliation-parallel layers and thus encourage foliation-parallel fluid flow away from the fault zone. During longer periods of fault quiescence, a number of subsidiary factors, such as later grain growth, the sealing of fractures and secondary mineral growth–precipitation on fracture surfaces and within pore space, will completely seal the fault zones, impeding both vertical and horizontal fluid flow, independent of host-rock lithology (Fig. 11c). Keulen *et al*. (2008) have shown, based on microstructural criteria, that such healing may occur within a few months at 300°C, through the processes of dissolution and grain growth. Any later reactivation of the fault zone, however, may restart the above-described cycle (Fig. 11a–c). The model implies that a fault zone formed at depths of 8–10km may,

depending on the host rock lithology, cyclically evolve from a fluid conduit, through a conduit–barrier, and finally a full fluid barrier.

Implications for passive margin evolution

The ultracataclasites observed in the Rekvika fault zone are suggested to be comparable with ultracataclasites described by Wibberley (1999) and thus reflect early stages of faulting. Their *in situ* presence indicates that the Late Permian–Early Triassic faulting came to a halt during early (deep) stages of faulting, to prevent subsequent formation of phyllosilicates within the fault zone. Thus, the preservation of these ultracataclasites may coincide with, and be a result of, the westward migration of fault activity to offshore fault complexes after Late Permian–Early Triassic (Davids *et al*. 2013; Indrevær *et al*. 2013). Furthermore, an average geothermal gradient for the upper continental crust is in the range of 25–30 °C km^{-1}. Within early stages of continental rifting, both palaeo- and present geothermal gradients tends to be elevated, especially within subsiding rift-basins, and may exceed 50 °C km^{-1} (Ru & Pigott 1986; Qiu & Wang 1998; Sandiford *et al*. 1998; Liu *et al*. 2001; Wang *et al*. 2011). The geothermal gradient of *c*. 30 °C km^{-1} calculated in this study suggest either that onshore faulting occurred during early phases of rifting along the SW Barents Sea margin, or that the faulting was located along the rift flanks, where geothermal gradients may have remained relatively unchanged.

An uplift of the coastal part of the SW Barents Sea margin has been suggested as part of the formation of the Scandes Mountains (see Corner 2005). The timing and nature of such uplift(s) have been widely discussed in the literature (see Doré *et al*. 2002). The depth estimates from the studied fault zones are used in conjunction with the Late Permian time constraints on faulting in the region (Davids *et al*. 2013) to calculate a minimum average exhumation rate of *c*. 40 m Ma^{-1} for the outer islands of Troms since the Late Permian. When we consider that continental average erosion rates typically range from *c*. 10 to 100 m Ma^{-1} (e.g. Stallard 1988; Schaller *et al*. 2001, 2002; Charreau *et al*. 2011) and that the SW Barents Sea region has experienced extensive glacial erosion in the last 2.7 Ma with an average erosion rate of *c*.380 m Ma^{-1} (Laberg *et al*. 2012), the values suggest that erosion alone can explain the regional exhumation since Permian times: the Late Cenozoic tectonic uplift of the margin may be due to climate deterioration after the formation of the North Atlantic Ocean, which caused subsequent isostatic recalibration and greater uplift of the marginal crust owing to a faster rate of erosion along the margin than inland.

In terms of fault permeability and fluid flow, the studied Late Permian–Early Triassic fault zones may have acted as fluid barriers since this rifting phase. If we assume that the permeability of the basement fault rocks onshore is analogous to that of basement-seated faults offshore, then faults such as those present on the proximal shelf along the SW Barents Sea margin (i.e. the Finnmark Platform and the Loppa High) have the potential to act as hydrocarbon traps. In contrast, any later reactivation of faults after the emplacement of hydrocarbons would most probably increase along-fault permeability and allow for migration of hydrocarbons up through the fault zone.

Conclusions

(1) Late Permian–Early Triassic brittle normal faults make up a network of basement-seated faults that occur both onshore and offshore along the SW Barents Sea passive margin. These faults show varying amounts of displacement from >3 km to hundreds of metres or less, and they comprise distinctive cataclastic fault rocks.

(2) Minimum *P–T* conditions during early stages of faulting are estimated to be *c*. 300 °C and *c*. 240 MPa (*c*. 10 km depth) based on greenschist-facies mineral assemblages of the cataclasites. Later fault movement introduced pumpellyite, yielding minimum *P–T* conditions of *c*. 275 °C and *c*. 220 MPa (*c*. 8.5 km depth).

(3) The quartzitic ultracataclasites that occur within granitoid fault rocks are interpreted to be preserved fault rocks from early stages of faulting that formed as a result of the chemical breakdown of feldspar to epidote with the release of quartz. Fault activity is interpreted to have come to a halt during early (and deep) stages of rifting, as there is no subsequent formation of phyllosilicates within the process zone.

(4) Microstructural evidence indicates that pore pressures locally reached lithostatic levels (240 MPa) during faulting. Fluidized cataclasites allowed for the estimation of the minimum fluid velocity necessary, yielding a value on the order of 10^{-1} m s^{-1}.

(5) The brittle faults within the basement rocks acted as important fluid conduits during rifting in the Late Permian–Early Triassic. A model is proposed, suggesting that fluid flow was concentrated in the core zone during faulting and in the damage zone during periods after faulting. Healing and precipitation processes probably sealed off the fault zones within a short time span after faulting.

(6) A maximum geothermal gradient during faulting in the Late Permian–Early Triassic of *c*. 30 °C km^{-1} is calculated based on the occurrence of pumpellyite. The un-elevated geothermal gradient suggests either that faulting occurred during early stages of continental rifting or that the studied fault zones were located along the rift flanks where little to no subsidence took place.

(7) A minimum average exhumation rate of *c*. 40 m Ma^{-1} since the Late Permian is estimated for the West Troms Basement Complex. When considering normal erosion rates, the proposed late Cenozoic uplift, which has been discussed widely in the literature, may be explained by climate deterioration after the formation of the North Atlantic Ocean, causing subsequent isostatic crustal recalibration and greater isostatic uplift of the margin crust owing to a greater amount of erosion along the margin than inland.

(8) As the studied fault zones are the onshore portions of large fault complexes that continue offshore, it is likely that the studied fault zones are analogous to basement-seated faults offshore. This implies that the conditions and nature of faulting observed onshore may be valid for offshore faults, including past and present fault zone permeability and potential for hydrocarbon entrapment.

Acknowledgements: This work was part of the Industrial PhD scheme organized by the Norwegian Research Council. The project is a collaboration between DONG E&P Norge and the University of Tromsø, financed by DONG E&P Norge and the Norwegian Research Council. We would like to express our gratitude to all those involved from these institutions.

References

Antonsdóttir, V. 2006. *Structural and kinematic analysis of the post-Caledonian Rekvika Fault Zone, Kvaløya, Troms.* Unpublished Master thesis, University of Tromsø, 84 pp.

Bergh, S. G., Eig, K, Kløvjan, O. S., Henningsen, T., Olesen, O. & Hansen, J-A. 2007. The Lofoten-Vesteralen continental margin: a multiphase Mesozoic-Palaeogene rifted shelf as shown by offshore-onshore brittle fault-fracture analysis. Norwegian Journal of Geology, v. **87**, 29 - 58.

Bergh, S. G., Kullerud, K., Armitage, P. E. B., Zwaan, K. B., Corfu, F., Ravna, E. J. K. & Myhre, P. I. 2010. Neoarchaean through Svecofennian tectono-magmatic evolution of the West Troms Basement Complex, North Norway. *Norwegian Journal of Geology*, v. **90**, 21-48.

Blanpied, M. L., Lockner, D. A. & Byerlee, J. D. 1992. An earthquake mechanism based on rapid sealing of faults. *Nature*, **358**(6387), 574-576.

Blystad, P., Brekke, H., Færseth, R. B., Larsen, B. T., Skogseid, J. & Tørudbakken, B. 1995: Structural elements of the Norwegian continental shelf, Part II. The Norwegian Sea Region. Norwegian Petroleum Directorate Bulletin, v. 8. 45pp.

Boone, G. M. 1969. Origin of clouded red feldspars; petrologic contrasts in a granitic porphyry intrusion. *American Journal of Science*, **267**(6), 633-668.

Bos, B. & Spiers, C. J. 2000. Effect of phyllosilicates on fluid-assisted healing of gouge-bearing faults. *Earth and Planetary Science Letters*, **184**(1), 199-210.

Brace, W. F. & Kohlstedt, D. L. 1980. Limits on lithospheric stress imposed by laboratory experiments. *Journal of Geophysical Research. Solid Earth (1978–2012)*, **85**(B11), 6248-6252.

Bruhn, R. L., Parry, W. T., Yonkee, W. A. & Thompson, T. 1994. Fracturing and hydrothermal alteration in normal fault zones. *Pure and Applied Geophysics*, **142**(3-4), 609-644.

Bucher, K. & Grapes, R. H. 2011. *Petrogenesis of metamorphic rocks*. Springer.

Byerlee, J. 1978. Friction of rocks. *Pure and applied Geophysics*, **116**(4-5), 615-626.

Byerlee, J. 1990. Friction, overpressure and fault normal compression. *Geophysical Research Letters*, **17**(12), 2109-2112.

Byerlee, J. D. 1993. Model for episodic flow of high-pressure water in fault zones before earthquakes. *Geology*, **21**(4), 303-306.

Caine, J. S., Evans, J. P. & Forster, C. B. 1996. Fault zone architecture and permeability structure. *Geology*, **24**(11), 1025-1028.

Caine, J. S., Bruhn, R. L. & Forster, C. B. 2010. Internal structure, fault rocks, and inferences regarding deformation, fluid flow, and mineralization in the seismogenic Stillwater normal fault, Dixie Valley, Nevada. *Journal of Structural Geology*, **32**(11), 1576-1589.

Charreau, J., Blard, P. H., Puchol, N., Avouac, J. P., Lallier-Vergès, E., Bourlès, D., ... & Roy, P. 2011. Paleo-erosion rates in Central Asia since 9Ma: A transient increase at the onset of Quaternary glaciations? *Earth and Planetary Science Letters*, **304**(1), 85-92.

Corfu, F. 2004. U–Pb age, setting and tectonic significance of the anorthosite–mangerite–charnockite–granite suite, Lofoten–Vesterålen, Norway. *Journal of Petrology*, **45**(9), 1799-1819.

Corfu, F., Armitage, P. E. B., Kullerud, K. & Bergh, S. G. 2003. Preliminary U-Pb geochronology in the West Troms Basement Complex North Norway: Archaean and Palaeoproterozoic events and younger overprints. *Geological Survey of Norway, Bulletin* **441**, 61-72.

Corner, G. D. 2005. Chap 12. Atlantic coast and fjords. In: Seppälä, M. (ed.). The physical Geography of Fennoscandia, *Oxford Regional Environments Series*, Oxford University Press, 203-228.

Crampin, S., Gudmundsson, A. & Stefánsson, R. 2002. Indication of high pore-fluid pressures in a seismically-active fault zone. *Geophysical Journal International*, **151**(2), F1-F5.

Dalland, A. 1981. Mesozoic sedimentary succession at Andøya, Northern Norway, and relation to structural development of the North Atlantic area. In: Kerr, J. W. & Fergusson, A. J. (eds.) Geology of the North Atlantic borderlands. *Canadian Society of Petroleum Geologists, Memoir* **7**, 563-584.

Davids, C., Wemmer, K., Zwingmann, H., Kohlmann, F., Jacobs, J. & Bergh, S. G. 2013. K–Ar illite and apatite fission track constraints on brittle faulting and the evolution of the northern Norwegian passive margin. *Tectonophysics*, **608**, 196-211.

Delaney, P. T., Pollard, D. D., Zioney, J. 1. & McKee, E. H. 1986. Field relations between dikes and joints: Emplacement processes and paleostress analysis. *Journal of Geophysical Research* **91***, p. 4920-4938.*

Doré, A. G., Lundin, E. R., Fichler, C. & Olesen, O. 1997. Patterns of basement structure and reactivation along the NE Atlantic margin. *Journal of the Geological Society of London* **154**, 85-92

Doré, A. G., Lundin, E. R., Jensen, L. N., Birkeland, Ø., Eliassen, P. E. & Fichler, C. 1999. Principal tectonic events in the evolution of the northwest European Atlantic margins. In: Fleet, A. J. & Boldy,

S. A. R. (eds.), Petroleum Geology of Northwest Europe*: Proceedings of the 5th Conference. Geological Society of London*, 41-61.

Doré, A. G., Cartwright, J. A., Stoker, M. S., Turner, J. P. & White, N. (eds.) 2002. Exhumation of the North Atlantic Margin: Timing, Mechanisms and Implications for Petroleum Exploration, *Special Publications - Geological Society of London*, v. **196**, 45-65.

Drake, H., Tullborg, E. L. & Annersten, H. 2008. Red-staining of the wall rock and its influence on the reducing capacity around water conducting fractures. *Applied Geochemistry*, **23**(7), 1898-1920.

Eichhubl, P. & Boles, J. R., 2000. Rates of fluid flow in fault systems; evidence for episodic rapid fluid flow in the Miocene Monterey Formation, coastal California. *American Journal of Science*, **300**(7), 571-600.

Eig, K. 2008. *Onshore and offshore tectonic evolution of the Lofoten passive margin, North Norway.* Unpublished PhD thesis, University of Tromsø, 256 pp.

Faulkner, D. R., Jackson, C. A. L., Lunn, R. J., Schlische, R. W., Shipton, Z. K., Wibberley, C. A. J. & Withjack, M. O. 2010. A review of recent developments concerning the structure, mechanics and fluid flow properties of fault zones. *Journal of Structural Geology*, **32**(11), 1557-1575.

Faleide, J. I., Tsikalas, F., Breivik, A. J., Mjelde, R., Ritzmann, O., Engen, O., Wilson, J. & Eldholm, O. 2008. Structure and evolution of the continental margin off Norway and Barents Sea. *Episodes* **31***(1),* 82-91.

Forslund, T. 1988. *Post-Kaledonske forkastninger i Vest-Troms, med vekt på Kvaløyslettaforkastningen, Kvaløya*. Unpublished Cand. Scient. thesis, University of Tromsø. 173 pp.

Fürsich, F. & Thomsen, E. 2005. Jurassic biota and biofacies in erratics from the Sortland area, Vesterålen, northern Norway. *Geological Society of Norway, Bulletin* **443**, 37-53.

Gabrielsen, R.H., Færseth, R.B., Jensen, L.N., Kalheim, J.E. & Riis, F. 1990. Structural elements of the Norwegian continental shelf — Part I: the Barents Sea Region. *Norwegian Petroleum Directorate Bulletin* **6**, 33 pp.

Ganerød, G. V., Braathen, A., & Willemoes-Wissing, B. 2008. Predictive permeability model of extensional faults in crystalline and metamorphic rocks; verification by pre-grouting in two sub-sea tunnels, Norway. *Journal of Structural Geology*, ***30***(8), 993-1004.

Gernigon, L. & Brönner, M. 2012. Late Palaeozoic architecture and evolution of the southwestern Barents Sea: insights from a new generation of aeromagnetic data. *Journal of the Geological Society*, **169**(4), 449-459.

Goodman, R. E. 1989. *Introduction to rock mechanics*, 2nd edn. Wiley, New York.

Gudmundsson, A., Berg, S. S., Lyslo, K. B. & Skurtveit, E. 2001. Fracture networks and fluid transport in active fault zones. *Journal of Structural Geology*, **23**(2), 343-353.

Haimson, B. & Fairhurst, C. 1967. Initiation and extension of hydraulic fractures in rocks. *SPE Journal*, **7**(3), 310-318.

Hansen, J.-A. 2009. *Onshore-offshore tectonic relations on the Lofoten and Vesterålen Margin - Mesozoic to early Cenozoic structural evolution and morpological implications.* PhD thesis, University of Tromsø, 229 pp.

Hansen, J. A., Bergh, S. G., & Henningsen, T. 2012: Mesozoic rifting and basin evolution on the Lofoten and Vesterålen Margin, North-Norway; time constraints and regional implications. *Norwegian Journal of Geology*, **91**, 203-228.

Hendriks, B. W. H., Osmundsen, P. T. & Redfield, T. F. 2010. Normal faulting and block tilting in Lofoten and Vesterålen constrained by apatite fission track data*. Tectonophysics* **485**, 154-163.

Hickman, S., Sibson, R. & Bruhn, R. 1995. Introduction to special section: Mechanical involvement of fluids in faulting. *Journal of Geophysical Research: Solid Earth (1978–2012)*, **100**(B7), 12831-12840.

Holdsworth, R. E. 2004: Weak Faults - Rotten Cores. *Science*, *303*(5655), 181-182.

Hubbert, M. K. & Rubey, W. W. 1959. Role of fluid pressure in mechanics of overthrust faulting I. Mechanics of fluid-filled porous solids and its application to overthrust faulting. *Geological Society of America Bulletin*, **70**(2), 115-166.

Indrevær, K., Bergh, S.G., Koehl, J-B, Hansen, J-A, Schermer, E., & Ingebrigtsen, A., 2013. Post-Caledonian brittle fault zones on the hyper-extended SW Barents Sea Margin: New insights into onshore and offshore margin architecture. *Norwegian Journal of Geology,* Vol. 93, pp. 167–188. Trondheim 2013, ISSN 029-196X.

Jaeger, J. C., Cook, N. G. & Zimmerman, R. 2009. *Fundamentals of rock mechanics.* Wiley. com.

Janecke, S. U., & Evans, J. P. 1988. Feldspar-influenced rock rheologies. *Geology*, *16*(12), 1064-1067.

Jefferies, S. P., Holdsworth, R. E., Wibberley, C. A. J., Shimamoto, T., Spiers, C. J., Niemeijer, A. R., & Lloyd, G. E. 2006. The nature and importance of phyllonite development in crustal-scale fault cores: an example from the Median Tectonic Line, Japan. *Journal of Structural Geology*, *28*(2), 220-235.

Kanagawa, K., Cox, S. F. & Zhang, S. 2000. Effects of dissolution-precipitation processes on the strength and mechanical behavior of quartz gouge at high-temperature hydrothermal conditions. *Journal of Geophysical Research: Solid Earth (1978–2012)*, **105**(B5), 11115-11126.

Karner, S. L., Marone, C. & Evans, B. 1997. Laboratory study of fault healing and lithification in simulated fault gouge under hydrothermal conditions. *Tectonophysics*, **277**(1), 41-55.

Keulen, N., Stünitz, H. & Heilbronner, R. 2008. Healing microstructures of experimental and natural fault gouge. *Journal of Geophysical Research: Solid Earth (1978–2012)*, **113**(B6). DOI: 10.1029/2007JB005039

Laberg, J. S., Andreassen, K. & Vorren, T. O. 2012. Late Cenozoic erosion of the high-latitude southwestern Barents Sea shelf revisited. *Geological Society of America Bulletin*, **124**(1-2), 77-88.

Mosar, J., Torsvik, T. H. & the BAT team 2002. Opening the Norwegian and Greenland Seas: Plate tectonics in Mid Norway since the Late Permian. In: Eide, E.A. (coord.), *BATLAS - Mid Norway plate reconstruction atlas with global Atlantic perspectives*, 48-59. The Geological Survey of Norway, Trondheim.

Nakano, S., Akai, J. & Shimobayashi, N. 2005. Contrasting Fe-Ca distributions and related microtextures in syenite alkali feldspar from the Patagonian Andes, Chile. *Mineralogical Magazine*, **69**(4), 521-535.

Nakatani, M. & Scholz, C. H. 2004. Frictional healing of quartz gouge under hydrothermal conditions: 1. Experimental evidence for solution transfer healing mechanism. *Journal of Geophysical Research: Solid Earth (1978–2012)*, **109**(B7). DOI: 10.1029/2001JB001522

Nansheng, Q. & Jiyang, W. 1998. The use of free radicals of organic matter to determine paleogeothermal gradient. *Organic geochemistry*, **28**(1-2), 77-86.

Olesen, O., Torsvik, T. H., Tveten, E., Zwaan, K. B., Løseth, H. & Henningsen, T. 1997. Basement structure of the continental margin in the Lofoten-Lopphavet area, northern Norway: constraints from potential field data, on-land structural mapping and palaeomagnetic data, *Norwegian Journal of Geology* **77**, 15–30.

Olsen, M. P., Scholz, C. H. & Léger, A. 1998. Healing and sealing of a simulated fault gouge under hydrothermal conditions: Implications for fault healing. *Journal of Geophysical Research: Solid Earth (1978–2012)*, **103**(B4), 7421-7430.

Opheim, J.A. and Andresen, A. 1989. Basement-cover relationships on northern Vanna, Troms, Norway. *Norwegian Journal of Geology*, v. **69**(2), 67-81.

Osmundsen, P. T., Redfield, T. F., Hendriks, B. H. W., Bergh, S., Hansen, J. A., Henderson, I. H. C., Dehls, J., Lauknes, T.R., Larsen, Y., Anda, E. & Davidsen, B. 2010: Fault-controlled alpine topography in Norway. Journal of the Geological Society, 167(1), 83-98.

Putnis, A., Hinrichs, R., Putnis, C. V., Golla-Schindler, U. & Collins, L. G. 2007. Hematite in porous red-clouded feldspars: evidence of large-scale crustal fluid–rock interaction. *Lithos*, **95**(1), 10-18.

Rice, J. R. 1992. Fault stress states, pore pressure distributions, and the weakness of the San Andreas fault. *International Geophysics Series*, **51**, p. 475-503.

Roberts, D. & Lippard, S.J. 2005. Inferred Mesozoic faulting in Finnmark: current status and offshore links. *Geological Survey of Norway Bulletin* **443**, 55-60.

Rodrigues, N., Cobbold, P. R. & Løseth, H. 2009. Physical modelling of sand injectites. *Tectonophysics*, **474**(3), 610-632.

Ru, K. & Pigott, J. D. 1986. Episodic rifting and subsidence in the South China Sea. *Am. Assoc. Pet. Geol., Bull.;(United States)*, **70**(9).

Rutter, E. H., Holdsworth, R. E., & Knipe, R. J. 2001: The nature and tectonic significance of fault-zone weakening: an introduction. *Geological Society, London, Special Publications*, *186*(1), 1-11.

Sandiford, M., Hand, M. & McLaren, S. 1998. High geothermal gradient metamorphism during thermal subsidence. *Earth and Planetary Science Letters*, **163**(1), 149-165.

Schaller, M., von Blanckenburg, F., Hovius, N. & Kubik, P. W. 2001. Paleo-Erosion Rates From in Situ ^{10}Be in Middle European River Terrace Sediments. In *AGU Fall Meeting Abstracts* (Vol. **1**, p. 0449).

Schaller, M., Von Blanckenburg, F., Veldkamp, A., Tebbens, L. A., Hovius, N. & Kubik, P. W. 2002: A 30 000 yr record of erosion rates from cosmogenic ^{10}Be in middle European river terraces. *Earth and Planetary Science Letters*, **204**(1), 307-320.

Schmidt, E. H. W. and F. Mayinger, 1963. Viscosity of Water and Steam at High Pressures and Temperatures Up to 800 Atmospheres and 700 C. Edited by Warren Ibele. *Modern Developments in Heat Transfer*, p. 265-278. Academic Press Inc, New York.

Seront, B., Wong, T. F., Caine, J. S., Forster, C. B., Bruhn, R. L. & Fredrich, J. T. 1998. Laboratory characterization of hydromechanical properties of a seismogenic normal fault system. *Journal of structural geology*, **20**(7), 865-881.

Sibson, R. H. 1973. Frictional constraints on thrust, wrench and normal faults. *Nature*, **249**, 542-544.

Sibson, R. H. 1977. Fault rocks and fault mechanisms. *Journal of the Geological Society*, **133**(3), 191-213.

Sibson, R. H. 1989. Earthquake faulting as a structural process. *Journal of Structural Geology*, **11**(1), 1-14.

Sibson, R. H., Moore, J. M. M. & Rankin, A. H. 1975. Seismic pumping—a hydrothermal fluid transport mechanism. *Journal of the Geological Society*, **131**(6), 653-659.

Smelror, M., Petrov, O.V., Larssen, G.B. & Werner, S.C. (eds.) + 16 co-authors 2009. *Geological history of the Barents Sea*. Geological Survey of Norway, Trondheim, 135 pp.

Smith, J. V. & Brown, W. L. 1988. *Feldspar minerals*. Springer-Verlag.

Stallard, R. F. 1988. Weathering and erosion in the humid tropics. In *Physical and Chemical Weathering in Geochemical Cycles* (pp. 225-246). Eds: Lerman, A. & Meybeck, M. Springer Netherlands.

Taylor, H. P. 1977. Water/rock interactions and the origin of H2O in granitic batholiths Thirtieth William Smith lecture. *Journal of the Geological Society*, **133**(6), 509-558.

Tegner, C. 1997. Iron in plagioclase as a monitor of the differentiation of the Skaergaard intrusion. *Contributions to Mineralogy and Petrology*, **128**(1), 45-51.

Thorstensen, L. 2011. *Land-sokkel korrelasjon av tektoniske elementer i ytre del av Senja og Kvaløya i Troms.* Unpublished Master thesis, University of Tromsø, 107 pp.

Torgersen, E., Viola, G. & Zwingmann, H. 2013. How can K-Ar geochronology of clay-size mica/illite help constrain reactivation histories of brittle faults? An example from a Paleozoic thrust fault in Northern Norway. In EGU General Assembly Conference Abstracts (Vol. 15, p. 2986).

Wang, W., Zhou, Z., Guo, T. & Xu, C. 2011. Early cretaceous-paleocene geothermal gradients and Cenozoic tectono-thermal history of Sichuan basin.*Journal of Tongji University. Natural Science*, **39**(4), 606-613.

Wibberley, C. 1999. Are feldspar-to-mica reactions necessarily reaction-softening processes in fault zones?. *Journal of Structural Geology*, **21**(8), 1219-1227.

Wintsch, R. P., Christoffersen, R., & Kronenberg, A. K. 1995. Fluid-rock reaction weakening of fault zones. *Journal of Geophysical Research: Solid Earth (1978–2012)*, **100**(B7), 13021-13032.

Yiqun, L., Mingsheng, Y., Dingwu, Z., Qiao, F. & Jun, J. 2001. New progresses on geothermal history of Turpan-Hami Basin, Xinjiang, China. *Science in China Series D: Earth Sciences*, **44**(2), 166-176.

Zoback, M. D. 1991. State of stress and crustal deformation along weak transform faults. *Philosophical Transactions of the Royal Society of London. Series A: Physical and Engineering Sciences*, **337**(1645), 141-150.

Zoback, M. D. & Townend, J. 2001. Implications of hydrostatic pore pressures and high crustal strength for the deformation of intraplate lithosphere. *Tectonophysics*, **336**(1), 19-30.

Zwaan, K. B. 1995. Geology of the West Troms Basement Complex, northern Norway, with emphasis on the Senja Shear Belt: a preliminary account. *Geological Survey of Norway, Bulletin* **427**, 33-36.

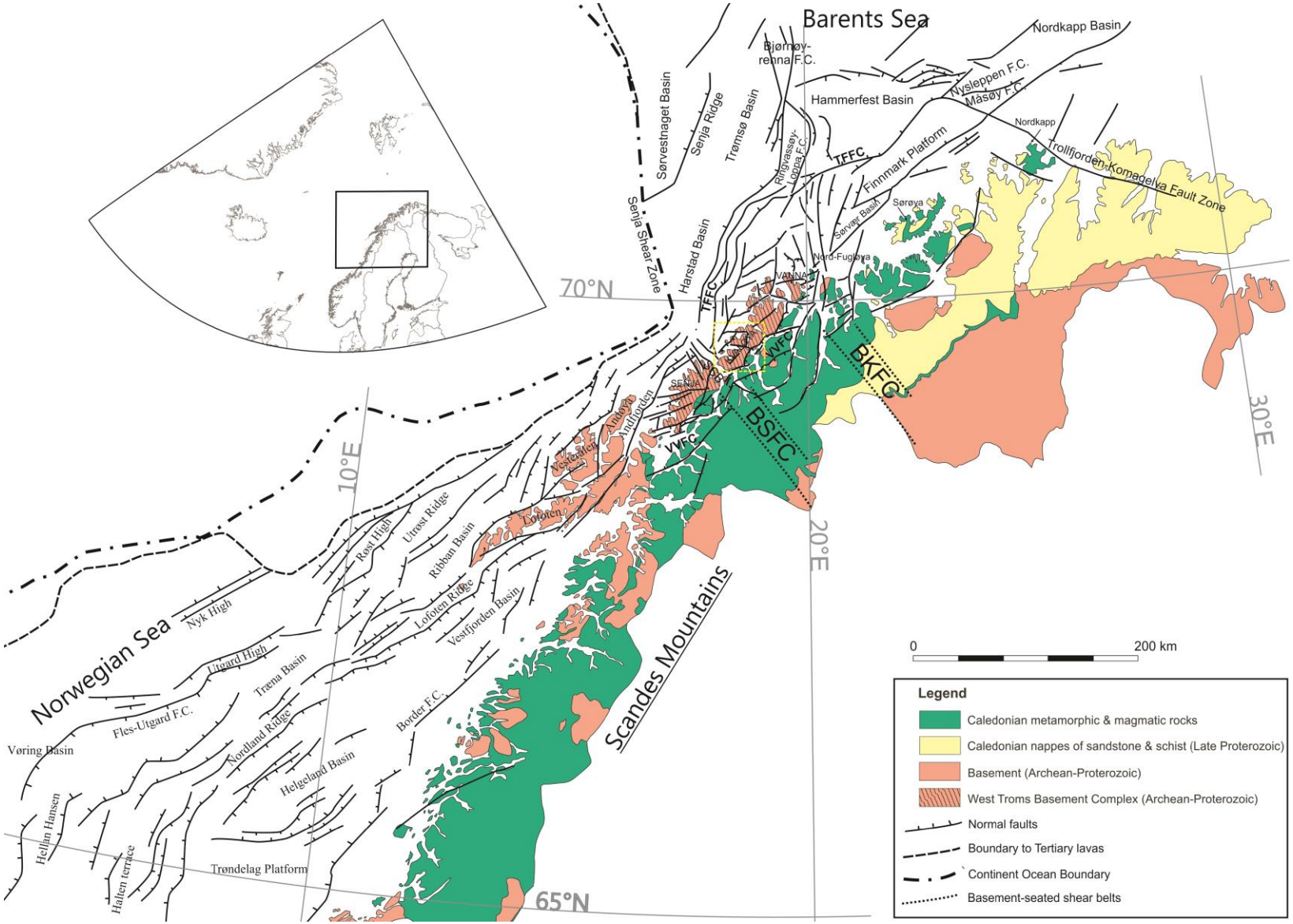

Fig. 1. Regional onshore–offshore tectonic map and setting of the mid-Norwegian shelf, the West Troms Basement Complex and the SW Barents Sea margin (after Blystad *et al.* 1995; Mosar *et al.* 2002; Bergh *et al.* 2007; Faleide *et al.* 2008; Hansen *et al.* 2012; Indrevær *et al.* 2014). Onshore geology is from the Geological Survey of Norway. The yellow box outlines Figure 2. BKFC, Bothnian-Kvænangen Fault Complex; BSFC, Bothnian-Senja Fault Complex; TFFC, Troms–Finnmark Fault Complex; VVFC, Vestfjorden-Vanna Fault Complex.

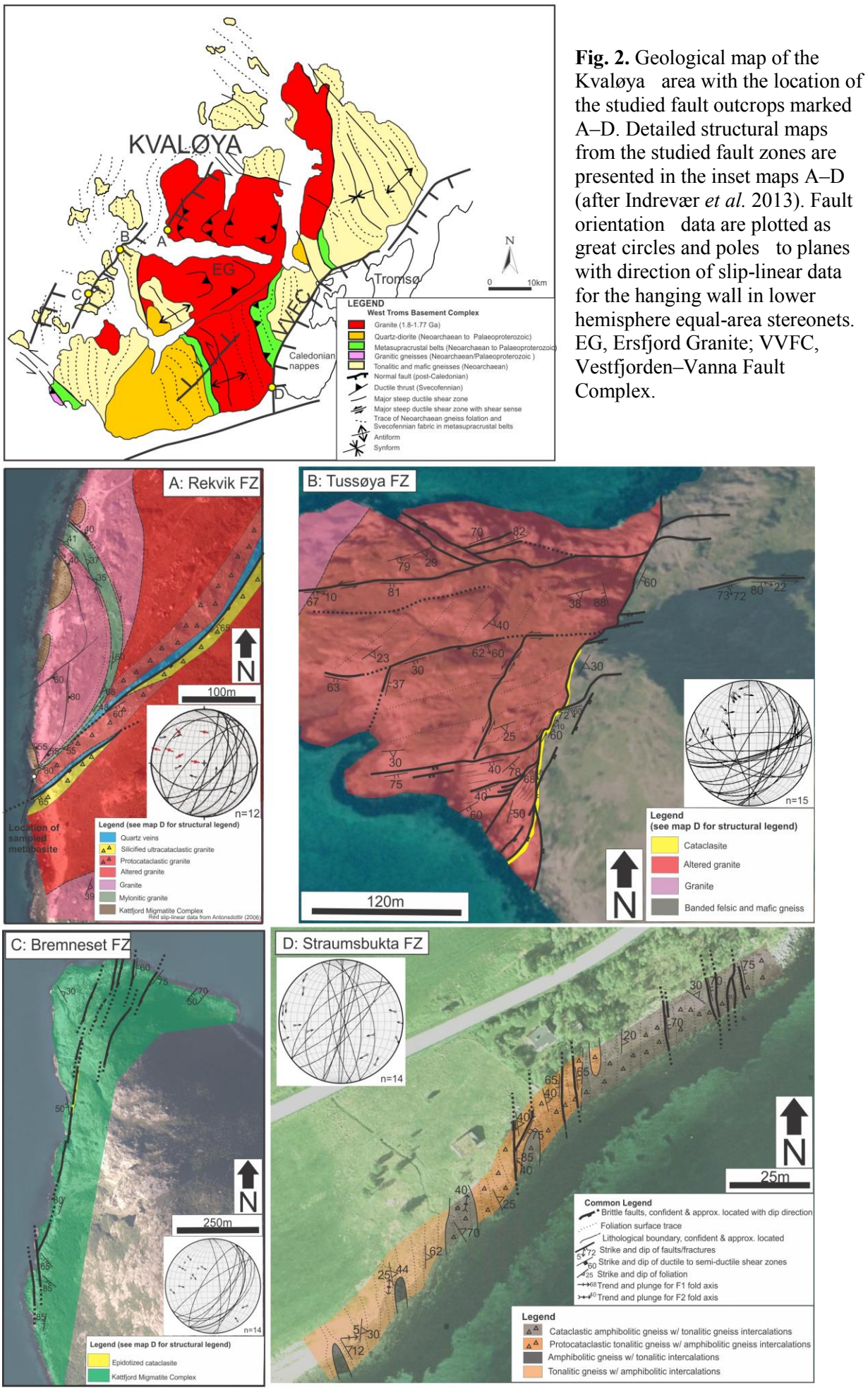

Fig. 2. Geological map of the Kvaløya area with the location of the studied fault outcrops marked A–D. Detailed structural maps from the studied fault zones are presented in the inset maps A–D (after Indrevær *et al.* 2013). Fault orientation data are plotted as great circles and poles to planes with direction of slip-linear data for the hanging wall in lower hemisphere equal-area stereonets. EG, Ersfjord Granite; VVFC, Vestfjorden–Vanna Fault Complex.

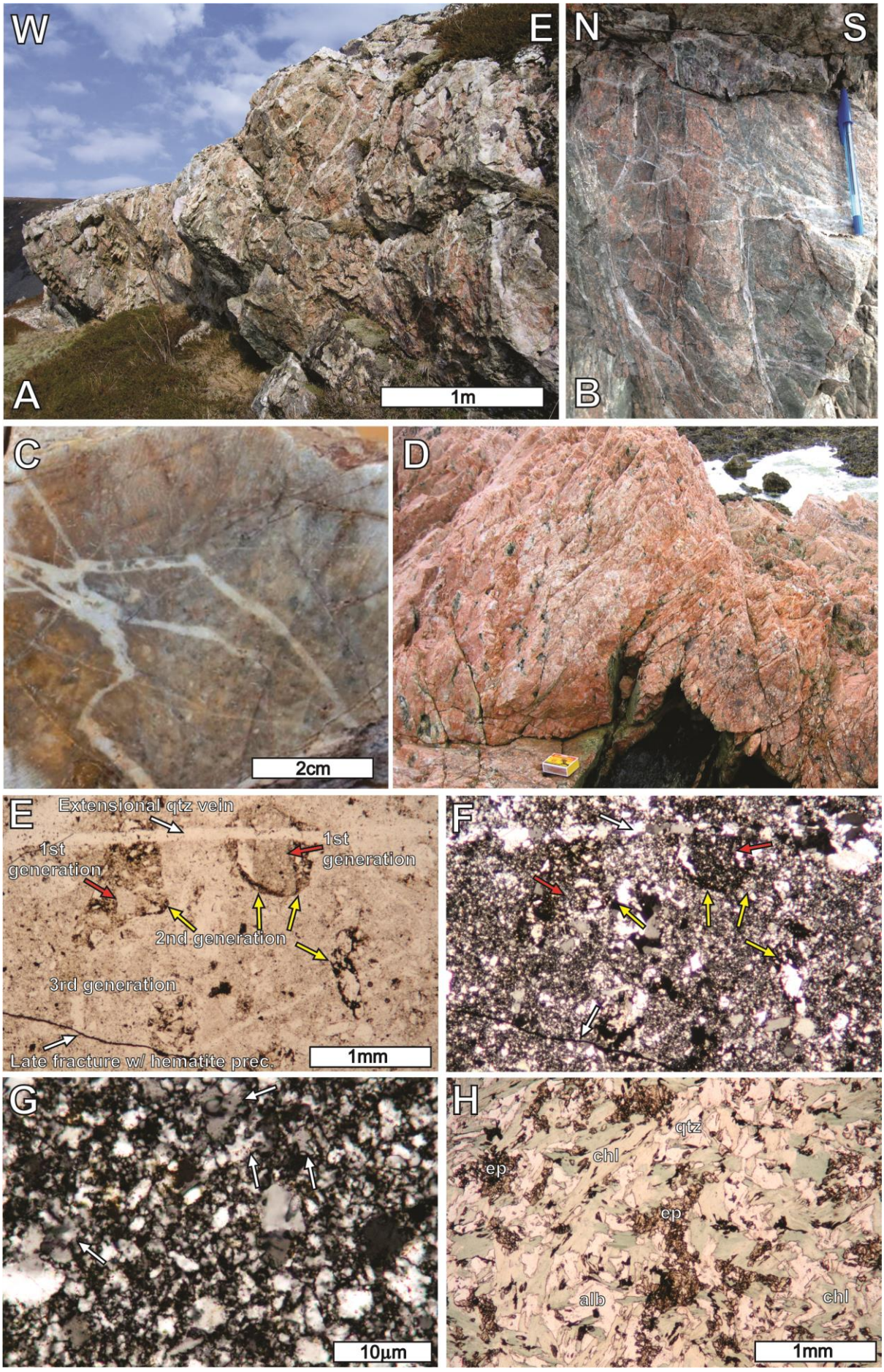
W
E
A
1m
N
S
B
C
2cm
D
E
Extensional qtz vein
1st generation
1st generation
2nd generation
3rd generation
Late fracture w/ hematite prec.
1mm
F
G
10µm
H
qtz
chl
ep
ep
alb
chl
1mm

Fig. 3. (Previous page) Outcrop photographs and photomicrographs from the Rekvik fault zone. (**a**) Damage zone of the Rekvika fault zone. The extensive occurrence of quartz veins should be noted. (**b**) Close-up of the damage zone close to the process zone. The occurrence of epidote, irregular quartz veins and clasts of red granite should be noted. (**c**) Close-up of quartzitic ultracataclasite from the process zone of the Rekvika fault zone. (**d**) A typical example of red stained granite from the damage zone surrounding the Rekvika fault zone. (**e**) Quartz-rich cataclasite matrix with fragments of former cataclasite cut by extensional quartz veins and late-stage fractures with precipitation of hematite; plane-polarized light. The three generations of cataclasites should be noted. Red arrows indicate first generation; yellow arrows indicate second generation cataclasites. The two first generations are embedded within the matrix of the third generation. (**f**) Same as (**e**) but with crossed polars. (**g**) Indications of grain growth within the fine-grained domain of the second generation of cataclasite in (**e**) and (**f**); crossed polars. (**h**) A statically recrystallized mafic cataclasite showing a typical greenschist- facies mineral assemblage. alb, albite; chl, chlorite; ep, epidote; qtz, quartz.

Fig. 4. (next page) Outcrop photographs and photomicrographs from the Tussøya fault zone. (**a**) Overview of the fault zone showing how the fault zone separates banded gneisses in the hanging wall from granite in the footwall. (**b**) Detailed photograph of the main fault zone and the hanging wall, indicating the spatial relationship between the main fault zone, subsidiary faults and the gneiss foliation. (**c**) Outcrop photograph of a fault segment from the Tussøya fault zone that cuts through granite. (Note the dark band of ultracataclasite that fills fault-related fractures that are at a high angle to the main fault zone (arrows).) (**d**) Close-up of a dark band of ultracataclasite within the granite host rock. Location is shown in (**c**). (Note how the cataclasite lacks any internal foliation consistent with high strain and the relatively undamaged sidewalls.) (**e**) Fault rock containing three generations of cataclasites, shown by cross-cutting relationships. (**f**) Same as (**e**) but with crossed

polars. (**g**) Microfracture composed of injected cataclasite. (**h**) Same as (**g**) but with crossed polars.

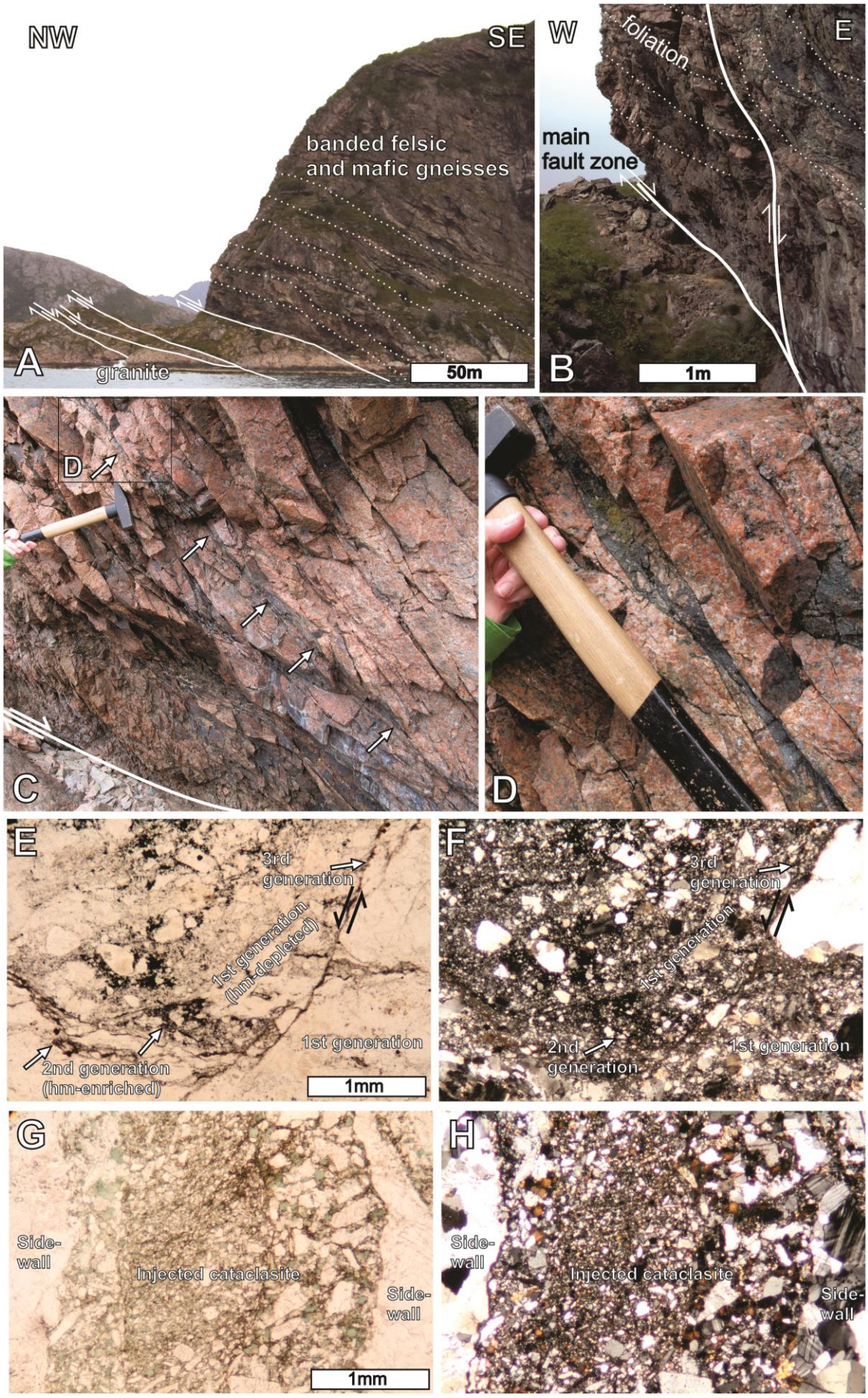

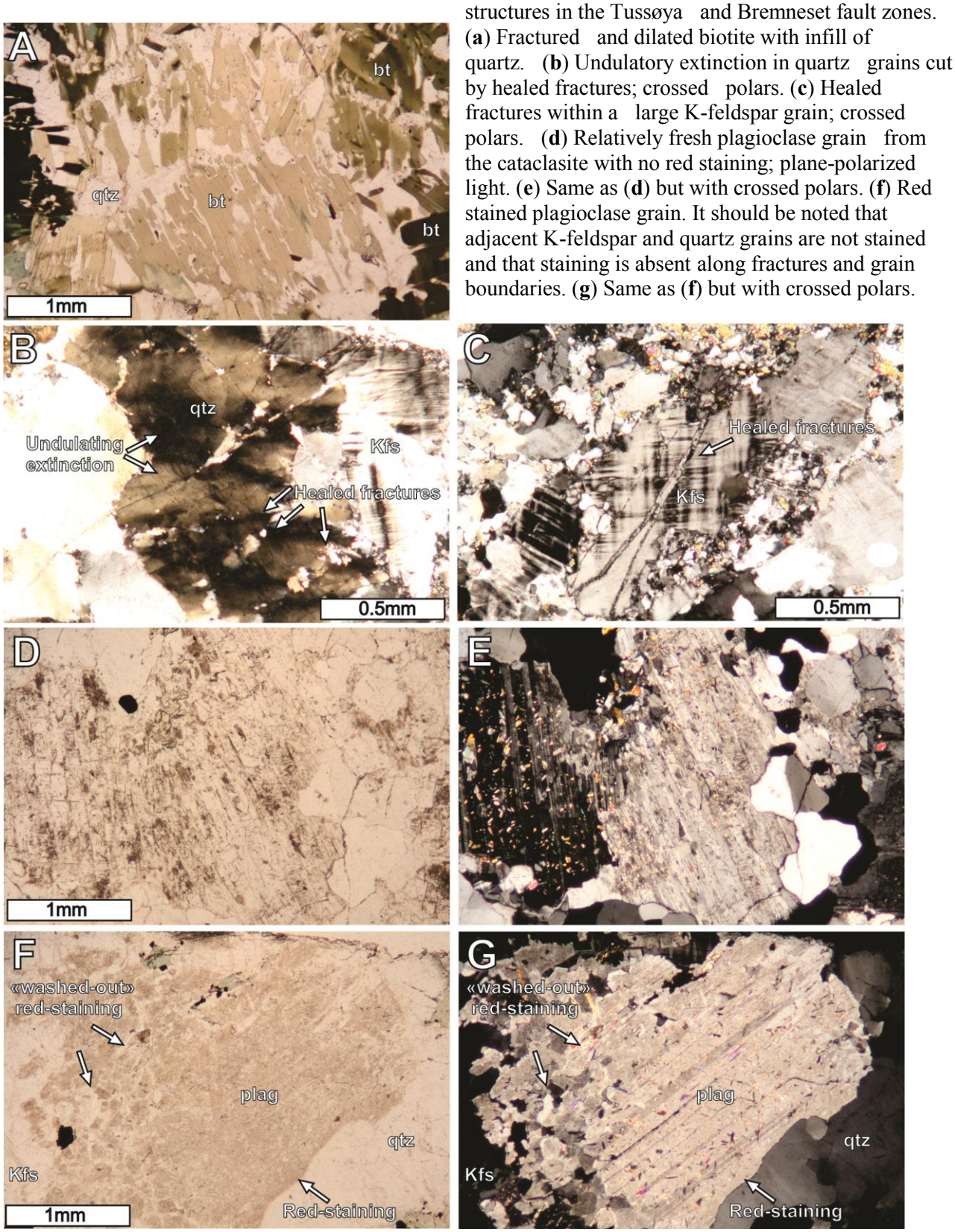

Fig. 5. Photomicrographs of observed deformation structures in the Tussøya and Bremneset fault zones. (**a**) Fractured and dilated biotite with infill of quartz. (**b**) Undulatory extinction in quartz grains cut by healed fractures; crossed polars. (**c**) Healed fractures within a large K-feldspar grain; crossed polars. (**d**) Relatively fresh plagioclase grain from the cataclasite with no red staining; plane-polarized light. (**e**) Same as (**d**) but with crossed polars. (**f**) Red stained plagioclase grain. It should be noted that adjacent K-feldspar and quartz grains are not stained and that staining is absent along fractures and grain boundaries. (**g**) Same as (**f**) but with crossed polars.

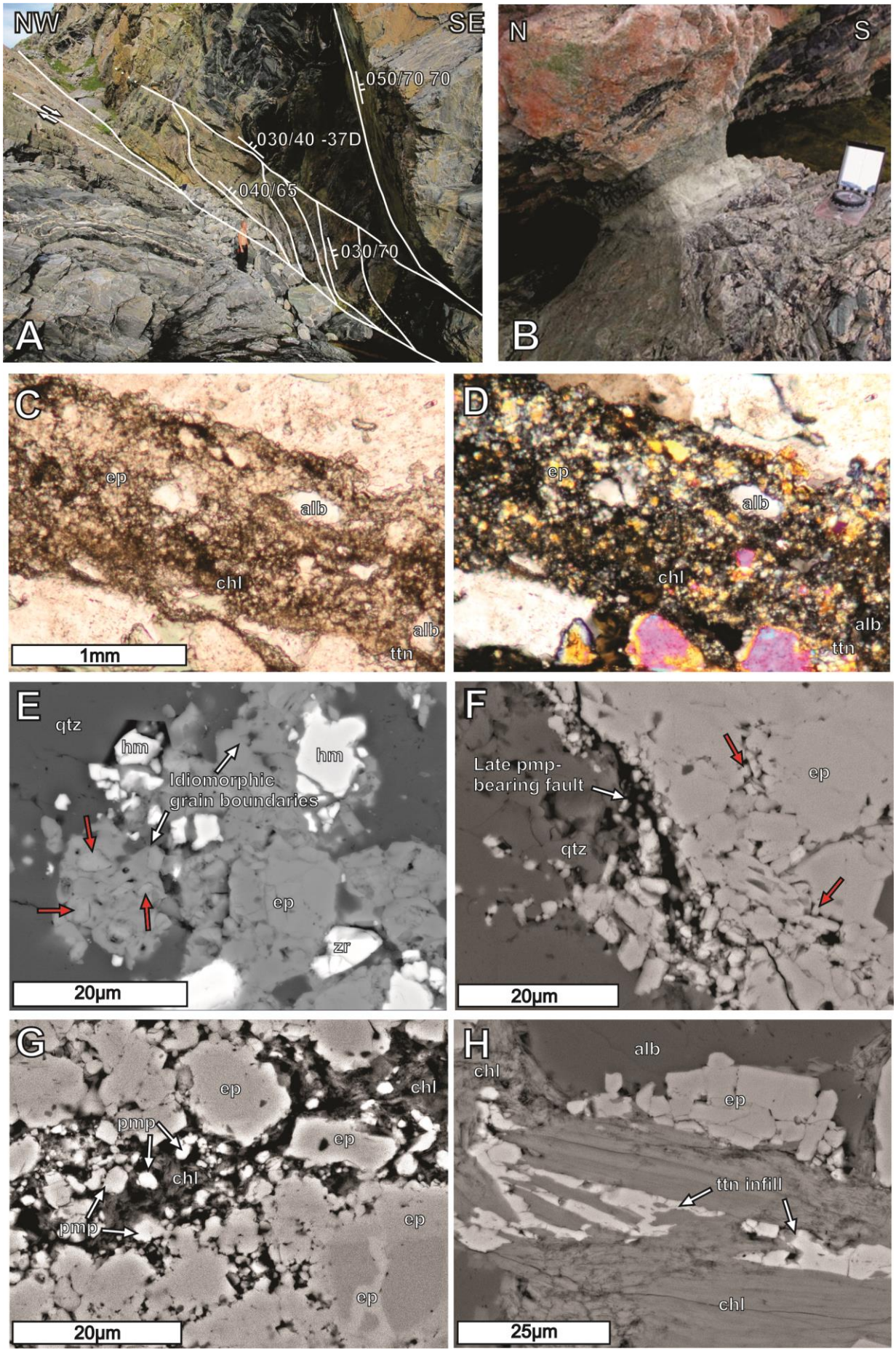
NW
SE
050/70 70
030/40 -37D
040/65
030/70
A
N
S
B
C
ep
alb
chl
alb
ttn
1mm
D
ep
alb
chl
alb
ttn
E
qtz
hm
hm
Idiomorphic grain boundaries
ep
zr
20µm
F
Late pmp-bearing fault
ep
qtz
20µm
G
ep
chl
pmp
ep
chl
pmp
ep
ep
20µm
H
alb
chl
ep
ttn infill
chl
25µm

Fig. 6. (previous page) Outcrop photographs, photomicrographs and BSD images of fault rocks from Bremneset. (**a**) Overview of parts of the Bremneset fault zone. (See person for scale.) (**b**) Close-up of a portion of the Bremneset fault zone. The red stained block of granite in the hanging wall should be noted. (**c**) Cataclastic mafic gneiss from the Bremneset fault zone composed of grains with greenschist-facies minerals. (**d**) Same view as (**c**) but with crossed polars. (**e**) BSD image illustrating how clasts of epidote (red arrows) have grown and developed idiomorphic grain boundaries, supporting that greenschist-facies conditions prevailed prior to, during and after early stages of faulting (from Tussøya fault zone). (**f**, **g**) Idiomorphic epidote grains cut by late-stage microfaults with the formation of pumpellyite (from Bremneset fault zone). The red arrows in (**f**) show examples of preserved epidote clasts from the earlier greenschist-facies fault activity. (**h**) BSD image of fractured and dilated chlorite with titanite infill (from Bremneset fault zone). alb, albite; chl, chlorite; ep, epidote; hm, hematite; ttn, titanite; qtz, quartz; zr, zircon.

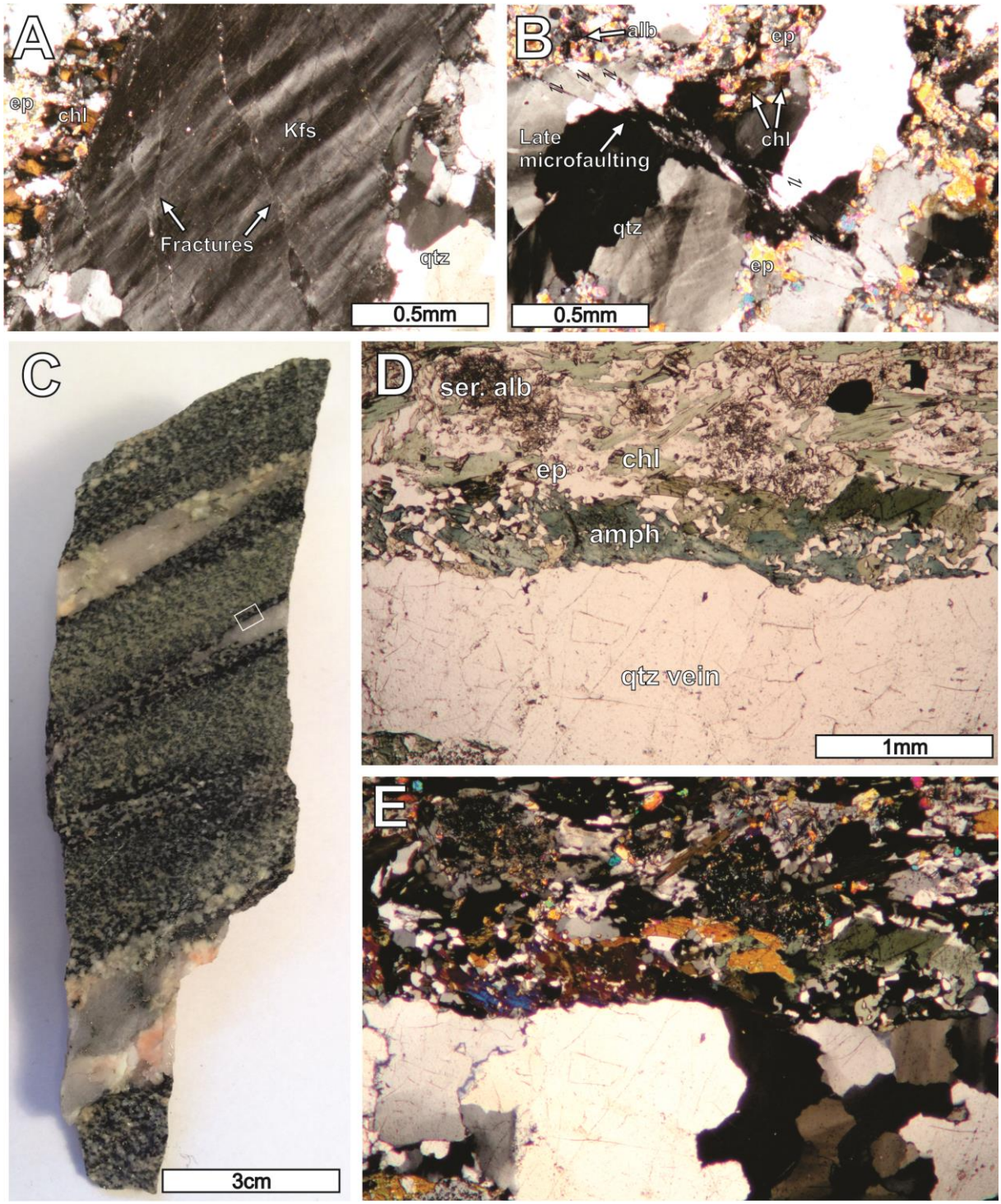

Fig. 7. Photomicrographs and hand-specimen photograph from the Bremneset fault zone. (**a**, **b**) Late microfaulting with no development of cataclasite. Crossed polars. (**c**) Hand-specimen of banded and retrograded amphibolite gneiss with foliation-parallel quartz veins. The preserved zone of amphibolite-facies mineral assemblage (dark bands) along quartz veins that are parallel to ductile foliation and predate the brittle deformation should be noted. Away from the quartz veins, the mafic gneiss is statically retrograded to a greenschist-facies mineral assemblage (green bands). (**d**) Micrograph showing the zone of preserved amphibole along the rim of the quartz vein in an otherwise statically recrystallized rock. Location is shown in (**c**). (**e**) Same as (**d**) but with crossed polars. amph, amphibole; chl, chlorite; ep, epidote; ser. alb, sericitic albite; qtz, quartz.

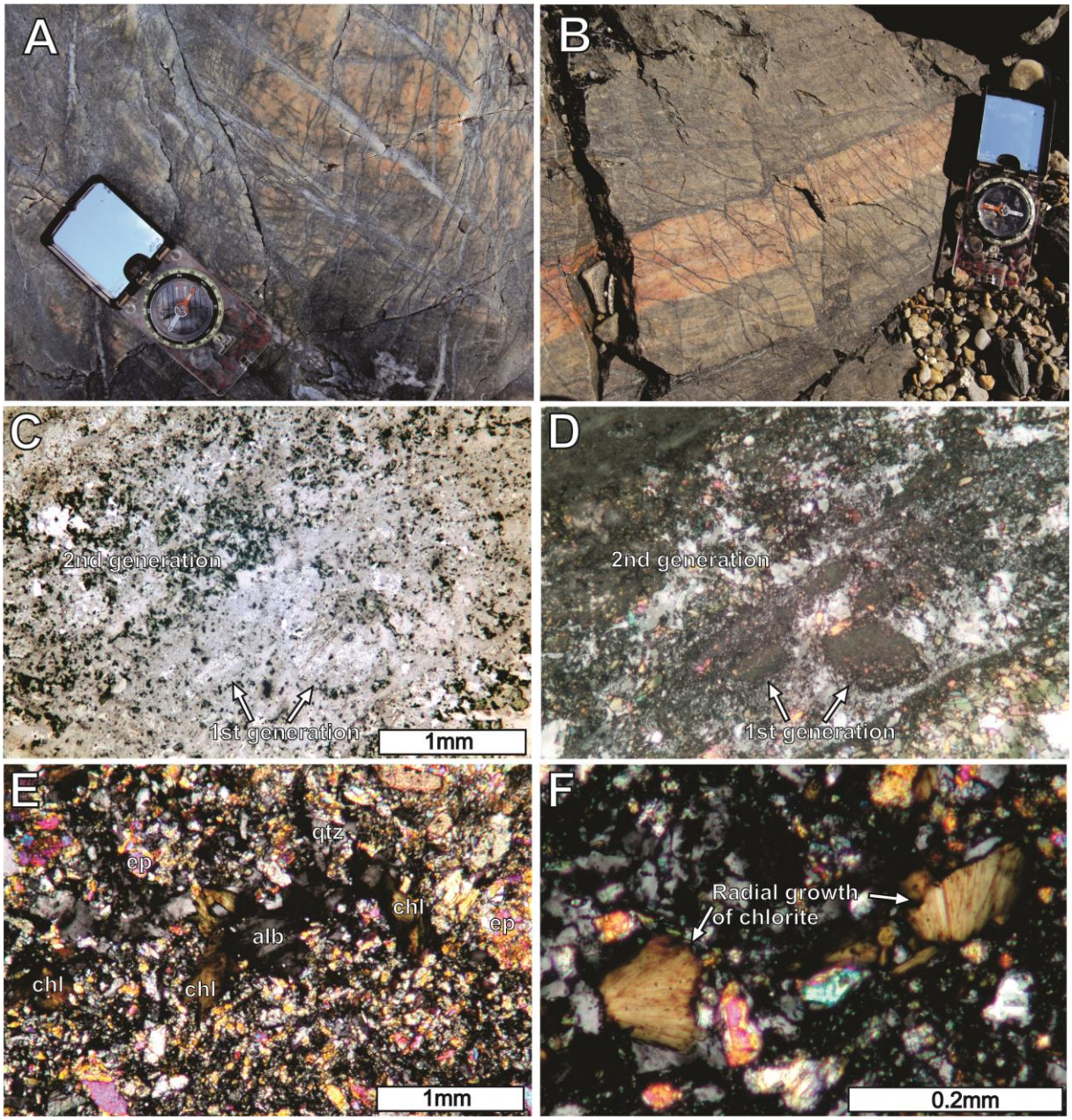

Fig. 8. Outcrop photographs and photomicrographs of cataclastic amphibolitic gneisses from the Kvaløysletta–Straumsbukta fault zone at Straumsbukta. (**a**, **b**) Outcrop photographs of cataclased tonalites from the footwall damage zone of the Kvaløysletta–Straumsbukta fault zone. The dark bands of chlorite should be noted. (**c**) A cataclastic zone showing at least two generations of mafic cataclasite outlined by very fine-grained (<1 μm) epidote, chlorite and quartz aggregates forming the first generation, which appear as clasts within a second generation of cataclasite with similar composition. (**d**) Same as (**c**) but with crossed polars. (**e**) Mafic cataclasite showing greenschist-facies mineral growth. The radial growth of chlorite in the matrix of the cataclasite should be noted. (**f**) Close-up of chlorite within the cataclasite showing radial growth. Crossed polars. alb, albite; chl, chlorite; ep, epidote; qtz, quartz.

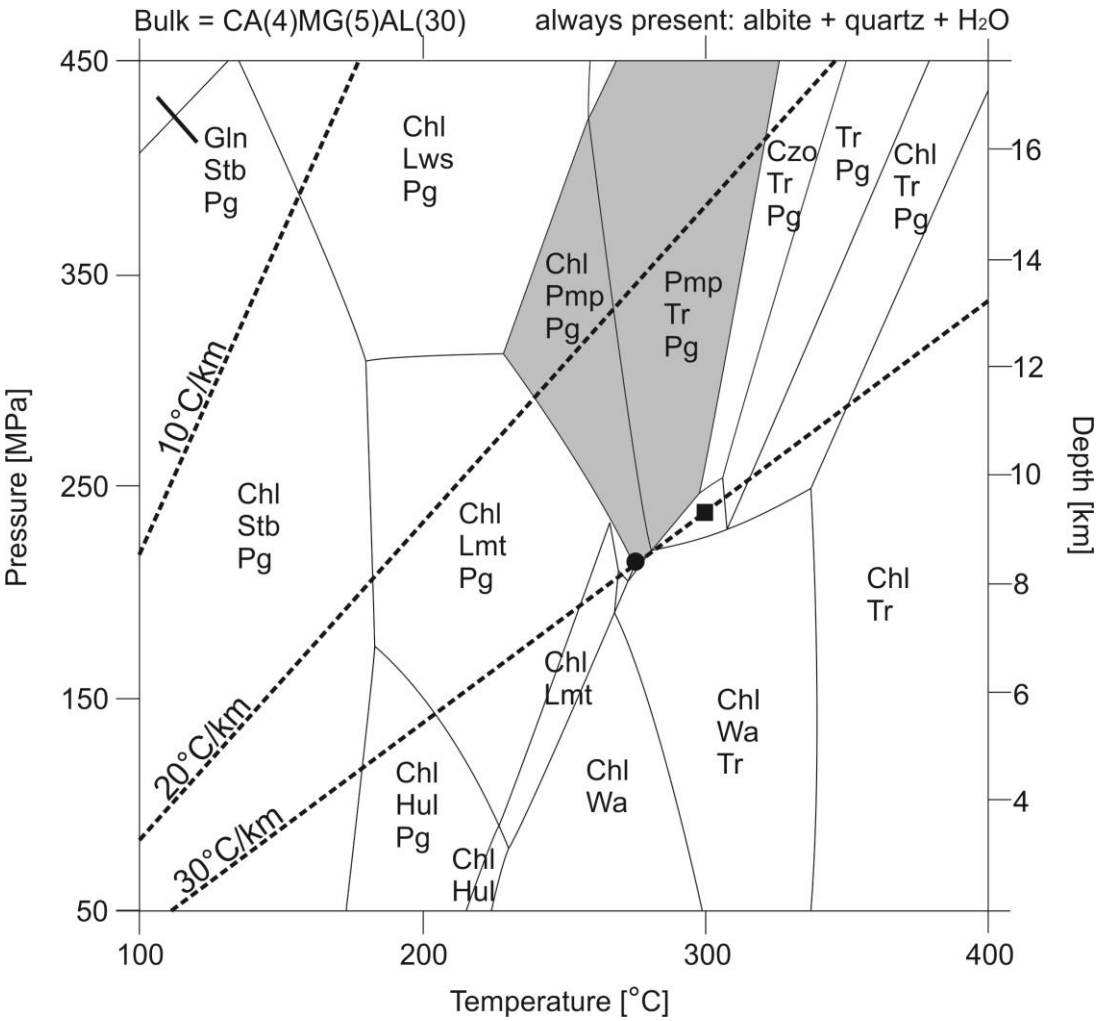

Fig. 9. *P–T* diagram showing mineral assemblages and stability fields of a CMASH system at low-grade metamorphic-facies conditions assuming an average meta-MORB composition. Dashed lines are geothermal gradients. The shaded area marks the stability field of pumpellyite. The black square indicates minimum *P–T* conditions for the early stage faulting; the black circle indicates minimum *P–T* conditions during later-stage faulting. The diagram is modified from Bucher & Grapes (2011). Chl, chlorite; Czo, clinozoisite; Gln, glaucophane; Hul, heulandite; Pg, paragonite; Pmp, pumpellyite; Lmt, laumonite; Lws, lawsonite; Stb, stilbite; Tr, tremolite; Wa, wairakite.

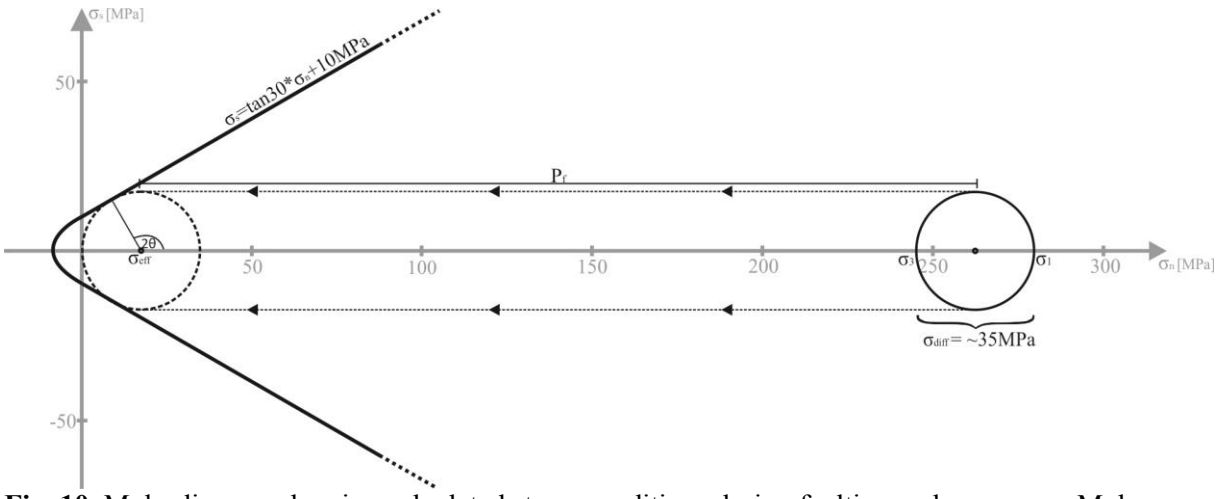

Fig. 10. Mohr diagram showing calculated stress conditions during faulting and a common Mohr–Coloumb failure criterion (see Goodman 1989). The evidence for lithostatic pore pressure suggests that the differential stress did not exceed *c*. 35 MPa.

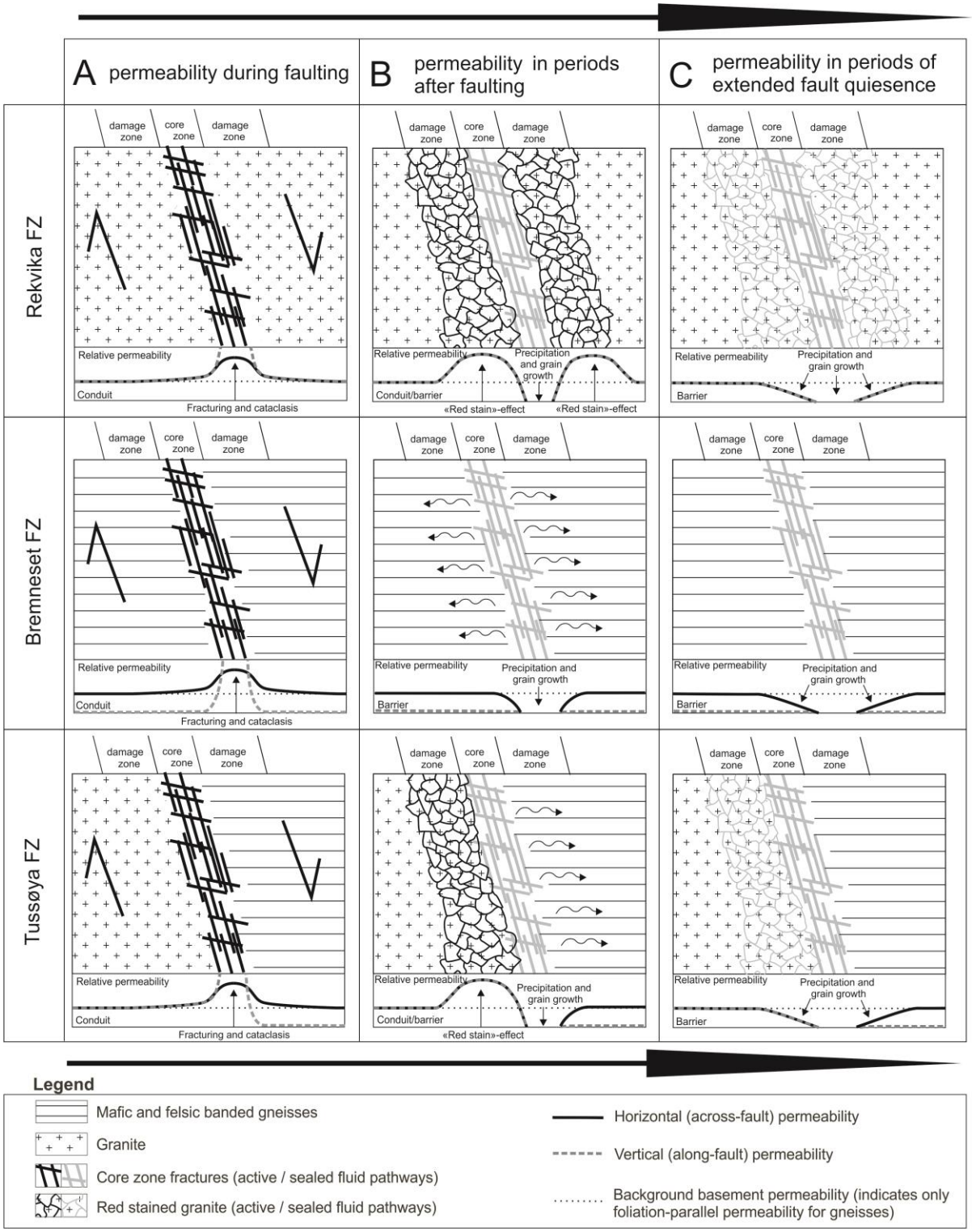

Fig. 11. Schematic illustrations of a model for cyclic changes in permeability contrast through time within fault zones of different host rock lithologies. Relative changes in across-fault and along-fault permeability are illustrated by the curves below each sketch. (**a**) With faulting, movement along a fault causes fracturing and cataclasis within the core zone and increases permeability. The core zone thereby acts as a fluid conduit. (**b**) Precipitation of minerals and grain growth within the core zone decreases permeability within the core zone and forces fluid flow into the damage zone. Within feldspar- rich host rocks, permeability increases with time owing to the red staining effect. (**c**) Grain growth (healing) and precipitation processes through time decrease permeability and with time seal the entire fault zone. Fault reactivation will initiate a new fluid flow cycle.

Paper 3

Linking onshore-offshore basement rock architecture and brittle faults on the submerged strandflat along the SW Barents Sea Margin; using high-resolution (5x5m) bathymetry data

Kjetil Indrevær[1,2,*] & Steffen G. Bergh[1]

1) Department of Geology, University of Tromsø, N-9037 Tromsø, Norway
2) DONG E&P Norge AS, Roald Amundsens Plass 1, N-9257 Tromsø, Norway

* Corresponding author (e-mail: kjetil@indrevar.no)

Abstract: High-resolution bathymetry data reveal astonishingly detailed and complex morphology on the shallow offshore shelf (strandflat) along the SW Barents Sea Margin, outboard Troms, northern Norway. The features are compared with, and interpreted based on, known onshore geology, including Precambrian basement structures of the West Troms Basement Complex, Caledonian thrust nappes and post-Caledonian passive margin brittle structures. The study reveals that Precambrian basement structures commonly observed onshore, such as a generally steep gneiss foliation, steeply plunging tight to isoclinal intrafolial folds, upright macro-fold limbs, duplexes and high-strain ductile shear zones are also present on the strandflat, including possible offshore continuations of Precambrian meta-supracrustal belts. The results suggest that the strandflat outboard Troms is largely comprised of rocks of West Troms Basement Complex affinity. A contact with Caledonian thrust nappes is interpreted to trend NW-SE within a sound in the northern parts of the study area, where it overlaps with the Late Palaeozoic-Mesozoic Fugløya transfer zone, a possible reactivated portion of a Proterozoic-Palaeozoic basement-seated fault complex. A set of linear NNE-SSW to ENE-WSW trending trenches truncate the ductile fabrics and are interpreted as post-Caledonian brittle faults that formed due to multiple rifting events in the Late Palaeozoic-Mesozoic as parts of the evolution of the passive continental margin of the SW Barents Sea. Aspect analysis reveals a strong correlation between the present day landscape and tectonic elements, which indicate a pervasive tectonic influence on the present day coastal landscape of western Troms and the outboard strandflat.

Introduction

The shallow coastal portion off the coast off northern Norway comprises a distinct morphological phenomenon, the strandflat (e.g. Reusch, 1894; Nansen, 1922; Dahl, 1947; Larsen & Holtedahl, 1985; Corner, 2005; Thorsnes et al., 2009). The strandflat is typically manifested as a horizontal to gently dipping, low-relief surface comprised of exposed basement rocks. In Troms, the strandflat is largely submerged but may potentially, due to its location, be a very important source of information for onshore-offshore correlation studies. Any minor relief such as scarps, gullies, trenches, slopes, ridges, etc. visible on data covering the submerged strandflat may be the product of tectonic processes, such as foliation, folds, shear zones, faults and cleavages, (cf. Thorstensen, 2011) and thus give valuable insight into the margin architecture.

In recent years, the Norwegian government has as a part of the MAREANO project collected high-resolution (5x5m) bathymetry data along the coast of Norway. The data is partly available online (mareano.no) and has been widely used within geological sciences to for example map and resolve the glaciation and deglaciation history of the Norwegian shelf or to study submarine canyons and evidence for mass movement (e.g. Ottesen et al., 2005; Rydningen et al., 2013; Rise et al., 2013). For tectonic onshore-offshore studies, however, examples using bathymetry data as a correlation tool are farther apart. This is mainly due to the military restrictions on the data, which limits the resolution to only 50x50m within 12 nautical miles of the coast. This includes more or less all of the submerged strandflat along the Norwegian coast, leaving any detailed study of the strandflat difficult.

However, for the purpose of this study we have been granted access to, and permission to publish, high-resolution (5x5m) MAREANO data within 12 nautical miles of the coast, covering the strandflat offshore Troms (Fig. 1). The dataset is astonishingly rich in detail and may likely be used to solve many very different scientific problems. In this study, however, we will solely focus within a tectonic framework, using the data as a tool in the ongoing onshore-offshore correlation project in Troms and western Finnmark (Gagama, 2005; Eig, 2008; Hansen, 2009; Thorstensen, 2011; Indrevær et al., 2013; 2014). We aim to interpret and explain the strandflat morphology on the basis of known onshore ductile basement fabrics and brittle fault trends. The study aims to improve the understanding of the onshore and offshore SW Barents Sea margin architecture, including (i) the lateral offshore extension of the West Troms Basement Complex (WTBC), (ii) the offshore distribution of Caledonian thrust nappes and (iii) the distribution and linkage of Late Palaeozoic-Mesozoic brittle fault zones and how they relate to onshore fault complexes, such as the Vestfjorden-Vanna Fault Complex (VVFC, e.g. Olesen et al., 1997) and offshore fault complexes, such as the Troms-Finnmark Fault Complex (TFFC, e.g. Gabrielsen et al., 1990).

Geological Setting

In order to interpret morpho-tectonic elements on the strandflat with confidence, it is crucial to have a good understanding of the onshore geology. In the following, a description of the main bedrock lithologies, the ductile and brittle fabrics onshore and the different models proposed for the formation of the strandflat is given.

Precambrian structures of the West Troms Basement Complex

The outer islands of Troms constitute a major basement horst, the West Troms Basement Complex (Fig. 1). The horst is made up of a range of Meso- and Neoarchaean (2.9-2.6 Ga) tonalitic, trondhjemitic and anorthositic gneisses (TTG-gneisses), metasupracrustal belts (2.85-1.9 Ga), and felsic, mafic and ultramafic igneous rocks (2.4-1.75 Ga) (Corfu et al., 2003; Bergh et al., 2010; Myhre et al., 2011, 2013). The ductile deformation is the result of a complex tectonic history in the region, covering a large time span (Bergh et al., 2010): The host-rocks of the TTG-gneisses were igneous tonalites metamorphosed and deformed during a Neoarchean orogenic event (2.69-2.56 Ga; Myhre et al., 2013), producing a main N-S striking gneiss foliation with variable dip, intrafolial ductile shear zones and tight folds (Bergh et al., 2010). This event was followed by crustal extension and mafic dyke intrusions (2.40 Ga). The main architecture of the TTG-gneisses and metasupracrustal belts was the result of a major orogenic event, the Svecofennian, in the Palaeoproterozoic (1.9-1.75 Ga), which included (Fig. 2): (i) tight to isoclinal, NW-SE trending folds with moderate plunges and SW-dipping mylonitic ductile shear zones formed by NE-SW crustal shortening (D1-event), (ii) regional NW-SE trending, open to tight upright folding of the mylonitic foliation (D2-event), (iii) steeply N-plunging sinistral shear folds and associated, steep conjugate NNW-SSE and NW-SE trending ductile strike-shear zones of regional significance (D3-event) and (iv) NE-SW trending upright folds, SE-directed ductile thrust faults and NE-SW and ESE-WNW trending semi-ductile strike-slip shear zones that formed synchronoulys, but orogen-parallel relative to the D3 event in the northern part of the WTBC.

The metasupracrustal belts consist of various meta-conglomerates, meta-psammites, mica-schists and mafic to intermediate meta-volcanic rocks (Zwaan, 1989; Pedersen, 1997; Motuza et al., 2001). They dominantly trend NW-SE and some may be traced for 10's of kilometers along strike, while others define folded, discontinuous inliers or dismembered enclaves that obliquely truncate the Neoarchean foliation in the surrounding gneisses (Bergh et al., 2010). The Svecofennian deformation of the meta-supracrustal belts produced similar structures in the adjacent TTG-gneisses (cf. Armitage & Bergh 2005).

The Senja Shear Belt (Zwaan, 1995; Bergh et al., 2010) defines a network of such metasupracrustal belts thought to be a Palaeoproterozoic terrane boundary. This more than 30 km wide shear belt is delimited from the surrounding TTG-gneisses by the Svanfjellet metasupracrustal belt in the southwest and the Torsnes meta-supracrustal belt in the northeast

(Fig. 3). Internally, several separated meta-supracrustal belts and inliers, including the Astridal and Nøringen belt, are sandwiched between granitic and mafic TTG-gneisses. The width of the belts varies along strike, and anastomosing and lens-shaped ductile shear zones can be traced into the surrounding gneisses. The dominant fabric of the Astridal belt is a mylonitic foliation formed axial-planar to isoclinal folds (D1), which is macrofolded into upright antiforms and synforms (D2), and later folded by steeply plunging mostly sinistral drag folds (D3) (Fig. 3: Bergh et al., 2010). Shear zones along the Astridal belt contacts to neighboring granitic gneisses define macroscale, sinistral duplexes that are affected by a steeply plunging sinistral macrofold in the north at Baltsfjorden (Fig. 3). The Astridal belt can be traced from Baltsfjorden along the coastline towards Nøringen (Figs. 3 & 4), where narrow bands of meta-volcanic and meta-psammitic rocks and intercalated ultramafic lenses dominate (Pedersen, 1997). Internally, the ultra-mafic lenses define sinistral duplexes and comprise multiple and cross-cutting smaller ductile shear zones, both sinistral and dextral types (Fig. 4). The Torsnes belt on Kvaløya (Figs. 3) trends NW-SE and is folded into a macroscale, upright syncline (D2) and affected by subvertical folds and sinistral strike-slip shear zones (D3). The N-S trending foliation of the adjacent TTG-gneisses is notably bent into parallelism with the Torsnes belt. An associated sub-vertical macrofold (D3) in the neighbouring gneisses is present farther north, on the islands of Sommarøya and Hillesøya (Fig. 3; Thorstensen, 2011).

The overall NW-SE structural trend in the WTBC is largely parallel with the Archaean and Palaeoproterozoic orogenic belts of the Fennoscandian Shield east of the Scandinavian Caledonides, that stretches from Kola through Finland and Sweden into the Bothnian basin of central Sweden (Gaal & Gorbatchev 1987; Hölttä et al., 2008; Lahtinen et al., 2008; Bergh et al., 2014). Despite its position as a basement outlier west of the Caledonides, the younger Caledonian overprint is generally weak within the WTBC, but is possibly manifested as arc-shaped refolding and SE-directed thrust zones (Corfu et al., 2003; Bergh et al., 2010).

Caledonain thrust nappes

In the Palaeozoic, a collision between Laurentia and Baltica led to the accretion of thrust nappes with a distinct tectonostratigraphy comprised of the Lower-, Middle-, Upper- and Uppermost Allochthons and the southeast- and eastwards translation of up to several hundreds of kilometers of these as a part of the Caledonian Orogeny (e.g. Roberts and Gee, 1985; Roberts, 2003). The Caledonian rocks in northern Troms and western Finnmark is characterised by gently NW-dipping, well-foliated thrust nappes and some large-scale folds.

Within the study area, the islands of Nord-Fugløya and Arnøya are comprised of units belonging to the Caledonian Kalak Nappe Complex (Middle Allochthon). The Kalak Nappe Complex on Nord-Fugløya and Arnøya consists mainly of gently NW-dipping garnet-mica schists and marble units (Roberts, 1974).

Post-Caledonian structures

The Late Palaeozoic-Mesozoic rift-related activity on the west Troms margin (Figs. 1 & 5) (Gabrielsen et al., 1990; Davids et al; 2013) is outlined by widespread NNE-SSW and ENE-WSW trending brittle normal faults that constitute at least two major fault complexes, the Vestfjorden-Vanna and the Troms-Finnmark fault complexes (Gabrielsen et al., 1984, 1990, 2002; Olesen et al., 1997; Indrevær et al., 2013) and a subsidiary NW-SE trending transfer fracture system (cf. Indrevær et al., 2013) (Fig. 5). The onshore fault zones can be divided into the Vestfjorden-Vanna Fault Complex (VVFC), which marks the southeastern boundary of the WTBC, down-dropping the Caledonian nappes to the east in the order of 1-3 km (Forslund, 1988; Opheim & Andresen, 1989; Olesen et al., 1997) and a less prevalent, SE-dipping fault system that runs along the outer rim of the islands of the WTBC (Fig. 1) (Antonsdottir, 2006; Thorstensen, 2011; Indrevær et al., 2013) with displacement in the order of 100's of meters or less (Indrevær et al., 2013). Offshore, the Troms-Finnmark Fault Complex is the dominant basin-bounding fault complex and defines the northwestern limit of the WTBC, down-faulting basement rocks from 4-5km depth on the Finnmark Platform to possibly more than ~10km depth in the Harstad Basin (Fig. 2) (cf. Gabrielsen et al., 1984, 1990; Indrevær et al., 2013). The Troms-Finnmark and Vestfjorden-Vanna Fault Complexes (Fig. 5) can be traced for 100's of kilometers along strike along the North-Norwegian margin, linking up major horst-bounding structural elements in the south, such as the Lofoten and Nordland Ridges, with offshore fault complexes in the north, such as the Ringvassøy-Loppa, Nysleppen and Måsøy Fault Complexes (c.f. Gabrielsen et al., 1990; Olesen et al., 1997; Dore et al., 1997, 1999; Indrevær et al., 2013). The margin is segmented along strike by at least two major transfer fault systems, the Senja Shear Zone and the Fugløya transfer zone, the possible continuations of the Proterozoic-Palaeozoic Bothnian-Senja (and Senja Shear Belt) and the Bothnian-Kvænangen fault complexes, respectively (Berthelsen & Marker, 1986; Gaal & Gorbatchev 1987; Olesen et al., 1990; Henkel, 1991; Doré et al., 1997; Olesen et al., 1997; Hölttä et al., 2008; Lahtinen et al., 2008; Indrevær et al., 2013; Bergh et al., 2014).

Geomorphology of the strandflat

The strandflat along the Norwegian coast is manifested as a horizontal to gently dipping, low-relief surface that typically ranges in elevation from about 40 meters below sea level to a maximum of 100 meters above sea level (cf. Corner, 2005). The strandflat is comprised of highly dissected bedrock commonly draped by a thin layer of Holocene sediments. It is present along large portions of the coast, from Stavanger in the south, to Nordkapp in the north and may locally reach 60km in width. The origin of the strandflat has been widely discussed in the literature (e.g. Reusch, 1894; Nansen, 1922; Asklund, 1928; Dahl, 1947; Büdel, 1978; Larsen & Holtedahl, 1985; Olesen et al., 2013). Several models for the its origin has been discussed, including the strandflat represent a surface of pre-Cretaceous age that formed due to tropical weathering (Asklund, 1928; Büdel, 1978; Olesen et al., 2013). There seems, however, to be a common concensus that the strandflat formed from a combination of frost weathering, sea-ice erosion and marine abrasion during the Quaternary (Reusch, 1894; Nansen, 1922; Dahl, 1947; Larsen & Holtedahl, 1985), likely re-excavating the pre-Cretaceous etch plain by the removal of easily erodable weathered bedrock (cf. Olesen et al., 2013).

In western Troms and Finnmark, the strandflat is at present mainly a submarine feature, varying in width from 2km, outboard northern parts of Senja, up to 30 km north of Nord-Fugløya (Fig. 1). The strandflat is delimited in the east by the high relief, alpine landscape of the outer islands of Troms, with topography reaching >1000 m above sea level. The western limit of the strandflat is defined by abrupt, steeper slopes that separate the strandflat from the bankflat area, which defines the continental shelf from the strandflat towards the continental break (Corner, 2005). The bankflat outboard Troms is characterised by thick glacigenic deposits forming glacially controlled morphology such as troughs and banks (Fig. 1, cf. Rydningen et al., 2013).

Methods and data bases

The 5x5m resolution dataset covers most of the strandflat off the coast of Troms (~4600 km^2), from Senja in the south to Vanna in the north. Minor areas are provided with 25x25m and 50x50m resolution only and a few areas, especially close to shore and in regions with shallow water depths, have no data available at all (Fig. 6). The strandflat outboard Troms seems well suited for a case study like this due to (i) the wide zone of submerged strandflat along this portion of the coast, (ii) the high degree of available high-resolution bathymetry data covering

the strandflat, (ii) the relatively well understood onshore basement geology of the outer islands of Troms, including both ductile and brittle deformation features (Zwaan, 1995; Corfu et al., 2003; Bergh et al., 2010; Myhre et al., 2011; Indrevær et al., 2013; 2014) and (iv) the overall margin-perpendicular, NW-SE structural and lithological trends of heterogeneous Precambrian bedrocks (e.g. Bergh et al., 2010), providing an excellent framework for onshore-offshore structural analysis.

The data has been used to produce dip maps, profiles, shadow relief maps (3D-view) and aspect maps in order to highlight morphological features. The aspect maps consider only slopes that dip more than 5°, where the slope direction for each data point is calculated based on the immidiate neighbouring data points (3x3 window). Aerial photographs are used to map and interpret morphology on smaller islands and skerries. Geological maps from NGU and other detailed studies (Pedersen, 1997; Armitage, 2007; Bergh et al., 2010) are used to compare and evaluate features visible on the high-resolution bathymetry data with nearby onshore basement structures.

Results

Regional slope aspect analysis

Aspects for surface slopes dipping more than 5° covering the entire WTBC horst and the outboard subsea strandflat (Fig. 5) shows that the island of Senja is dominated by NE-SW striking slopes, except in its northern portion, where NW-SE trending slopes are common, clearly reflected by the NW-SE trending fjords that spatially overlap with the basement gneiss foliation and the Senja Shear Belt (Figs. 1 & 7). The islands of Kvaløya and Ringvassøya are in general dominated by NNE-SSW to ENE-WSW striking slopes, while the Vanna island is characterised by ~N-S trending larger ridges (Fig. 7). The combined aspect values of all islands within the WTBC reveal that the onshore slope topography is dominated by NW-SE and NE-SW to E-W striking slopes (Fig. 7).

The morphology of the strandflat shows, as expected, a much lower relief and slope variation than onshore topography, with much of the strandflat being characterised by slopes that dip less than 5°. Of steeper slopes, N-S and ENE-WSW striking slopes dominate, including a minor maximum of slopes striking NNW-SSE (Fig. 5). The latter population of slopes are

more common outboard the northern portions of Senja and northwest of Nord-Fugløya (Fig. 7).

Comparing onshore and offshore aspect values reveal that slopes of very similar orientations dominate both the bathymetry and the topography, indicating that there are at least some common aspects to the controlling elements of terrain-forming processes on the strandflat and on land.

Morpho-tectonic elements on the strandflat

On a regional scale, the strandflat within the study area is more or less continuous along the outer coast of the WTBC, only interrupted by a few, up to 200m deep, ~E-W trending trenches located at the mouths of sounds and fjords, carved out by glaciers extending from the inland and feeding large glacial ice streams during previous glacial periods (Fig. 1; Vorren et al., 1983; Dahlgren et al., 2005; Rydningen et al., 2013). On a more local scale, the strandflat is dissected by relatively less prevalent trenches that define the outer boundaries of basement blocks and which internally show a lower relief variation, commonly defined by smaller, linear to curved, parallel ridges and truncating trenches.

We describe in detail three areas of the strandflat in western Troms and Finnmark (Fig. 1) that cover key morpho-tectonic elements that may be used to characterise this portion of the SW Barents Sea margin.

Area 1

Local onshore geology

Area 1 (Fig. 8) covers the northwestern parts of Senja and southwestern parts of Kvaløya. Onshore, the geology is dominated by N-S trending, foliated Neoarchaean TTG-gneisses, locally with intercalations of the Ersfjord granite, several NW-SE trending meta-supracrustal belts, including the Astriddal, Nøringen and Torsnes belts and ductile shear zones belonging to the Svecofennian Senja Shear Belt (Figs. 3 & 8; Zwaan, 1995; Bergh et al., 2010).

Post-Caledonian brittle structures within Area 1 include the Bremneset, Tussøya and Hillesøya fault zones (Figs. 3 & 8), which are a part of the SE-dipping fault system that run along the outer rim of the WTBC islands. The Tussøya fault zone (Indrevær et al., 2013, 2014) defines a normal-oblique sinistral fault that dips moderately ESE and separates granitic TTG-gneisses in the footwall from banded mafic and felsic gneisses in the hanging wall. The

Hillesøy fault zone (Fig. 8; Thorstensen, 2011; Indrevær et al., 2013) is comprised of several ENE-dipping faults that merge into subsidiary ENE-dipping fault set. The fault zone is located on the steep northwestern limb of a sub-vertical macrofold on the islands of Sommarøya and Hillesøya (Thorstensen, 2011; Indrevær et al., 2013). Further north, the Bremneset fault zone dips ESE and can be traced along the shore for c. 200 meters, cutting migmatitic TTG-gneisses of the Kattfjord Complex (Fig. 8; Indrevær et al., 2013, 2014).

Morpho-tectonic elements on the strandflat

The strandflat northwest of Nøringen (Fig. 9), is dominated by lens-shaped, flat-topped plateaus and ridges surrounded by anastomosing 25-50 m deep and internally smooth depressions that have a distinct NW-SE trend (Fig. 9a & b). These anastomosing features are well displayed on the aspect map of slope directions in the area (Fig. 9c). E-W trending parallel ridges (red aspect values) to the north truncate and/or curve into parallelism with the anastomosing NW-SE features. A few, more or less developed, NNE-SSW trending, sub-linear trenches (blue aspect values) cut the anastomosing features and curved ridges. Aspect analysis of seabed slopes shown on the map (Fig. 9c) and slope azimuth histograms (Fig. 9d), with dips exceeding 5°, reveals that slopes trending NW-SE dominate the morphology on the seabed.

The strandflat north in Area 1 (Figs. 8 & 10) shows NW-SE trending, linear to curved parallel ridges in the northwest that may be traced for 20 km from the Torsnes Belt in the southeast (Fig. 10). The elongated ridges are typically 1-30m high and 100-500 m wide (Fig. 10a, cross-sections). Northwest of Edøya, these ridges curve into a macroscale z-shaped feature before continuing northwestward. Close to the outer edge of the strandflat, these parallel ridges are obliquely truncated by a E-W trending trench that apparantly displace the morpho-tectonic pattern, thus defining a boundary toward a portion of the strandflat that is characterized by rounded knobs rather than elongated ridges (Fig. 10a & 11a). Outside the zone of parallel ridges, cross-cutting trenches and a chaotic assembly of irregular, often rectangular depressions dominate the strandflat (Fig. 10a). The depressions have variable trends NNE-SSE to ENE-WSW and NW-SE, as illustrated by the aspect map (Fig. 10c). Aspect analysis of slopes with dips > 5° show that slopes trending NW-SE (red and blue aspect values) dominate the seabed morphology within the area (Fig. 10d). Onshore aspects (Fig. 10d; black line) show a larger variation in trends than offshore aspects, which include NE-SW trends, but reveals that slopes striking NW-SE are common onshore as well.

Interpretation

The anastomosing, morpho-tectonic feature visible northwest of Nøringen (Fig. 9) show similar geometry as the sinistral duplexes observed onshore in lenses of foliated granitic gneisses of the Astridal belt (Fig. 3) and ultramafic rocks in meta-supracrustal units of the Nøringen belt (Fig. 4), including an apparent sinistral displacement of the lense along a curved lineament. The anastomosing feature is therefore interpreted as a sinistrally duplexed lens (Fig. 11b). Based on the direct bathymetric link of this feature along the seabed to Nøringen (Fig. 9a), the feature is interpreted to be the offshore continuation of the Palaeoproterozoic Astridal belt, or alternatively a separate meta-supracrustal inlier of the TTG-gneisses, common within the Senja Shear Belt. The outline of this zone on the strandflat is overall similar in trend and width to onshore meta-supracrustal belts, supporting the above interpretation. To the northeast of this zone, distributed elongated ridges and depressions are considered to reflect the exposed TTG-gneiss foliation. The gneiss foliation is transposed and/or tight to isoclinally folded and modified along the contact to the meta-supracrustal belt in a similar manner as observed onshore along the Astridal belt (Fig. 3), suggesting a sinistral sense of shear (Fig. 11b).

The zone of NW-SE trending elongated and parallel ridges north in area 1 (Fig. 10) can be traced directly southeastward into the Torsnes meta-supracrustal belt. Thus, these ridges may represent the offshore continuation of the upright macrofolded (D2) units of the Torsnes belt (Fig. 11c). This linkage is supported by the fact that meta-supracrustal rocks partly step onshore Edøya (Zwaan et al., 1998). Northwest of Edøya (Fig. 11c), the macroscale z-shaped curvature of the belt is interpreted as a sub-vertical macrofold (D3) formed by NW-SE directed, sinistral ductile shearing along the Torsnes belt boundaries. A similar, but more localized Svecofennian ductile shear zone may be present on the northern limb of this macrofold, merging southeastward just east of Hillesøya (Fig. 11c). Close to the strandflat edge, the presumed continuation of the Torsnes belt is truncated by an E-W trending lineament, separating homogenous rocks in the north from the well-foliated rocks in the south (Fig. 11a & c). This lineament is interpreted as either a ductile shear zone that displaced portions of the Torsnes belt, or a lithological, intrusive contact. Granitoid intrusive rocks of both Archean and Svecofennian age, are common within the TTG-gneisses (Andresen, 1980; Corfu et al., 2003), where they truncate ductile Svecofennian fabrics and shear zones (e.g. Bergh et al., 2010). Therefore we suggest this abrupt contact to be lithological and related to some of these intrusions. This inferred granite-gneiss contact may have been tectonically

reactivated during e.g. the late Svecofennian deformations events (Bergh et al., 2010), or alternatively during Palaezoic-Mesozoic brittle normal faulting (Indrevær et al., 2013).

Linear and curved, variably trending trenches that truncate many of the curved and parallel ridges must therefore be younger (Fig. 11b & c). In general, these trenches inhabit the same trends as known Late Palaozoic-Mesozoic brittle fault zones onshore (Indrevær et al., 2013). Consequently, the linear trenches are interpreted as fault scarps, partly excavated by strandflat-forming processes. The chaotic array of rectangular to orthogonal depressions (Fig. 11c), with long axes oriented parallel to trends of brittle faults, can tentatively be interpreted as smaller basins delimited by normal faults.

In summary, Area 1 shows morpho-tectonic elements interpreted to be the offshore continuation of two metasupracrustal belts, the Astridal/Nøringen belt and the Torsnes belt. In addition, the inferred ductile structures are truncated by NNE-SSW and ENE-WSW trending trenches that are interpreted as Late Palaeozoic-Mesozoic brittle normal faults.

Area 2:

Local onshore geology

Area 2 covers the strandflat outboard the northern parts of Kvaløya, Ringvassøya and Rebbensøya in the central portion of the WTBC, and includes the smaller islands of Vengsøya, Gjøssøya, Sandøya and Sørfugløya (Fig. 12). The islands of Vengsøya and Gjøssøya are comprised of heterogenous TTG-gneisses and amphibolitic gneisses of the Kattfjord Complex, with intercalations of biotite schists, meta-psammites, quartzites and some meta-volcanic rocks (Grogan & Zwaan, 1997). On Vengsøya, the foliation is in general striking NW-SE and is tightly folded into a steeply plunging (D3) macrofold on the southwestern part of the island (Fig. 12; Grogan & Zwaan, 1997). On Gjøssøya, the foliation strikes NNE-SSW. Granitic intrusions are widespread both as lenses parallel to the foliation and as irregular, truncating bodies and pegmatite veins.

The islands of Ringvassøya and Rebbenesøya in the north are composed of well-foliated TTG-gneisses that have numerous intercalations of amphibolitic gneisses, and commonly cut by irregular granite intrusions (Grogan & Zwaan, 1997). The TTG-gneiss foliation on Rebbenesøya and northern parts of Ringvassøya trend on average N-S, but is bent into a NW-SE orientation in the south, adjacent to a high-strain, migmatitic ductile shear zone presumed

to be a Neoarchaean terrane boundary and termed the Kvalsund shear zone (Fig. 12; Myhre et al., 2013).

Farther northwest, on the island of Sandøya, the foliation within quartz-feldspathic biotite gneisses dips steeply toward WNW (Fig. 12, inset map). A ~0.5km wide, foliation-parallel quartzite layer traverses the island on its eastern side (Armitage, 2007; Gjerløv, 2008).

Morpho-tectonic elements on the strandflat

The strandflat just west of Vengsøya and Gjøssøya (Fig. 12), is characterized by a plateau surrounded by narrow, deep trenches (Fig. 13). The plateau shows an internal morphology outlined by parallel elongated ridges that trend NW-SE and curve around in a somewhat complex dome-shaped pattern (Fig. 13a & b). Minor, linear ENE-WSW trending trenches on the plateau truncate the curved parallel ridges. The plateau is delimited in the north by a NE-SW to ENE-WSW trending, ~1km wide, 50 m deep trench and to the south by a c. 2km wide, ~200m deep E-W trending depression that can be traced for ~30km eastward, merging into Skulsfjord on Kvaløya (visible as green and red slopes on the aspect map, Fig. 13c). The elongated ridges on the plateau correspond in attitude with the main TTG-gneiss foliation on the island of Vengsøya (Fig. 12), including the tight isoclinal fold that occurs in the southwestern parts of Vengsøya (also visible from aerial photographs, Fig. 13a). Aspect analysis of slopes with dips exceeding 5° reveals that slopes striking NE-SW and NW-SE (green and red aspect values) dominate the seabed morphology within the area (Fig. 13c & d), which corresponds to the orientation of the large trenches delimiting the plateau.

Within the strait between the islands of Rebbenesøya and Sandøya (Fig. 12), a similar morphological pattern is observed (Fig. 14). The two islands comprise well-foliated TTG-gneisses, with foliation striking mostly N-S, but with opposite dips, i.e. steeply to the east and west, respectively (Fig. 14a & b). Aerial photographs have allowed for interpretative mapping and linkage of the basement foliation surface traces between many smaller islands and skerries (Fig. 14a). The bathymetry data between the two islands reveals a distinct curved ridge that may be traced from the eastern rim of Sandøya northeastward until it curves into a NNW-SSE trend and proceeds southwards to match up with the foliation on Rebbenesøya (Fig. 14a & b). A distinct NNE-SSW trending trench can also clearly be observed east of Sandøya. Aspect analysis reveals that slopes striking N-S to NNE-SSW and WNW-ESE

dominate the seabed morphology (Fig. 14c & d, yellow and blue aspect values). The same trends also dominate the onshore topography (Fig. 14d; grey lines).

West of Sandøya, close to the strandflat edge, a >5km wide zone of NNW-trending, parallel ridges is present (Fig. 12, see Figs. 15 & 16 for details). The individual ridges vary from 100-500m in width and 20-75m in height. Within this zone, tightly curved ridges and internally anastomosing wedge-shaped lenses are observed (Fig. 15), enclosed by irregular, aligned depressions (blue and red-yellow aspect values, Fig. 15c & d). Towards the east, the area comprises well-developed parallel ridges separated from a slightly more elevated area. This ridge is mainly covered by 50x50m resolution bathymetry data, but still show less developed lineated morphology. The widespread red to orange and blue aspect values (Fig. 15c & d) reveal that slopes trending N-S to NNW-SSE and NE-SW dominate the seabed morphology in this subarea, which is similar to the main orientation of the zone of parallel ridges. The northern portion of this zone (Fig. 16) shows a network of irregular, variable trending trenches that truncate the parallel ridges such that the strandflat is split up into blocks of distinct geometric characters. Notably, there is a marked east-west change in the elevation of the strandflat across a major escarpment, apparent on the profile (Fig. 16a). This escarpment dips steeply west and displaces the strandflat from less than c. 100 m depth in the east to c. 250 m depth in the west. The escarpment runs northward to link up with the edge of the strandflat (Fig. 16a & b). Aspect analysis reveals that slopes striking NNW-SSE (orange and blue aspect values, Fig. 16c & d) dominate the seabed morphology in this subarea, which reflects the flanks of the NNW-SSE trending ridges visible on the bathymetry data.

The northernmost part of Area 2, northwest of the small island of Sørfugløya (Figs. 12), shows morpho-tectonic elements that are dominated by a set of linear, distinct 200-500m wide steeper slopes trending N-S and NNE-SSW that link up in a system of scarps with a zigzag geometry (Fig. 17a & b). This structure defines an escarpment that separates the inner and outer portions of the strandflat, with c. 200m difference in elevation (Fig. 17a). Weakly developed curved ridges are visible (Fig. 17a). Aspect analysis (Fig. 17c & d) reveals that blue to purple aspect values, corresponding to the NNE-SSW striking escarpments, dominate the seabed morphology in this region, with a minor maximum striking ENE-WSW (green aspect values).

Interpretation

The curved, parallel ridges observed west of Vengsøya and Gjøssøya (Fig. 13) can be directly linked with the basement fabric observed onshore these islands, and thus are interpreted to reflect the bedrock foliation. The dome-shaped and curved nature of ridges on the strandflat suggests that the foliation is folded around a sub-vertical fold axis (D3), making up a tight macrofold with fold limbs trending ~NW-SE (Fig. 18a). This interpretation is supported by similar fold patterns onshore the island of Vengsøya. The minor ENE-WSW trending trenches that truncate the TTG-gneiss foliation, together with the larger and deeper trenches in the north and south of this portion of the strandflat are, based on the similarity in orientations with onshore brittle normal faults (Indrevær et al., 2013), interpreted to represent brittle faults and/or fracture systems.

A similar fold structure (D3) is interpreted to exist in the strait between Sandøya and Rebbenesøya (Fig. 18b). The ridge that continues northward from Sandøya is interpreted to be the continuation of the meta-quartzite unit mapped on Sandøya (Fig. 12, inset map), as a competent unit like quartzite likely would manifests itself as a positive feature on the seabed (Fig. 18b). The ridge curves around and link up with the foliation onshore Rebbenesøya, suggesting that this area represent a major fold hinge with a steeply N-plunging (D3) fold axis. Thus, the fold may explain the opposite dips of foliation onshore Sandøya and Rebbenøya, due to their location on opposite fold limbs.

The wide zone of NNW-SSE trending parallel ridges west of Sandøya (Fig. 12) resemble that of a high-strain ductile shear zone present within TTG-gneisses and meta-supracrustal belts onshore. The internally merging ridges and wedge-shaped lenses within its southern portion (Fig. 19a) are thought to reflect intrafolial tight to isoclinal (D1) macrofolds with transposed shear-lenses, features also commonly identified onshore in Svecofennian ductile shear zones (e.g. Bergh et al., 2010). The orientation of the foliation and hence the contact towards the low-strain zone along the northern portion of the zone is estimated to dip ~35° towards west, based on the asymmetric relief of the ridges (Fig. 16a & b). The shear zone foliation is bent and asymmetrically folded (sinistrally), likely by steep-plunging folds (D3) (Fig. 19a). Importantly, this shear zone may be the strandflat impression of the offshore continuation of the Kvalsund shear zone (Myhre et al., 2013). The abrupt divide from well-foliated ridges against less lineated morphology to the east of this inferred high-strain zone is interpreted to represent a hinge zone of a sub-horizontal, upright NW-SE trending (D2) anticlinal fold (Fig.

19a & b), as is present along the Kvalsund shear zone onshore. Alternatively, this zone may be interpreted as a shear zone or lithologicial boundary against the high-strain shear zone in the west, with e.g. non-migmatized tonalitic gneisses and/or meta-quartzite horizons such as those observed on the island of Sandøya (Armitage, 2007).

The inferred offshore continuation of the Kvalsund shear zone is cut and offset by numerous NNE-SSW to ENE-WSW trending gullies and narrow depressions (Fig. 19a & b). These depressions are interpreted as major brittle faults transecting the entire strandflat in localized zones. The boundary between the high-strain ductile shear zone and an apparently less strained zone to the east (interpreted as a hinge zone) may be dextrally displaced across one such major brittle fault zone in the south of this subarea (Fig. 19b). By assuming pure normal dip-slip displacement along the major brittle fault, a northwards 60° dip of the fault plane and a 35° westward dip of the foliation surface, the apparent 2.2km dextral displacement of the high-strain zone across the fault is calculated to correspond to 1.8km down to the north, normal displacement. Notably, NNE-SSW trending brittle faults are observed to curve into the ENE-WSW trending faults and vica-versa (Fig. 19a).

North in Area 2, an escarpment with zigzag geometry is dominating the seabed morphology (Fig. 20). The zigzag character of the escarpment corresponds with the character of the offshore Troms-Finnmark Fault Complex and the onshore Vestfjorden-Vanna Fault Complex (Gabrielsen et al., 1990; Olesen et al., 1997; Indrevær et al., 2013), and is therefore considered to reflect Late Palaeozoic-Mesozoic brittle normal faults that are defining the western boundary of the strandflat. These presumed faults are well outlined in the cross-sections (Fig. 17a) as a major, overall NW-dipping set of escarpments that vertically offsets the basement surface of the strandflat to a lower elevation and thus allowing for glacigenic sediments to be partly deposited on top (Fig. 20). A set of curved ridges just to the east of the major scarp suggests that the foliation in this area is tightly folded by a N-S trending steeply dipping macrofold (D3).

In summary, the seabed morphology within Area 2 is interpreted to contain at least three D3 macrofolds (Figs. 18 & 20). The folds are associated with the offshore continuation of the Kvalsund shear zone (Figs. 19), which is interpreted to show intrafolial D1-folding (Fig. 19a), and the hinge zone of an upright D2-fold (Fig. 19a, b). The ductile fabrics are cut by numerous inferred Late Palaeozoic-Mesozoic brittle normal faults that truncate the strandflat.

The westernmost scarp of the strandflat is suggested to be connected to Late Palaeozoic-Mesozoic brittle faulting (Fig. 20).

Area 3:

Local onshore geology

Area 3 covers the islands of Vanna and Nord-Fugløya and the strandflat north of these islands (Fig. 21). Vanna is the northernmost island of the exposed West Troms Basement Complex and consists of Neoarchaean tonalitic gneisses that locally are unconformably overlain by the para-autochthonous meta-supracrustal units, the Vanna Group and the Skipsfjord Nappe (Fig. 21; Binns et al., 1980; Johansen 1987; Opheim & Andresen, 1989; Bergh et al., 2007a). The Vanna Group meta-supracrustal unit is also exposed on the island of Spenna, 5 km along strike east of Vanna (Roberts, 1974). In general, the tonalitic gneiss foliation on Vanna is folded by a N-S trending, macroscale, upright antiform plunging southward (Fig. 21). The Skipsfjord nappe is in the north down-faulted by at least 3 km by the SSE-dipping Vannareid-Brurøysund fault zone (Fig. 21), of presumed Mesozoic age (Opheim & Andresen, 1989). This fault zone constitutes a well-defined ENE-WSW trending topographic valley underlain by a >20m wide zone of brittle, cataclastic fault rocks.

The islands of Nord-Fugløya and Arnøya northeast of Vanna (Fig. 21) are both comprised of Palaeozoic, metamorphic Caledonian rocks of the Middle Allochthonous thrust sheets (Roberts, 1974; Ramsay et al., 1985). Dominant rocks are garnet-mica schists and marble units (Roberts 1974) with a foliation on average dipping gently to the NW. The sound between Vanna and the two islands therefore define a prominent regional boundary between the Caledonian thrust nappes to the northeast and the Precambrian rocks of the WTBC to the southwest. Indrevær et al. (2013) considers this sound to be underlain by a major Late Palaozoic-Mesozoic transfer fault zone that formed by reactivation of a Proterozoic-Palaeozoic ductile shear zone (the Bothnian-Kvænangen Fault Complex) (Doré et al., 1997).

Morpho-tectonic elements on the strandflat

The bathymetry data north of Vanna seem to be more influenced by glacial-induced morphology than farther south (Fig. 21). Still, within the western parts of the area, N-S to NNW-SSE trending parallel ridges and gullies are visible (Fig. 22 a & b). In the northern parts, a larger raised portion of the strandflat defines a plateau delimited by a major south-facing escarpment in the south, marked as a green coloured feature on the aspect map (Fig.

22c). The escarpment separates seabed morphology that differs ~ 200m in depth (Figs. 21 & 22a). While the southern, down-dropped part has a diffuse glacial-fill morphology, the plateau itself shows distinct sets of intersecting trenches: the western portion of the plateau comprises smaller E-W, NE-SW and ~N-S trending rhombic bedrock patterns, which are illustrated by blue, red and green values on the aspect map (Fig. 22c). This pattern is abruptly replaced further east on the plateau by a c. 6 km wide zone of ~NNW-SSE trending parallel ridges that run within in a major trough (Fig. 22a & b). East of the N-S trending trough, the rhombic bedrock pattern visible on the western portion of the plateau appear again.

The prominent zone of ~NNW-SSE trending parallel ridges that run across the plateau can be traced southwards along the western side of the island of Nord-Fugløya, where it merges into a system of broad, E-W to NE-SW trending undulating ridges and trenches (Fig. 22a & b). This zone of parallel ridges thus reflect a major change in the orientation of morphologic elements on the strandflat, from dominantly NNW-SSE trending lineated morphology SW of Nord-Fugløya, to a dominantly NE-SE trending lineated morpholgy NE of Nord-Fugløya. This change is clearly visible on the aspect map (Fig. 22c).

Interpretation

The N-S to NNW-SSE trending diffuse and locally curved ridges north of Vanna, including similar morphologies on the western part of the raised plateau, are interpreted as the continuation of the TTG-gneiss foliation and possibly, meta-supracrustal lithologies analogue to the Skipsfjord Nappe rocks exposed onshore Vanna (Fig. 23). The wide zone of NNW-SSE trending parallel ridges, that may be traced northwest of Nord-Fugløya and north onto the raised plateau, is suggested to reflect the boundary zone between the crystalline Precambrian basement of the WTBC and the gently NW-dipping Caledonian thrust nappes present onshore Nord-Fugløya (Fig. 23; Roberts, 1974). Northeast of Nord-Fugløya, the observed NE-SW trending parallel ridges are interpreted to reflect the outcrop of Caledonian nappe foliation on the seabed. North of Nord-Fugløya, these ridges bend to a northwest trend, which is interpreted to be an apparent effect of the oblique truncation between the in general gently NW-dipping Caledonian foliation and the seabed.

The contact between the Caledonian rocks and the WTBC rocks must be present in the sound somewhere in between the islands of Spenna and Nord-Fugløya, as the two islands are comprised of WTBC rocks and Caledonian rocks, respectively (Fig. 24). The contact must thus trend NW-SE, parallel to the general morpho-tectonic trends present on the seabed within

this sound. A possible continuation of this contact zone is visible on the raised plateau northwest of Nord-Fugløya, defined by the zone of ~NNW-SSE trending parallel ridges within the major trough (Fig. 23). Here, however, the zone does not separate ~NNW-SSE trending linear morphology, typical for basement lithologies, in the southwest from NE-SW trending linear morphology, typical for the Caledonian units, in the northwest, but rather obliquely truncate presumed basement lithologies on both sides. The exact location and southeastward trace of the Caledonian-WTBC contact, and its regional implications are discussed in a later section.

The south-facing escarpment delimiting the plateau and displacing the strandflat vertically by c.200m to the south is interpreted as a Late Palaeozoic-Mesozoic brittle fault. Consequently, this fault may be linked to the Vestfjord-Vanna Fault Complex, and thus imply that the WTBC rocks can be traced further northeastward along the Barents Sea margin (Fig. 24). This is also inferred from the N-S trend of the ductile basement fabrics visible on the raised plateau. The major brittle fault apparently displaces the strandflat and may therefore post-date the strandflat, (i.e. the Quaternary), thus inferring neotectonic activity.

Discussion

Above we have described and interpreted morpho-tectonic features visible on the strandflat offshore western Troms and compared them with local onshore ductile and brittle fabric elements. In order to further link and correlate these features, we have combined the two data-packages into a simplified onshore-offshore map of all the interpreted morpho-tectonic features along the studied portion of the WTBC and the transition to the Caledonian nappes in the northeast (Fig. 25). In the following, we will discuss the implications of these features in a regional context of onshore-offshore correlation and margin architecture.

A) Precambrian rocks and ductile fabrics

The morpho-tectonic elements observed on the strandflat clearly mimic onshore Precambrian basement structures in great detail, both in the form of interpreted lithologies and ductile structures. Dominant lithological elements such as the strongly foliated TTG-gneisses, more competent and massive granitic intrusions and meta-supracrustal belts can be tentatively identified and separated. Major ductile structures observed onshore, such as the prominent steep NW-SE trending, irregular and anastomosing Neoarchaean foliation in the TTG-gneisses and the complex Neoarchaean and later Svecofennian fold structures and ductile

shear zones may be identified on the strandflat. In fact, even specific time-generations of folds and shear zones can be inferred in TTG gneisses on the strandflat bathymetry, including macro-scale isoclinal (D1), upright (D2) and steeply plunging folds (D3). Distinct zones of high-strain deformation that may represent terrane boundaries are identified on the strandflat (Fig. 25). These include the Astridal and Torsnes meta-supracrustal belts of the Senja Shear Belt, which are interpreted to continue NW onto the strandflat (Fig. 11b & c, Zwaan, 1995; Bergh et al., 2010). Further north, the possible offshore continuation of the Kvalsund shear zone is identified (Figs. 18 & 19). Onshore, the Kvalsund shear zone is related to a terrane boundary where adjacent gneisses are commonly heavily deformed and folded by upright, horizontal folds (Myhre et al., 2013). On the strandflat, along the trend of this zone, the occurrence of upright (D2) and steeply dipping (D3) macro folds (Fig. 25) indicate that the Kvalsund shear zone continues northwestward onto the strandflat. The great degree of similarity and correlation of morpho-tectonic elements on the strandflat with the onshore basement features (Fig. 25), suggests that the strandflat to a large extent is comprised of lithologies of WTBC affinity. In fact, the WTBC suite can be traced westward from the WTBC, all the way out to the western edge of the strandflat, from the the island of Senja in the south and northward to Nord-Fugløya. The contact zone to Caledonian rocks is interpreted to run just west and south of Nord-Fugløya (Figs. 24 & 25). The contact zone is clearly observed on the strandflat west and south of Nord-Fugløya (Fig. 23) and mirrored by a distinct change in the morpho-tectonic character of the seabed, strongly indicating that gently dipping Caledonian nappes and structures make up the strandflat northeast of this boundary.

B) Caledonian rocks and ductile fabrics

The Caledonian rocks of western Troms are outlined by flat-lying to gently NW-dipping thrust nappes with a marked structural difference relative to those of the WTBC rocks. In the northeastern part of the study area (Fig. 24), on the island of Nord-Fugløya and Arnøya, the onshore geology is overlain by Caledonian Kalak Nappe Complex units and northeast of these islands is the only area on the strandflat where Caledonian nappes are interpreted to crop out on the seafloor. Here, curved, parallel ridges that trend NE-SW dominate, as opposed to the NW-SE trending parallel ridges commonly observed within lithologies associated with the WTBC.

In a regional context, the onshore Caledonian-WTBC boundary of the SW Barents Sea margin (Figs. 1 & 2) is outlined by a zigzag pattern of NNE-SSW to ENE-WSW trending (mostly SE-dipping), brittle normal fault segments of the Vestfjord-Vanna Fault Complex

(Forslund, 1988; Olesen et al., 1997) and locally Caledonian thrust faults (on Senja and the northern parts of Ringvassøya). South of Nord-Fugløya, the orientation changes to a NNW-SSE trend, suggesting that the contact is no longer defined by coast-parallel brittle normal faults, but rather a thrust fault or a transfer fault zone of post-Caledonian age. The latter is supported by recent studies of Indrevær et al. (2013), which advocate the presence of a major sinistral transfer zone (Fugløya) of Late Palaeozoic-Mesozoic age, as a reactivated portion of the Proterozoic-Palaeozoic Bothnian-Kvænangen Fault Complex, running in the sound between Vanna and Nord-Fugløya. The wide zone of localised, parallel ridges observed on the raised plateau northeast of Vanna (Fig. 22) is therefore interpreted as the continuation of this transfer zone. However, since morphologies similar to that of exposed WTBC bedrock lithologies do occur on the eastern and western parts of the raised plateau, it is suggested that this zone, on the plateau, does not mark the direct continuation of the Caledonian-WTBC boundary, but rather reflect a Palaeoproterozoic meta-supracrustal belt, or the continuation of a pre-existing major, basement-seated ductile shear zone within WTBC rocks (Fig. 24). This strengthens the idea that the Fugløya transfer zone formed along a pre-existing zone of weakness within Precambrian basement rocks: The conspicuous overlap (Fig. 25) of (i) the Fugløya transfer zone, (ii) the contact between WTBC and Caledonian thrust nappes, (iii) a possible Svecofennian high-strain ductile shear zone and (iv) the Proterozoic-Palaeozoic Bothnian-Kvænangen Fault Complex, suggest that this zone may have played a major role in controlling and accommodating crustal deformation through a very long time span. This zone may have initiated during the Neoarchean and/or Palaeoproterozic orogenies, e.g. the Svecofennian, and later been overridden by thrust nappes during the Caledonian orogeny. Later Palaeozoic-Cenozoic crustal rifting, which led to the opening of the North-Atlantic Ocean, then potentially reactivated this zone as a transfer zone, displacing the Caledonian thrust nappes sinistrally and allowing Late Palaeozoic-Mesozoic brittle faults to step and change fault polarity across the transfer zone (Indrevær et al., 2013).

C) Post-Caledonian brittle structures

Post-Caledonian brittle faults are present throughout the studied passive margin (Indrevær et al., 2013) and are largely controlled by two major fault complexes, the partly onshore Vestfjord-Vanna Fault Complex and the offshore Troms-Finnmark Fault Complex that bound the WTBC horst (Gabrielsen et al., 1990; Olesen et al., 1997; Indrevær et al., 2013). The margin is segmented along strike by at least two Late Palaeozoic-Mesozoic transfer faults, the Senja Shear Zone and the Fugløya transfer zone (Olesen et al., 1997; Indrevær et al., 2013)

The two major fault complexes are both comprised of alternating NNE-SSE and ENE-WSW trending subsidiary fault zones (Gabrielsen et al., 1990; Olesen et al., 1997; Indrevær et al., 2013). A wide spectrum of irregular and linear trenches and escarpments truncate the strandflat bathymetry and the presumed bedrock structures, thus segmenting the strandflat into blocks. These features, including major boundary escarpments such as the westernmost scarp that defines the western edge of the strandflat, produce a zig-zag pattern of alternating ~NNE-ENE and ~ENE-WSW trending segments (Fig. 25) similar to those observed onshore (e.g. the VVFC) and on the deep shelf (e.g. the TFFC). We thus infer that these trenches and escarpments are in total, the result of Late Palaeozoic-Mesozoic rifting and brittle faulting that formed the present passive continental margin. The distribution of these faults, as evident from the bathymetry data, suggests that they are a part of a continuous system of horst-internal fault segments that link up onshore fault complexes with offshore complexes across the horst (Fig. 25).

Displacement

Estimating the amount of displacement across the trenches on the strandflat interpreted as brittle faults is important in order to understand their regional significance. In general, the VVFC, including the Vannareid-Brurøysund fault zone on Vanna have estimated amounts of displacement of 1-3km (Olesen et al., 1997). The less prevalent, linked fault system along the outer islands of the WTBC have estimated amounts of displacement of 100's of meters or less (Indrevær et al., 2013).

From this study, it is evident that the outer faults (e.g. the Bremneset, Tussøya and Hillesøya fault zones (Fig. 8 & 10) produce only weak bathymetric morphology. In areas where they are possible to trace onto the strandflat, they are not comparable in width nor depth with the many trenches that are observed on the strandflat. This suggests that the amount of displacement along the inferred fault-related trenches on the strandflat must have been greater than 100's of meters in order to produce wider damage zones (so that they may have been more heavily excavated by strandflat-forming processes and glacial erosion). However, the Vannareid-Brurøysund fault zone, for example, defines a topographic valley along its strike that is comparable in size with the offshore trenches (Fig. 21). The larger offshore trenches are thus suggested to have similar amounts of displacement as the VVFC and the Vannareid-Brurøysund fault zone (i.e. 1-3km). This is supported by the apparent dextral offset of the interpreted fold hinge zone running along the Kvalsund shear zone (Fig. 19b), which yielded an estimated amount of normal displacement of ~1.8km, down to the northwest.

The estimated displacement for interpreted brittle faults on the strandflat are thus similar to those estimated for the VVFC and implies that fault zones with displacements comparable with the VVFC may be widely distributed across the WTBC horst. Since very few fault zones comparable in displacement with the VVFC have been mapped onshore (e.g. Opheim & Andresen, 1989; Gagama, 2005), these major fault zones may tentatively be located within the larger sounds and fjords along the margin.

Timing of brittle faulting

Onshore, the brittle fault activity occurred in the Permian/Late-Triassic and came to a halt during early and deep stages of rifting as the rift activity propagated westward to offshore fault complexes in the Late Jurassic/Early Cretaceous (Davids et al., 2013; Indrevær et al., 2013; 2014). A similar westward progressive migration of fault activity may thus be expected for the brittle faults located on the strandflat. However, in order to preserve the entire WTBC horst as a uniform basement outlier, it is likely that most of these faults also became largely inactive after the Late Permian/Early Triassic rift event.

Several other indicators, which may shed light on the relative timing of fault segments and possible later reactivation, have been observed on the strandflat bathymetry. First, the relative timing of the alternating NNE-SSW and ENE-WSW trending brittle faults that constitute the two major fault complexes of the WTBC horst (Indrevær et al., 2013) can be inferred since both the NNE-SSW and ENE-WSW trending faults merge into parallelism with each other (Fig. 19a), suggesting that the two fault sets formed contemporaneously.

Secondly, the apparent sub-planar strandflat shows a vertical offset of c. 200m across inferred fault scarps. Examples include (i) the westernmost escarpment running along larger portions of the studied strandflat, which apparently has down-faulted the strandflat ~200m to the west (Fig. 20), (ii) the brittle fault zone that defines the southern limit of the raised plateau in Area 3, where the strandflat is displaced by ~200m down to the south (Fig. 22) and (iii) the presence of strandflat-internal smaller basins within Area 1 (Fig. 11b). The apparent ~200m vertical displacement across these scarps may be interpreted as the reactivation of the Late Palaeozoic-Mesozoic brittle faults after the formation of the strandflat, i.e. advocating Quarternary fault activity. Fenton (1991, 1994) and Muir Wood (1993) have listed criterias that may be used to separate neotectonic faults from older faults. The two most relevant criterions for this study is (i) that the amount of displacement is more or less constant along the entire length of the fault scarp and (ii) that the hight-to-length ratio of neotectonic fault

scarps are typically in the range of 1:10.000 to 1:1.000, rarely exceeding the latter. The observed scarps do not show an increase in hight from the scarp tips to their centers (e.g. Fig. 20), thereby supporting their origin as neotectonic. However, if considering individual scarp segments, the hight-to-length ratio of the scarps does exceed 1:1000, typically falling in the range of c. 1:100 (Fig. 20). Only by considering the entire c. 200 km western boundary of the strandflat as one continuous fault scarp (Fig. 25) does the ratio approach 1:1.000.

The scarps may also be the result of glacitectonic ice-plucking of the hangingwall of the Late Palaeozoic-Mesozoic faults. Alternatively, the scarps may separate basement lithologies with contrasting susceptibility to the pre-Cretacous tropical weathering, thus leaving the apparent displacement of the strandflat across the scarps purely as a result of different amounts of Quarternary erosion.

D) Relation of bathymetry to present onshore topography and landscape forms

The analysis of aspect values (dip directions) for topographic surfaces dipping more than 5° (Fig. 5) shows that NNW-SSE, N-S and ENE-WSW trending slopes dominate on the strandflat. The N-S and ENE-WSW striking slopes make up the same zigzag pattern as evidently characterize the onshore WTBC-boundary fault zones and fault segments (i.e. VVFC) as well as the offshore Troms-Finnmark Fault Complex (Fig. 25; Indrevær et al., 2013). Onshore, the topography is dominated by NW-SE and NE-SW to E-W striking slopes, mirroring the orientations of ductile and brittle fabrics, respectively (Fig. 25, upper left corner). The SW Barents Sea margin landscape is therefore clearly influenced by Late Palaeozoic-Mesozoic brittle faulting, and to some extent, also Precambrian fabric elements. Both the topography and bathymetry show strong NW-SE trends close to the Senja Shear Belt and Fugløya transfer zone (Fig. 5 & 25), indicating the regional significance of these structures as terrane boundaries and later transfer zones (Olesen et al., 1997; Indrevær et al., 2013).

A similar study of the margin in Lofoten-Vesterålen has shown that the local topography is strongly influenced by brittle faults and fracture sets (Bergh et al., 2007b; Eig, 2008; Hansen, 2009). The brittle faults in Troms have similar orientation as faults and fractures in Lofoten-Vesterålen, but their effect on topography is apparently less. A possible explanation for this is the heterogeneous nature of the WTBC. In Lofoten, the basement is in large dominated by homogenous Palaeoproterozoic magmatic rocks (Griffin et al., 1978; Corfu, 2004). As few pre-existing zones of weakness existed for faults to utilize, the fault zones formed freely, in

that they reflected the regional stress field and produced the alternating NNE-SSW and ENE-WSW trending fault zones as is present today. These were then the only zones of weakness that the main landscape forming element, the glaciers, could utilize and excavate during the Quaternary, enhancing the tectonic effect on topography. In the relatively heterogeneous WTBC, however, zones of weakness with more variable orientation, as produced by lithological boundaries, macro-scale folds, foliation and ductile shear zones were present and free to be utilized by faults and glaciers alike. As a result, the topography of the WTBC shows a larger degree of correlation with ductile basement structures and a lesser correlation with Late Palaeozoic-Mesozoic brittle faults than that of the Lofoten-Vesterålen margin.

Conclusions

- Morpho-tectonic features observed on the high-resolution bathymetry data covering the strandflat outboard Troms, mimics in great detail basement structures observed onshore, such as duplexes, steeply plunging tight folds, intrafolial macro-folds and shear zones, including the offshore continuations of high-strain meta-supracrustal belts. This strongly suggests that the lithologies of the WTBC are also present on the strandflat.
- The contact between WTBC lithologies with mainly sub-vertical N-S striking foliation and gently NW-dipping Caledonian thrust nappes is interpreted to run in the sound southwest of Nord-Fugløya, clearly visible as a distinct change in seabed morphology across the contact zone. The same sound marks the location of the Mesozoic Fugløya transfer zone, a possible reactivated portion of the Svecofennian Bothnian-Kvænangen Fault Complex, which has displaced the Basement-Caledonian contact sinistrally. The spatial overlap of these features suggests that the sound has exerted an important role in controlling and accommodating deformation of the margin through a very long time span.
- NNE-SSW to ENE-WSW trending trenches commonly truncate interpreted ductile structures on the strandflat and are interpreted as brittle faults based on their similar orientation as known onshore fault zones and fault zones on the continental shelf. Based on comparison of onshore fault zones impact on topography and the apparent offset of bedrock structures across a trench, the fault zones on the strandflat are suggested to have accommodated displacement on the order of kilometres.

- The structural relationship between faults of different orientation suggests that the Late Palaeozoic-Mesozoic fault zones, independent of their orientations, formed contemporaneous. Still, some interpreted fault zones on the strandflat defines escarpments that displaces the strandflat vertically with as much as 200m, inferring neo-tectonic activity. Alternatively, the vertical offset across the fault scarps may be due to glacitectonics, or lithological contrasts in susceptibility to pre-Cretaceous tropical weathering.
- Comparing topography and strandflat slope aspects reveals that the common orientations of basement structures and brittle faults onshore are reflected in the topography as well as the strandflat bathymetry. This supports a tectonic influence on the present day coastal landscape and the SW Barents Sea margin architecture.

Ackowledgements: This work was part of the Industrial PhD scheme organized by the Norwegian Research Council. The project is a collaboration between DONG E&P Norway and the University of Tromsø, financed by DONG E&P Norway and the Norwegian Research Council. We would like to express our gratitude to all persons involved from these institutions. We would also like to thank the Norwegian Mapping Authority and the Norwegian Armed Forces for sharing and allowing us to publish illustrations of the high-resolution bathymetry data.

References

Andresen, A. 1980: The age of the Precambrian basement in western Troms, Norway. *GFF*, *101*(4), 291-298.

Antonsdòttir, V. 2006: *Structural and kinematic analysis of the post-Caledonian Rekvika Fault Zone, Kvaløya, Troms*. Unpublished Master thesis, University of Tromsø, 84 pp.

Armitage, 2007: *Geological reconnaissance on Sandøya, West Troms Basement Complex, 04-07 September 2007*. Unpublished report, NunaMinerals A/S.

Armitage, P.E.B. & Bergh, S.G. 2005: Structural development of the Mjelde-Skorelvvatn Zone on Kvaløya, Troms: a metasupracrustal Shear Belt in the Precambrian West Troms Basement Complex, North Norway. *Norwegian Journal of Geology 85*, 117-132.

Bergh, S. G., Kullerud, K., Corfu, F., Armitage, P. E., Davidsen, B., Johansen, H. W., Pettersen, T & Knudsen, S. 2007a: Low-grade sedimentary rocks on Vanna, North Norway: a new occurrence of a Palaeoproterozoic (2.4-2.2 Ga) cover succession in northern Fennoscandia. *Norwegian Journal of Geology 87* (3), 301.

Bergh, S. G., Eig, K, Kløvjan, O. S., Henningsen, T., Olesen, O. & Hansen, J-A., 2007b: The Lofoten-Vesteralen continental margin: a multiphase Mesozoic-Palaeogene rifted shelf as shown by offshore-onshore brittle fault-fracture analysis. *Norwegian Journal of Geology 87*, 29 - 58.

Bergh, S. G., Kullerud, K., Armitage, P. E. B., Zwaan, K. B., Corfu, F., Ravna, E. J. K. & Myhre, P. I., 2010: Neoarchaean through Svecofennian tectono-magmatic evolution of the West Troms Basement Complex, North Norway. *Norwegian Journal of Geology*, *v*. *90*, 21-48.

Bergh, S. G., Kullerud, K., Myhre, P. I., Corfu, F., Armitage, P. E. B., Zwaan, K. B., & Ravna, E. J. K. 2014: Archaean Elements of the Basement Outliers West of the Scandinavian Caledonides in Northern Norway: Architecture, Evolution and Possible Correlation with Fennoscandia. In *Evolution of Archean Crust and Early Life* (pp. 103-126). Springer Netherlands.

Binns, R.E., Chroston, P.N. & Matthews, D.W., 1980: Low-grade sediments on Precambrian gneiss on Vanna, Troms, Northern Norway. *Norges geologiske undersøkelse Bulletin 359*, 61-70.

Corfu, F. (2004). U–Pb age, setting and tectonic significance of the anorthosite–mangerite–charnockite–granite suite, Lofoten–Vesterålen, Norway. *Journal of Petrology*, *45*(9), 1799-1819.

Corfu, F., Armitage, P. E. B., Kullerud, K. & Bergh, S. G., 2003: Preliminary U-Pb geochronology in the West Troms Basement Complex North Norway: Archaean and Palaeoproterozoic events and younger overprints. *Geological Survey of Norway, Bulletin 441*, 61-72.

Corner, G. D., 2005: Chapter 12. Atlantic coast and fjords. In: Seppälä, M. (ed.). The physical Geography of Fennoscandia, *Oxford Regional Environments Series*, Oxford University Press, 203-228.

Dahl, E., 1947: Litt om forholdene under og etter den siste istid i Norge. *Naturen*, *71*, 232-252.

Dahlgren, K. I., Vorren, T. O., Stoker, M. S., Nielsen, T., Nygård, A., & Petter Sejrup, H., 2005: Late Cenozoic prograding wedges on the NW European continental margin: their formation and relationship to tectonics and climate. *Marine and Petroleum Geology*, *22*(9), 1089-1110.

Davids, C., Wemmer, K., Zwingmann, H., Kohlmann, F., Jacobs, J. & Bergh, S.G. 2013: K–Ar illite and apatite fission track constraints on brittle faulting and the evolution of the northern Norwegian passive margin. *Tectonophysics 608*, 196–211.

Doré, A. G., Lundin, E. R., Fichler, C. & Olesen, O., 1997: Patterns of basement structure and reactivation along the NE Atlantic margin. *Journal of the Geological Society of London 154*, 85-92

Doré, A. G., Lundin, E. R., Jensen, L. N., Birkeland, Ø., Eliassen, P. E. & Fichler, C., 1999: Principal tectonic events in the evolution of the northwest European Atlantic margins. In: Fleet, A. J. & Boldy, S. A. R. (eds.), Petroleum Geology of Northwest Europe*: Proceedings of the 5th Conference*. *Geological Society of London*, 41-61.

Eig, K. 2008: *Onshore and offshore tectonic evolution of the Lofoten passive margin, North Norway*. Unpublished PhD thesis, University of Tromsø, 256 pp.

Fenton, C.H. 1991: Neotectonics and Palaeoseismicity in North West Scotland. Unpubl. Ph.D. Thesis, Univ. of Glasgow, 403 pp.

Fenton, C.H. 1994: Postglacial faulting in eastern Canada. Geological Survey of Canada Open file Report 2774, 98 pp.

Forslund, T. 1988: *Post-Kaledonske forkastninger i Vest-Troms, med vekt på Kvaløyslettaforkastningen, Kvaløya*. Unpublished Cand. Scient. thesis, University of Tromsø. 173 pp.

Gaal, G & Gorbatschev, R. 1987: An outline of the Precambrian evolution of the Baltic Shield. *Precambrian Research 35*, 15-52.

Gabrielsen, R. H. 1984: Long-lived fault zones and their influence on the tectonic development of the southwestern Barents Sea. *Journal of the Geological Society*, *141*(4), 651-662.

Gabrielsen, R.H., Færseth, R.B., Jensen, L.N., Kalheim, J.E. & Riis, F. 1990: Structural elements of the Norwegian continental shelf — Part I: the Barents Sea Region. *Norwegian Petroleum Directorate Bulletin 6*, 33 pp.

Gabrielsen, R. H., Braathen, A., Dehls, J. & Roberts, D. 2002: Tectonic lineaments of Norway. *Norwegian Journal of Geology*, *v*. *82*, 153-174.

Gagama, M. F. V., 2005: *Strukturell analyse av post-kaledonske lineamenter ved Sifjorden, Vest-Senja, Troms*. Unpublished Master thesis, University of Tromsø, 85 pp.

Gjerlow, E. 2008: *Petrologi og alder av hoymetamorfe mafiske bergarter i det vestlige gneiskomplekset i Troms*. Unpublished Master thesis, University of Tromsø, 90 pp.

Grogan, P. & Zwaan, K.B. 1997: *Geologisk kart over Norge, berggrunnskart Helgøy, M 1:250 000,* Norges geologiske undersøkelse.

Griffin W. L., Taylor P. N., Hakkinen J. W., Heier K. S., Iden I. K., Krogh E. J. Malm O., Olsen K. I., Ormaasen D. E., and Tveten E., 1978: Archaean and Proterozoic crustal evolution in Lofoten-Vesterålen, N. Norway, *Journal of the Geological Society London, 135*, 629–647.

Hansen, J.-A. 2009: *Onshore-offshore tectonic relations on the Lofoten and Vesterålen Margin - Mesozoic to early Cenozoic structural evolution and morpological implications*. PhD thesis, University of Tromsø, 229 pp.

Hölttä, P. H., Balagansky, V., Garde, A. A., Mertanen, S., Peltonen, P., Slabunov, A.,Sorjonen-War, P. & Whitehouse, M. 2008: Archean of Greenland and Fennoscandia. *Episodes 31(1),* 13-19.

Indrevær, K., Bergh, S.G., Koehl, J.-B., Hansen, J.-A., Schermer, E.R. & Ingebrigtsen, A. 2013: Post-Caledonian brittle fault zones on the hyper-extended SW Barents Sea Margin: New insights into onshore and offshore margin architecture. *Norwegian Journal of Geology, Vol 93*, pp. 167-188.

Indrevær, K., Stunitz, H., & Bergh, S. G., 2014: On brittle normal faults along the SW Barents Sea margin: fault processes and implications for basement permeability and margin evolution. *Journal of the Geological Society, London, v. 171, no. 6.*

Johansen, H. 1987: *Forholdet mellom det prekambriske underlaget og overliggende sedimentære bergarter sørøst på Vanna, Troms*. Unpublished Cand. Scient thesis, University of Tromsø, 129 pp.

Lahtinen, R., Garde, A. A. & Melezhik, V. A., 2008: Paleoproterozoic evolution of Fennoscandia and Greenland. *Episodes 31(1),* 20.

Larsen, E., & Holtedahl, H., 1985: The Norwegian strandflat: A reconsideration of its age and origin. *Norsk geologisk tidsskrift*, *65*(4), 247-254.

Motuza, G., Motuza, V., Beliatsky, B. & Savva, E. 2001: *The Ringvassøya greenstone belt (Tromso, North Norway): implications for a Mesoarchaean subduction zone*. EUROPROBE time-slice symposium "Archaean and Proterozoic Plate Tectonics: Geological and Geophysical Records", St. Petersburg, Russia, October 1-November 3, 2001, 43-44.

Muir Wood, R. 1993: A review of the seismotectonics of Sweden. Swedish Nuclear Fuel and Waste Management Co. (SKB) Technical Report 93-13, 225 pp.

Myhre, P. I., Corfu, F., & Bergh, S., 2011: Palaeoproterozoic (2.0–1.95 Ga) pre-orogenic supracrustal sequences in the West Troms Basement Complex, North Norway. *Precambrian Research*, *186*(1), 89-100.

Myhre, P.I., Corfu, F., Bergh S.G. & Kullerud, K. 2013: U–Pb geochronology along an Archaean geotransect in the West Troms Basement Complex, North Norway. *Norwegian Journal of Geology, Vol 93*, pp. 1–24. Trondheim 2013, ISSN 029-196X.

Nansen, F., 1922: *The strandflat and isostasy (No. 11)*. I kommission hos J. Dybwad.

Nyheim, H., Bergh, S. G., Krogh, E. J. & Zwaan, K. B. 1994: Torsnesskjærsonen i det vestlige (nord-norske) gneisterreng, Kvaløya, Troms; evidenser for kompleks skorpeforkortning og orogenparallelloblik strike-slip. *Nordic Geological Winter Meeting, Lulea*, p. 149.

Olesen, O., Torsvik, T. H., Tveten, E., Zwaan, K. B., Løseth, H. & Henningsen, T. 1997: Basement structure of the continental margin in the Lofoten-Lopphavet area, northern Norway: constraints from potential field data, on-land structural mapping and palaeomagnetic data, *Norwegian Journal of Geology, v. 77*, 15-30.

Opheim, J.A. and Andresen, A. 1989: Basement-cover relationships on northern Vanna, Troms, Norway. *Norwegian Journal of Geology*, *v. 69*(2), 67-81.

Ottesen, D., Dowdeswell, J. A., & Rise, L., 2005: Submarine landforms and the reconstruction of fast-flowing ice streams within a large Quaternary ice sheet: The 2500-km-long Norwegian-Svalbard margin (57–80 N). *Geological Society of America Bulletin*, *117*(7-8), 1033-1050.

Pedersen, B., R., S., 1997: *Strukturell analyse av en prekambrisk, duktilt deformert metasuprakrustalsone (Astridal-skjarsonen?) på NO-Senja, Troms*. Unpublished Cand. scient. thesis, University of Tromso, 166 pp.

Ramsay, D. M., Sturt, B. A., Jansen, Ø., Andersen, T. B., & Sinha-Roy, S. 1985: The tectonostratigraphy of western Porsangerhalvøya, Finnmark, north Norway. In: Gee, D.G. and Sturt, B.A. (eds): *The Caledonide Orogen: Scandinavia and related areas*. John Wiley, Chichester, UK, 611-619.

Reusch, H. (1894). Strandfladen, et nyt træk i Norges geografi. *Norges geologiske undersøkelse 14*, 1-12.

Rise, L., Bøe, R., Riis, F., Bellec, V. K., Laberg, J. S., Eidvin, T., Elvenes, S. & Thorsnes, T. 2013: The Lofoten-Vesterålen continental margin, North Norway: Canyons and mass-movement activity. *Marine and Petroleum Geology*, *45*, 134-149.

Roberts, D. 1974: Kartblad Hammerfest. Beskrivelse til det 1:250 000 berggrunnsgeologiske kart. *Norges geologiske undersøkelse Bulletin 301,* 66 p.

Roberts, D., 2003: The Scandinavian Caledonides: event chronology, palaeogeographic settings and likely modern analogues. *Tectonophysics 365*, p. 283-299

Roberts, D., Gee, D.G., 1985: An introduction to the structure of the Scandinavian Caledonides. In: Gee, D.G., Sturt, B.A. (Eds.), *The Caledonide Orogen—Scandinavia and Related Areas*. Wiley, Chichester, pp. 55– 68.

Roberts, D., Chand, S., & Rise, L. 2011: A half-graben of inferred Late Palaeozoic age in outer Varangerfjorden, Finnmark: evidence from seismic reflection profiles and multibeam bathymetry. *Norwegian Journal of Geology 91*(3), 193-202.

Rydningen, T.A., Vorren T.O., Laberg, J.S. & Kolstad, V. 2013: The marine-based NW Fennoscandian ice sheet: glacial and deglacial dynamics as reconstructed from submarine landforms. *Quaternary Science Reviews, v. 68*, 126-141.

Thorsnes, T, Erikstad, L., Dolan, M. F. J. & Bellec, V. K. 2009: Submarine landscapes along the Lofoten-Vesterålen-Senja margin, northern Norway. *Norwegian Journal of Geology*, *v. 89* (1-2), 5-16.

Thorstensen, L. 2011: *Land-sokkel korrelasjon av tektoniske elementer i ytre del av Senja og Kvaløya i Troms*. Unpublished Master thesis, University of Tromsø, 107 pp.

Vorren, T. O., Edvardsen, M., Hald, M., & Thomsen, E., 1983: Deglaciation of the continental shelf off southern Troms, North Norway. *Norges Geologiske Undersøkelse Bulletin*, (70), 173-187.

Zwaan, K. B., 1989: Berggrunnsgeologisk kartlegging av det prekambriske grønnsteinsbeltet pa Ringvassoy, Troms. *Norges geologiske undersøkelse Rapport 89*.101.

Zwaan, K. B. 1995: Geology of the West Troms Basement Complex, northern Norway, with emphasis on the Senja Shear Belt: a preliminary account. *Geological Survey of Norway, Bulletin 427*, 33-36.

Zwaan K. B., Fareth, E. & Grogan, P.W. 1998: *Geologisk kart over Norge, berggrunnskart TROMSØ, M 1:250.000*. Norges geologiske undersøkelse.

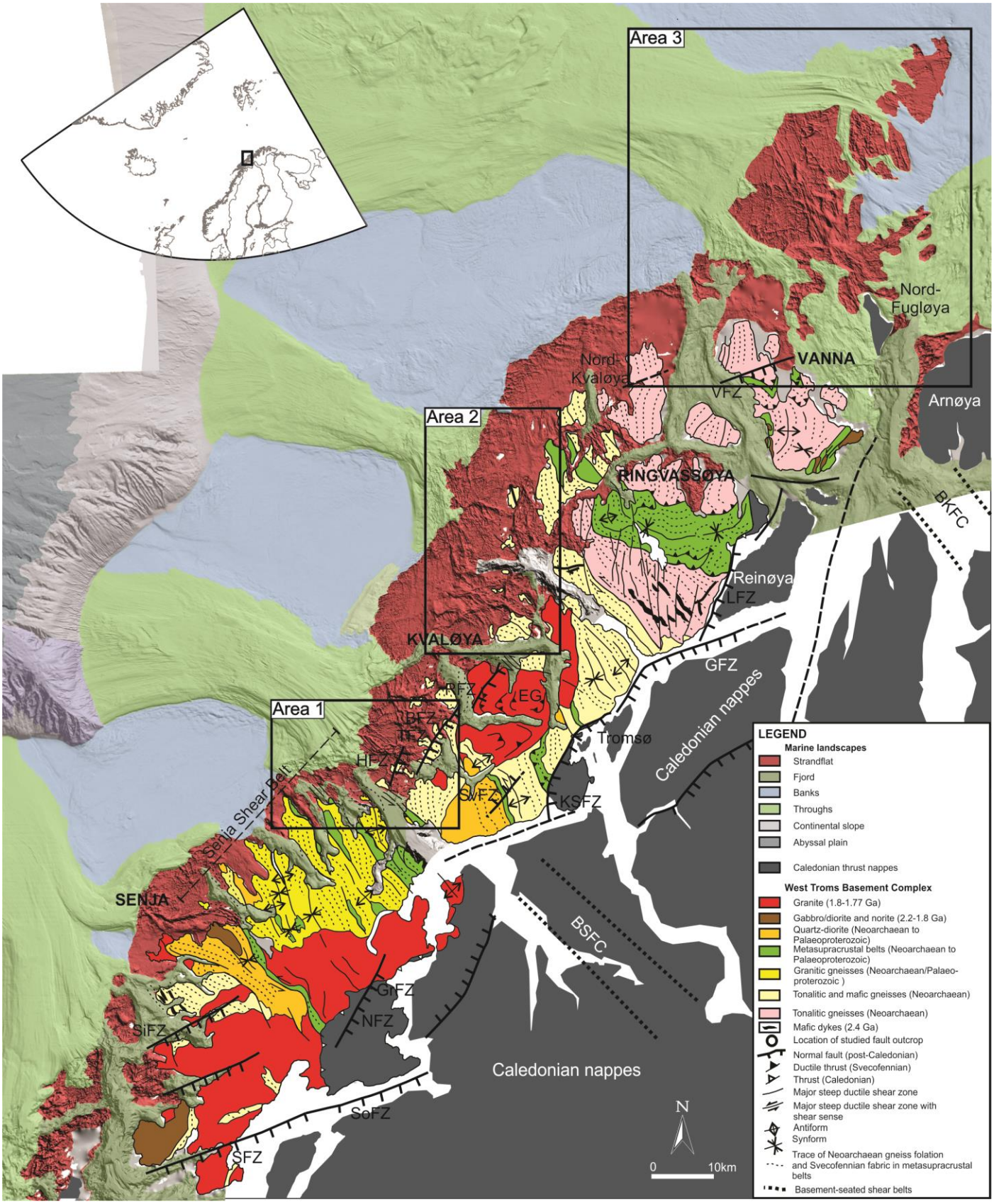
Area 3
Area 2
Area 1
Nord-Fugløya
VANNA
Nord-Kvaløya
VFZ
Arnøya
RINGVASSØYA
BKFC
Reinøya
LFZ
KVALØYA
GFZ
Caledonian nappes
RFZ
EGI
BFZ
TFZ
HFZ
Tromsø
SWFZ
TKSFZ
Senja Shear Belt
SENJA
BSFC
GrFZ
NFZ
SiFZ
Caledonian nappes
SoFZ
SFZ
N
0
10km
LEGEND
Marine landscapes
Strandflat
Fjord
Banks
Throughs
Continental slope
Abyssal plain
Caledonian thrust nappes
West Troms Basement Complex
Granite (1.8-1.77 Ga)
Gabbro/diorite and norite (2.2-1.8 Ga)
Quartz-diorite (Neoarchaean to Palaeoproterozoic)
Metasupracrustal belts (Neoarchaean to Palaeoproterozoic)
Granitic gneisses (Neoarchaean/Palaeo-proterozoic)
Tonalitic and mafic gneisses (Neoarchaean)
Tonalitic gneisses (Neoarchaean)
Mafic dykes (2.4 Ga)
Location of studied fault outcrop
Normal fault (post-Caledonian)
Ductile thrust (Svecofennian)
Thrust (Caledonian)
Major steep ductile shear zone
Major steep ductile shear zone with shear sense
Antiform
Synform
Trace of Neoarchaean gneiss folation and Svecofennian fabric in metasupracrustal belts
Basement-seated shear belts

Figure 1 (previous page): Detailed geological map of the West Troms Basement Complex showing main Archaean-Palaeoproterozoic fabrics and post-Caledonian brittle normal faults that separate the basement horst from down-dropped Caledonian nappes to the east (after Bergh et al., 2010). Offshore, marine landscape types are given, including the lateral distribution of the strandflat (mareano.no). Three areas of focus of the present paper are marked. Abbreviations: BFZ = Bremneset fault zone, BKFC=Bothnian-Kvænangen Fault Complex, BSFC=Bothnian-Senja Fault Complex, EG=Ersfjord Granite, GFZ=Grøtsundet fault zone, GrFZ=Grasmyrskogen fault zone, HFZ = Hillesøy fault zone, KSFC=Kvaløysletta-Straumsbukta fault zone, LFZ=Langsundet fault zone, NFZ=Nybygda fault zone, RFZ=Rekvika fault zone, SFZ=Stonglandseidet fault zone, SiFZ=Sifjorden fault zone, SoFZ=Solbergfjorden fault zone, SvFZ=Skorelvvatn fault zone, TFZ=Tussøya fault zone, VFZ=Vannareid-Brurøysund fault zone, VVFC=Vestfjorden-Vanna Fault Complex.

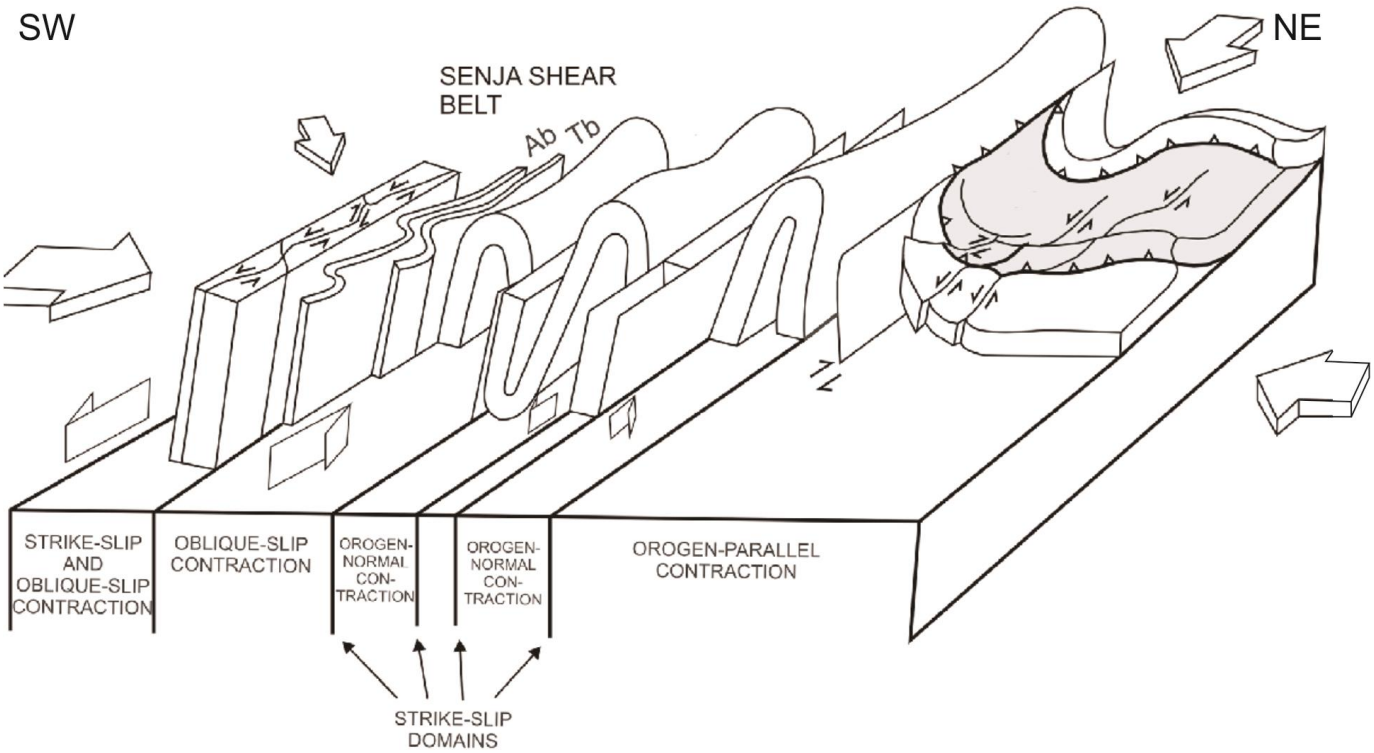

Figure 2: Schematic (not to scale) geometric/kinematic model for the development of Svecofennian structures observed in the WTBC. Early-stage formation of NE-directed thrusts and a low-angle main mylonitic foliation in the metasupracrustal belts was continued by orthogonal NE-SW contraction that produced upright macro-folds with steep limbs. Late-stage Svecofennian tectonism involved NE-SW orthogonal and/or oblique to orogen-parallel contraction (NW-SE) and mostly sinistral strike-slip reactivation of steep macro-fold limbs, e.g. in the Senja Shear Belt. The eastern, more flatlying macro-fold hinges accommodated NW-SE shortening and SE-directed thrusting. From Bergh et al. (2010). Abbreviations: Ab=Astridal belt, Tb=Torsnes belt.

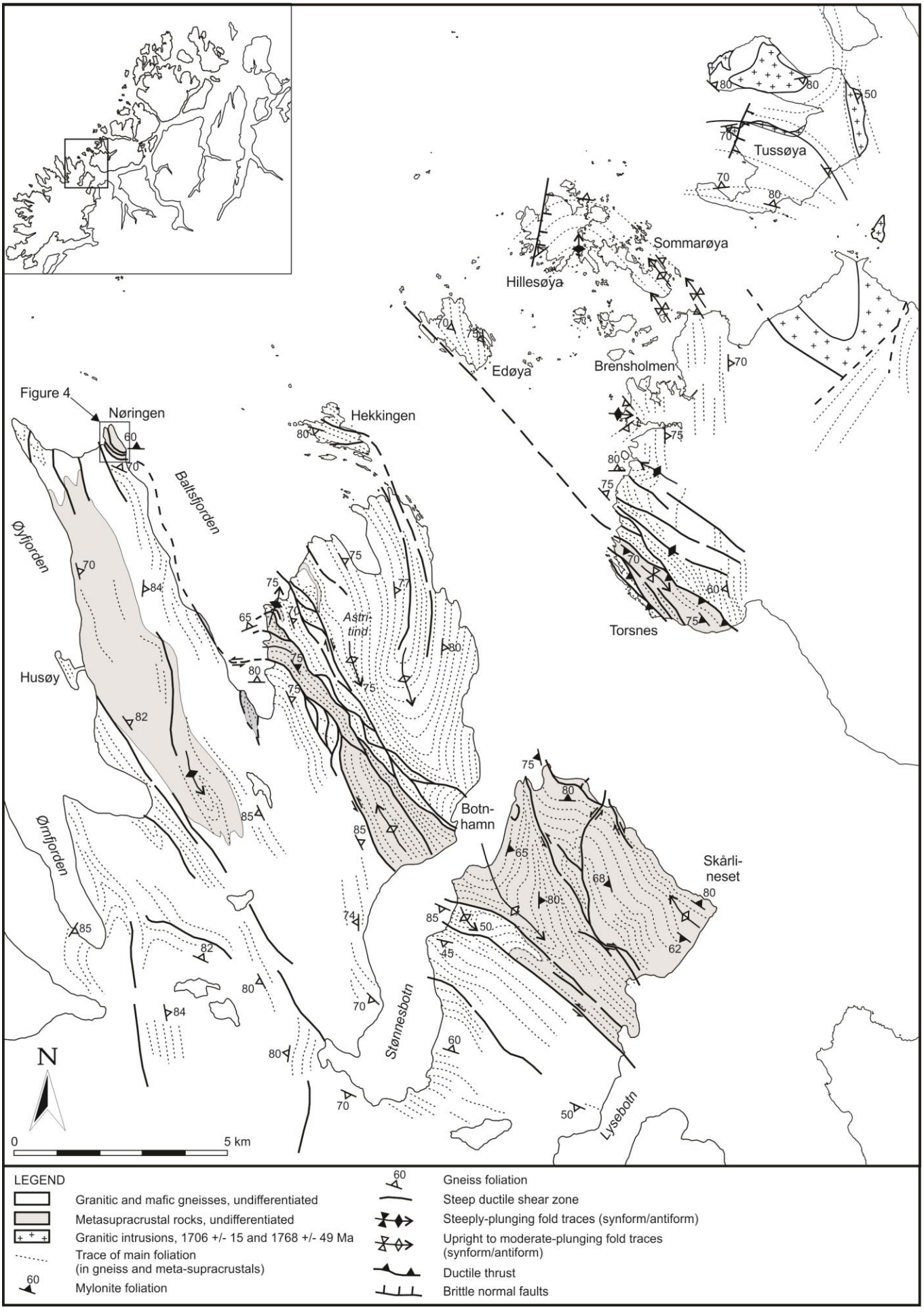
Figure 4
Nøringen
Hekkingen
Baltsfjorden
Øyfjorden
Husøy
Ørnfjorden
Astri-tind
Botn-hamn
Stønnesbotn
Lysebotn
Skårli-neset
Torsnes
Edøya
Hillesøya
Sommarøya
Tussøya
Brensholmen
N
0
5 km
LEGEND
Granitic and mafic gneisses, undifferentiated
Metasupracrustal rocks, undifferentiated
Granitic intrusions, 1706 +/- 15 and 1768 +/- 49 Ma
Trace of main foliation (in gneiss and meta-supracrustals)
Mylonite foliation
Gneiss foliation
Steep ductile shear zone
Steeply-plunging fold traces (synform/antiform)
Upright to moderate-plunging fold traces (synform/antiform)
Ductile thrust
Brittle normal faults

Figure 3 (previous page): Tectonic map of the Senja Shear Belt in northeastern Senja and southwestern Kvaløya, illustrating the lens-shaped architecture of the Astridal and Torsnes belts. Note macro-scale folds in the adjacent tonalitic gneisses where fold hinges are rotated into parallelism with the trace of the Astridal belt. The map is modified from Nyheim et al. (1994), Pedersen (1997), Zwaan et al. (1998), Corfu et al. (2003) and Bergh et al. (2010).

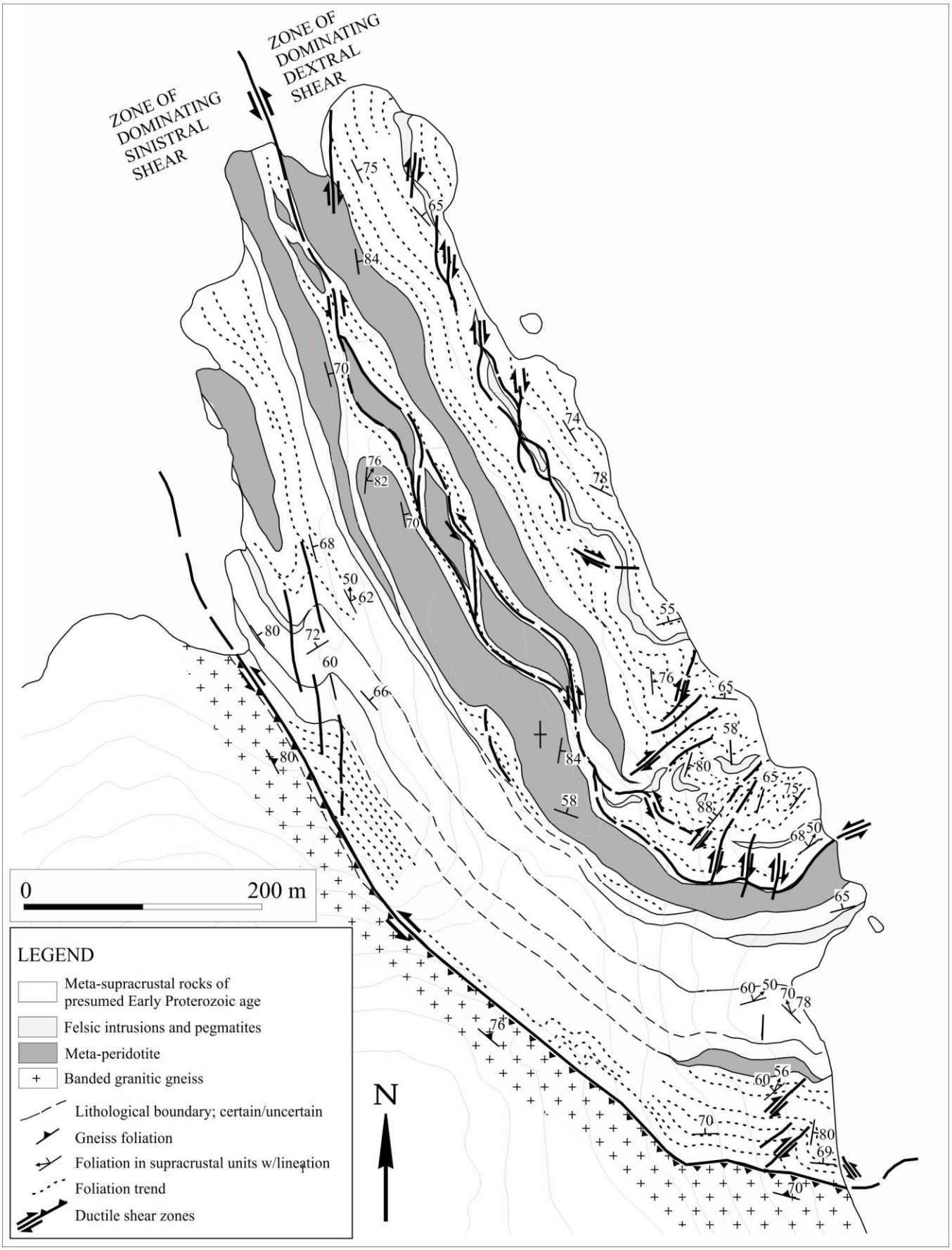

Figure 4: Detailed geological and structural map covering meta-supracrustal rocks that crop out at Nøringen. Note how meta-peridotites are sinistrally duplexed. Simplified from Pedersen (1997).

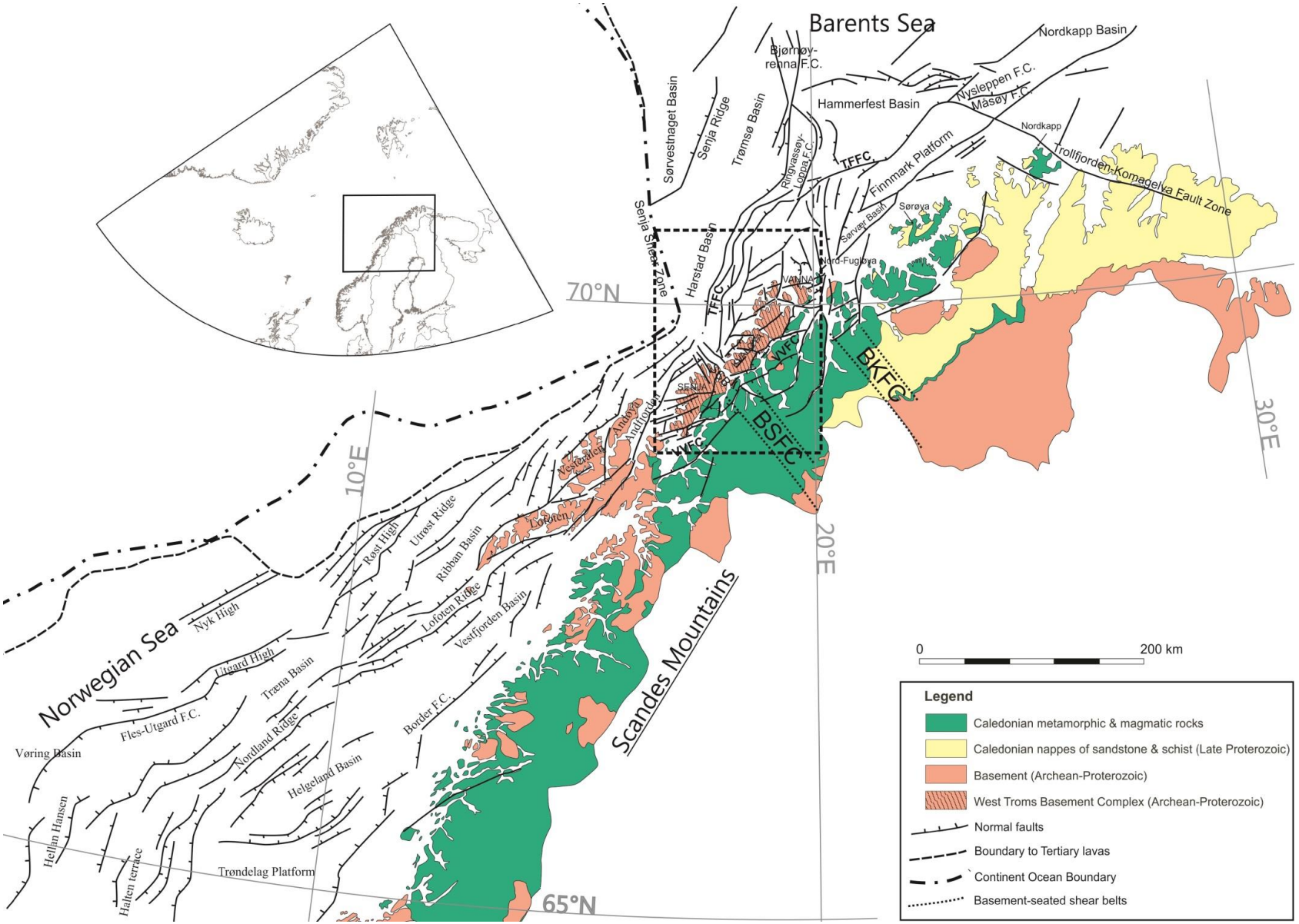

Figure 5: Regional onshore-offshore tectonic map and setting of the Lofoten-Vesterålen archipelago and the SW Barents Sea margin (after Blystad et al., 1995; Mosar et al., 2002; Bergh et al., 2007a; Faleide et al., 2008; Hansen et al., 2012; Indrevær et al., 2014). Onshore geology is from the Geological Survey of Norway. Areas of focus in are outlined. Abbreviations: BKFC=Bothnian-Kvænangen Fault Complex, BSFC=Bothnian-Senja Fault Complex, TFFC=Troms-Finnmark Fault Complex, VVFC=Vestfjorden-Vanna Fault Complex.

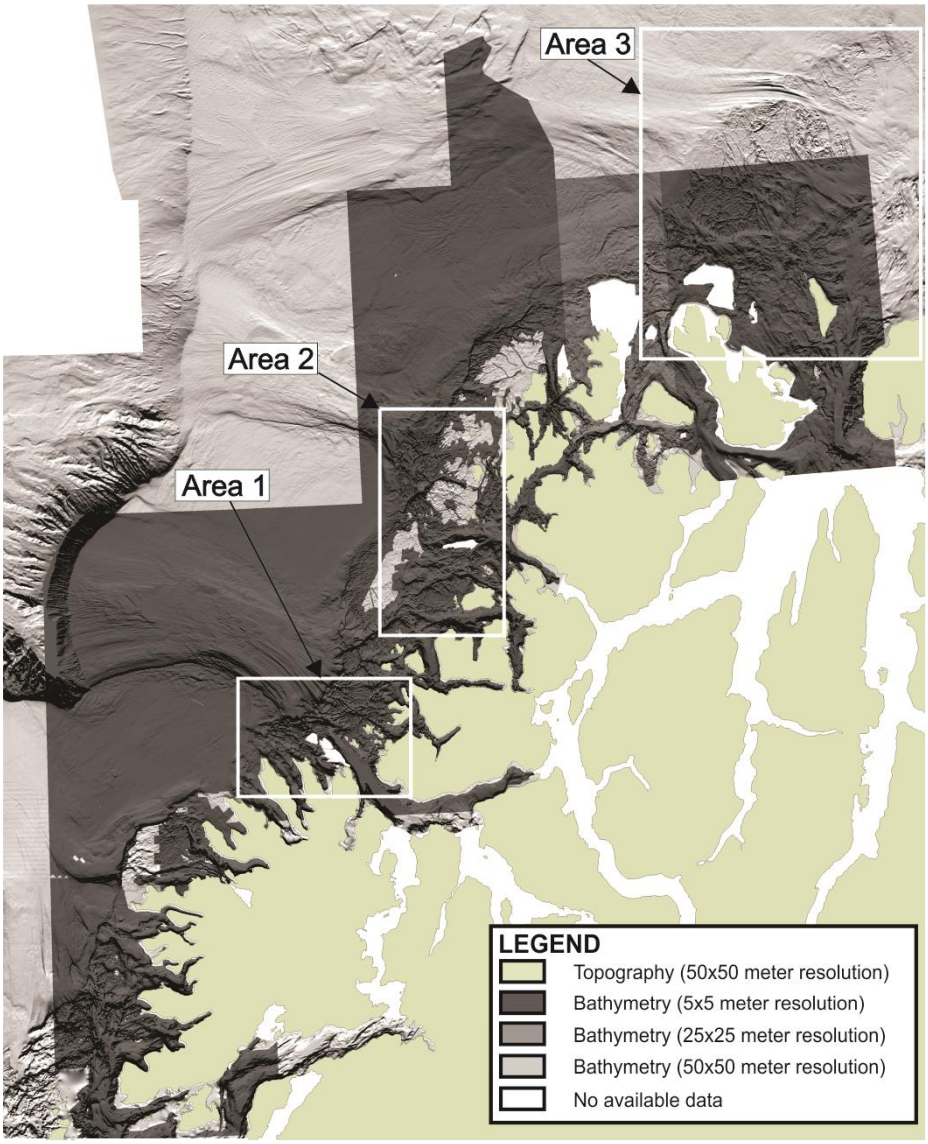

Figure 6: Overview of the available bathymetry data and its resolution. Note that there are several gaps in the 5x5m resolution data set covering the strandflat.

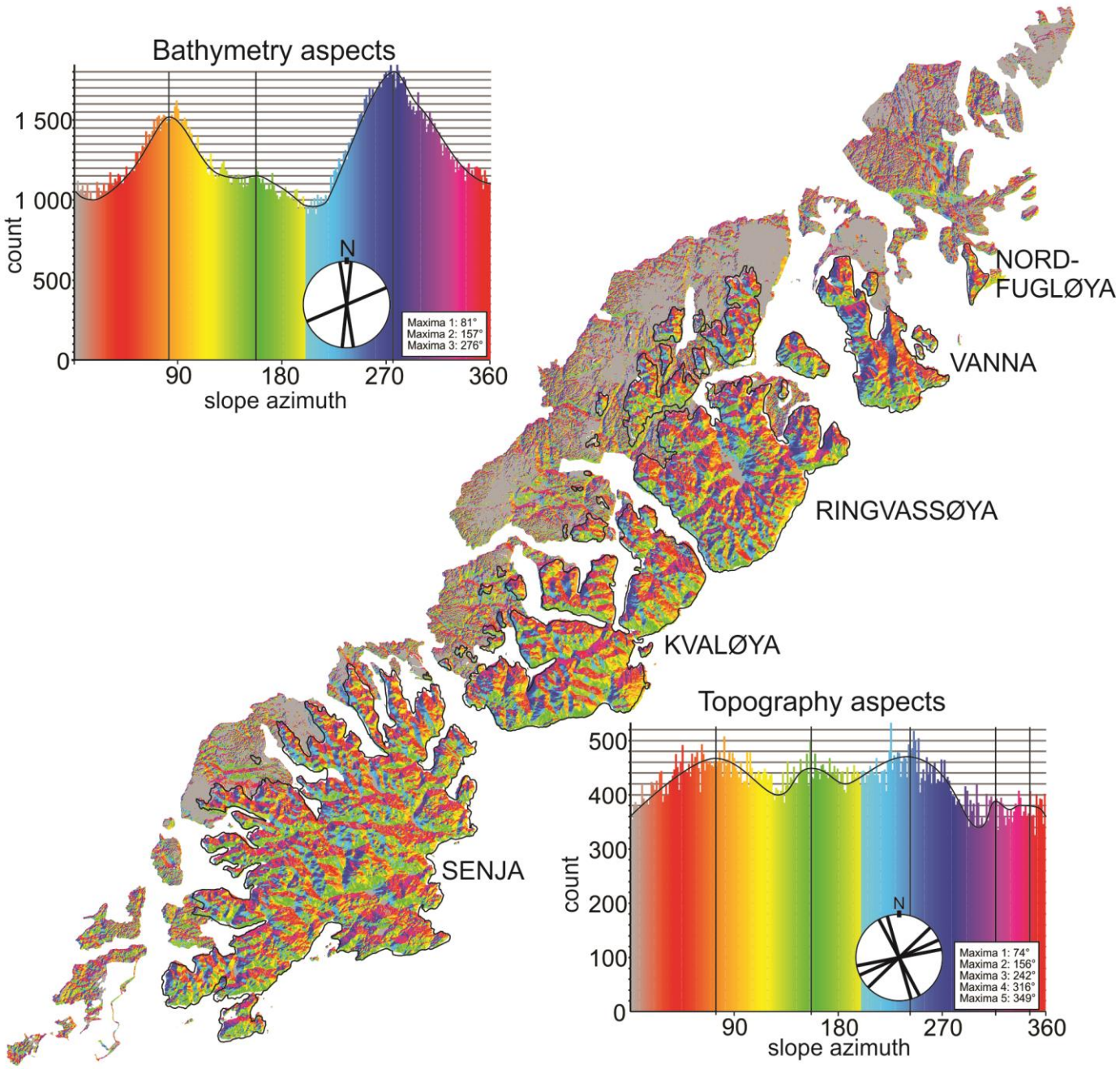

Figure 7: Aspect analysis of slopes steeper than 5°, for the outer islands and strandflat off Troms. Bathymetry (strandflat) aspects and topography aspects are shown separately (black lines indicate a running average of the aspects). Circular insets represent simplified rose diagrams. The analysis shows that N-S and NE-SW trending slopes are common on the strandflat, while NW-SE and NE-SW to E-W trending slopes are common onshore. These orientations are the same as orientations that dominate both ductile and brittle structures onshore.

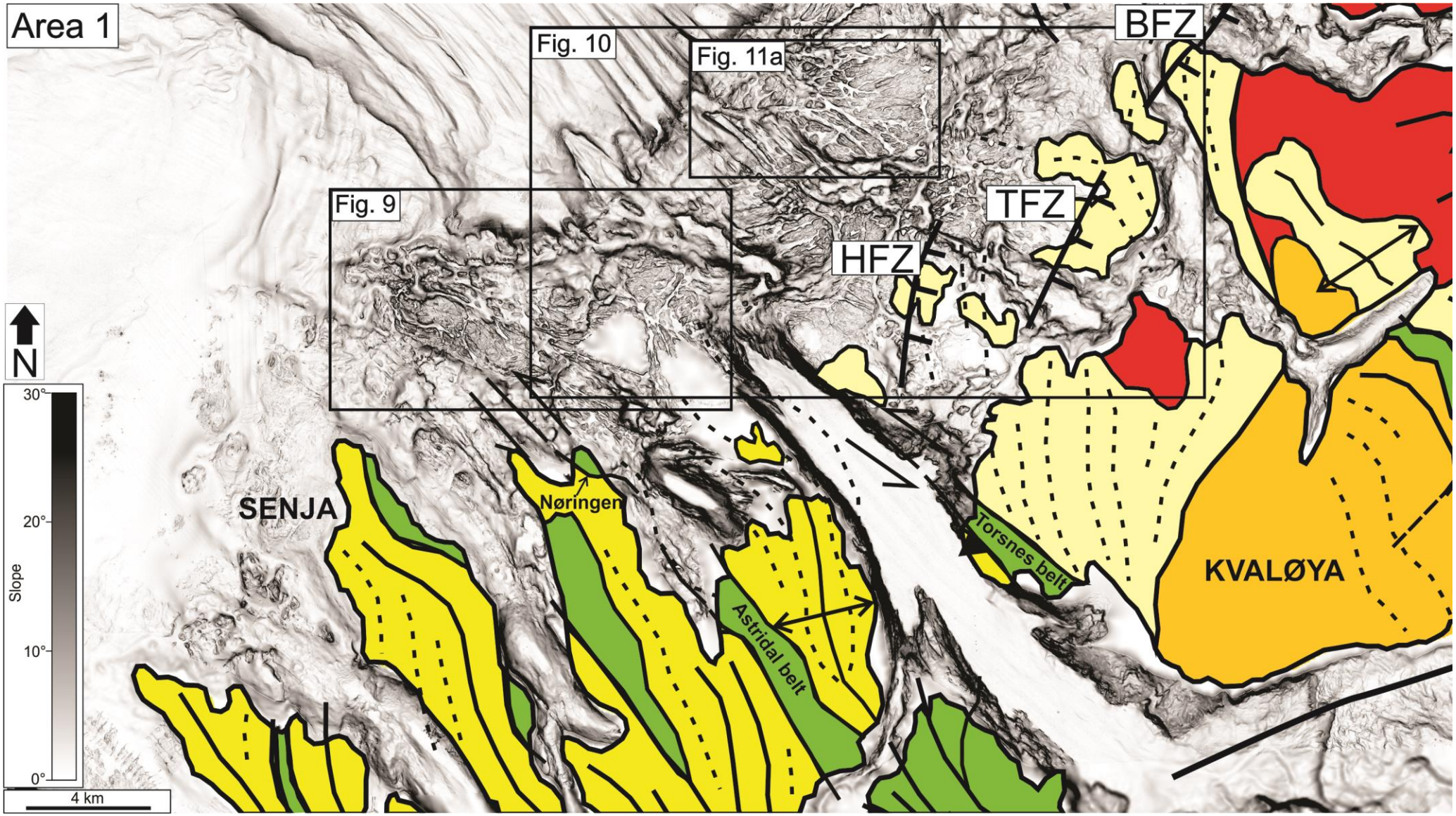

Figure 8: Overview of Area 1 covering the strandflat outboard northern portions of Senja and the southeastern portions of Kvaløya. Onshore geology from Bergh et al., (2010). Figures 9 and 10 are outlined.

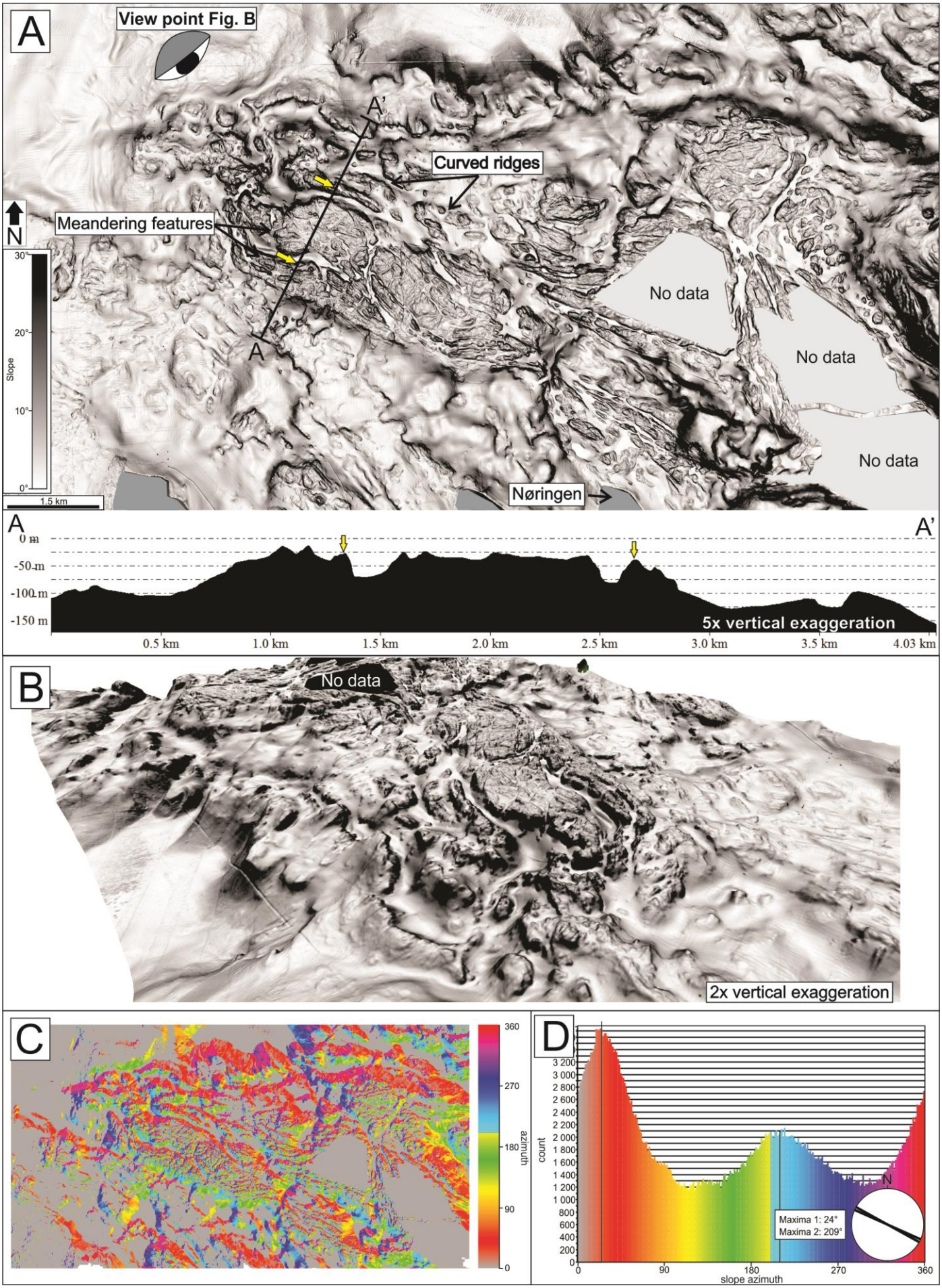
A
View point Fig. B
A'
Curved ridges
Meandering features
N
Slope
30°
20°
10°
0°
1.5 km
No data
No data
No data
Nøringen
A
A'
0 m
-50 m
-100 m
-150 m
5x vertical exaggeration
0.5 km
1.0 km
1.5 km
2.0 km
2.5 km
3.0 km
3.5 km
4.03 km
B
No data
2x vertical exaggeration
C
360
270
180
90
0
azimuth
D
count
3 200
3 000
2 800
2 600
2 400
2 200
2 000
1 800
1 600
1 400
1 200
1 000
800
600
400
200
0
N
Maxima 1: 24°
Maxima 2: 209°
0
90
180
270
360
slope azimuth

Figure 9 (previous page): Detailed illustrations of the strandflat within Area 1 (see Fig. 8 for location). (**a**) Dip map covering the strandflat with location of cross-section given and shown below. Yellow arrows indicate points of reference. Note the NW-SE trending meandering feature. Point of view for 3D illustration is marked. (**b**) 3D bathymetry illustration of the subarea, which highlights the meandering nature of the seabed morphology. (**c**) Aspect map and (**d**) histogram showing the prefered dip direction for slopes steeper than 5°. The preferred strikes of slopes from the aspect analysis are shown in the small circular insets (simplified rose diagrams).

Figure 10 (next page): Detailed illustrations of the strandflat within Area 1 (see Fig. 8 for location). (**a**) Dip map bathymetry data covering the strandflat with onshore portions of the subarea covered by aerial photographs. Locations of cross-sections are shown and given below. Yellow arrows indicate points of reference. Point of view for 3D illustration is marked. (**b**) 3D illustration of the subarea, which highlights the continuation of the Torsnes belt with a notable rounded z-shape. (**c**) Aspect map and (**d**) histogram showing the prefered direction of dips for slopes steeper than 5°. Grey line shows the preferred aspects of the topography (not to scale along the Y-axis). The preferred strikes of slopes from the aspect analysis are shown in the small circular insets (simplified rose diagrams, grey lines shows *topography* maxima).

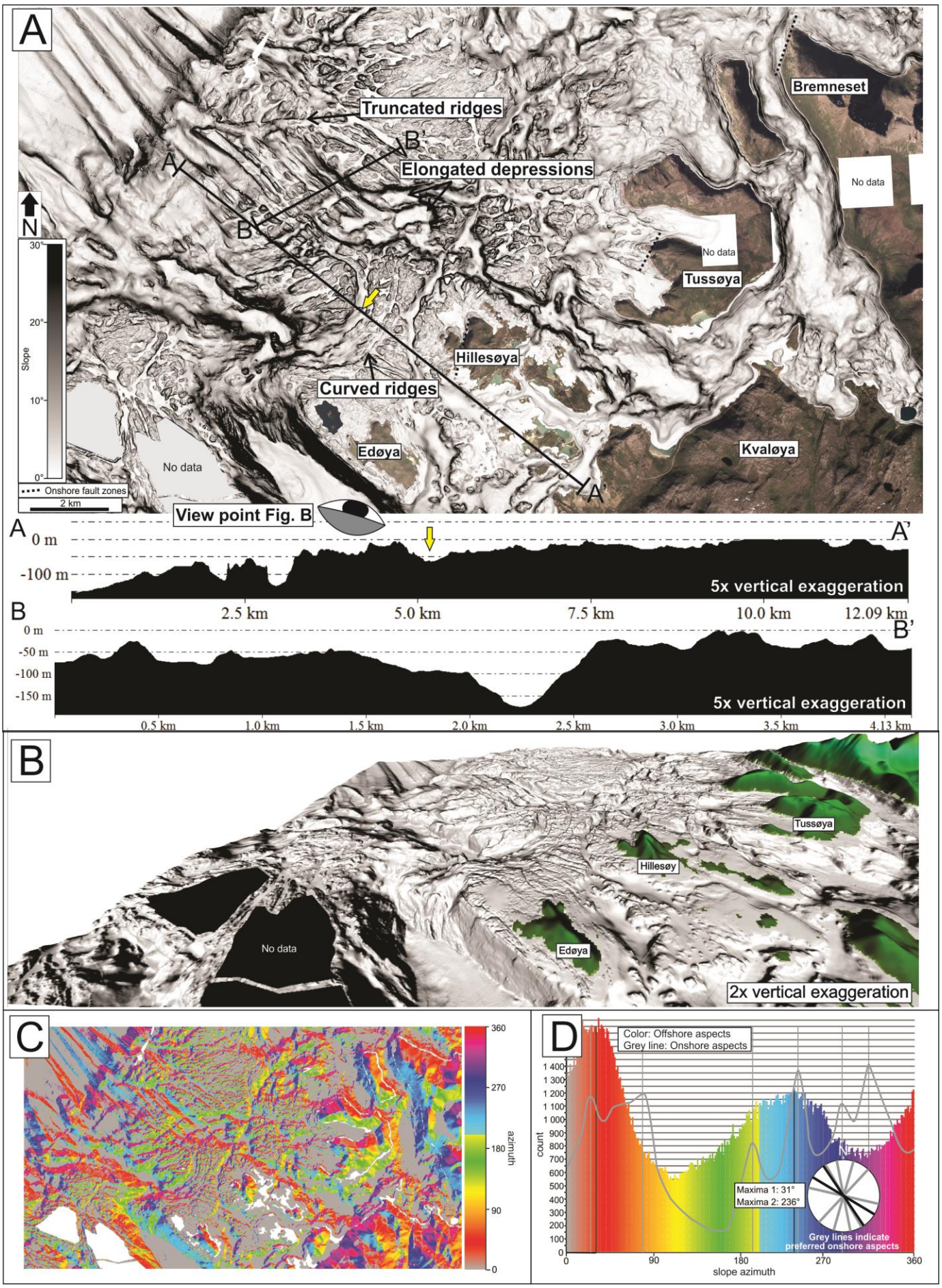
A
Truncated ridges
Elongated depressions
Curved ridges
Bremneset
No data
Tussøya
Hillesøya
Edøya
Kvaløya
No data
N
Slope
30°
20°
10°
0°
Onshore fault zones
2 km
View point Fig. B
A
A'
0 m
-100 m
5x vertical exaggeration
2.5 km
5.0 km
7.5 km
10.0 km
12.09 km
B
B'
0 m
-50 m
-100 m
-150 m
5x vertical exaggeration
0.5 km
1.0 km
1.5 km
2.0 km
2.5 km
3.0 km
3.5 km
4.13 km
B
Tussøya
Hillesøy
Edøya
No data
2x vertical exaggeration
C
360
270
180
90
0
azimuth
D
Color: Offshore aspects
Grey line: Onshore aspects
count
1 400
1 300
1 200
1 100
1 000
900
800
700
600
500
400
300
200
100
0
N
Maxima 1: 31°
Maxima 2: 236°
Grey lines indicate
preferred onshore aspects
0
90
180
270
360
slope azimuth

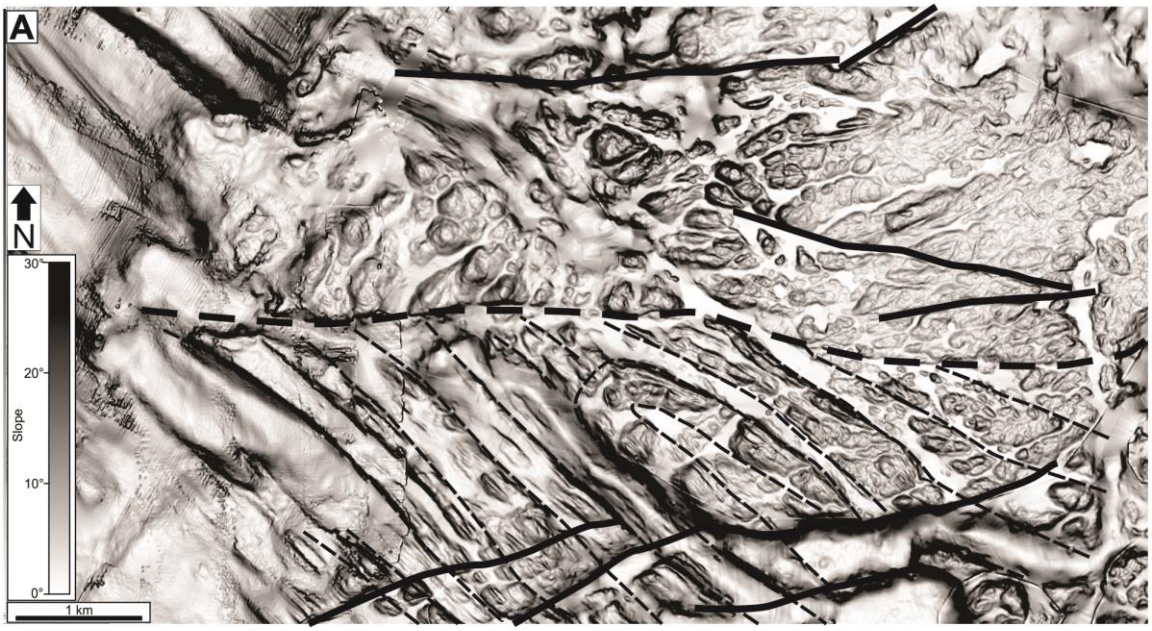
A
N
30°
20°
10°
0°
Slope
1 km

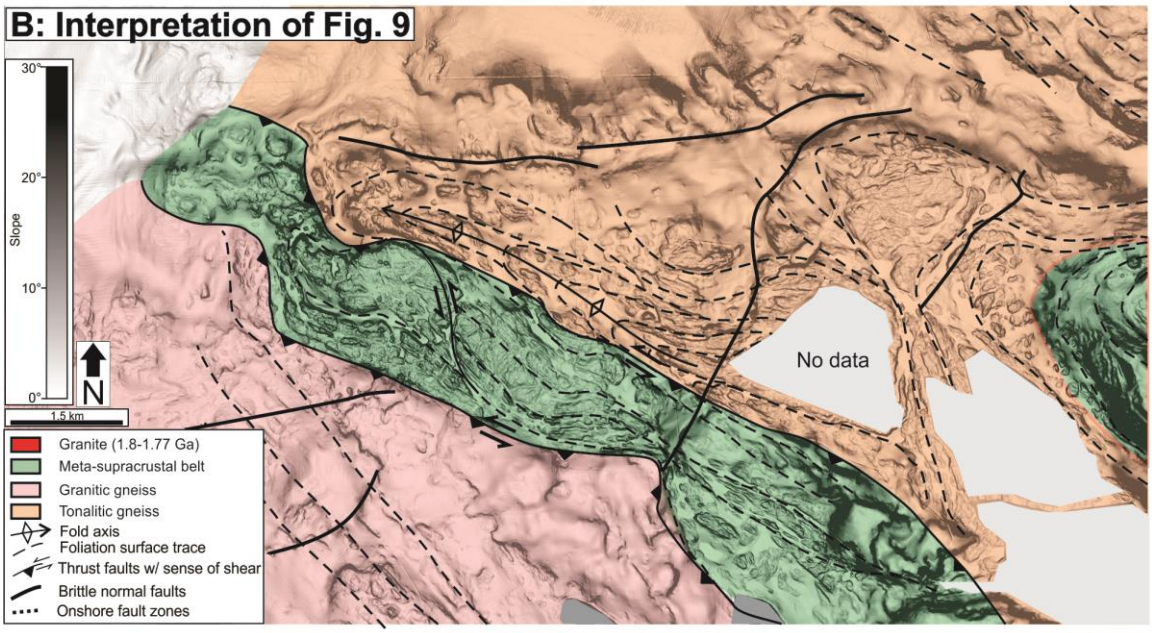
B: Interpretation of Fig. 9
30°
20°
10°
0°
Slope
N
1.5 km
No data
Granite (1.8-1.77 Ga)
Meta-supracrustal belt
Granitic gneiss
Tonalitic gneiss
Fold axis
Foliation surface trace
Thrust faults w/ sense of shear
Brittle normal faults
Onshore fault zones

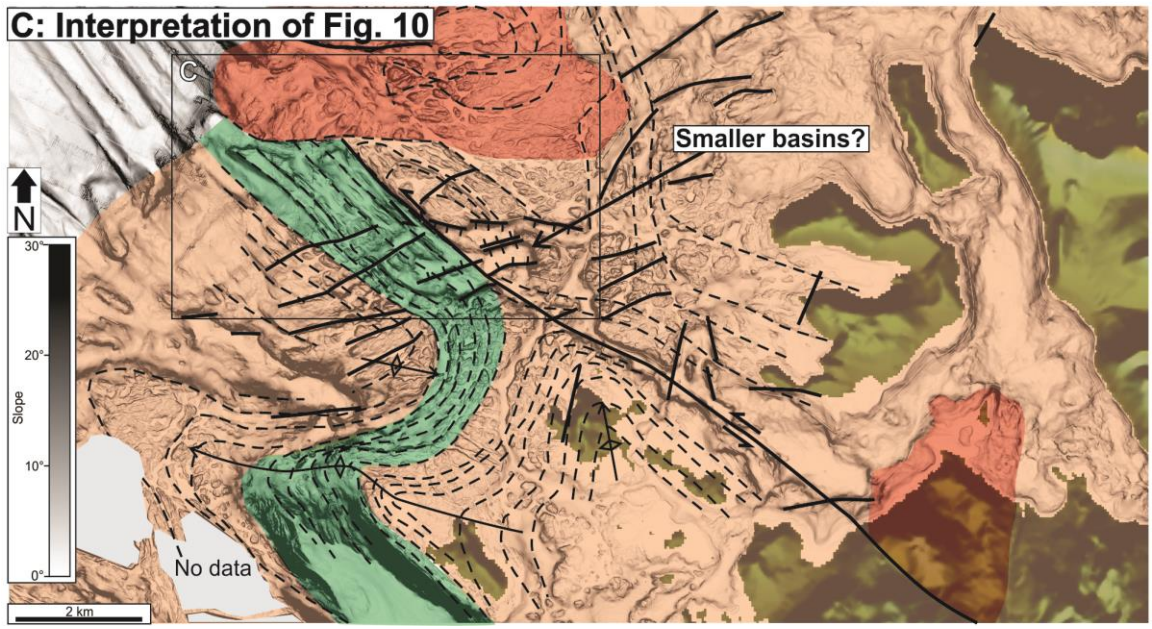
C: Interpretation of Fig. 10
C
Smaller basins?
N
30°
20°
10°
0°
Slope
No data
2 km

Figure 11 (previous page): Interpretative mapping of lithologies and structures covering the strandflat in Area 1 (see Fig. 8 for locations), based on correlation with known onshore structures. (**a**) Detailed outline of the northern portion of the offshore continuation of the Torsnes belt, which is truncated by a E-W trending lineament, separating homogenous and unfoliated rocks interpreted as a granitic intrusion in the north from the well-foliated rocks in the south. (**b**) The meandering feature visible northwest of Nøringen is interpreted as the offshore continuation of the Nøringen and Astridal belt. The belt is sinistrally duplexed and bounded by drag-folded gneiss to the north, consistent with an overall sinstral sense of shear. (**c**) Interpretative mapping of the northern portion of Area 1. The offshore continuation of the Torsnes belt is folded into a rounded z-shape and runs in the north parallel to a sinistral shear zone that may be traced from land.

Figure 12 (next page): Overview of Area 2 covering the strandflat outboard northern portions of Kvaløya and west of Ringvassøya, including the islands of Vengsøya, Gjøssøya, Rebbenesøya, Sandøya and Sørfugløya. Onshore geology from Bergh et al. (2010). Figures 13 to 17 are outlined by boxes and the location of two cross-sections are given and shown below. Inset: Simplified geological map of Sandøya. Note the NNE-SSW trending quartzite layer that dominates the eastern portion of the island. From Armitage (2007).

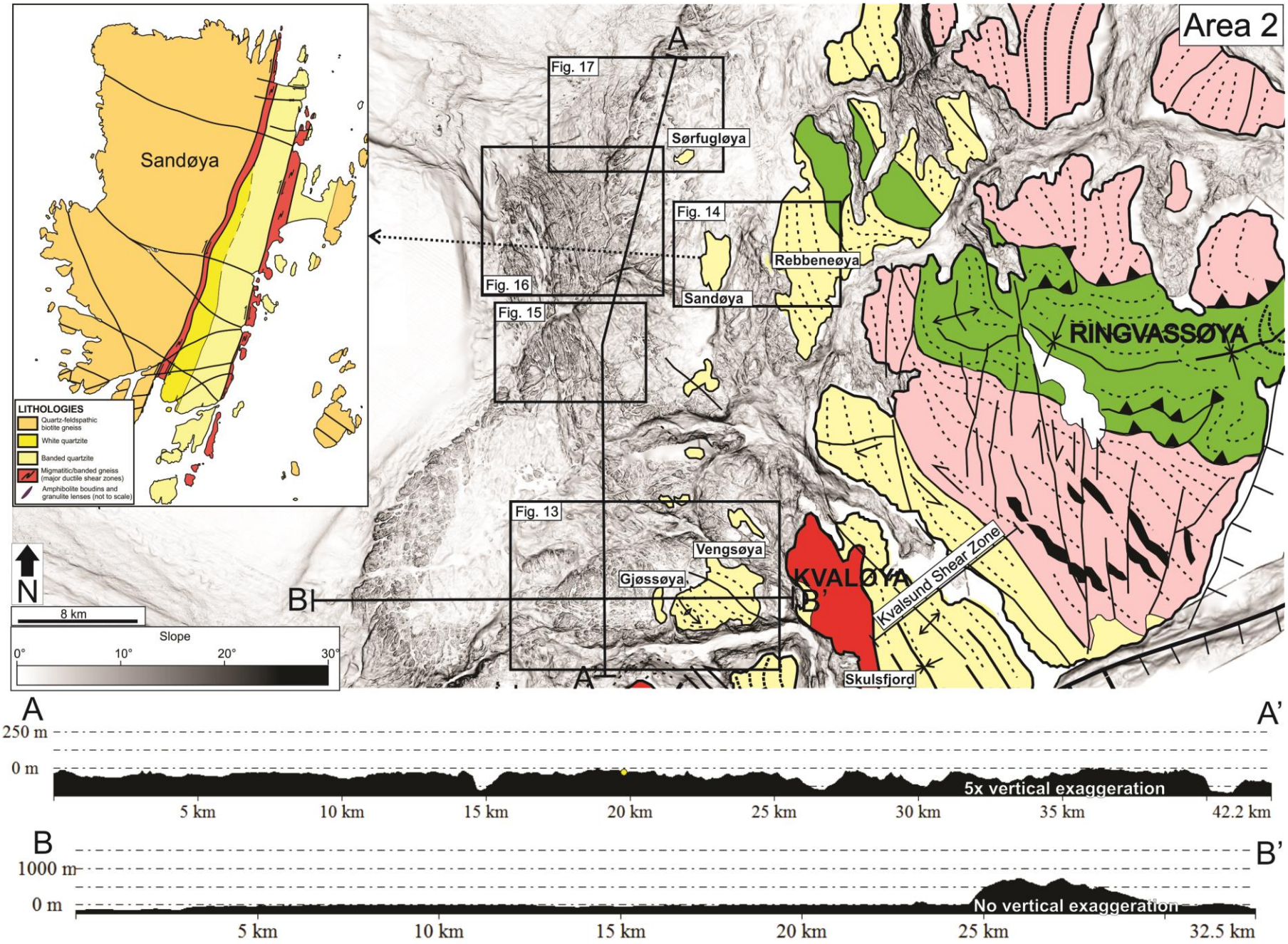
Area 2
Sandøya
LITHOLOGIES
Quartz-feldspathic biotite gneiss
White quartzite
Banded quartzite
Migmatitic/banded gneiss (major ductile shear zones)
Amphibolite boudins and granulite lenses (not to scale)
N
8 km
Slope
0°
10°
20°
30°
A
A'
B
B'
Fig. 17
Fig. 16
Fig. 15
Fig. 14
Fig. 13
Sørfugløya
Sandøya
Rebbeneøya
RINGVASSØYA
Vengsøya
Gjøssøya
KVALØYA
Kvalsund Shear Zone
Skulsfjord
250 m
0 m
5 km
10 km
15 km
20 km
25 km
30 km
35 km
42.2 km
5x vertical exaggeration
1000 m
0 m
5 km
10 km
15 km
20 km
25 km
32.5 km
No vertical exaggeration

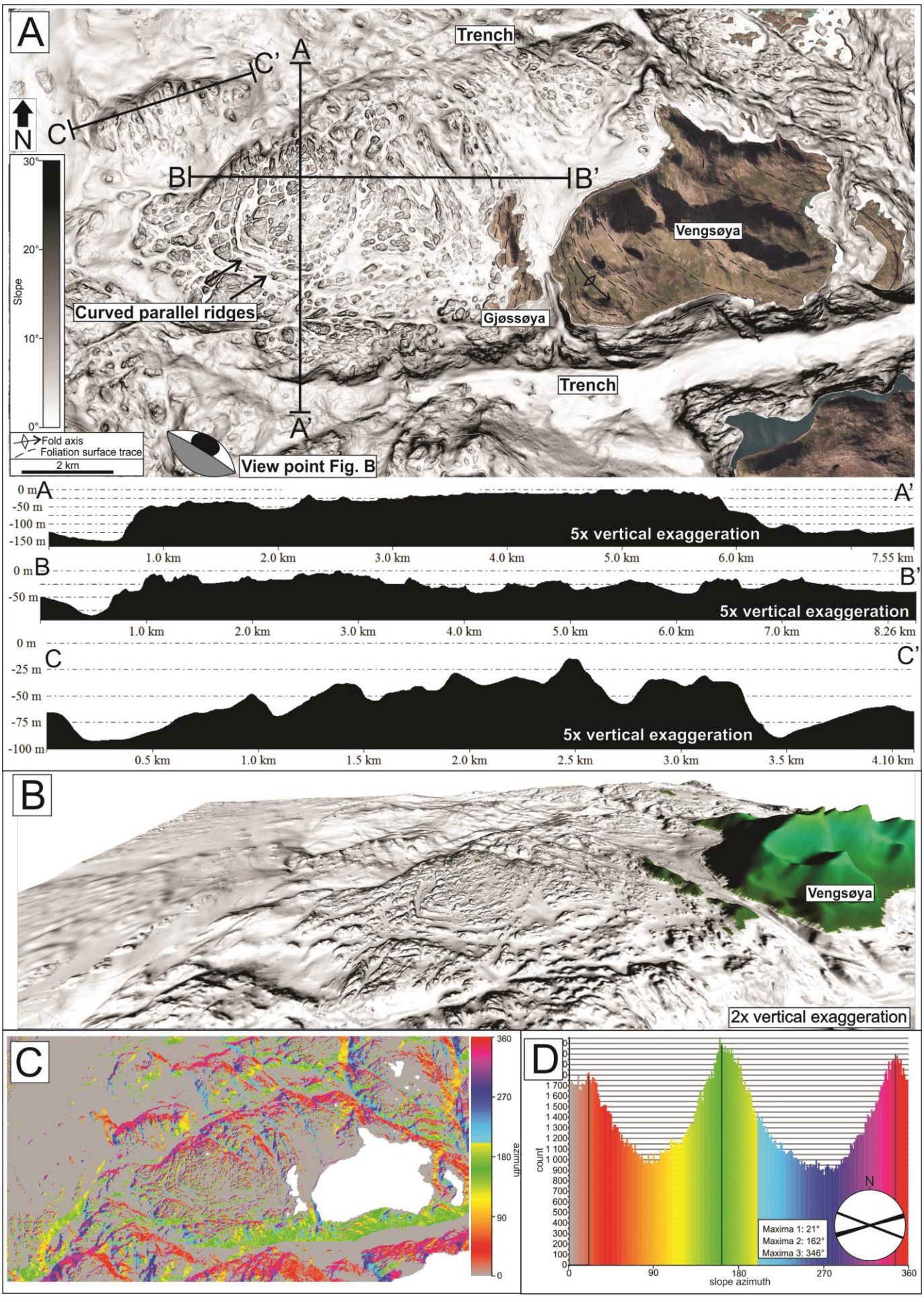
A
Trench
A
C'
C
N
B
B'
30°
20°
10°
0°
Slope
Vengsøya
Curved parallel ridges
Gjøssøya
Trench
A'
Fold axis
Foliation surface trace
2 km
View point Fig. B
0 m
-50 m
-100 m
-150 m
A
A'
5x vertical exaggeration
1.0 km
2.0 km
3.0 km
4.0 km
5.0 km
6.0 km
7.55 km
0 m
B
B'
-50 m
5x vertical exaggeration
1.0 km
2.0 km
3.0 km
4.0 km
5.0 km
6.0 km
7.0 km
8.26 km
0 m
C
C'
-25 m
-50 m
-75 m
-100 m
5x vertical exaggeration
0.5 km
1.0 km
1.5 km
2.0 km
2.5 km
3.0 km
3.5 km
4.10 km
B
Vengsøya
2x vertical exaggeration
C
360
270
180
90
0
azimuth
D
count
slope azimuth
N
Maxima 1: 21°
Maxima 2: 162°
Maxima 3: 346°

Figure 13 (previous page): Detailed illustrations of the strandflat within area 2 (see Fig. 12 for location). (**a**): Dip map covering the strandflat with onshore portions of the subarea covered by aerial photographs. Note the curved parallel ridges of the basement block adjacent to Vengsøya and Gjøssøya and bounded by larger trenches. Locations of cross-sections are given and shown below. Point of view for 3D illustration is marked. (**b**) 3D illustration of the subarea, which highlights the curved, parallel ridges. (**c**) Aspect map and (**d**) histogram showing the preferred direction of dips for slopes steeper than 5°. The preferred strikes of slopes from the aspect analysis are shown in the small circular insets (simplified rose diagrams).

Figure 14 (next page): Various detailed illustrations of the (see Fig. 12 for location). (**a**) Dip map covering the strandflat with onshore portions of the subarea covered by aerial photographs. Areas covered with aerial photographs of the sea surface indicate area where no 5x5m resolution bathymetry data is available. Note the curved ridge traceable from Sandøya and northwards before it curves around to a SSE-NNW trend. The line illustrates locations of the cross-section. Point of view for the 3D illustration is marked. (**b**) 3D illustration of the subarea, which highlights the cruved ridge northeast of Sandøya. (**c**) Aspect map and (**d**) histogram showing the preferred direction of dips for slopes steeper than 5°. Grey line shows the preferred aspects of the topography (not to scale along the Y-axis). The preferred strikes of slopes from the aspect analysis are shown in the small circular insets (simplified rose diagrams, grey lines shows topography maxima).

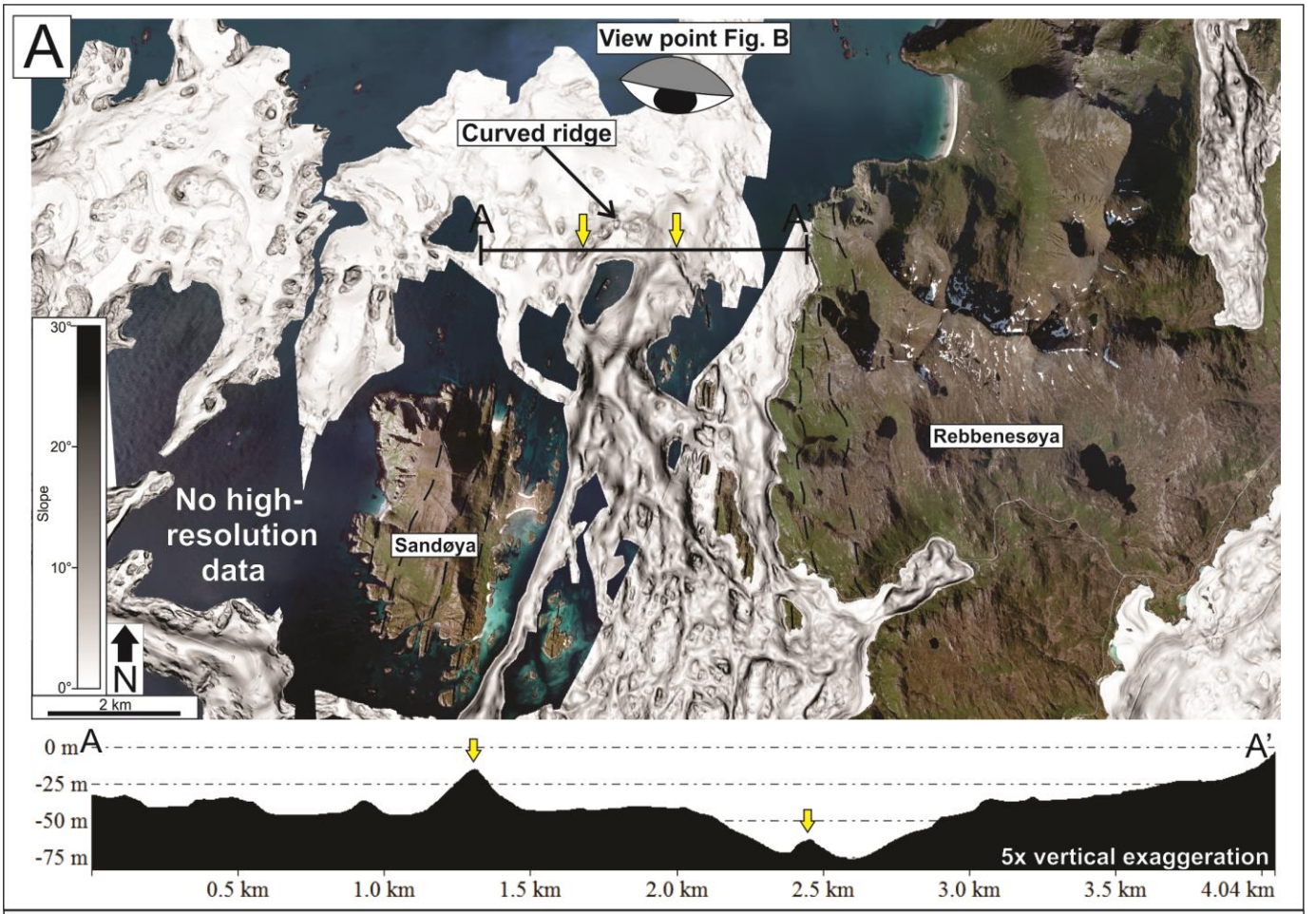
A
View point Fig. B
Curved ridge
A
A'
30°
20°
10°
0°
Slope
No high-resolution data
Sandøya
Rebbenesøya
N
2 km
0 m
-25 m
-50 m
-75 m
A
A'
5x vertical exaggeration
0.5 km
1.0 km
1.5 km
2.0 km
2.5 km
3.0 km
3.5 km
4.04 km

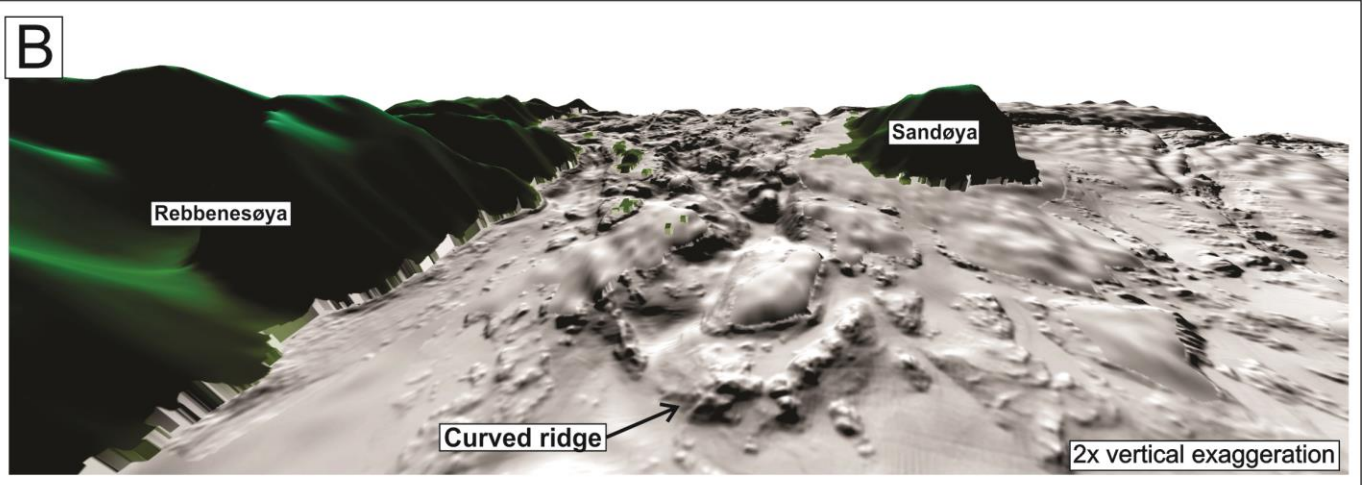
B
Rebbenesøya
Sandøya
Curved ridge
2x vertical exaggeration

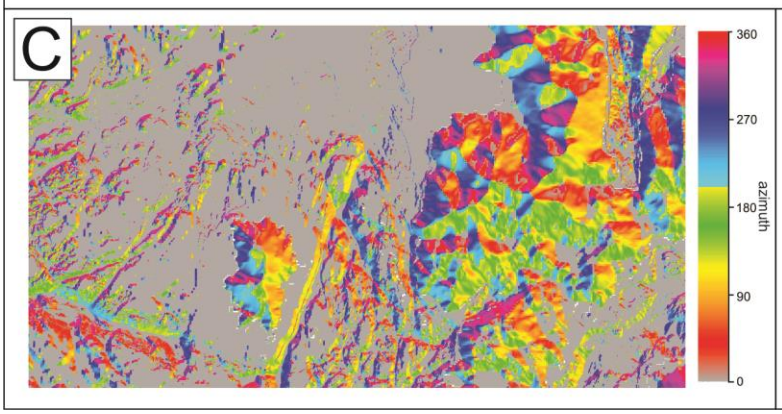
C
360
270
180
90
0
azimuth

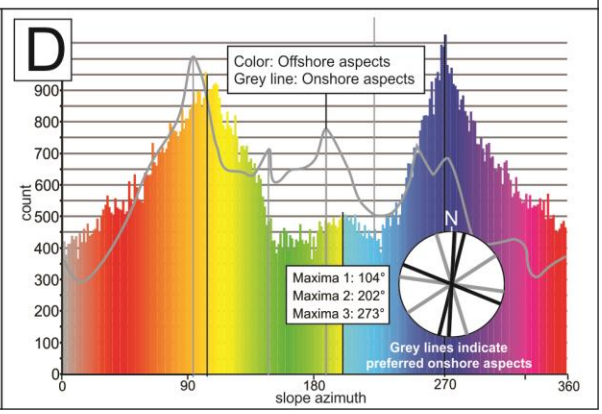
D
Color: Offshore aspects
Grey line: Onshore aspects
900
800
700
600
500
400
300
200
100
0
count
N
Maxima 1: 104°
Maxima 2: 202°
Maxima 3: 273°
Grey lines indicate preferred onshore aspects
0
90
180
270
360
slope azimuth

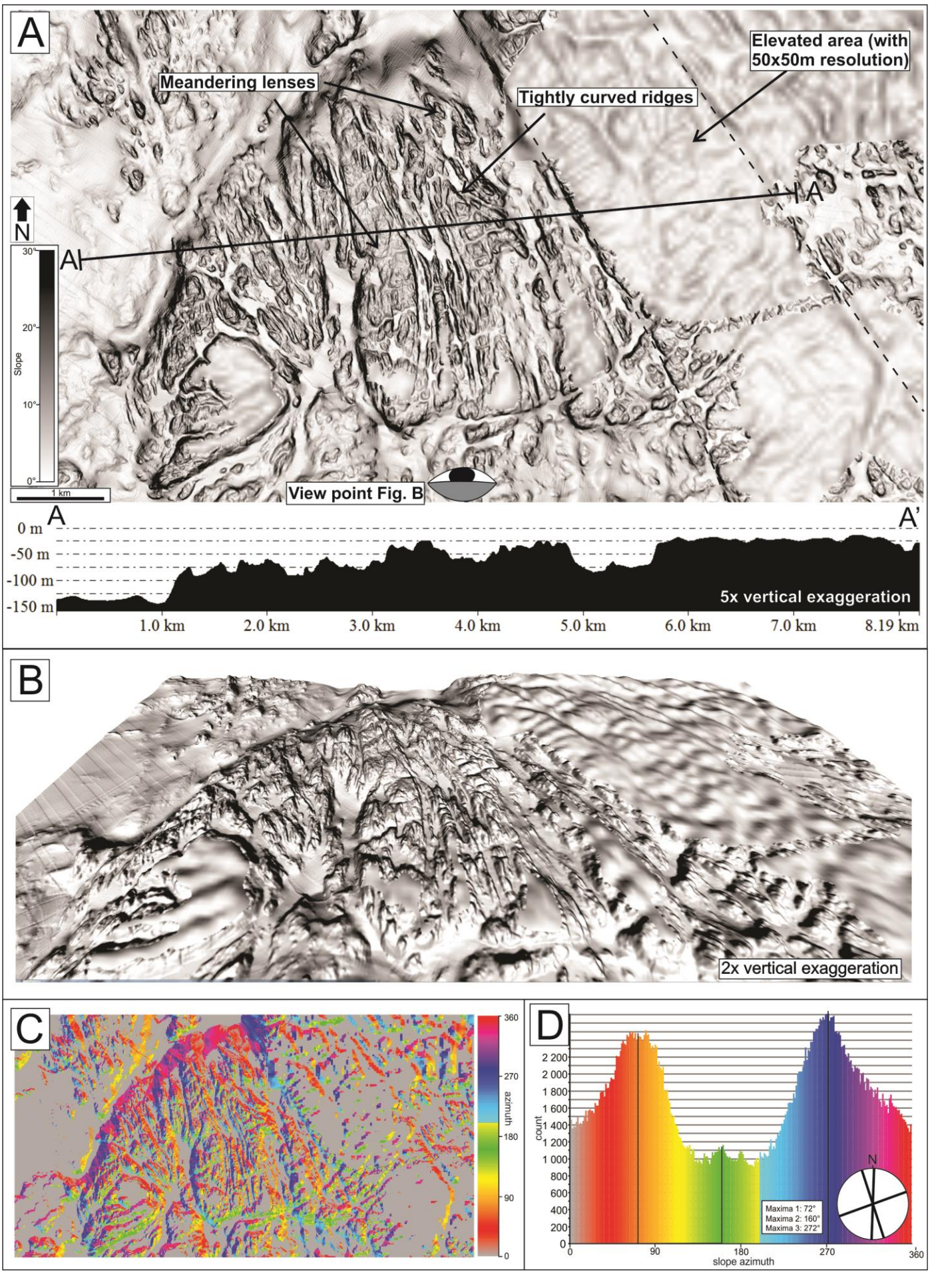
A
Meandering lenses
Tightly curved ridges
Elevated area (with 50x50m resolution)
A
A'
N
30°
20°
10°
0°
Slope
1 km
View point Fig. B
A
A'
0 m
-50 m
-100 m
-150 m
5x vertical exaggeration
1.0 km
2.0 km
3.0 km
4.0 km
5.0 km
6.0 km
7.0 km
8.19 km
B
2x vertical exaggeration
C
360
270
180
90
0
azimuth
D
2 200
2 000
1 800
1 600
1 400
1 200
1 000
800
600
400
200
0
count
0
90
180
270
360
slope azimuth
N
Maxima 1: 72°
Maxima 2: 160°
Maxima 3: 272°

Figure 15 (previous page): Detailed illustrations of the strandflat within area 2 (see Fig. 12 for location). (**a**) Dip map covering the strandflat with location of cross-section given and shown below. Note the internally curved, parallel ridges and meandering lenses. Point of view for 3D illustration is marked. (**b**) 3D illustration of the subarea, which highlights the internally curved, parallel ridges. (**c**) Aspect map and (**d**) histogram showing the prefered direction of dips for slopes steeper than 5°. The preferred strikes of slopes from the aspect analysis are shown in the small circular insets (simplified rose diagrams).

Figure 16 (next page): Illustrations of the strandflat within Area 2 (see Fig. 12 for location). (**a**): Dip map covering the strandflat east of Sandøya with location of the cross-section shown below. Note the NNW-SSE trending curved, parallel ridges and the NE-SW trending trench in the southern portion of the subarea. Point of view for the 3D illustration is marked. (**b**) 3D illustration of the subarea, which highlights the curved, parallel ridges. Interpretation of the dip of a major foliation surface (ductile shear zone?) is shown. (**c**) Aspect map and (**d**) histogram showing the preferred direction of dips for slopes steeper than 5°. The preferred strikes of slopes from the aspect analysis are shown in the small circular insets (simplified rose diagrams).

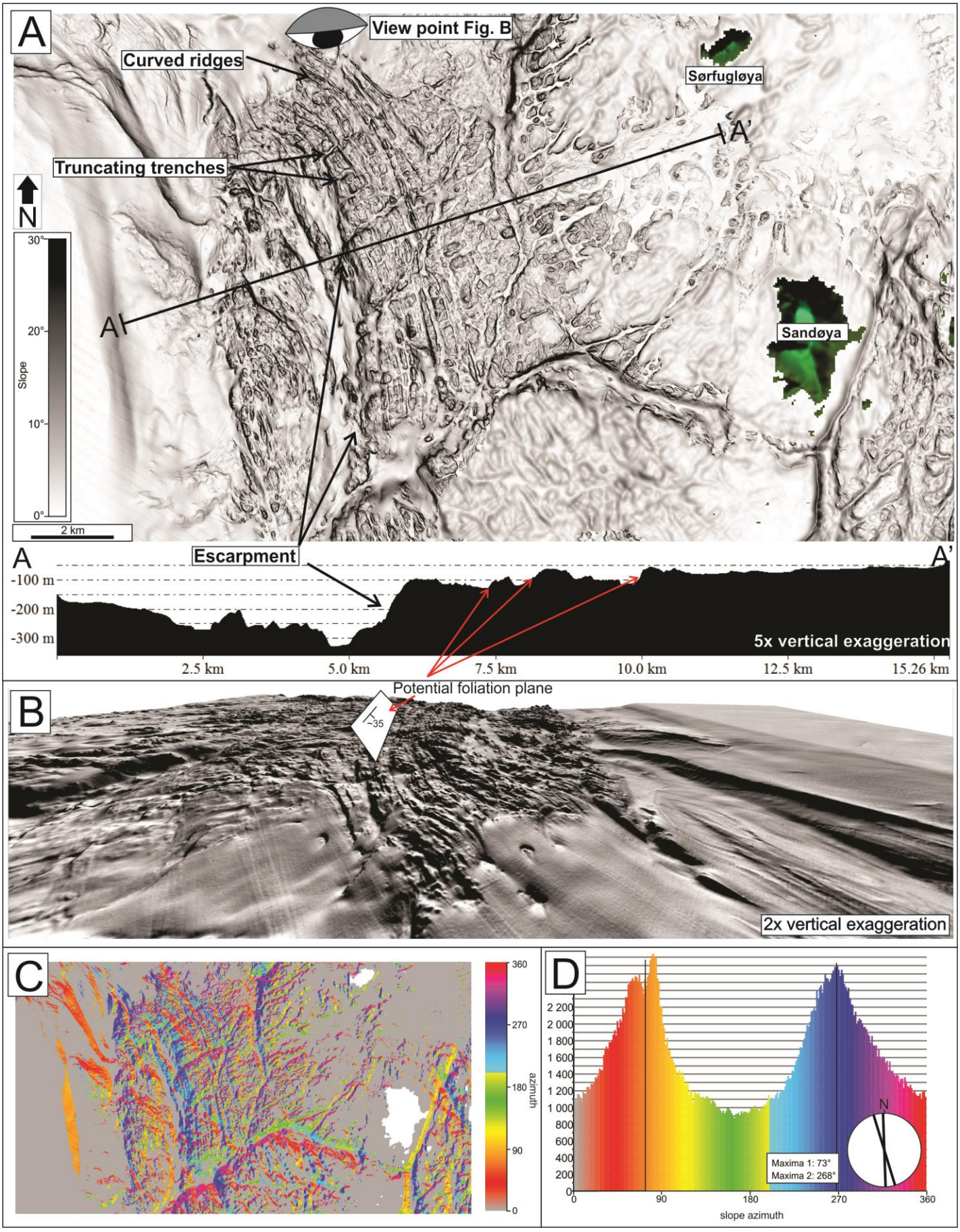
A
View point Fig. B
Curved ridges
Truncating trenches
Sørfugløya
Sandøya
A
A'
N
30°
20°
10°
0°
Slope
2 km
A
A'
Escarpment
-100 m
-200 m
-300 m
5x vertical exaggeration
2.5 km
5.0 km
7.5 km
10.0 km
12.5 km
15.26 km
B
Potential foliation plane
~35
2x vertical exaggeration
C
360
270
180
90
0
azimuth
D
2 200
2 000
1 800
1 600
1 400
1 200
1 000
800
600
400
200
0
0
90
180
270
360
slope azimuth
N
Maxima 1: 73°
Maxima 2: 268°

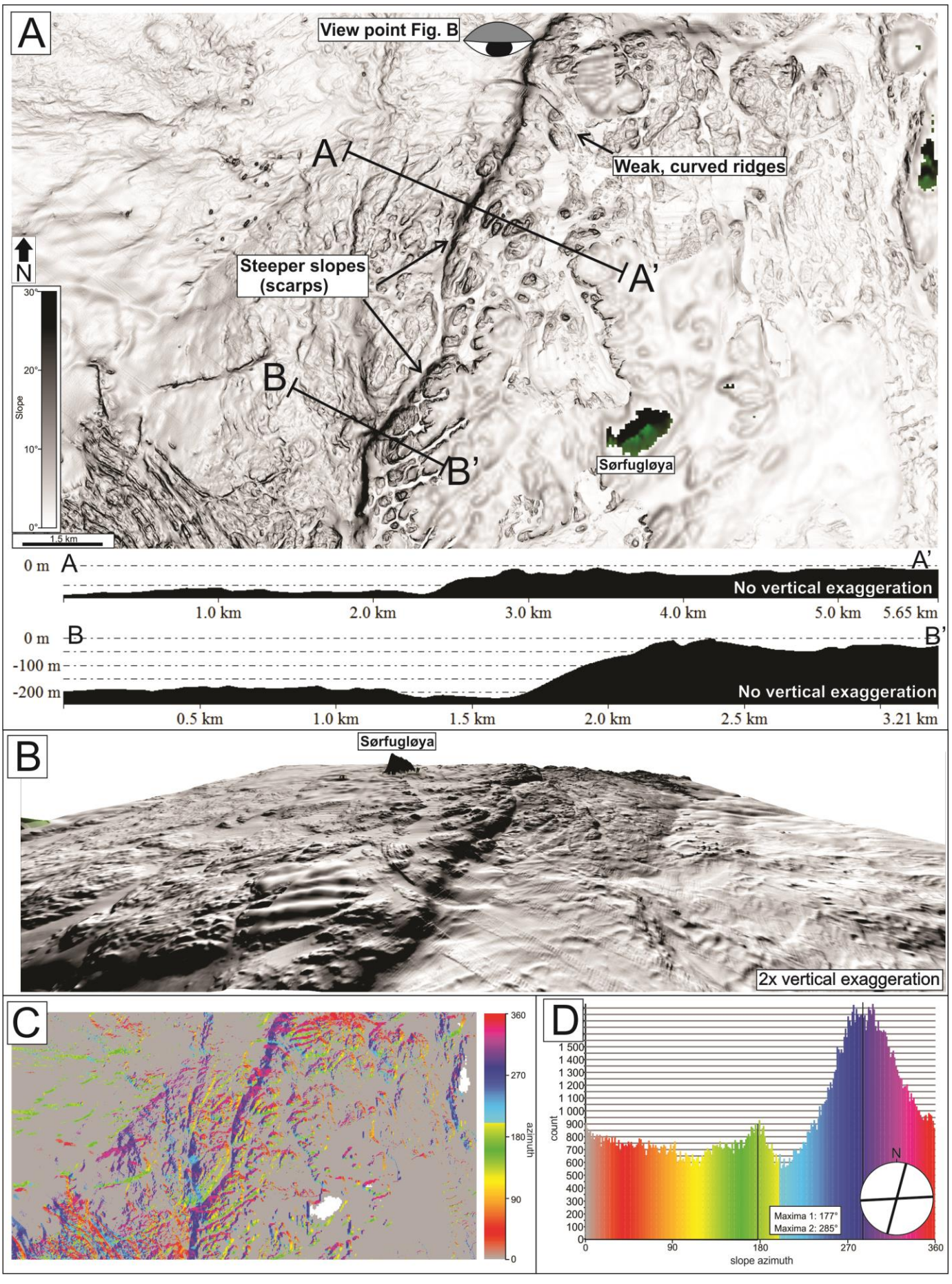
A
View point Fig. B
A
A'
Weak, curved ridges
Steeper slopes
(scarps)
N
30°
20°
10°
0°
Slope
1.5 km
B
B'
Sørfugløya
0 m
A
A'
No vertical exaggeration
1.0 km
2.0 km
3.0 km
4.0 km
5.0 km
5.65 km
0 m
B
B'
-100 m
-200 m
No vertical exaggeration
0.5 km
1.0 km
1.5 km
2.0 km
2.5 km
3.21 km
B
Sørfugløya
2x vertical exaggeration
C
360
270
180
90
0
azimuth
D
1 500
1 400
1 300
1 200
1 100
1 000
900
800
700
600
500
400
300
200
100
0
count
N
Maxima 1: 177°
Maxima 2: 285°
0
90
180
270
360
slope azimuth

Figure 17 (previous page): Detailed illustrations of the strandflat within Area 2 (see Fig. 12 for location). (**a**) Dip map covering the strandflat northwest of Sørfugløya with location of the cross-section shown below. Note the zigzag shape of the slope trending in general NE-SW and the weak trace of curved, parallel ridges in the northern parts of the subarea. Point of view for the 3D illustration is marked. (**b**) 3D illustration of the subarea, which highlights the slope and the weak curved parallel ridges. (**c**) Aspect map and (**d**) histogram showing the preferred direction of dips for slopes steeper than 5°. The preferred strikes of slopes from the aspect analysis are shown in the small circular insets (simplified rose diagrams).

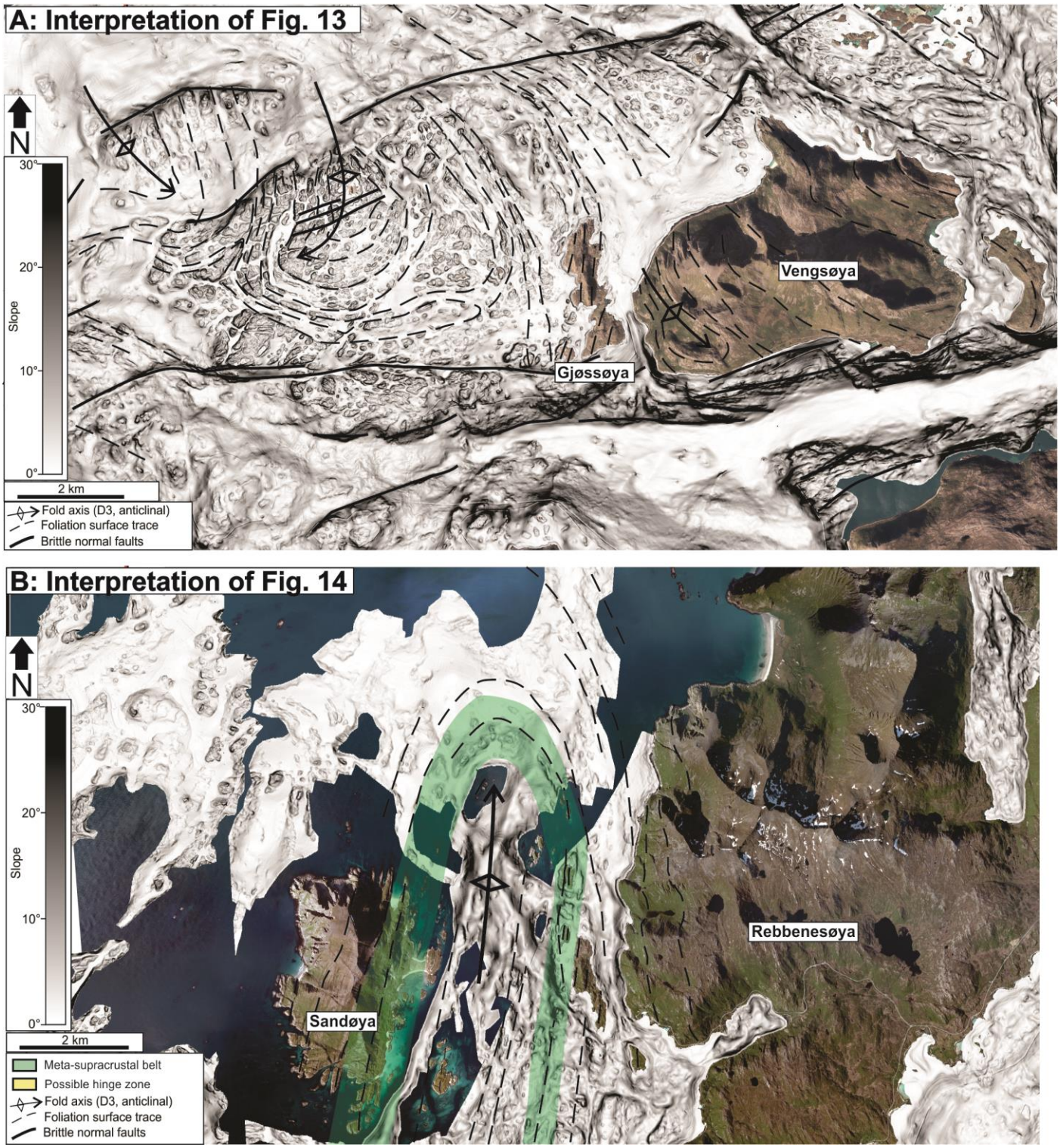

Figure 18: Interpretation of lithologies and structures present on the strandflat in Area 2 (see Fig. 12 for locations), based on correlation with known onshore structures. (**a**) The curved, parallel ridges of subarea 2.1 are interpreted as folded TTG-gneiss foliation, similar to what is observed on Vengsøya. The truncating trenches in the centre of the fold are interpreted as minor brittle faults while the larger trenches to the north and south of the fold are interpreted as major brittle faults. (**b**) The ridge tracable from Sandøya is thought to be the continuation of the quartzite unit on Sandøya. It is interpreted to be folded around a N-S trending, subvertical fold axis and may explain the opposing strikes of the foliation on Sandøya and Rebbenesøya.

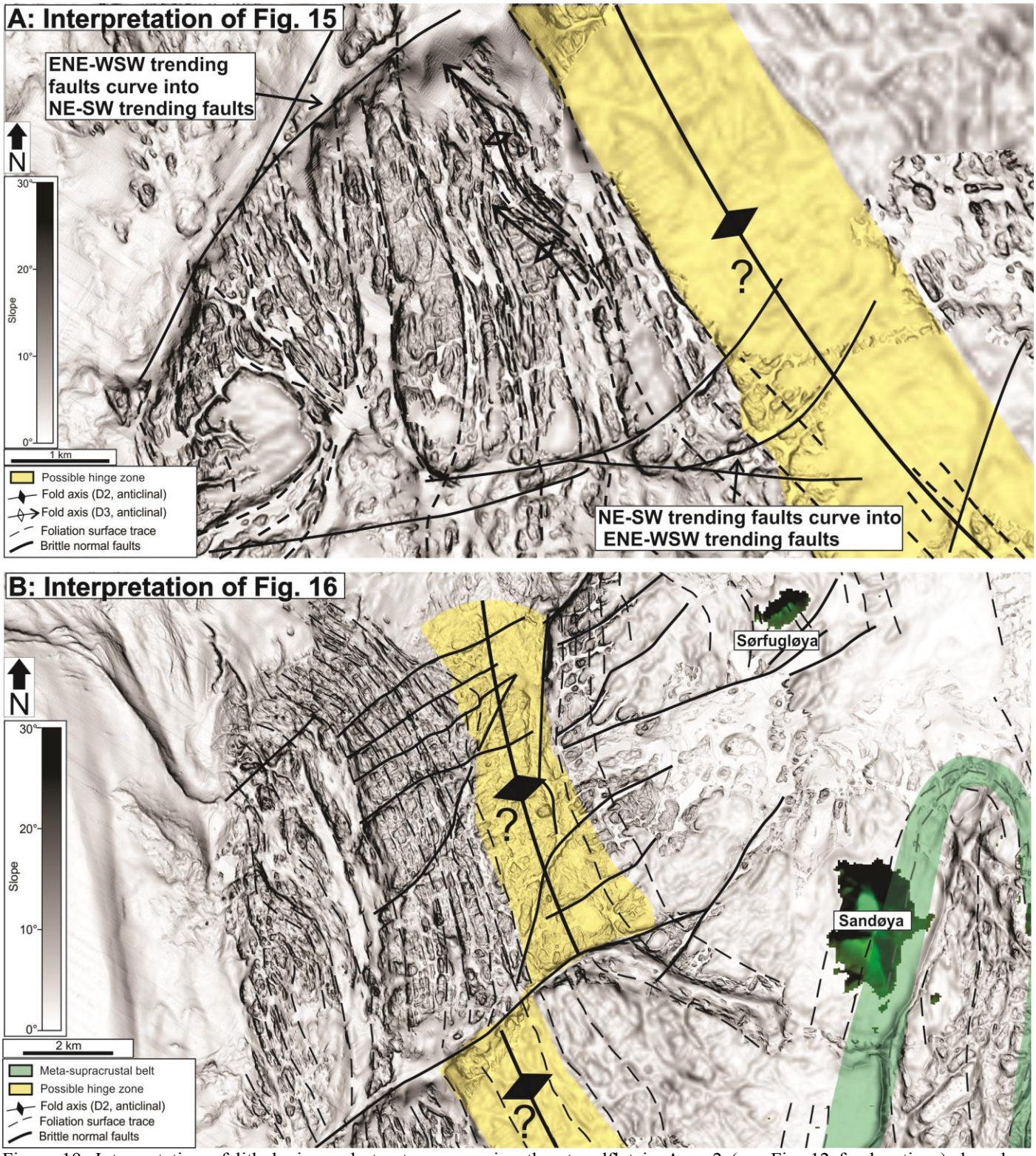

Figure 19: Interpretation of lithologies and structures covering the strandflat in Area 2 (see Fig. 12 for locations), based on correlation with known onshore structures. (**a**) The internally curved parallel ridges are interpreted as intrafolial folds that formed within a high-strain ductile shear zone. The highlighted NNW-SSE trending more diffuse area to the east is, interpreted to mark the position of either a more competent lithology, such as e.g. quartzite, or the hinge zone of an upright, sub-horizontal macro-fold. Truncating trenches are interpreted as brittle faults that bend into parallelism with each other. Note that NNE-SSW trending faults bend into parallelism with ENE-WSW trending faults in the south of the subarea, while the opposite is apparent in the northern part of the subarea. (**b**) The curved, parallel ridges are the northwards continuation of the high-strain ductile shear zone in (a). The ENE-WSW trending trench in the southern parts of the subarea is interpreted as a major brittle fault that apparently displaces the interpreted quartzite unit or macro-fold hinge-zone dextrally (yellow colour).

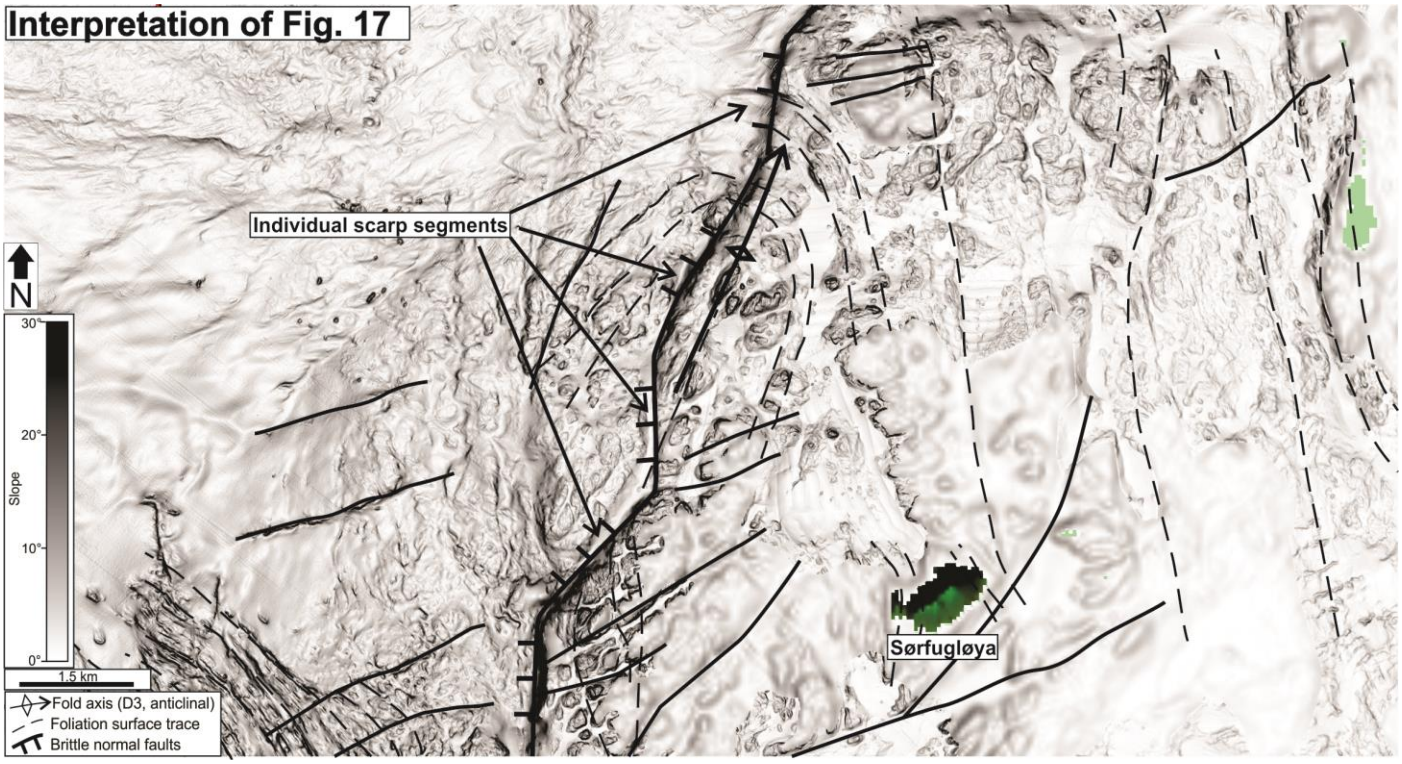

Figure 20: Interpretation of main structural features within a subarea on the strandflat in Area 2 (see Fig. 12 for location), based on correlation with known onshore structures. The zigzag-shaped slope is interpreted as an array of alternating N-S and NE-SW trending brittle normal faults that down-drop basement rocks to the west. The weak curved, parallel ridges in the northern parts of the subarea are interpreted to mark the position of a north-trending sub-vertical fold.

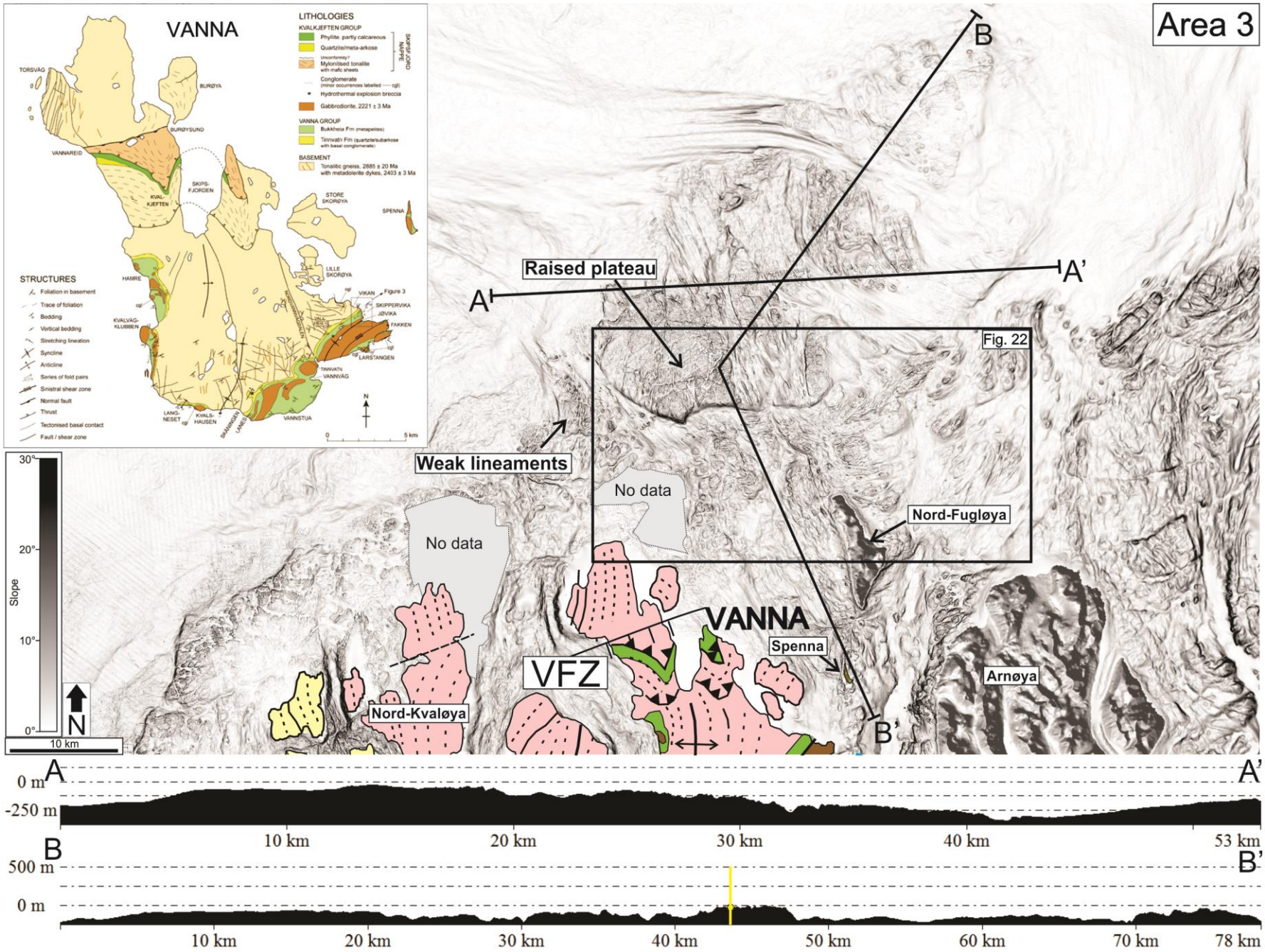
Area 3
VANNA
LITHOLOGIES
KVALKJEFTEN GROUP
Phyllite, partly calcareous
Quartzite/meta-arkose
Mylonitised tonalite with mafic sheets
Conglomerate
Hydrothermal explosion breccia
Gabbrodiorite, 2221 ± 3 Ma
VANNA GROUP
Bukkheia Fm (metapelites)
Tinnvatn Fm (quartzite/subarkose with basal conglomerate)
BASEMENT
Tonalitic gneiss, 2885 ± 20 Ma with metadolerite dykes, 2403 ± 3 Ma
STRUCTURES
Foliation in basement
Trace of foliation
Bedding
Vertical bedding
Stretching lineation
Syncline
Anticline
Series of fold pairs
Sinistral shear zone
Normal fault
Thrust
Tectonised basal contact
Fault / shear zone
TORSVÅG
BURØYA
BURØYSUND
VANNAREID
SKIPS-FJORDEN
KVAL-KJEFTEN
STORE SKORØYA
SPENNA
LILLE SKORØYA
HAMRE
VIKAN
Figure 3
SKIPPERVIKA
JØVIKA
TAKKEN
KVALVÅG-KLUBBEN
LARSTANGEN
TINNVATN
VANNVÅG
LANG-NESET
KVALS-HAUSEN
VANNSTUA
0
5 km
A
A’
B
B’
Raised plateau
Weak lineaments
Fig. 22
No data
No data
Nord-Fugløya
VANNA
VFZ
Spenna
Arnøya
Nord-Kvaløya
Slope
30°
20°
10°
0°
N
10 km
0 m
-250 m
10 km
20 km
30 km
40 km
53 km
500 m
0 m
10 km
20 km
30 km
40 km
50 km
60 km
70 km
78 km

Figure 21 (previous page): Overview of the strandflat of Area 3 north of Vanna and Nord-Fugløya, with onshore geology from Bergh et al. (2010). Location of Fig. 22 is outlined. VFZ=Vannareid-Brurøysund fault zone. **Inset map**: Geological and tectonic map of the island of Vanna. From Bergh et al. (2007b).

Figure 22 (next page): Detailed illustrations of the strandflat within Area 3 (see Fig. 21 for location). (**a**) Bathymetric dip map of the strandflat and northern parts of Nord-Fugløya. Note the prominent rise in elevation in the north, the NE-SW trending ridges northeast of Nord-Fugløya and the NW-SE trending ridges southwest of Nord-Fugløya. Location of the cross-sections are given by lines and shown below. Point of view for 3D illustration is marked. (**b**) 3D illustration of the subarea, which highlights NW-SE trending ridges to the west and north of Nord-Fugløya. (**c**) Aspect map and (**d**) histogram showing the prefered direction of dips for slopes steeper than 5°. The preferred strikes of slopes from the aspect analysis are shown in the sircular inset (simplified rose diagram).

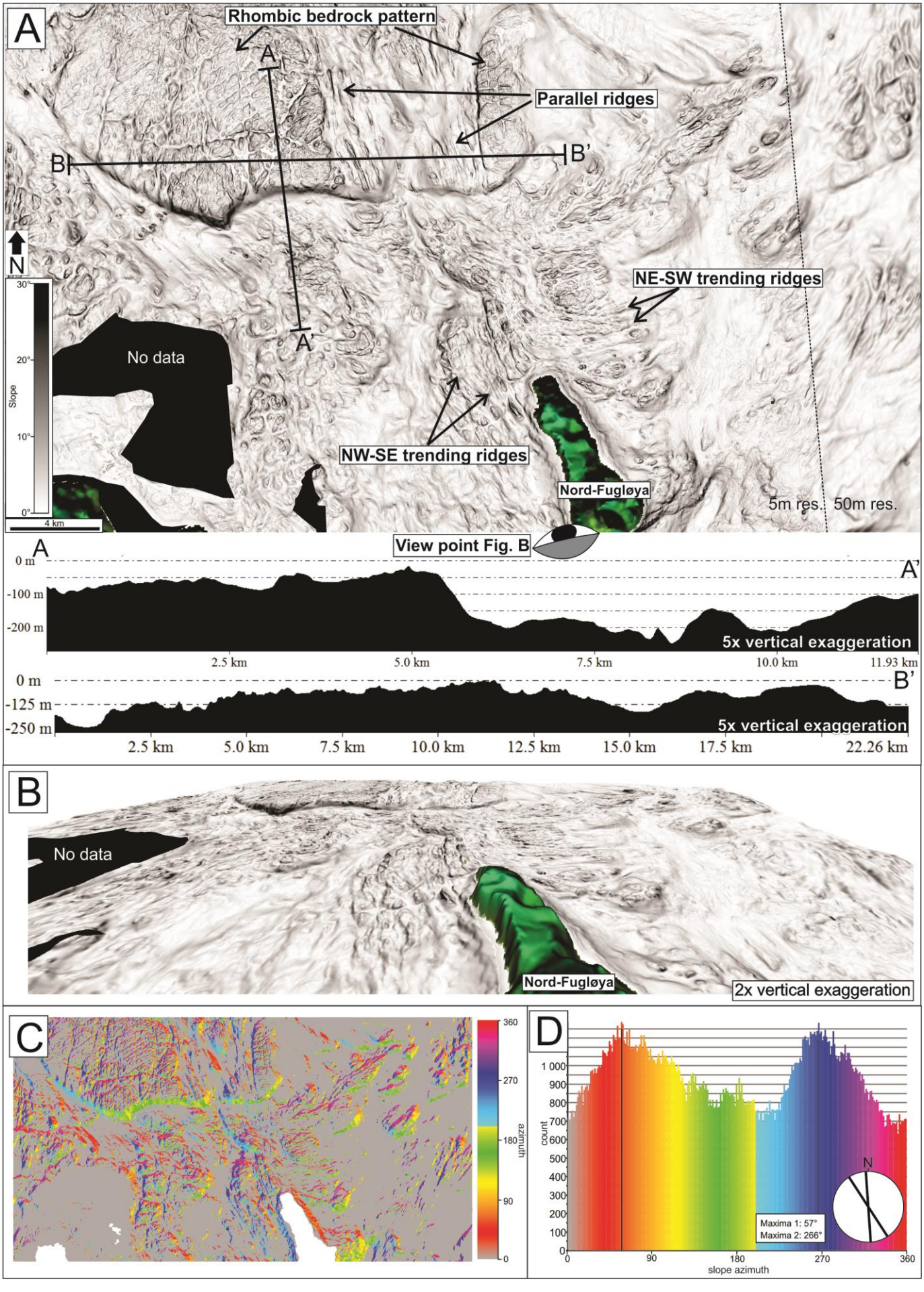
A
Rhombic bedrock pattern
A
A'
Parallel ridges
B
B'
N
NE-SW trending ridges
30°
20°
10°
0°
Slope
4 km
No data
NW-SE trending ridges
Nord-Fugløya
5m res.
50m res.
View point Fig. B
A
A'
0 m
-100 m
-200 m
5x vertical exaggeration
2.5 km
5.0 km
7.5 km
10.0 km
11.93 km
0 m
B'
-125 m
-250 m
5x vertical exaggeration
2.5 km
5.0 km
7.5 km
10.0 km
12.5 km
15.0 km
17.5 km
22.26 km
B
No data
Nord-Fugløya
2x vertical exaggeration
C
360
270
180
90
0
azimuth
D
1 000
900
800
700
600
500
400
300
200
100
0
count
N
Maxima 1: 57°
Maxima 2: 266°
0
90
180
270
360
slope azimuth

Figure 23: Detailed interpretation of the presumed WTBC – Caledonian contact and related structures covering the strandflat within Area 3 (see Fig. 21 for location), based on correlation with known onshore structures. The contact is marked by a change in the preferred orientation of NE-SW trending ridges to the northeast, relative to N-S trending ridges in the northwest, i.e. N-S trending ridges just west of Nord-Fugløya.

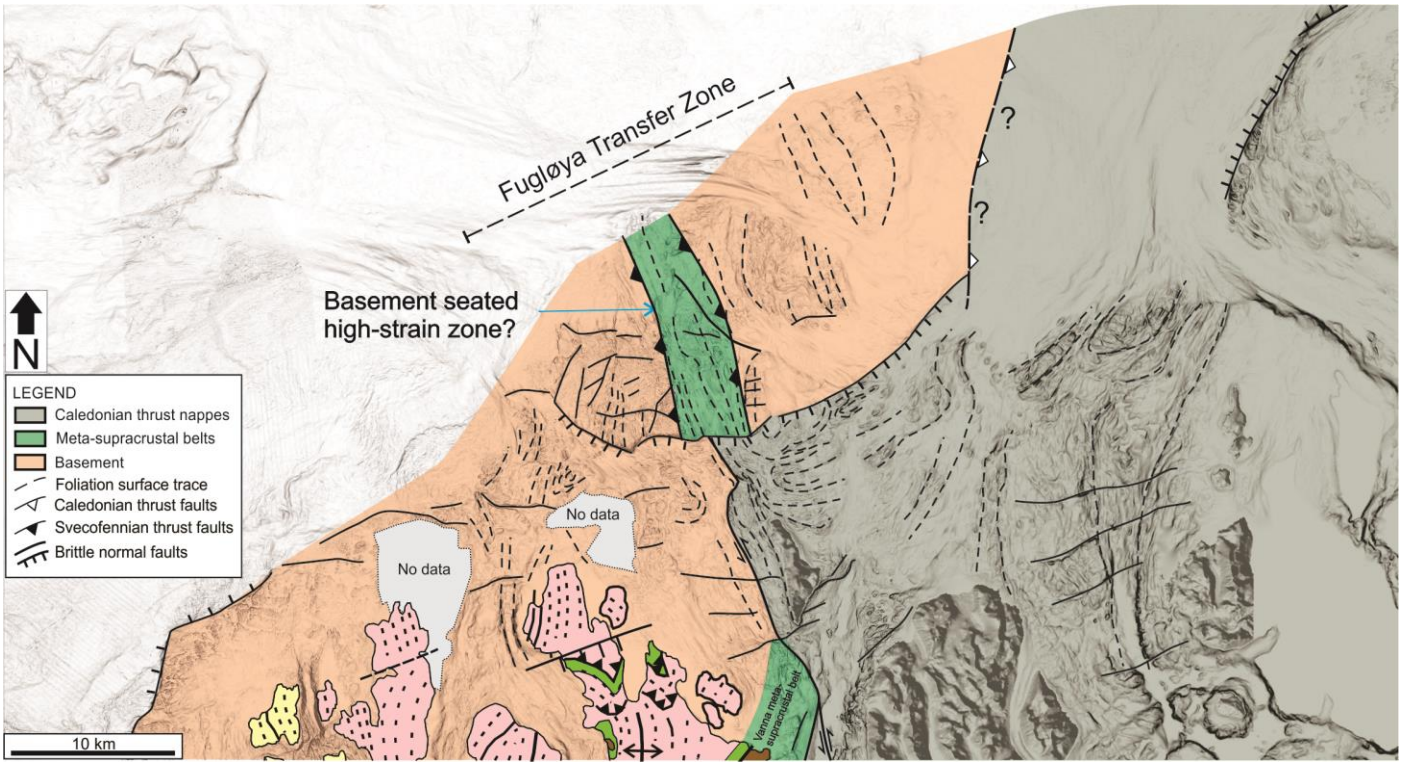

Figure 24: Interpretation of the strandflat bathymetry in Area 3, based on observation and correlation with onshore structures. The interpreted fault that defines the southern limit of the continental rise has down-faulted Caledonian nappes to the southeast, similar to what is observed along the inner portions of the WTBC. The NNW-SSE trending parallel ridges that truncate the rise are interpreted as part of a high-strain ductile zone within WTBC rocks, possibly a meta-supracrustal belt. If so, the meta-supracrustal belt, the contact towards Caledonian nappes and the Fugløya transfer zone overlap in the strait between Vanna and Nord-Fugløya.

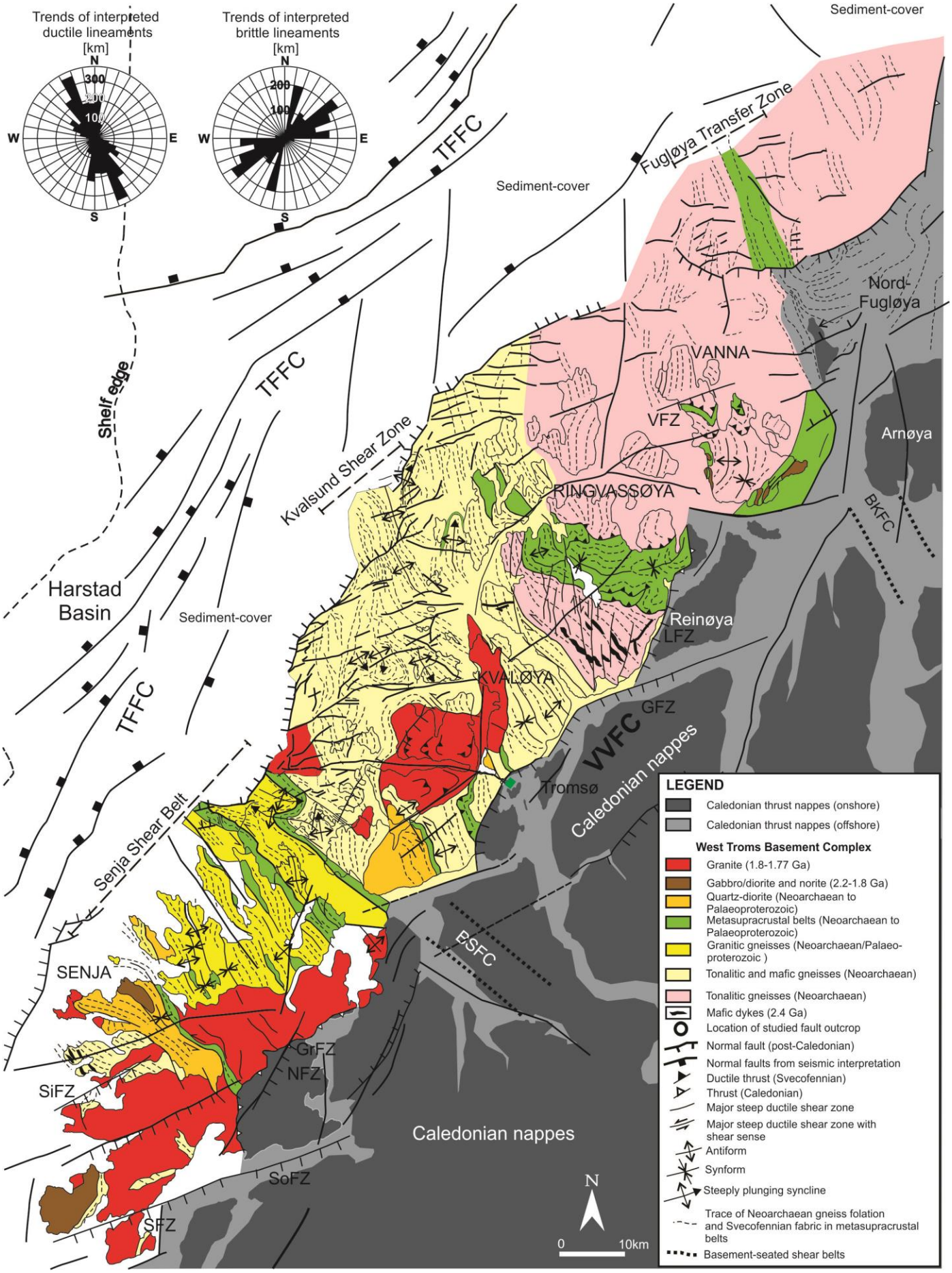
Trends of interpreted ductile lineaments [km]
N
300
200
100
W
E
S
Trends of interpreted brittle lineaments [km]
N
200
100
W
E
S
Sediment-cover
Fugløya Transfer Zone
TFFC
Sediment-cover
Nord-Fugløya
VANNA
VFZ
Arnøya
Shelf edge
TFFC
Kvalsund Shear Zone
RINGVASSØYA
BKFC
Harstad Basin
Sediment-cover
Reinøya LFZ
KVALØYA
TFFC
GFZ
VVFC
Caledonian nappes
Tromsø
Senja Shear Belt
BSFC
SENJA
GrFZ
NFZ
SiFZ
Caledonian nappes
SoFZ
SFZ
N
0
10km
LEGEND
Caledonian thrust nappes (onshore)
Caledonian thrust nappes (offshore)
West Troms Basement Complex
Granite (1.8-1.77 Ga)
Gabbro/diorite and norite (2.2-1.8 Ga)
Quartz-diorite (Neoarchaean to Palaeoproterozoic)
Metasupracrustal belts (Neoarchaean to Palaeoproterozoic)
Granitic gneisses (Neoarchaean/Palaeo-proterozoic)
Tonalitic and mafic gneisses (Neoarchaean)
Tonalitic gneisses (Neoarchaean)
Mafic dykes (2.4 Ga)
Location of studied fault outcrop
Normal fault (post-Caledonian)
Normal faults from seismic interpretation
Ductile thrust (Svecofennian)
Thrust (Caledonian)
Major steep ductile shear zone
Major steep ductile shear zone with shear sense
Antiform
Synform
Steeply plunging syncline
Trace of Neoarchaean gneiss folation and Svecofennian fabric in metasupracrustal belts
Basement-seated shear belts

Figure 25 (previous page): Tentative compiled bed rock and structural map of the strandflat and adjacent onshore and offshore portions of the SW Barents Sea margin, summarizing the interpretations from all areas of the strandflat by extending the onshore geology onto the strandflat. Note how the Senja Shear Belt, the Vengsøya high-strain zone and the Fugløya transfer zone segment the margin laterally. The combined length of all mapped and interpreted ductile and brittle lineaments with respect to their trends are shown in rose diagrams in the top left corner. BKFC=Bothnian-Kvænangen Fault Complex, BSFC=Bothnian-Senja Fault Complex, GFZ=Grøtsundet fault zone, GrFZ=Grasmyrskogen fault zone, LFZ=Langsundet fault zone, NFZ=Nybygda fault zone, SFZ = Stonglandseidet fault zone, SiFZ=Sifjorden fault zone, SoFZ=Solbergfjorden fault zone, VFZ=Vannareid-Brurøysund fault zone, VVFC=Vestfjorden-Vanna Fault Complex, TFFC=Troms-Finnmark Fault Complex.